

**Photoinduced Electron Transfer Processes in
Homogeneous and Microheterogeneous Media
Involving Organic and Inorganic Donor-Acceptor
Systems**

By

PAPU SAMANTA

CHEM01201604001

BHABHA ATOMIC RESEARCH CENTRE, MUMBAI

A thesis submitted to the

Board of Studies in Chemical Sciences

In partial fulfillment of requirements for the Degree of

DOCTOR OF PHILOSOPHY

of

HOMI BHABHA NATIONAL INSTITUTE



March, 2021

CERTIFICATION FROM GUIDE

This is to certify that the Ph.D. thesis entitled "Photoinduced Electron Transfer Processes in Homogeneous and Microheterogeneous Media Involving Organic and Inorganic Donor-Acceptor Systems" submitted by Shri. Papu Samanta is based on the research work carried out by him under our supervision.



Dr. Sharmistha Dutta Choudhury
(PhD Co-guide)



Dr. Haridas Pal
(PhD Guide)

Recommendations of the Viva-Voce Board

1. Date of Viva Voce Examination: 10-07-2021

2. Recommendations for the award of the Ph.D. degree: ☒ Recommended / ~~Not Recommended~~

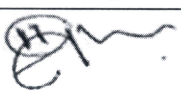
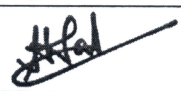
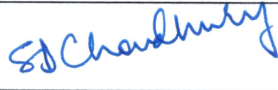
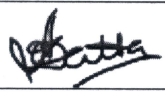
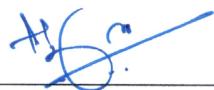
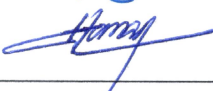
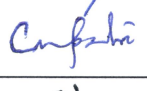

(If Recommended, give summary of main findings and overall quality of thesis)

(If Not Recommended, give reasons for not recommending and guidelines to be communicated by Convener of the Doctoral committee to the student for further work)

As the Committee members of the Ph.D. Viva Voce examination of Shri Papu Samanta, we have carefully attended his deliberation and critically read his dissertation, entitled, "*Photoinduced electron transfer processes in homogeneous and microheterogeneous media involving organic and inorganic donor-acceptor systems*". In the present thesis, Shri Samanta has carried out an impressive amount of high quality research work in the subject area of photoinduced electron transfer (PET) processes in homogeneous and microheterogeneous media. Two noteworthy findings of his research work are: (i) Unambiguously demonstrating the "Marcus Inversion Behavior" for PET reactions in microheterogeneous media, and (ii) Observing "Multichannel PET Reactions" involving lanthanide ions as unique electron acceptors. Shri Samanta had performed all the experiments very meticulously and analyzed the observed results very thoroughly to draw the inferences very convincingly. As the members of the Viva Voce Committee, we are very pleased with the dissertation and recommend the acceptance of the thesis in its present form for the award of Ph.D. Degree to Shri Papu Samanta.

In case, Not Recommended, another date will be fixed by the Dean-Academic, CI, which shall not be earlier than a month after and not later than six months from the date of first viva.

1. Name and Signature of the Viva Voce Board (Doctoral Committee & External Examiner):

Sr No	Composition	Name	Signature with date
a.	Chairman	Prof. H. N. Ghosh	 14-07-2021
b.	Convener (Guide)	Prof. Haridas Pal	 14-07-2021
c.	Co-Guide/External Guide (if any)	Prof. S. Dutta Choudhury	 14.7.21
d.	External Examiner	Prof. Anindya Datta	 14-07-2021
e.	Member	Prof. A. C. Bhasikuttan	 14-07-2021
f.	Member	Prof. P. A. Hassan	 14-07-2021
g.	Member	Prof. C. N. Patra	 14-07-2021
h.	The Technology Adviser, if any	Prof. P. K. Pujari	 14/7/21

Dean-Academic, CI

STATEMENT BY AUTHOR

This dissertation has been submitted in partial fulfillment of requirements for an advanced degree at Homi Bhabha National Institute (HBNI) and is deposited in the Library to be made available to borrowers under rules of the HBNI.

Brief quotations from this dissertation are allowable without special permission, provided that accurate acknowledgement of source is made. Requests for permission for extended quotation from or reproduction of this manuscript in whole or in part may be granted by the Competent Authority of HBNI when in his or her judgment the proposed use of the material is in the interests of scholarship. In all other instances, however, permission must be obtained from the author.

Papu Samanta
(PAPU SAMANTA)

DECLARATION

I, hereby declare that the investigation presented in the thesis has been carried out by me. The work is original and has not been submitted earlier as a whole or in part for a degree/diploma at this or any other Institution/University.

Papu Samanta
(PAPU SAMANTA)

List of publications arising from the thesis

Journal: Published (04)

1. "Tetronic star block copolymer micelles: photophysical characterization of microenvironments and applicability for tuning electron transfer reactions", **P. Samanta**, S. Rane, P. Bahadur, S. Dutta Choudhury and H. Pal, *J. Phys. Chem. B*, **2018**, 122, 6079–6093.
2. "Effect of ionic liquids as cosurfactants on photoinduced electron transfer in tetronic micelles", **P. Samanta**, P. Halder, P. Bahadur, S. Dutta Choudhury and H. Pal, *J. Phys. Chem. B*, **2018**, 122, 10190–10201.
3. "Kinetics and energetics of ultrafast bimolecular photoinduced electron transfer reactions in pluronic-surfactant supramolecular assemblies", **P. Samanta**, S. Dutta Choudhury and H. Pal, *J. Phys. Chem. B*, **2019**, 123, 5942–5953.
4. "Lanthanide (III) ions as multichannel acceptors for bimolecular photoinduced electron transfer reactions with coumarin dyes", **P. Samanta**, S. Dutta Choudhury and H. Pal, *J. Photochem. Photobiol. A*, **2020**, 401, 112774(1-11).

Conferences (02):

1. Effect of ionic liquid as co-surfactant on photoinduced electron transfer in tetronics®1304 micelles, **P. Samanta**, P. Halder, P. Bahadur, S. Dutta Choudhury and H. Pal, 14th Trombay Symposium on Radiation & Photochemistry (TSRP), January 3-7, 2018, BARC, Mumbai, India.
2. Kinetics and energetics of ultrafast photoinduced electron transfer in pluronic-surfactant micelles, **P. Samanta**, S. Dutta Choudhury and H. Pal, 15th Trombay Symposium on Radiation & Photochemistry (TSRP), January 5-9, 2020, BARC, Mumbai, India.

Papu Samanta
(PAPU SAMANTA)

Dedicated to My Family

ACKNOWLEDGEMENTS

The realization of this thesis was accomplished with the support and encouragement of numerous people including my well-wishers, friends and colleagues to whom I would like to show my greatest appreciation. Firstly, I would like to express my sincere gratitude to my research guide **Dr. Haridas Pal** and co-guide **Dr. Sharmistha Dutta Choudhury** for their continuous guidance, support and motivation. Their encouragement, knowledge, and experience helped me a lot during the course of my Ph.D. work. I would like to thank **Prof. H. N. Ghosh (Chairman, doctoral committee)** and other members of my doctoral committee; **Prof. A. C. Bhasikuttan, Prof. P. A. Hassan, Prof. C. N. Patra** and **Prof. P. K. Pujari**, for their time, encouragement, thoughtful ideas and critical evaluation during the course of my Ph.D.

I am very thankful to **Vivek Bhasin**, Group Director, Nuclear Fuels Group (NFG), **Rakesh Kumar**, Head, Integrated Fuel Fabrication Facility (IF3) and **Dr. Pradeep Kumar**, Head, Chemical Quality Control Section, IF3, for their interest, continuous support and motivation, which helped me a lot during the course of my Ph.D. work.

My sincere thanks to **my lab mates** for all their precious help, valuable discussions, and cooperation. Special Thanks to **Sonal Rane** and **Pritesh Halder** for their valuable help and support. I sincerely thank **Dr. Arun Kumar Mora** for his scientific help during the ultrafast studies. I acknowledge **Dr. Biswajit Manna** for his extended help in laser flash photolysis study. I also acknowledge **Shri Ramapada Das** for his help during zeta potential measurements. I would also like to thank my colleagues **Dr. M. Kumbhakar, Dr. P.K. Singh, Dr. M. Sayed, Dr. S. Nath and all other members of MPS** for their help, encouragement, and support during the course of my research work.

I wish to express my sincere thanks to all my dear friends for their moral support, encouragement and constant positivity when it was needed. I would also like to thank all **my training school batch mates** for their warm friendship and support. I would like to acknowledge my **teachers** since my childhood; I would not have been here without their guidance, blessings, and support.

I am eternally grateful to **my father (Shri Churamani Samanta)** and **mother (Smt. Rupa Samanta)** for their unconditional love, support, faith, encouragement and

confidence in me. They have been my driving force and inspiration in all pursuits of my life and I owe all my accomplishments to them. Heartfelt thank goes to my in-laws for their unconditional love and blessings in my life. I would like to express my warm gratitude towards my wife **Debodyity Das** for her love and understanding at every step of life, without her support I would not have been able to make it. My heartiest thanks to my **Didi (Moumita Barui)** and **brother (Devmya Samanta)**, for their love, inspiration and confidence endowed on me in all my endeavors.

Lastly, I wish to express my appreciation and thanks to the individuals who were important in the realization of this thesis, as well as apologize that I could not mention everyone personally.

Papu Samanta
(PAPU SAMANTA)

CONTENTS

Items	Page No.
<i>Synopsis</i>	i
<i>List of Abbreviations</i>	viii
<i>List of Figures</i>	ix
<i>List of Charts</i>	xiii
<i>List of Schemes</i>	xiii
<i>List of Tables</i>	xiv

Chapter 1: *General Introduction*

1.1.	Introduction	3
1.2.	Electron Transfer Reaction: Theoretical Background	4
1.2.1.	Classical Marcus Outer-sphere Electron Transfer Theory	4
1.2.2.	Quantum Mechanical Refinement of the Marcus ET Theory: Adiabatic and Non-adiabatic ET Reactions	9
1.2.3.	Effect of High Frequency Vibrational Modes on ET Rates	11
1.2.4.	ET Rate versus Solvent Relaxation Dynamics: Sumi-Marcus Two-dimensional ET (2DET) Theory	14
1.3.	Photoinduced Processes	17
1.4.	Energetics of Photoinduced Electron Transfer Processes	19
1.5.	Predicted Kinetics of PET Reactions under Diffusive Condition	20
1.5.1.	Correlations of the Quenching Constants with the Free Energy Changes for Bimolecular PET Reactions under Diffusive Condition	22
1.6.	Solvation Dynamics	25
1.7.	General Micellar Characteristics of Block Copolymers (Pluronics and Tetronics) in Aqueous Solutions	27
1.8.	Lanthanide Ions as Electron Acceptors in PET Studies	34
1.9.	Motivation and Objective of the Present Thesis	35

Chapter 2: *Instruments and Methods*

2.1.	Introduction	43
2.2.	Ground State Absorption Measurements	43
2.3.	Steady-State Fluorescence Measurements	45

2.3.1.	Correction of the Emission Spectra	45
2.4.	Time-resolved Fluorescence Measurements	46
2.5.	Time-Correlated Single Photon Counting (TCSPC) Technique	47
2.5.1.	Basic Principles of TCSPC Technique	47
2.5.2.	Important Components of a TCSPC Spectrometer	49
2.5.3.	Time Calibration of the MCA Channels in a TCSPC Spectrometer	52
2.5.4.	Analysis of the Fluorescence Decay Measured using TCSPC Instrument	53
2.6.	Fluorescence Up-conversion Measurements	54
2.6.1.	Brief Description of the Present Fluorescence Up-conversion Setup	55
2.7.	Fluorescence Anisotropy Measurements	57
2.8.	Time Resolved Transient Absorption Measurements	61
2.9	Zeta potential Measurements	62

Chapter 3: *Tuning Photoinduced Electron Transfer Reactions in Tetronic Star Block Copolymer Micelles*

3.1.	Introduction	65
3.2.	Materials and Methods	68
3.3.	Results and Discussion	69
3.3.1.	Characterization of the Microenvironments in T1304 and T1307 Micelles	69
3.3.1.1.	Micropolarity Estimations in T1304 and T1307 Micellar Systems	69
3.3.1.2.	Microviscosity Measurements in T1304 and T1307 Micelles	70
3.3.1.3.	Solvation Dynamics Study in T1304 and T1307 Micelles	72
3.3.2.	Photoinduced Bimolecular Electron Transfer Studies in Tetronic Micelles	76
3.3.2.1.	Ground State Absorption and Steady-State Fluorescence Studies	76
3.3.2.2.	Time-Resolved Fluorescence Quenching Measurements	80
3.3.2.3.	Calculation of Free Energy Changes and Correlation with the observed PET Rates	84
3.3.2.4.	Salt effect on the micellar micropolarity and ET kinetics	89
3.4.	Conclusion	94

Chapter 4: *Ionic Liquids as Co-Surfactants for Tetronic Micelles in Modulating Photoinduced Electron Transfer Process*

4.1.	Introduction	99
4.2.	Materials and Methods	101
4.3.	Results and Discussion	101
4.3.1.	Ground State Absorption and Steady-State Fluorescence Studies	101

4.3.2.	Time-Resolved Fluorescence Quenching Measurements	104
4.3.3.	Correlations of the Observed PET rates with the Free Energy Changes (ΔG^0) of the PET Reaction in the Studied Micellar Media	106
4.3.4.	Time-Resolved Fluorescence Anisotropy Studies: Microviscosity Estimations	109
4.3.5.	Solvent Relaxation Dynamics Studies in the Investigated Micellar Media	111
4.3.6.	Modulations of Marcus Inversion (MI) Behavior by the Presence of the ILs as Co-surfactants in T1304 Micelles	113
4.4.	Conclusion	116

Chapter 5: *Ultrafast Photoinduced Electron Transfer in Pluronic-Surfactant Supramolecular Assemblies*

5.1.	Introduction	121
5.2.	Materials and Methods	124
5.3.	Results and Discussion	125
5.3.1.	Ground State Absorption and Steady-State Fluorescence Studies on the Interaction of Coumarin Dyes with DMAN Donor	125
5.3.2.	Time-resolved Fluorescence Quenching Studies for Coumarin-DMAN Pairs in Different Micellar Media using TCSPC measurements	127
5.3.3.	Correlation of the Bimolecular Quenching Constants with the Free Energy Changes of the ET Reactions	129
5.3.4.	Ultrafast Time-resolved Fluorescence Studies for Coumarin-DMAN Pairs in Different Micellar Media using Up-Conversion Measurements	132
5.4.	Conclusion	137

Chapter 6: *Lanthanide (III) Ions as Multichannel Acceptors for Photoinduced Electron Transfer Reactions*

6.1.	Introduction	141
6.2.	Materials and Methods	144
6.3.	Results and Discussion	145
6.3.1.	Interaction of Ground State Coumarin Dyes with Ln(III) Ions	145
6.3.2.	Interaction of Excited (S_1) Coumarin Dyes with the Ln(III) Quenchers	145
6.3.2.1.	Steady-state (SS) Fluorescence Quenching Study	145
6.3.2.2.	Time-resolved (TR) Fluorescence Quenching Study	147
6.3.3.	Laser Flash Photolysis Studies on Coumarin-Ln(III) Systems	150
6.3.4.	Correlation of k_q Values with Free Energy Changes of PET Reactions	154
6.4.	Conclusion	163

Chapter 7: *Summary of the Present Research Work and Future Prospects*

7.1.	Introduction	167
7.2.	Studies on the Bimolecular PET Reactions in Micellar Media	167
7.3.	PET Reactions in Aqueous Media Involving Lanthanide (III) ions	169
7.4 .	Future Perspectives of the Work Carried out in the Present Thesis	170

References	173
-------------------	-----

LIST OF ABBREVIATIONS

Electron Transfer	ET
2-Dimentional Electron Transfer	2DET
Photoinduced Electron Transfer	PET
Marcus Inversion	MI
Time Correlated Single Photon Counting	TCSPC
Time to Amplitude Converter	TAC
Instrument Response Function	IRF
Photomultiplier Tube	PMT
Ultraviolet	UV
Charge Coupled Device	CCD
Time-Resolved Emission Spectra	TRES
Time-resolved Area Normalized Emission Spectra	TRANES
Critical Micelle Temperature	CMT
Critical Micelle Concentration	CMC
Constant Fraction Discriminator	CFD
Multichannel Analyzer	MCA
Analog-to-Digital Converter	ADC
Light Emitting Diodes	LED
Full Width at Half Maximum	FWHM
Laser Flash Photolysis	LFP
Phase Analysis Light Scattering	PALS

LIST OF FIGURES

Chapter 1

Figure 1.1.	Schematic presentation of the free energy surfaces of reactant (R) and product (P) states according to classical Marcus' outer-sphere ET theory.	5
Figure 1.2.	Pictorial representation of the "Marcus Inversion Behavior".	9
Figure 1.3.	Avoided crossing for the free energy surfaces of the R and P states and the electronic coupling matrix element (V_{el}).	11
Figure 1.4.	Schematics for the participation of the high-frequency vibrational modes in ET reactions.	12
Figure 1.5.	Schematics of the symmetric and asymmetric k_{et} versus $-\Delta G^0$ correlations.	13
Figure 1.6	Conceptual presentation of the free energy contours of R and P states for 2DET model.	15
Figure 1.7.	Schematic presentation of the 2DET process for equilibrium and non-equilibrium free energy curves of R state with regard to solvent relaxation.	16
Figure 1.8.	Energetics involved for dark ET and PET reactions.	18
Figure 1.9.	The Jablonski diagram depicting the photoexcitation of a chromophoric system and its subsequent relaxation processes.	19
Figure 1.10.	Rehm-Weller behavior and its comparison with Marcus inversion behavior.	23
Figure 1.11.	Changes in the ΔG^* and k_{obs} values with reaction exergonicity, as governed by Rehm-Weller relations.	24
Figure 1.12.	Qualitative presentation of the appearance of MI under diffusive condition at exceedingly high $-\Delta G^0$ values.	25
Figure 1.13.	Conceptual presentation of dynamic fluorescence Stokes' shift due to solvent relaxation process.	26
Figure 1.14.	Representative structures of the Pluronic and Tetronic block copolymers and their micelle formation.	28
Figure 1.15.	Hartely's 'oil' drop model for a micellar structure.	31
Figure 1.16.	Schematic of the mixed micellar assemblies formed by ionic surfactant with a block copolymer micelle.	33

Chapter 2

Figure 2.1.	Schematics of a double beam UV-vis absorption spectrometer.	44
Figure 2.2.	Schematics of a steady-state fluorescence spectrometer.	45
Figure 2.3.	Schematic of a Time Correlated Single Photon Counting spectrometer.	48
Figure 2.4.	Schematics of the functioning of a TAC unit in TCSPC measurements.	52
Figure 2.5.	Schematics of the femtosecond fluorescence up-conversion setup.	55
Figure 2.6.	Schematic presentation of the spatial and temporal overlap of fluorescence and gate pulses in fluorescence up-conversion method.	56
Figure 2.7.	Creation of anisotropic distribution of excited chromophores by polarized light.	58
Figure 2.8.	Schematics of the fluorescence anisotropy measurement.	58
Figure 2.9.	Schematics of the nanosecond laser flash photolysis setup.	61

Chapter 3

Figure 3.1.	Fluorescence spectra of C153 probe in different solvents and tetronic micelles, and the constructed calibration plot with respect to the solvent polarity function (Δf).	70
Figure 3.2.	Fluorescence anisotropy decay of C153 dye in T1307 and T1304 micelles.	71
Figure 3.3.	Wavelength dependent fluorescence kinetic traces for C153 dye in T1307 and T1304 micelles.	73
Figure 3.4.	Time-resolved emission spectra of C153 dye in T1307 and T1304 micelles.	73
Figure 3.5.	Spectral shift correlations of C153 dye in T1307 and T1304 micelles.	74
Figure 3.6.	Absorption and fluorescence spectra for coumarin-DMAN systems and the Stern-Volmer (SV) plot for SS fluorescence quenching in tetronic micelles.	77
Figure 3.7.	Fluorescence decay traces of C151-DMAN systems in T1307 micelles and the corresponding SV plot.	81
Figure 3.8.	Calibration plot for the estimation of $E_T(30)$ values in T1304 and T1307	85

micelles.

Figure 3.9	The $\ln(k_{q(TR)})$ versus ΔG^0 plots for the coumarin-amine systems in T1304 and T1307 micelles.	88
Figure 3.10.	Fluorescence spectra of C153 dye in T1307 micelles in the presence of different NaCl concentrations and estimation of polarity in the corresponding micelles from the calibration plot.	90
Figure 3.11.	Fluorescence anisotropy decays and spectral shift correlation functions of C153 dye in T1307 micelle in the presence of different NaCl concentrations.	90
Figure 3.12.	The SV plots obtained from TR fluorescence quenching and correlation of the $\ln(k_{q(TR)})$ values with ΔG^0 for coumarin-amine system in T1307 micelle in the presence of different NaCl concentrations.	92
Figure 3.13.	Pictorial representation on the modulation of PET kinetics using either different Tetronic micelles or using NaCl as the additive.	94

Chapter 4

Figure 4.1.	Fluorescence quenching for C153-DMAN system in pure T1304 and in T1304-[DMIm][BF ₄] mixed micelles. Absorption spectra and the SV plot in the studied micelles are also shown.	102
Figure 4.2.	Fluorescence quenching of C151-DMAN system in pure T1304 and in T1304-[BMIm][BF ₄] mixed micelle. The SV plots for the studied systems are also shown.	102
Figure 4.3.	Changes in the emission maxima of C153 dye with increasing concentration of T1304 in the absence and presence of IL, to estimate CMC values.	104
Figure 4.4.	Fluorescence decay traces of C153-DMAN system in pure T1304 and T1304-[DMIm][BF ₄] mixed micelles.	105
Figure 4.5.	Polarity dependent fluorescence spectra of C153 probe and the constructed calibration plots for the estimations of Δf and $E_T(30)$ parameters in different T1304-IL mixed micelles.	108
Figure 4.6.	The $\ln(k_{q(TR)})$ versus ΔG^0 plots in pure T1304 and in different T1304-IL mixed micelles.	108
Figure 4.7.	Fluorescence anisotropy decay traces of C153 in pure T1304 and T1304-IL mixed micelles.	110

Figure 4.8.	Wavelength dependent fluorescence decay traces for C153 dye and the constructed TRES in T1304-[DMIm][BF ₄] mixed micellar system.	111
Figure 4.9.	Spectral shift correlations for C153 dye in pure T1304 and T1304-IL mixed micellar systems.	112

Chapter 5

Figure 5.1.	Absorption spectra of coumarin-DMAN system in pure P123 micelle and in a typical SDS-P123 mixed micelle.	125
Figure 5.2.	SS fluorescence quenching and corresponding SV plots for coumarin-DMAN systems in pure P123 micelle and in a typical SDS-P123 mixed micelle.	126
Figure 5.3.	TR fluorescence quenching and corresponding SV plots for coumarin-DMAN systems in pure P123 micelle and in a typical SDS-P123 mixed micelle.	128
Figure 5.4.	Polarity dependent fluorescence spectra of C153 probe and the constructed calibration plots for the estimations of Δf and $E_T(30)$ parameters for pure P123 and different SDS-P123 mixed micelles.	130
Figure 5.5.	The $\ln(k_{q(TR)})$ versus ΔG^0 plots in pure P123 and in different SDS-P123 mixed micelles.	132
Figure 5.6.	Ultrafast fluorescence decays for coumarin-DMAN pairs in pure P123 and in different SDS-P123 mixed micelles.	133
Figure 5.7.	The τ_i^{-1} vs ΔG^0 plots for all the three decay components of coumarin-DMAN pairs in pure P123 and in different SDS-P123 mixed micelles.	135

Chapter 6

Figure 6.1.	Absorption spectra of different coumarin-Ln(III) pairs in aqueous solution.	145
Figure 6.2.	SS fluorescence quenching and corresponding SV plots for coumarin-Ln(III) pairs in aqueous solution.	146
Figure 6.3.	TR fluorescence quenching and corresponding SV plots for coumarin-Ln(III) systems in aqueous solution.	148
Figure 6.4.	Transient absorption spectra for C339 dye and C339-Eu(III) system	151

obtained from LFP studies.

Figure 6.5.	Transient absorption spectra for C339 and C339-Eu(III) system plotted specifically for shorter wavelength region.	151
Figure 6.6.	Transient absorption spectra for C339 and C339-Eu(III) systems plotted specifically for longer wavelength region.	151
Figure 6.7.	Transient absorption spectra for C102 dye and C102-Eu(III) system obtained from LFP studies.	152
Figure 6.8.	Transient absorption spectra for C102 and C102-Eu(III) system plotted specifically for shorter wavelength region.	153
Figure 6.9.	Transient absorption spectra for C102 and C102-Eu(III) system plotted specifically for longer wavelength region.	153
Figure 6.10.	Transient kinetic traces for C339 radical cation in different C339-Ln(III) systems.	154
Figure 6.11.	The k_q vs ΔG^0 plots for the coumarin-Ln(III) systems in aqueous media.	157
Figure 6.12.	Partial energy diagram of the lanthanide ions and comparison with the available exergonicity of the PET reaction in coumarin-Ln(III) systems.	160

LIST OF CHARTS

Chart 3.1.	Chemical structures of T1304 and T1307 star block copolymers, the coumarin acceptors and the aromatic amine donors.	66
Chart 4.1.	Chemical structures of T1304 star block copolymer, the $[C_nMIm][BF_4]$ series of ILs, the coumarin dyes and the DMAN donor.	100
Chart 5.1.	Chemical structures of the P123 tri-block copolymer, the SDS surfactant, the coumarin acceptors and DMAN donor.	123
Chart 6.1.	The 4-methyl-7-aminocoumarin dyes and Ln(III) ions used in this study along with their redox potentials.	143

LIST OF SCHEMES

Scheme 4.1.	Schematics of the T1304+IL mixed micelles formed on addition of ILs of differential chain lengths and conceptual presentation of the tuning in PET reactions in the mixed micellar systems.	116
Scheme 5.1.	Schematics of the formation of copolymer-surfactant mixed micellar aggregates on addition of an ionic surfactant into pluronic micelles.	122
Scheme 5.2.	Modulation of ET kinetics from subnanosecond to subpicosecond time domain in P123-SDS mixed micelles.	136
Scheme 6.1.	Kinetic scheme for bimolecular PET reactions taking place under standard diffusive condition.	158

LIST OF TABLES

Chapter 3

Table 3.1.	Anisotropy decay parameters of the C153 probe in T1304 and T1307 micellar systems.	71
Table 3.2.	Parameters related to solvent relaxations in T1304 and T1307 micelles estimated from the dynamic Stokes' shifts of C153 dye.	74
Table 3.3.	Various micellar parameters for the T1304 and T1307 systems.	79
Table 3.4.	The list of $k_{q(SS)}$ and $k_{q(TR)}$ values for coumarin-DMAN pairs in T1307 and T1304 micellar media.	82
Table 3.5.	Various parameters related to PET process for coumarin-DMPT and coumarin-DMAN systems in T1304 and T1307 micelles.	83
Table 3.6.	Calculated electrochemical properties of the donors (DMAN and DMPT) and acceptors (coumarin dyes) in T1304 and T1307 micelles.	87
Table 3.7.	Fitted parameters for time-resolved fluorescence anisotropy decay and solvent relaxation dynamics for C153 probe in T1307 micelles in the presence varying NaCl concentrations.	91
Table 3.8.	List of the PET parameters and the free energy changes for the coumarin-amine systems in T1307 micelle at different NaCl concentrations.	91
Table 3.9.	Calculated electrochemical properties of the donor (DMAN/DMPT) and acceptors (coumarin dyes) in T1307 micelles in the presence of different NaCl concentrations.	93

Chapter 4

Table 4.1.	Various micellar parameters of pure T1304 and T1304-IL mixed micelles.	103
Table 4.2.	Various energy parameters for PET reactions involving coumarin acceptors and DMAN donor in pure T1304 and T1304-IL mixed micelles.	106
Table 4.3.	Calculated electrochemical properties of the coumarin acceptors and DMAN donors in T1304 and T1304+IL micellar media.	107
Table 4.4.	Fluorescence anisotropy decay parameters of C153 in pure T1304 and T1304-IL micelles.	110
Table 4.5.	Fitted parameters for the spectral shift correlation function $C(t)$ in pure	112

T1304 and T1304-IL micelles.

Table 4.6.	Zeta potential values in T1304 and T1304-IL micelles.	115
-------------------	---	-----

Chapter 5

Table 5.1.	Various micelle parameters of SDS-P123 (n=0-2) systems.	127
Table 5.2.	Parameters related to PET reactions between coumarin acceptors and DMAN donor in the SDS-P123 (n=0-2) mixed micellar systems.	128
Table 5.3.	Calculated electrochemical properties for the DMAN donor and coumarin acceptors in SDS-P123 systems.	131
Table 5.4.	Fitted parameters for the ultrafast fluorescence kinetic traces recorded using up-conversion measurements.	134

Chapter 6

Table 6.1.	Electronic configurations, reduction potentials, diffusion coefficients and hydrated radii of Ln(III) ions in aqueous solution.	141
Table 6.2.	The $k_{q(SS)}$ and $k_{q(TR)}$ values estimated for the coumarin-Ln(III) systems.	147
Table 6.3.	Various parameters for the PET Reactions between coumarin donors and Ln(III) acceptors.	149
Table 6.4.	Calculated electrochemical properties for the coumarin dyes in aqueous solution.	155
Table 6.5.	Calculated free energy changes (ΔG^0) for coumarin-Ln(III) systems following Rehm-Weller relation.	155

CHAPTER-7

SUMMARY OF THE PRESENT RESEARCH WORK AND FUTURE PROSPECTS

7.1. Introduction

The primary objective of the present thesis has been to understand the modulations in the kinetic and energetic details of bimolecular photoinduced electron transfer (PET) reactions,^{3,4,9-11,29,30,42,102} either by using selected constrained microheterogeneous reaction media, where physiochemical properties of reaction microenvironments can be tailored suitably to influence the PET reactions, or by the use of uniquely chosen PET systems, whereby the mechanistic pathways of the reactions can be amended in a fascinating manner to control the outcome of the PET reactions. In the first part of the present thesis, the studies on the bimolecular PET reactions have been carried out between organic donors (aromatic amines) and acceptors (coumarin dyes) in different tetronic and pluronic block copolymer micelles, both in the absence and presence of unconventional (ionic liquid; IL) and conventional (sodium dodecyl sulfate; SDS) co-surfactants, respectively.^{161,347,400} In the second part of the thesis, the details of the bimolecular PET reactions have been investigated in homogeneous aqueous media, using conventional organic dyes (coumarin dyes) as the donors and the rarely used redox active inorganic systems (trivalent lanthanide ions, Ln(III)) as the unique electron acceptors. In this study, intriguing participation of multichannel PET mechanism has been anticipated through the involvement of the low lying electronic states of the Ln(III) species.²¹¹ The summary of the overall results obtained from the detailed research work carried out in this thesis are briefly given below. Finally, we discuss the future perspectives of the research work undertaken in this Ph.D. program, to substantiate the objectives of the present thesis work.

7.2. Studies on the Bimolecular PET Reactions in Micellar Media

In the pursuit of our PET studies in constrained microheterogeneous media, we have used micelles of two newly introduced tetronic series of star block copolymers, namely tetronic-1304 (T1304) and tetronic-1304 (T1307). Also we used micelles of T1304, both in the absence and presence of different 1-alkyl-3-methylimidazolium tetrafluoroborate ($[C_n\text{MIm}][\text{BF}_4]$) ILs with varying chain length (C_n) of the 1-alkyl substituent of the $[C_n\text{MIm}]^+$ cation as the unconventional co-surfactants. In these studies, N,N-dimethylaniline (DMAN) and N,N-dimethyl-*p*-toluidine (DMPT) have been used as the typical organic donors and a series of coumarin dyes have been used as the typical organic acceptors to understand the modulations in the kinetic and energetic of the PET processes as a function of the tetronic copolymer systems as well as that of the IL co-surfactants used. The kinetics of the observed bimolecular PET reactions in the concerned micelles were evaluated following sub-nanosecond time-resolved fluorescence quenching studies following time-correlated single photon counting (TCSPC) measurements. For the micellar systems used in these studies, the microenvironments of their corona region, especially in regard to their micropolarity, hydration, microviscosity, and solvent relaxation, have also been investigated independently, to rationalize the

observed PET results in a comprehensive manner. In both T1304 and T1307 micelles, and also in T1304-IL mixed micellar systems, it is indicated that observed PET reactions apparently occur under non-diffusive condition of the reactants, suggesting that the PET reactions in these systems mainly occur in those pre-existing donor-acceptor pairs where the reactants are already within the interaction zone (i.e. the reaction sphere) at the point of photoexcitation of the sample. In all the micellar systems used, the correlation of the observed bimolecular quenching rate constants ($k_{q(TR)}$) with the exergonicity of the PET reactions ($-\Delta G^0$) demonstrate the most desired Marcus Inversion (MI) behavior. Interestingly, the onset of the MI in all the cases appear at a much lower exergonicity as compared to the expected solvent reorganization energy (λ_s) in the corona regions of the concerned micelles, suggesting the involvement of two-dimensional ET (2D-ET) mechanism in all the studied cases. The observations of the relatively higher $k_{q(TR)}$ values and the reasonable shift for the onset of MI towards higher exergonicity in T1307 micelle as compared to those in T1304 micelle correlate very nicely with the higher micropolarity, lower microviscosity and faster solvent relaxation in the corona region of the former micelle than the latter. That the $k_{q(TR)}$ values also gradually decrease and the onset of MI shifts significantly towards lower exergonicity with the increasing salt (NaCl) concentration in T1307 micelle substantiate nicely with the salt induced dehydration of the studied micelles, as revealed independently from micropolarity, microviscosity and solvent relaxation dynamics studies. Similarly, the observation that the $k_{q(TR)}$ values gradually increase and the onset of MI systematically shifts towards higher exergonicity with the increasing alkyl chain length of the $[C_nMIm][BF_4]$ ILs as the co-surfactants in T1304 micelle also corroborate nicely with the increased micropolarity, reduced microviscosity and faster solvent relaxation dynamics estimated for these T1304-IL mixed micellar systems as a function of the increasing C_n value of the ILs used. Observed results demonstrate the intriguing strategies of using either added salt or a suitable IL co-surfactant in a tetronic micelle to modulate the observed reaction rates as well as the onset of the observed MI for bimolecular PET reactions very effectively.

To substantiate the indicated fact from sub-nanosecond TCSPC measurements that the PET reactions in the constrained micellar media occur mainly through the involvement of the pre-existing donor-acceptor pairs that have the concerned interacting species already within the interaction zone at the point of photoexcitation, we have also carried out ultrafast fluorescence up-conversion studies on the bimolecular PET reactions, involving coumarin dyes as the acceptors and DMAN as the donor. These studies have been carried out in the micellar and mixed micellar systems of a triblock copolymer, namely pluronic-123 (P123), using SDS as a co-surfactant, with the anticipation that the PET process occurring in the pre-existed donor-acceptor pairs would be captured directly in the measured kinetic traces with sub-picosecond time resolution, as can be achieved easily through fluorescence up-conversion measurements. It was observed that either in P123 micelle or in SDS-P123 mixed micelles, the individual decay rate constants (τ_i^{-1}) estimated from the tri-exponential analysis of the ultrafast fluorescence kinetic traces recorded through up-conversion measurements

display the unique Marcus Inversion (MI) behavior on plotting against the $-\Delta G^0$ values of the PET reactions, which is also indicated similarly while we correlate the observed $k_{q(TR)}$ values obtained through sub-nanosecond TCSPC measurements with the concerned $-\Delta G^0$ values. Observations of the similar MI behaviors throughout the time scales of the observations (from sub-nanoseconds to sub-picoseconds) inevitably suggest the involvement of the non-diffusive PET reactions in the studied micellar assemblies. Similar to the studies in tetroic micelles, in the present cases also, the onset of MI appears at a substantially lower exergonicity, suggesting the involvement of 2DET mechanism for the PET reactions investigated in the studied micellar systems. In the present cases, it is further observed that the maximum reaction rates, either in terms of the individual τ_i^{-1} values or in regard to the $k_{q(TR)}$ values, as well as the exergonicity values for the onset of the MI in all these cases, gradually increase on increasing the [SDS]/[P123] molar ratio (n -value) of the concerned mixed micellar systems, which correlate nicely with the increasing micropolarity in corona region of these mixed micelles with an increase in their n -values.

The intriguing modulations in the energetic and kinetics of the PET reactions in the studied micellar systems are not only very appealing from the academic point of view, but would also definitely find prospective uses in different applied areas.

7.3. PET Reactions in Aqueous Media Involving Lanthanide (III) ions

Trivalent lanthanide ions, Ln(III), have wide range of redox potentials and many of these ions can act as good electron acceptors in the presence of suitable electron donors to participate especially in the photoinduced electron transfer (PET) reactions. In a part of the study carried out in the present thesis, the bimolecular PET reactions have been explored quite extensively involving three Ln(III) ions, namely Eu(III), Yb(III) and Sm(III), as the electron acceptors, and a series of coumarin dyes as the electron donors in homogeneous aqueous medium, unlike the previously discussed studies that had been carried out in microheterogeneous micellar media. A thorough investigation in the present part of the studies has shown that among the different coumarin-Ln(III) pairs, only the coumarin-Eu(III), coumarin-Yb(III) and coumarin-Sm(III) systems can provide favorable free energy changes (negative ΔG^0 values) for the PET reactions and accordingly reasonable extent of PET mediated fluorescence quenching could be observed for the above three coumarin-Ln(III) systems using the steady state and the TCSPC based sub-nanosecond time-resolved fluorescence measurements. Interestingly, in the present cases, the correlations of the $k_{q(TR)}$ values with the exergonicity ($-\Delta G^0$) of the PET reactions do not follow a common correlation incorporating all the three coumarin-Ln(III) systems together. More surprisingly, even though the exergonicity for the studied coumarin-Ln(III) systems followed the order, coumarin-Eu(III) > coumarin-Yb(III) > coumarin-Sm(III), the $k_{q(TR)}$ values for these systems unexpectedly showed a reverse trend, i.e. coumarin-Eu(III) > coumarin-Sm(III) > coumarin-Yb(III), indicating the differential electron accepting propensities of

different Ln(III) ions towards the studied PET reactions. On correlating the $k_{q(TR)}$ values with the $-\Delta G^0$ values for different coumarin-Ln(III) systems independently for each of the Ln(III) ions following the well-known diffusion mediated bimolecular reaction scheme^{29,38,148,236} the total reorganization energy (λ) is found to be as high as ~ 2.3 eV for the coumarin-Yb(III) systems, while the concerned λ value for coumarin-Sm(III) and coumarin-Eu(III) systems are found to be in the usual range of ~ 1.3 eV.^{130,260,264,375,416,442} The differences observed in the $k_{q(TR)}$ versus ΔG^0 correlations for different coumarin-Ln(III) systems along with the unusually high λ value obtained for the coumarin-Yb(III) systems are rationalized considering the differential participations of the low lying electronic states of the used Ln(III) ions in supporting the multichannel PET reactions in these donor-acceptor systems. It is realized that for the coumarin-Eu(III) and coumarin-Sm(III) systems more than one electronic states of the Eu(III) and Sm(III) ions can suitably accept an electron from the excited coumarin donors, as these states are accessible by the available exergonicity of the PET reactions in the concerned coumarin-Ln(III) systems, and thus the multichannel PET reactions is supported in these systems, causing the observed $k_{q(TR)}$ values substantially higher and the associated λ value substantially lower in these cases, as are observed experimentally. For the coumarin-Yb(III) systems, however, only the lowest electronic state of the Yb(III) ion can accept an electron from the excited coumarin donors, because there is no other higher electronic states for this Yb(III) ion quencher which is accessible by the available exergonicity of the PET reactions in these cases and accordingly the multichannel PET is not supported for the studied coumarin-Yb(III) systems. Accordingly, for these PET systems, we observe significantly lower $k_{q(TR)}$ values in general along with a substantially higher λ value on correlating the observed $k_{q(TR)}$ values with the $-\Delta G^0$ values of the PET reactions following the well-known diffusion-mediated bimolecular reaction scheme.^{29,38,148,236} The modulations observed in the PET kinetics for the studied coumarin-Ln(III) systems is expected to find suitable applications in controlling the PET processes in different applied areas where appropriate Ln(III) ions can be used as the electron acceptors to achieve the desired PET results.

7.4. Future Perspectives of the Work Carried out in the Present Thesis

As we have mentioned earlier (Section 1.7 in Chapter 1 and Section 3.1 in Chapter 3), among various surfactant systems, the ones constituted with unique arrangements of the polyethyleneoxide (PEO or (EO)_n) and polypropyleneoxide (PPO or (PO)_m) blocks have attracted considerable research interests during last two decades because of the intriguing thermo-responsive behavior of these block copolymer based surfactant systems in aqueous solution,^{175,445-449} and also because of their wide-spread applications in detergent, lubricant, emulsifier and related industries.⁴⁵⁰⁻⁴⁵⁶ While the family of the linear block copolymer systems, designated with their trade names as “Pluronics” and are constituted with the general formula as (EO)_n-(PO)_m-(EO)_n, have been investigated quite

extensively,^{117,118,235,331-335} the family of the star block copolymer systems, designated with their trade names as “Tetronics” and are constituted with the general formula as $[(EO)_n-(PO)_m]_2-[N(CH_2)-(CH_2)N]-[(EO)_n-(PO)_m]_2$, have not been investigated that extensively till date, as these star block copolymers are quite new entrants in the surfactant systems. Interestingly, however, the star block copolymer systems have attracted a lot of research interests in recent years, because the supramolecular assemblies of these copolymer based surfactants display many improved properties in aqueous solution in regard to their prospective applications in the drug delivery and related areas of applied sciences as compared to the linear block copolymer systems.^{151,156-158,160,167,188,326-328}

In the present thesis, our major endeavour has been to understand if the kinetics and energetics of bimolecular photoinduced electron transfer (PET) reactions can be modulated in any useful manner in the tetronic and pluronic micellar systems, either by changing the block copolymers as such, or by adding suitable additives, either as the co-surfactants (e.g. ionic liquids) or as the dehydrating agents (e.g. NaCl salt). Using the micelles formed by the tetronic series of the star block copolymers, namely T1304 and T1307, we indeed find very intriguing modulations in the kinetics and energetic of the studied PET reactions, realized either by changing the copolymer system directly, or by changing the concentration of the added NaCl salt suitably as the dehydrating agent in a single tetronic micelle, which are not only very interesting from the academic point of view but also of the relevance for the PET processes take place in the areas like photovoltaics, solar energy conversions, drug stabilizations, and so on.

In the present study, we have also observed that the biologically friendly and quite benign ionic liquid (IL) systems can be suitably used as the co-surfactants for the tetronic star block copolymer systems forming unique mixed micellar assemblies in the solution whereby the kinetics and energetic of the studied PET reactions can be modulated very significantly for the possible control of the PET processes. In different drug delivery systems based on the block polymeric assemblies, various conventional surfactant molecules are often used as the co-surfactants to improve the performance of the delivery vehicles. The results obtained in the present study demonstrating large modulations in the PET processes in the tetronic-IL mixed micellar systems would certainly invite many such studies as these are directly relevant to the drug stabilization, drug formalism and drug delivery systems.

Our studies on ultrafast bimolecular PET reactions in pure pluronic micelle (P123) and in the surfactant-pluronic mixed micelle (SDS-P123) using femtosecond fluorescence up-conversion measurements unambiguously establish the non-diffusive nature of the bimolecular PET reactions carried out in the constrained micellar assemblies. This is clearly indicated because all the three time constants, as are estimated from the tri-exponential analysis of the observed ultrafast fluorescence kinetic traces, and whose values range from sub-picosecond to sub-nanosecond time domains, display very clear Marcus inversion (MI) behavior independently, which would not have been possible if diffusion of the reactants was influencing the observed PET reactions, especially at the

sub-nanosecond time domains. In the present cases also, substantial modulations in the kinetics and energetic are achieved simply by changing the [SDS]/[P123] molar ratio which allows a suitable control over these PET processes for their better utilizations.

Our studies on bimolecular PET reactions in the coumarin-Ln(III) systems fascinatingly indicated the unique behavior of the Ln(III) ions as the electron acceptors, that can support multichannel PET processes, as these ions are having number of low lying electronic states,¹⁹⁶ which can become accessible easily by the available free energy change in the form of exergonicity ($-\Delta G^\theta$) of the concerned PET reactions. Unique participation of the Ln(III) ions as the multichannel electron acceptors is a very intriguing finding from our present study, which is hardly reported in the literature except for just one earlier report from our laboratory.¹⁹⁷ Considering that the participation of the multichannel mechanism for the forward PET process is an extremely unusual phenomenon, the results obtained in the present study using coumarin-Ln(III) systems would expectedly draw the attention of the researchers working in the area of the PET reactions to investigate many more of such PET systems to get a better insight of this interesting aspect of multichannel reactions for the forward PET processes. Further, the noteworthy modulations observed in the kinetics and energetics of the bimolecular PET reactions in the coumarin-Ln(III) systems with the changing Ln(III) ions as the acceptors will certainly find many uses because Ln(III) ions as the electron acceptors are directly involved in optoelectronics,²⁰⁵⁻²⁰⁷ bio-sensing,^{199-202,220,221} bio-imaging,^{200-202,220,221} biotechnology,¹⁹⁹⁻²⁰² and many others.²²²⁻²²⁸

Overall the PET studies carried out in the present thesis are not only very interesting in regard to the scientific results obtained and the inferences drawn from these studies, the intriguing findings made in the present thesis are also expected to draw the interests of many researchers to explore a lot more insights of such systems, considering the academic and applied relevance of the studies taken up in the present thesis. While future studies on the micellar and mixed micellar systems involving tetronic and pluronic block copolymer systems can enrich our understanding for the utilization of such systems in the areas like photovoltaics, solar energy conversions, drug stabilizations, drug formulation, drug delivery systems, and so on, the extensive studies involving Ln(III) ions as electron acceptors are warranted to understand the details of the multichannel forward PET processes, which might help in the uses of these ions in different luminescent applications.

SYNOPSIS

This thesis reports Photoinduced Electron Transfer (PET) processes in homogeneous and microheterogeneous media involving organic and inorganic donor-acceptor systems. The objective of this thesis is to understand the energetics and kinetics of PET reactions, especially in regard to the modulations of the outcome of the PET processes in the desired manner through the changes in the microenvironments of the reaction media, to explore the intriguing details of the PET processes for their better utilizations in the areas like solar energy conversion, photovoltaics and photocatalysis [1-5]. The detailed photophysical investigations on the PET process between 7-aminocoumarin dyes as the acceptors and aromatic amines as the donors in different micellar microenvironment, especially those of newly introduced Tetronic star block copolymers has been carried out with regards to modulation of the ET parameters by tailoring the microenvironments of concerned microheterogeneous media. In this regards, photophysical characterization of the micellar microenvironments of the newly introduced star block Tetronics copolymers have been carried out in detailed and the results were utilized for the better correlation of the ET results pertaining to the present micellar media. We have also investigated ultrafast PET process between 7-aminocoumarin dyes and aromatic amine donors in Pluronic-surfactant mixed micellar media to establish the non-diffusive nature of the PET reactions in micellar microenvironments for the whole time windows covering subpicosecond to subnanosecond ranges. Subsequently we investigated the PET reactions involving trivalent Lanthanides ions, Ln(III), as electron acceptors and 4-methyl-7-aminocoumarin derivatives as electron donors in aqueous media, exploring the intriguing modulations in ET rates by the differential involvements of the multichannel ET for different Ln(III) ions used.

This thesis is organized into seven different chapters to present and discuss different aspects of the thesis work. The first chapter provides the general introductory aspects related to the Marcus ET theory along with a brief description of block copolymeric systems and the objectives of the present work. The second chapter describes the various experimental techniques along with the sources of various chemical systems employed in the present study. Chapters 3 to 6 systematically present the results and discussion on the different PET systems investigated in the present work in different reaction media and under different reaction conditions. Finally, Chapter 7 summarizes the thesis work along with the future prospective of the observed results. Short descriptions on the contents of different chapters included in the present thesis are given below for their better appreciations.

Chapter 1: General Introduction

This introductory chapter describes the important aspects of ET reactions, giving a brief account of the development of the outer-sphere ET theory, describing first in its classical formulation as proposed initially by Prof. R. A. Marcus [6-8]. This is subsequently followed by the discussions on quantum chemical modifications of the Marcus ET theory and also on the concepts of two-

dimensional ET model, as developed through the contributions of many researchers including Prof. Marcus himself, for the progressive refinements of the ET theory [9,10]. A brief account of the solvent relaxation process has also been discussed in this chapter, as ET reactions are strongly coupled with the dynamics associated with the solvent relaxation. Since a significant part of the present study deals with the PET reactions in micellar microheterogeneous media, this chapter also describes the general aspects of the micellar and mixed-micellar aggregates, as are used in the present study. The motivation and objective of the present research work is also discussed in this chapter to provide a background of the research problem taken up in the present PhD thesis.

Chapter 2: *Instruments and Methods*

This chapter provides the brief account of different experimental techniques used in the present study. In the present work, different studies were carried out using photochemical techniques like UV-vis absorption, steady-state fluorescence, time-correlated single photon counting (TCSPC) based time-resolved emission, up-conversion based time-resolved fluorescence, and laser flash photolysis based transient absorption, to understand the details of the PET processes for the studied donor-acceptor systems in the suitably modulated micellar microenvironments or in the homogeneous solution using different Ln(III) ions as the unique electron acceptors. Number of these photochemical techniques has also been used in exploring the static and dynamic characteristics of different microheterogeneous systems used in the present study as the unique reaction media to modulate the energetic and kinetics of the PET reactions. Brief account of all these photophysical techniques have been discussed in this chapter providing the necessary details of the concerned instruments and the working principles.

Chapter 3: *Tuning Photoinduced Electron Transfer Reactions in Tetronic Star Block Copolymer Micelles*

The micellar assemblies formed by various block copolymers have wide range of applications in pharmaceutical industries, cosmetics, targeted drug delivery mechanisms, catalysis, micro-reactor systems, and many others [11-17]. In the present chapter we have discussed the characterization of the micellar microenvironments of two structurally related star block copolymers, Tetronic 1304 (T1304) and Tetronic 1307 (T1307), as investigated using various photophysical measurements. Interesting to note that both T1304 and T1307 copolymers have the same (PO)_m block length but their (EO)_n block sizes are largely different [18,19]. In the present study, using a fluorescent probe, namely, coumarin-153 (C153), as a local reporter for the micellar microenvironments, we have estimated the micropolarity, microviscosity and solvation dynamics in the corona region of these Tetronic micelles, following the changes in the absorption, steady-state emission and time-resolved fluorescence characteristics of the dye. It is revealed that the T1307 micelle is more polar, less viscous and more hydrated in nature as compared to the T1304 micelle. Subsequent to the

characterisation of the micellar microenvironments, we then investigated the effectiveness of the T1304 and T1307 micelles in modulating the kinetics and energetics of bimolecular photoinduced electron transfer (PET) reactions carried out using a series of 7-aminocoumarin dyes as the electron acceptors and aromatic amines like *N,N*-dimethylaniline (DMAN) and *N,N*-dimethyl-*p*-toluidine (DMPT) as the electron donors. Interestingly, Marcus Inversion (MI) behavior is clearly observed in both T1304 and T1307 micellar media on correlating the quenching constant ($k_{q(TR)}$) values with the concerned exergonicity ($-\Delta G^0$) of the ET reactions. Moreover, in both the micelles, the onset of the MI appears at a much lower exergonicity than one can anticipate from the consideration of the conventional Marcus ET theory. Such a shift in the onset of MI towards lower exergonicity suggested the involvement of 2D-ET mechanism in the present PET systems in studied micellar media. Interestingly, it is found that the $k_{q(TR)}$ values are higher and the onset of MI appears at a relatively higher exergonicity for the T1307 micelle as compared to those in T1304 micelle, which correlate nicely with higher micropolarity of the former micelle as compared to the latter micelle.

Chapter 4: Ionic Liquids as Co-Surfactants for Tetronic Micelles in Modulating Photoinduced Electron Transfer Process

As realized in Chapter 3, characteristics of the micellar microenvironments are extremely important in tuning the PET reactions. In this regard, the endeavor of our present study was to understand the influence of ionic liquids (IL) as the co-surfactants for the T1304 tetronic copolymer micelle in tuning the bimolecular PET reactions in the so formed mixed micellar assemblies. As the molten salts, ILs display many unique properties like low vapor pressure, non-flammability, high ionic mobility and excellent chemical stability, and accordingly various ILs have been explored extensively for their utilizations as the popular “green solvents” [20,21]. Being biologically friendly in general, ILs can be considered as the preferred co-surfactants than the conventional co-surfactants like SDS, TX100, CTAC, etc. used in modifying the microenvironments of different copolymer micelles through the formation of the mixed micellar systems, which can have wide applications in different areas [22-25]. In the present study, we have investigated the PET reactions between a series of 7-aminocoumarin dyes as electron acceptors and DMAN as electron donor using T1304 micelle and T1304+IL mixed micelles as the constrained reaction media involving 1-alkyl-3-methylimidazolium tetrafluoroborate ($[C_nMIm][BF_4]$) type of IL series as the co-surfactants for T1304 star block copolymer micelle. Along with the PET studies, we have also carried out elaborate characterization of the micropolarity, microviscosity, and solvent relaxation dynamics in these micellar systems, to correlate the energetics and kinetics of the PET processes adequately, especially in reference to the Marcus ET theory and Marcus Inversion (MI) behavior. The $[C_nMIm][BF_4]$ series of ILs used in this study have varying 1-alkyl chains with n values equal to 4, 6 and 10, and we abbreviate them as $[BMIm][BF_4]$, $[HMIm][BF_4]$, and $[DMIm][BF_4]$, respectively, where B, H, and D signify the 1-butyl, 1-hexyl and 1-decyl chains, respectively. Results indicate that the ILs with

longer alkyl chain influence the micellar microenvironments more effectively, causing an increased hydration for the mixed micelle and accordingly an increased micropolarity, reduced microviscosity and faster solvent relaxation dynamics in the micellar corona region. Correlations of the $k_{q(TR)}$ values with the reaction exergonicities ($-\Delta G^0$) in different micellar media display clear Marcus Inversion (MI) behaviors, and interestingly the onset of the MI in all the cases is seen to arise at much lower exergonicity than otherwise expected following conventional Marcus 1DET theory, suggesting the PET reaction in the present systems to follow the unique 2DET mechanism. In T1304+IL mixed micelles, it is further noticed that the $k_{q(TR)}$ value gradually increases and the onset of MI systematically shifts towards higher exergonicity as the alkyl chain length for the co-surfactant IL is increased systematically. These results are ascribed to the effect of the gradually increasing hydration and enhanced micropolarity of the corona region of the studied mixed micellar systems with the increasing alkyl chain lengths of the ILs used.

Chapter 5: Ultrafast Photoinduced Electron Transfer in Pluronic-Surfactant Supramolecular Assemblies

In the earlier chapters it is seen that the constrained micellar media can provide a unique opportunity to modulate their microenvironments (polarity, viscosity, solvation dynamics, etc.) by some easy means, which can in effect change the dynamics and energetics of chemical reactions, especially the PET reactions, carried out in these media. Micellar assemblies of triblock pluronic copolymers are important constrained media where microenvironments can be modulated very effectively just by adding a suitable co-surfactant [24-27]. Since the ET reaction in constrained media mainly involves the closely placed donor-acceptor pairs that pre-exist at the moment of photoexcitation [28-31], it was felt encouraging to reinvestigate the PET reactions in such a mixed micellar system following ultrafast fluorescence up-conversion measurements having subpicosecond time resolution, which can provide a direct insight of the ultrafast kinetics and their correlations with the concerned exergonicities, especially with regard to the MI behavior [6-8]. In the present study, we have investigated bimolecular PET reactions involving a series of 7-aminocoumarin dyes as the acceptors and *N,N*-dimethylaniline (DMAN) as the donor in different SDS-P123 mixed micelles with varying *n*-values, where $n = [\text{SDS}]/[\text{P123}]$. The objective of the present study was to understand how the changing *n*-values for the SDS-P123 mixed micellar systems (*SDS to P123 molar ratio*) can affect the kinetics and energetics of the studied PET reactions, especially in regard to the observation of the MI behavior and the applicability of the 2DET model of the theory for the studied systems. It is seen that in all the studied SDS-P123 mixed micelles, the quenching rate constants (k_q) obtained from sub-nanosecond time-resolved (TR) fluorescence studies, as well as the individual decay rate constants (τ_i^{-1}) estimated from the tri-exponential analysis of the ultrafast fluorescence kinetic traces recorded through femtosecond fluorescence up-conversion measurements display the unique Marcus Inversion (MI) behavior. Observation of such MI behavior throughout the time scales of the

observations (from sub-nanoseconds to sub-picoseconds) inevitably suggests that the non-diffusive PET reaction condition is always prevailed in the studied micellar assemblies. Further, the onsets of the MI in all the cases are found to appear at appreciably lower exergonicity ($-\Delta G^0$) than expected from the estimated solvent reorganization energy (λ_s), suggesting the suitability of the 2DET model to rationalize the observed results in the present cases. It is revealed that, with the increasing n value for the SDS-P123 mixed micelles there is a sequential increase in the micropolarity for the corona region of the micellar system, which in turn modulate the kinetics and energetic of the studied PET reactions in these media in the desired manner.

Chapter 6: *Lanthanide (III) ions as Multichannel Acceptors for Photoinduced Electron Transfer Reactions*

Till the last chapter we have discussed the bimolecular PET reactions in constrained reaction media where both electron acceptors and donors used were organic molecules. In the present study, we have used inorganic lanthanides in their trivalent states, Ln(III), as the electron acceptors in combination with organic donors, to understand their bimolecular PET reactions in homogeneous medium, namely in aqueous solution. The reason for the selection of Ln(III) ions as the electron acceptor is the consideration of the intense research interests on trivalent lanthanide ions (Ln(III)) in the electron transfer (ET) reactions owing to their direct involvement in many areas like geo-mitigation, optoelectronics, luminescence sciences, bio-sensing, bio-imaging, biotechnology, and many others [32-41]. In the present study, we have investigated the bimolecular PET reactions employing four different 4-methyl-7-aminocoumarin dyes as the electron donors and three different Ln(III) ions as the electron acceptors in aqueous medium and the detailed investigations have been carried out following steady-state (SS) and time-resolved (TR; sub-nanosecond to nanosecond) fluorescence quenching studies and laser flash photolysis (LFP) based transient absorption studies. Due to favorable free energy changes (negative ΔG^0 values) for the PET reactions, among all the coumarin-Ln(III) pairs, only coumarin-Eu(III), coumarin-Yb(III) and coumarin-Sm(III) systems were realized to have favorable exergonicity ($-\Delta G^0$) for the PET reactions. For these systems, it is found that the plot of the estimated k_q values against the exergonicity ($-\Delta G^0$) of the PET reactions do not display a generalized single correlation, as otherwise observed for most other donor-acceptor systems reported in the literature [42-45]. It is interestingly seen that even if the exergonicity values for the presently studied donor-acceptor systems follow the order, coumarin-Eu(III) > coumarin-Yb(III) > coumarin-Sm(III), the concerned k_q values surprisingly follow the unexpected reverse trend of coumarin-Eu(III) > coumarin-Sm(III) > coumarin-Yb(III). Following diffusion mediated bimolecular reaction scheme, the correlations of the k_q values with the ΔG^0 values of the PET reactions was attempted which show unreasonably high reorganization energy (λ) for the coumarin-Yb(III) pairs, even though the λ value seems to be quite lower for the coumarin-Sm(III)/coumarin-Eu(III) systems. The anomaly observed in the orders for the ΔG^0 and k_q values along with the

unusually high λ value for the coumarin-Yb(III) systems imply the differential involvements of the multichannel PET reactions for the current donor-acceptor systems, whereby different Ln(III) ions involve different numbers of their low lying electronic energy states to support the PET process, accessible through the available exergonicity for the concerned PET reactions. Thus, the Eu(III) and Sm(III) ions being able to involve multiples of their low energy electronic states, the efficiency of the PET reactions for the coumarin-Eu(III) and coumarin-Sm(III) systems are quite facile to give higher k_q values. For Yb(III) ion, only the lowest electronic state being energetically permissible for the PET reaction, the coumarin-Yb(III) pairs display remarkably lower k_q values, much lower than the k_q values estimated for the coumarin-Sm(III) pairs, in spite of the more favorable ΔG^θ values for the coumarin-Yb(III) systems than the coumarin-Sm(III) systems.

Chapter 7: Summary of the Present Research Work and Future Prospects

This is the concluding chapter of the thesis and provides the overall summary of the observed results, their interpretations and inferences. This chapter also presents a brief description on the perspectives of the present research work in regards to the possible future research and the utilization of the observed results in various academic and applied areas.

References

1. G. R. Fleming, J. L. Martin and J. Breton, *Nature*, **1988**, 333, 190.
2. M. R. Wasielewski, *Chem. Rev.*, **1992**, 92, 435.
3. J. Barber, *Chem. Soc. Rev.*, **2009**, 38, 185.
4. M. Gratzel, *J. Photochem. Photobiol. C*, **2003**, 4, 145.
5. D. Gust, T. A. Moore and A. L. Moore, *Acc. Chem. Res.*, **2009**, 42, 1890.
6. R. A. Marcus, *J. Chem. Phys.*, **1956**, 24, 966–978.
7. R. A. Marcus, *J. Chem. Phys.*, **1956**, 24, 979.
8. R. A. Marcus, *J. Electroanal. Chem.*, **2000**, 483, 2.
9. H. Sumi and R. A. Marcus, *J. Chem. Phys.*, **1986**, 84, 4894.
10. W. Nadler and R. A. Marcus, *J. Chem. Phys.*, **1987**, 86, 3906.
11. H. Feng, X. Lu, W. Wang, N.-G. Kang and J. W. Mays, *Polymers*, **2017**, 9, 494(1).
12. Y. Mai and A. Eisenberg, *Chem. Soc. Rev.*, **2012**, 41, 5969.
13. A. Rösler, G. W. Vandermeulen and H. A. Klok, *Adv. Drug Deliv. Rev.*, **2012**, 64, 270.
14. R. K. O'Reilly, C. J. Hawker and K. L. Wooley, *Chem. Soc. Rev.*, **2006**, 35, 1068.
15. P. Alexandridis, *Curr. Opin. Colloid Interface Sci.*, **1996**, 1, 490.
16. A. Rösler, G. W. Vandermeulen and H.-A. Klok, *Adv. Drug Deliv. Rev.*, **2012**, 64, 270.
17. H.-C. Kim and S.-M. H. Park, W.D., *Chem. Rev.*, **2009**, 110, 146.
18. P. Alexandridis, D. Zhou and A. Khan, *Langmuir* **1996**, 12, 2690.
19. P. Alexandridis and T. A. Hatton, *Col. Surf. A: Physicochem. Eng. Aspects*, **1995**, 96, 1.

20. Y. U. Paulechka, D. H. Zaitsau, G. J. Kabo and A. A. Strechan, *Thermochim. Acta*, **2005**, 439, 158.
21. L. P. N. Rebelo, J. N. C. Lopes, J. M. S. S. Esperanca and E. Filipe, *J. Phys. Chem. B*, **2005**, 109, 6040.
22. M. Kumbhakar, S. Dey, P. K. Singh, S. Nath, A. K. Satpati, R. Ganguly, V. K. Aswal and H. Pal, *J. Phys. Chem. B*, **2011**, 115, 1638.
23. P. Verma and H. Pal, *Phys. Chem. Chem. Phys.*, **2015**, 17, 23214.
24. R. Ganguly, V.K. Aswal, P.A. Hassan, I. K. Gopalakrishnan, S. K. Kulshreshtha, *J. Phys. Chem. B* **2006**, 110, 9843–9849.
25. J. Jansson, K. Schillen, M. Nilsson, O. Soderman, G. Fritz, A. Bergmann and O. Glatter, *J. Phys. Chem. B*, **2005**, 109, 7073–7083.
26. P. K. Singh, M. Kumbhakar, H. Pal, S. Nath, *J. Phys. Chem. B* **2008**, 112, 7771–7777.
27. T. Thurn, S. Couderc, J. Sidhu, D. M. Bloor, J. Penfold, J. F. Holzwarth, E. Wyn-Jones, *Langmuir* **2002**, 18, 9267–9275.
28. M. Kumbhakar, H. Pal, *Sci. Lett. J.* **2015**, 4, 1–17.
29. H. Pal, *J. Indian Chem. Soc.* **2017**, 94, 1311–1334.
30. A. K. Satpati, M. Kumbhakar, S. Nath, H. Pal, *J. Phys. Chem. B* **2007**, 111, 7550–7560.
31. A. Chakraborty, D. Seth, P. Setua, N. Sarkar, *J. Chem. Phys.* **2008**, 128, No. 204510.
32. M. C. Chuan, G.Y. Shu, J.C. Liu, *Water, Air, Soil Pollut.* **1996**, 91 543–556.
33. J. F. McCarthy, W. E. Sanford, P. L. Stafford, *Sci. Technol.* **1998**, 32, 3901–3906.
34. D. A. Atwood, (Ed.), *Radionuclides in the Environment*, John Wiley & Sons, **2010**.
35. M. R. Kesama, S. R. Dugasani, S. Yoo, P. Chopade, B. Gnapareddy, S. H. Park, *ACS Appl. Mater. Interfaces*, **2016**, 8, 14109–14117.
36. X. Chen, T. Sun, F. Wang, *Chem. Asian J.*, **2019**, 15, 21–33.
37. J.-C. G. Bnzli, C. Piguet, *Chem. Soc. Rev.*, **2005**, 43, 1048–1077.
38. W. D. Horrocks Jr, *Coord. Chem. Rev.*, **1999**, 185–186, 307–319.
39. M. V. DaCosta, S. Doughan, Y. Han, U. J. Krull, *Anal. Chim. Acta*, **2014**, 832 1–33.
40. N. Sabbatini, S. Perathoner, G. Lattanzi, S. Dellonte, V. Balzani, *Inorg. Chem.*, **1988**, 27 1628–1633.
41. D. Sykes, A. J. Cankut, N. M. Ali, A. Stephenson, S. J. P. Spall, S. C. Parker, J. A. Weinstein, M. D. Ward, *Dalton Trans.*, **2014**, 43, 6414–6428.
42. C. Turr, J. M. Zaleski, Y. M. Karabatsos, D. G. Nocera, *J. Am. Chem. Soc.*, **1996**, 118, 6060–6067.
43. I. R. Gould, S. Farid, *Acc. Chem. Res.*, **1996**, 29, 522–528.
44. A. K. Satpati, S. Nath, M. Kumbhakar, D. K. Maity, S. Senthilkumar, H. Pal, *J. Mol. Struct.*, **2008**, 878, 84–94.
45. D. Rehm, A. Weller, *Israel J. Chem.* **1970**, 8, 259–271.

CHAPTER-1

GENERAL INTRODUCTION

1.1. Introduction

Electron transfer (ET) is the most fundamental redox reaction that is omnipresent in both chemistry and biology. It has been a long term goal to understand the intricate details of electron-transfer reactions using simplified model systems. A significant part of such studies involve photoinduced charge separation reactions associated directly with the conversion of solar energy into chemical or electrical energy.¹⁻⁵ In ET reactions, an electron is transferred from a donor (D) unit to an acceptor (A) unit, either in an intramolecular or in an intermolecular fashion. For many biological processes, ET is the most fundamental step required to initiate a sequence of chemical and biochemical reactions that effectively produce the overall changes essential for the bio-systems.⁶⁻⁹ Among the many factors that have to be satisfied for ET reactions to be feasible, the most important requirement is that the reacting donor and acceptor units should first come close to each other within the reaction zone to support the reaction.

Although apparently an ET reaction might seem to be a very simple chemical process where an electron is transferred from one chemical species (donor, D) to another (acceptor, A), in reality, an ET process is controlled by many parameters in such a complex manner that a clear understanding of the kinetics, dynamics, and energetic of the ET reactions is extremely difficult. Prof. R. A. Marcus worked extensively on the kinetics and dynamics of ET processes and theoretically correlated these aspects with the energetic of the ET reactions, namely with the free energy change (ΔG^0) and the reorganization energy (λ). Prof. Marcus proposed his revolutionary outer sphere ET theory in 1956, predicting an inversion of the ET rate with the increasing exergonicity ($-\Delta G^0$) of the ET reaction.¹⁰⁻¹² Following his theoretical prediction, there have been extensive studies to explicitly understand various factors that are responsible in the progress of ET reactions, and the subject has remained as an attractive research area in chemical physics for last about 6 decades. Considering the direct relevance of the ET reactions in various chemical and biological processes, and taking into account the outstanding theoretical work carried out by Prof. Marcus, he was conferred with the prestigious Noble prize in the year 1992.

To comprehend the efficiency and dynamics of ET processes, one needs to understand the following important aspects; (i) electronic coupling between the interacting ET partners, i.e. the D-A pairs at the encounter separations, (ii) energetics associated with the transition state, a condition where an electronic resonance between D and A moieties of the interacting pairs is feasible, and (iii) the dynamics of the D-A pairs to cross over the activation barrier. These aspects are of utmost importance to understand the correlation between the energetics and kinetics of the ET reactions both under homogeneous and heterogeneous reaction conditions. The objective of the present thesis is to investigate the kinetics and energetics of bimolecular photoinduced electron transfer (PET) processes in constrained microheterogeneous media as well as in homogeneous aqueous solution. It

is intended to understand various factors that modulate the kinetics and energetic of ET reactions involving different donor-acceptor pairs and various confined micellar systems used in the present work. This introductory chapter of the thesis describes the important aspects of the ET reactions, giving a brief account of the development of the outer-sphere ET theory, describing first the one-dimensional classical formulation of the theory as proposed initially by Prof. Marcus, which will be followed by the discussions on the quantum chemical modifications of the Marcus ET theory and also the concepts of the two-dimensional ET theory, as developed over the years by many renowned researchers including Prof. Marcus himself. A brief account of the aspects of solvent relaxation process is also discussed in this chapter, as the ET reactions in condensed phase are strongly coupled with the dynamics associated with the solvation process. Since a significant part of the present study deals with the PET reactions in micellar media, this chapter also describes the general aspects of the micellar and mixed micellar aggregates that are used in the present study. The motivation and objective of the present research work are also discussed at the end of this chapter to provide a background of the research problem taken up in this PhD thesis.

1.2. Electron Transfer Reaction: Theoretical Background

1.2.1. One Dimensional Classical Marcus Outer-sphere Electron Transfer Theory

Prof. R. A. Marcus from CalTech, California, initiated his in-depth research on electron transfer processes mainly around 1955, when he got attracted by an interesting article by W. F. Libby, reporting quite unusual ET rates for the isotopic exchange reactions in the redox systems comprising of inorganic ions of different sizes.¹³ Libby and co-workers observed that some smaller ions had unexpectedly slower ET rates while some other larger ions provided surprisingly faster rates. The authors rationalized these unusual observations by providing a unique theoretical model whereby the well-known Franck-Condon principle for electronic transition was introduced as a governing factor for the progress of the studied redox reactions and the energy required for the reorganization of the solvent molecules around the reactanting systems was considered to be associated with the energy barrier encountered with the concerned redox reaction.¹³ Encouraged by these intriguing results and explanations, Prof. Marcus started working extensively on the ET processes, describing the progress of these reactions in terms of the solvent polarizations around the interacting donor-acceptor (D-A) pairs and eventually developed the classical version of his “Outer-sphere ET Theory” in the year 1956.^{10,11} According to this classical one-dimensional ET theory, the rate constant for the ET reaction (k_{et}) is expressed uniquely in terms of the standard free energy change (ΔG^0) and the associated reorganization energy (λ) for the concerned ET reaction.^{10-12,14-19} In this theoretical model, it was considered that ET takes place only at the transition state (TS) following the Franck-Condon principle such that the nuclei of the reactant and product states do not undergo any displacement during the ET process and the overall energy of the system remains conserved during

the transfer of the electron from D to A.^{10-12,14-28} To be mentioned that the conservation of energy was a drawback of the theory proposed earlier by W. F. Libby and co-workers,¹³ and this drawback was removed justifiably in the ET Theory developed by Prof. R. A. Marcus.

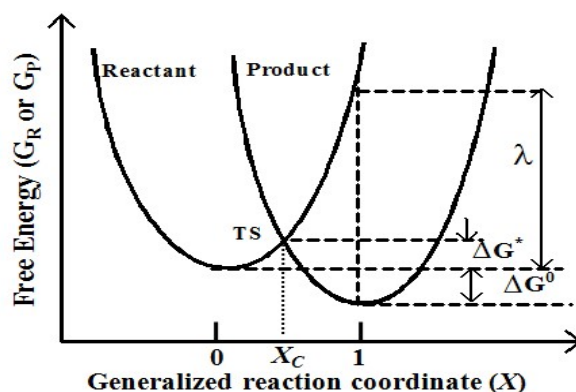


Figure 1.1. Schematic presentation of the free energies of reactant and product states in accordance with classical Marcus' outer-sphere ET theory. Here ΔG^0 is the free energy change, ΔG^* is the free energy of activation and λ is the total reorganization energy for the ET reaction. Free energies for both reactant and product states are quadratic functions of the generalized reaction coordinate (X) and are symmetric to each other. While TS represents the transition state, X_C represents its corresponding reaction coordinate.

The classical version of the outer-sphere ET theory was developed by Prof. R. A. Marcus with the basic consideration that the free energy of the reactant (R, comprising of D-A) and product (P, comprising of D^+-A^-) states, say G_R and G_P , respectively, are the quadratic functions of a generalized reaction coordinate, X . Thus, describing the progress of the ET reaction in terms of the solvent polarizations around the interacting D-A or D^+-A^- pairs, Prof. Marcus arrived at the conclusion that this solvent polarization around the R and P states at any stage can suitably be considered as the coordinate X for the ET reaction. Accordingly, the G_R and G_P functions for the reactant and product states, respectively, and the crossing of these two free energy surfaces at the TS for the ET reaction can be represented graphically as in Figure 1.1, where ΔG^0 and λ are the same as defined before, and ΔG^* is the associated free energy of activation for the ET reaction. The important point to be mentioned in regard to Figure 1.1 is that both R and P states and consequently their free energies are directly influenced by the solvent polarizations around these states and accordingly the D-A and D^+-A^- pairs in association with their surrounding solvent cages are considered as a whole the supramolecular R and P states of the concerned ET process.^{10-12,14-30}

For the ET to take place, it is essential that the R state first reaches the TS where the ET would occur from the donor moiety to the acceptor moiety maintaining the conservation of energy. In this sense, alike many other chemical reactions, ET is also the case of a free energy surface crossing process, as schematically represented in Figure 1.1. Evidently, the reaching of the R state to the TS is achieved through the thermal fluctuations in the nuclear and solvent coordinates for the R state, which is an ensemble of the interacting D-A pair along with its surrounding solvent cage. Due

to these thermal fluctuations, all the R states in the concerned systems will maintain a thermal equilibrium in regard to the distributions for all possible nuclear and solvent configurations, causing a small fraction of these R states to reach the TS, though the majority of R states will be in their minimum energy configuration. Truly, the same consideration is also equally valid for the P states of the system, which are the ensembles of the D^+-A^- pairs along with their surrounding solvent cages maintain a thermal equilibrium in the solution. Only the fraction of the R states that reach the TS geometry can actually participate in the transfer of an electron from the D to the A unit, and it happens following the Franck-Condon principle and maintaining the energy conservation of the concerned ET system. Once the electron is transferred, the so produced P states dissipate their excess energy through the thermal fluctuations of their nuclear and solvent coordinates, and thereby relax to the thermal equilibrium for the P state configurations. Accordingly, following this classical Marcus' outer-sphere ET theory, the distributions of both R and P states would always maintain a quasi-equilibrium condition along the reaction coordinate X during the progress of the ET reaction.^{10-12,14-30} This assumption otherwise suggests that the rate of relaxation for the nuclear and solvent configurations for the R and P states to attain their respective thermal equilibrium are much faster than the rate of ET process that takes place at the TS. Another important assumption in the classical Marcus' outer-sphere ET theory is that at the transition state geometry, as the activation barrier height is reached, the ET system simply moves forward along the reaction coordinate X , converting the R states to the P states with unit probability. Hence, the reactive trajectories cross the barrier top on the free energy surface only once during the progress of the ET reaction.³¹⁻³³

According to the classical Marcus' ET theory, the ET rate constant (k_{et}) for the interacting D-A pairs, which are also considered as the D-A encounter complexes as the D and A units are within the reaction zones, should be expressed as the product of three factors, i.e. (i) the nuclear frequency ν_n , the frequency with which R states can oscillate at the TS, (ii) the probability parameter κ_{el} with which R states can cross the TS to produce the P states, and (iii) the nuclear reorganization factor κ_N , that measures the thermodynamic probability for the R states to have an excess energy to reach the TS. Thus, for an ET system, the k_{et} can be expressed as,

$$k_{et} = \nu_n \kappa_{el} \kappa_N \quad (1.1)$$

In this equation, the frequency parameter ν_n is usually very high, in the order of about 10^{13} s^{-1} . In the classical Marcus' ET theory, the probability factor κ_{el} was arbitrarily considered to be unity, i.e. it was assumed that the reactants that reach the TS once, are eventually converted to the product states.¹⁶ The nuclear reorganization factor κ_N is effectively related to the free energy of activation for the ET reaction, ΔG^* , and would be given by the following exponential relation as,

$$\kappa_N = \exp\left(-\frac{\Delta G^*}{k_B T}\right) \quad (1.2)$$

where k_B is the Boltzmann's constant and T is the absolute temperature of the reaction medium.

As mentioned before, according to classical version of the Marcus' outer-sphere ET theory, the free energy surfaces, G_R and G_P , of the reactant and product states, are the quadratic functions of a generalized reaction coordinate, X . In this respect, it was further considered that the parabolic nature of both G_R and G_P functions are symmetric to each other, which in other words suggests that the vibrational modes associated with the free energy surfaces for both reactant and product states have just similar force constants (similar curvatures). Therefore, for the ET reactions, representing the concerned reaction coordinate in the normalized form such that the minimum free energy configuration for the R states appears at $X = 0$ and that of the P states appears at $X = 1$, the G_R and G_P functions for the R and P states can be expressed respectively as,^{9-12,14-16,26-30,34-55.}

$$G_R = \lambda X^2 \quad (1.3)$$

$$G_P = \lambda(1 - X)^2 + \Delta G^0 \quad (1.4)$$

where ΔG^0 is the standard free energy change (difference between the free energy minima of P and R states) for the ET system and λ is the total reorganization energy for the ET reaction. The G_R and G_P functions as represented by the above relations are graphically presented as in Figure 1.1. Following above relations, if X_c is considered as the value of the X coordinate that corresponds to the crossing of the G_R and G_P curves at the TS (cf. Figure 1.1), we can write,

$$\lambda X_c^2 = \lambda(1 - X_c)^2 + \Delta G^0 \quad (1.5)$$

Solving eq. 1.5, we can arrive at the expression for X_c as,

$$X_c = \frac{\lambda + \Delta G^0}{2\lambda} \quad (1.6)$$

Accordingly, following eq. 1.3, the free energy of activation ΔG^* for ET reaction can be obtained as,

$$\Delta G^* = \lambda X_c^2 = \lambda \left(\frac{\lambda + \Delta G^0}{2\lambda} \right)^2 \quad (1.7)$$

Eq. 1.7 relates the free energy of activation ΔG^* in terms of the standard free energy change ΔG^0 and the total reorganization energy λ of the ET reaction, which is often expressed in its more simplified form as eq. 1.8.^{10-12,14-19}

$$\Delta G^* = \frac{(\Delta G^0 + \lambda)^2}{4\lambda} \quad (1.8)$$

In ET reactions, the physical significance of the total reorganization energy λ is that it provides a measure of the energy associated with the nuclear and solvent rearrangements required for the equilibrium reactant state to reach the equilibrium configuration of the product state, but without having the electron being transferred, as clearly indicated in Figure 1.1. In true sense, λ is the measure of the effective force constant (k) associated with the G_R and G_P surfaces such that $\lambda = k/2$. The total reorganization energy λ has two contributions into it, one is the intramolecular reorganization energy, λ_i , arising due to the reorganizations of the intramolecular vibrational modes of the D-A system, and the other is the solvent reorganization energy, λ_s , arising due to the

reorganizations of the intermolecular vibrational modes of the surrounding solvent systems. Accordingly, the total reorganization energy λ is expressed as,

$$\lambda = \lambda_i + \lambda_s \quad (1.9)$$

As one can understand, the term λ_i would measure the reorganization energy involved as the normal coordinates for the intramolecular vibrational modes of the D-A system change from their equilibrium positions in reactant states to those of the product states, and would be given as,^{19,20,26}

$$\lambda_i = \frac{1}{2} \sum_j f_j (\Delta q_j) \quad (1.10)$$

where f_j is the force constant for the j^{th} vibrational mode and Δq_j is the change in the normal coordinate for this vibrational mode for going from the reactant state to the product state. The parameters associated with λ_i are in general very difficult to be estimated, though suitable vibrational spectroscopy or X-ray studies can sometimes help in estimating these complicated parameters.

Physically the parameter λ_s gives the measure of the reorganization energy contribution arising from the rearrangements of the polar solvent molecules around the reacting D-A system and consequently the changes in the solvent polarizations around the R state. A reasonable estimate for λ_s can be obtained by considering the reacting species (donors and acceptors) as the effective spheres, and treating the surrounding solvent as the polar dielectric continuum. Accordingly, Prof. R. A. Marcus derived an expression for λ_s in a polar solvent as,^{10-12,14-30}

$$\lambda_s = \frac{e^2}{2} \left(\frac{1}{r_A} + \frac{1}{r_D} - \frac{1}{r} \right) \left(\frac{1}{n^2} - \frac{1}{\epsilon} \right) \quad (1.11)$$

where r_D , r_A , r , n , and ϵ are the radius of the donor, radius of the acceptor, the separation between the donor and acceptor centers, the optical dielectric constant of the solvent and the static dielectric constant of the solvent, respectively. Since all the parameters associated with λ_s can be obtained independently, an estimate of the λ_s value for a concerned ET reaction in a polar solvent can be obtained easily with quite a reasonable accuracy.^{10-12,29,56,57}

The most important prediction from Marcus' outer sphere ET theory is the parabolic dependence of k_{et} on the free energy change (ΔG^0) of the ET reaction. Figure 1.2 shows the graphical presentation of the ΔG^0 dependence of k_{et} along with the qualitative presentation of the changing ΔG^* values as a function of the changing ΔG^0 . As indicated from Figure 1.2, the ΔG^0 dependence of k_{et} is clearly divided into three regions. Thus, in the “*The Normal Marcus Region*”, represented by the condition $-\Delta G^0 < \lambda$, the ΔG^* value gradually decreases and consequently k_{et} value increases in an asymptotic manner on increasing the exergonicity ($-\Delta G^0$) of the reaction. Similarly, in “*The Inverted Marcus Region*”, represented by the condition $-\Delta G^0 > \lambda_s$, the ΔG^* value interestingly suffers a reverse trend, undergoing an increase with the increasing $-\Delta G^0$, and thus causing the k_{et} value to display an intriguing decrease with the increasing reaction exergonicity. Evidently, there is a “*Marcus Barrierless Condition*”, represented by the situation $-\Delta G^0 = \lambda$, when the ΔG^* just

vanishes (eq. 1.8), causing the k_{et} to reach its maximum value. Therefore, if we plot k_{et} for the whole region of the $-\Delta G^0$ values, the Marcus' outer-sphere ET theory suggest the appearance of a bell-shaped curve, commonly referred as the “*Marcus Inversion (MI) Behavior*”, as qualitatively shown in Figure 1.2. Although this MI behavior was predicted theoretically way back in 1956, it effectively took more than 25 years of extensive research work to demonstrate this unique behavior experimentally for the first time in the year 1984, from the classic work of Closs and Miller involving charge shift reactions in the pulse radiolytically produced radical species in the wisely designed donor-spacer-acceptor kind of intramolecular ET systems.⁵⁷⁻⁵⁹

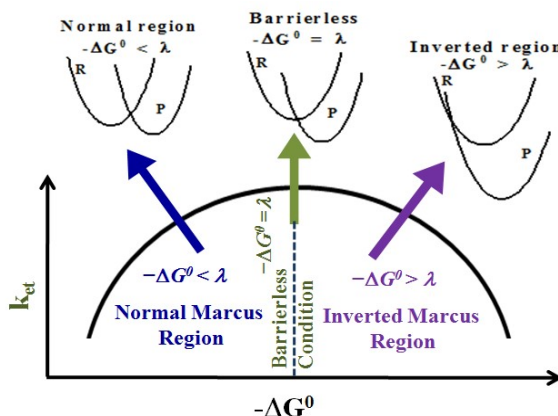


Figure 1.2. Pictorial representation of the “*Inversion Behavior*” as predicted from Marcus' outer sphere ET theory on correlating the ET rate constants (k_{et}) with the changing exergonicity ($-\Delta G^0$) of the ET reactions.

1.2.2. Quantum Mechanical Refinement of the Marcus ET Theory: Adiabatic and Non-adiabatic ET Reactions

In the classical Marcus ET theory, it was assumed that there is strong electronic coupling between the reactant (R) and product (P) states such that the probability factor κ_{el} for the transformation of the R state to the P state at the TS is unity (cf. eq. 1). In real ET systems, however, considering κ_{el} as unity seems to be extremely unrealistic. In real ET systems, κ_{el} can have any value between zero to unity, and this must be determined by the extent of electronic coupling between the R and P states near the crossing point of their adiabatic energy surfaces. To incorporate this aspect of electronic coupling between R and P states into the probability factor κ_{el} , it was essential to introduce a quantum mechanical refinement of the classical Marcus ET theory. Such a treatment is in fact very important when electronic coupling between R and P states is quite weak such that the probability parameter κ_{el} is very low ($\kappa_{el} \ll 1$), and in these cases κ_{el} can be calculated using the Fermi's golden rule formalism.^{14,50,60,61} Conceptually, quantum mechanical refinement of ET theory emanates from the basic rate equation only, as given by eq. 1.1 for the classical Marcus ET theory.^{10-12,14-30,43-50,62-87} Using this basis relation and considering the transmission probability κ_{el} based on the magnitude of the electronic-coupling matrix element, V_{el} , between the R and P states, the generalized equation for the ET rate constant, k_{et} , based on quantum chemical refinement is expressed as,^{45-47,73}

$$k_{et} = \frac{1}{1 + \kappa_{ad}} \left\{ \frac{2\pi}{\hbar} V_{el}^2 (4\pi\lambda k_B T)^{-1/2} \exp\left(\frac{-\Delta G^*}{k_B T}\right) \right\} \quad (1.12)$$

where κ_{ad} is termed as the adiabaticity parameter. In a polar solvent, the parameter κ_{ad} can be expressed approximately as,^{45-47,73}

$$\kappa_{ad} = \frac{4\pi V_{el}^2}{\hbar\lambda} \tau_s \quad (1.13)$$

where τ_s is the time constant for the relaxation dynamics of the solvent medium.

Following eq. 1.12, under the situation of very small V_{el} such that $\kappa_{ad} \ll 1$, the ET is considered to be nonadiabatic in nature, and in this situation the k_{et} can be expressed as,^{14,28}

$$k_{et,NA} = \frac{2\pi}{\hbar} V_{el}^2 (4\pi\lambda k_B T)^{-1/2} \exp\left(\frac{-\Delta G^*}{k_B T}\right) \quad (1.14)$$

To be noted from eq. 1.14 that for the nonadiabatic ET reactions for which V_{el} is very small (typically, $2V_{el} \ll \lambda$, or $V_{el} \leq k_B T$, where $k_B T$ represents the thermal energy, i.e. $\sim 200 \text{ cm}^{-1}$), the ET rate becomes proportional to the parameter V_{el}^2 . It is also to be noted from equation 1.14 that the rate for a nonadiabatic ET reaction is determined solely by the static relaxation parameter of the reacting system, i.e. the total reorganization energy λ , of which the solvent reorganization energy λ_s makes a major contribution in a polar solvent system, but the relaxation dynamics of the reacting system, e.g. the solvent relaxation time τ_s , does not affect the rate of a nonadiabatic ET reaction.

The other extreme of the nonadiabatic ET condition is the situation where V_{el} is very large, typically, $2V_{el} \geq \lambda$, or $V_{el} \gg k_B T$; i.e. V_{el} is few tens of times higher than the thermal energy. Under this situation, the adiabaticity parameter κ_{ad} becomes much higher than unity ($\kappa_{ad} \gg 1$; cf. eq. 1.13) and the ET is considered to occur under adiabatic condition for which the k_{et} is simplified as,^{26,45,47}

$$k_{et,AD} = \frac{1}{\tau_s} \sqrt{\frac{\lambda}{16\pi k_B T}} \exp\left(\frac{-\Delta G^*}{k_B T}\right) \quad (1.15)$$

At room temperature, since the value of “ $16\pi k_B T$ ” is about 1.3 eV, and because in a polar dielectric solvent the solvent reorganization energy λ_s is in the range of about 1 eV, it is expected that for ET reaction in a polar medium the total reorganization energy λ ($=\lambda_s + \lambda_i$) would be very close to the “ $16\pi k_B T$ ” value. Thus, from eq. 1.15, it is expected that for adiabatic ET reactions the maximum ET rate constant (at the barrierless condition) would approximately be in the order of $1/\tau_s$.

As understood from the discussions above, the parameter V_{el} plays a very significant role in determining the kinetics and dynamics of the ET reactions. The physical significance of the electronic-coupling matrix element V_{el} can be understood from the graphical presentation in Figure 1.3. It arises due to the mixing of the reactant (R) and product (P) states at the crossing point (TS) of their free energy surfaces, and it happens as an outcome of the quantum mechanical principle of “*avoided crossing*” of two potential energy surfaces, a principle which says that the two eigenvalues of a quantum chemical observable (free energies of R and P states, here) cannot become equal to

each other, unless some special circumstances are prevailed, which we avoid to discuss here. As indicated from Figure 1.3, following the avoided crossing principle, there is a splitting in the free energy surfaces of the R and P states at the crossing point (TS) and the magnitude of this energy splitting is twice the concerned electronic-coupling matrix element, i.e. $\Delta E_{split} = 2V_{el}$.

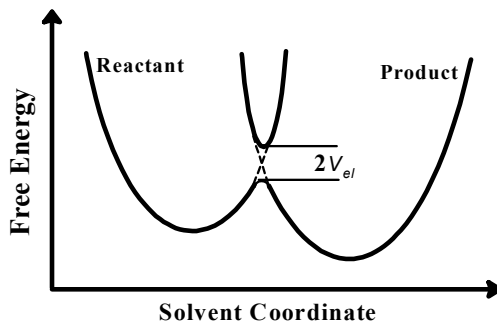


Figure 1.3. Conceptual presentation of avoided crossing for the free energy surfaces of R and P states and the concerned electronic coupling matrix element (V_{el}) for the donor-acceptor pairs participating in ET reaction.

1.2.3. Effect of High Frequency Vibrational Modes on ET Rates

In the discussion so far, the effects of the low frequency ($h\nu \ll k_B T$) vibrational modes of the reactant (R) and product (P) states, i.e. the low frequency intramolecular vibrations in D and A units (contributing towards λ_i) and the low frequency intermolecular vibrations for the solvent shells around R and P states (contributing towards λ_s and τ_s), have been considered mainly to understand the kinetics and dynamics of the ET reactions. The effects of the high frequency ($h\nu \gg k_B T$) vibrational modes of the reactant and product states, mainly those of the D and A units participating in the ET reactions, had not been considered yet to keep the discussion simple. To be mentioned that the high frequency vibrational modes of the R and P states do not usually participate in the ET reactions, especially under normal circumstances where reaction exergonicity ($-\Delta G^0$) is not extremely high. There are however situations, especially when $-\Delta G^0$ is very high, when the upper vibrational levels of the high frequency vibrational modes of R and P states can be accessed with the available free energy from the concerned reaction. Accordingly, these ET systems can involve the high frequency vibrational modes of the R and/or P states, modulating the kinetics and dynamics of the ET reactions quite substantially. This can be understood easily from the consideration that while the low-frequency vibrational modes ($h\nu \ll k_B T$) can be excited easily by the thermal energy ($k_B T$) available in the reaction bath and thus their reorganizations can be treated simply by using the classical concepts (as applied to estimate λ_i and λ_s values), the high frequency modes ($h\nu \gg k_B T$) cannot be excited by the available thermal energy and thus their contributions are necessary to be incorporated using quantum mechanical treatment.

Conceptually, the high frequency vibrational modes of the ET systems provide multiple channels for ET reactions, where each of these ET channel is effectively driven by the support of the

low-frequency vibrational modes that are accessible by thermal energy available in the reaction bath. In these cases thus, the overall rate of the ET reaction becomes the sum of the ET rates arising from each of these high frequency vibrational channels. For an ET system, it is generally assumed that only one high frequency vibrational mode is actively associated with the reaction. Further, it is expected that under normal reaction conditions the upper vibrational levels of the high frequency mode of the R state can hardly be excited, though such upper levels of the high frequency mode of the P state can be excited easily if the available reaction exergonicity is sufficiently large ($-\Delta G^0 > h\nu$). Therefore, considering that the ET process involves different upper vibrational levels (n) of the active high frequency mode of the P state, and assuming that the ET reactions along all these channels occur through nonadiabatic mechanism, the overall rate constant for the ET reaction can be expressed as^{12,14,20-30,45-50,73-87}

$$k_{NA} = \sum_n k_{NA,n} \quad (1.16)$$

where $k_{NA,n}$ is the rate constant involving the ground vibrational level ($n = 0$) of the reactant state and the n^{th} vibrational level of the product state and the sum in eq. 1.16 is over all the vibrational levels of the high frequency vibrational mode accessible by the available exergonicity of the ET reaction ($-\Delta G^0 \geq n h\nu$). The situation discussed here is pictorially presented in Figure 1.4.

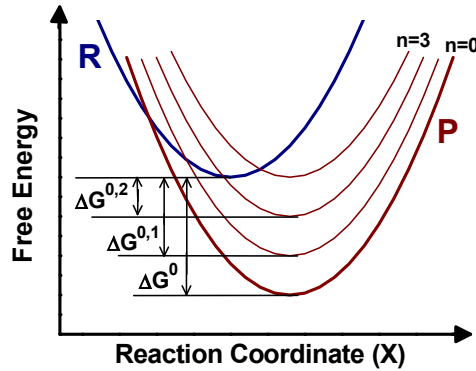


Figure 1.4. Schematic presentation for the participation of the high-frequency vibrational modes of the product state on the ET reaction, involved mostly at the higher exergonicity region.

For the present situations, the effective free energy gap $\Delta G^{0,n}$ for each of the reaction channels involving $n = 0$ vibrational level of the R state and n^{th} vibrational level of the P state should be considered as,

$$\Delta G^{0,n} = \Delta G^0 + n h\nu \quad (1.17)$$

Similarly, for the ET reaction involving $n = 0$ vibrational level of the R state and n^{th} vibrational level of the P state, the electronic coupling matrix element V_{el} is also needed to be weighted accordingly based on the Franck-Condon factor (vibronic overlap matrix element), $\langle 0|n \rangle$, such that,

$$V_{el,n}^2 = V_{el,0}^2 |\langle 0|n \rangle|^2 \quad (1.18)$$

where $V_{el,0}^2$ is the electronic coupling matrix element involving $n = 0$ vibrational levels of the high frequency mode for both reactant and product states. The square of the Franck-Condon factor in eq. 1.18 can further be expanded in terms of the electron-vibrational coupling strength (S) as,

$$|\langle 0|n \rangle|^2 = (S^n / n!) \exp(-S) \quad (1.19)$$

where S is given as $S = \lambda_h / h \nu_h$, λ_h being the reorganization energy and ν_h is the frequency of the concerned high frequency vibrational mode. Following the discussion above, the effective ET rate constant involving zero vibrational level of the reactant state and n^{th} vibrational level of the product state would be expressed as,

$$k_{NA,n} = \frac{2\pi}{\hbar} (V_{el,n})^2 (4\pi\lambda_s k_B T)^{-1/2} \exp\left(\frac{-(\Delta G^{0,n} + \lambda_s)^2}{4\lambda_s k_B T}\right) \quad (1.20)$$

It is important to mention here that the contributions of the high frequency vibrational modes to the ET reaction mostly arise in the “Marcus Inverted Region” (cf. Figure 1.2), as this effect becomes gradually more efficient with higher reaction exergonicity. The experimental demonstration of this effect is the observation in some experimental findings that the bell-shaped curves obtained from the k_{et} vs ΔG^0 correlations for various ET systems show an asymmetric Marcus inversion behavior, where the curvature of the plot is always less stiffer in the “Inverted Region” than in the “Normal Region”, as schematically shown in Figure 1.5.^{9,29,30,42} To be recalled here that in the absence of the participation of the high frequency mode, the conventional Marcus expression for the ET rate constant would be expressed by eq. 1.14, and based on this relation the k_{et} vs ΔG^0 correlation should lead to a symmetric bell-shaped curve, as schematically shown before in Figure 1.2. It is evident from the discussion here that the contribution of the high frequency vibrational mode becomes significant mainly in the inverted region of the ET reaction while its contribution in the normal Marcus region is essentially very insignificant.

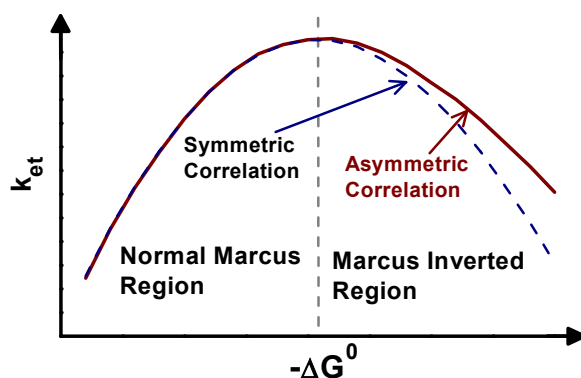


Figure 1.5. Schematic presentations of the symmetric and asymmetric correlations in the k_{et} versus $-\Delta G^0$ plots as expected in the absence and presence of the contributions of high frequency vibrational modes in the ET reactions, respectively.

1.2.4. ET Rate versus Solvent Relaxation Dynamics: Sumi-Marcus Two-dimensional ET (2DET) Theory

In the classical theories of the reaction rates, e.g. in the transition state theory, it is assumed that the population distribution of the reactant states (R) always maintains a thermal equilibrium in the system such that fraction of the reactants in the TS always remains unperturbed during the progress of the reaction. For most of reactions, this assumption seems to be quite adequate to be adopted. There are some limited cases of the reacting systems, however, where this assumption does not hold good. In conventional low viscosity homogeneous solvents, owing to the extremely fast solvent relaxation process, the R states for the photoinduced ET (PET) reactions always maintain a thermal equilibrium along the solvent relaxation coordinate, which is the effective reaction coordinate (X) for the concerned process (cf. Figure 1.1). Therefore, for these PET reactions, the conventional model of one dimensional ET (1DET) is quite applicable, and under this situation the rate constant k_{et} for the reaction can be described well using either eq. 1.14 or eq. 1.15, considering the ET process to be either nonadiabatic or adiabatic in nature. For ET reactions in micro-heterogeneous media, however, as the solvent relaxation dynamics is unexpectedly slow, it is expected that in these reaction media the population distribution of the R states cannot maintain a thermal equilibrium along the solvent relaxation coordinate X , during the ET reaction, as otherwise assumed in 1DET model. Thus, in micro-heterogeneous media, the non-equilibrium population of the R states along X , which is produced at the point of its photoexcitation (because of different dipolar character for excited state than ground state), maintains this non-equilibrium distribution during the PET reaction than attaining a thermal equilibrium quickly, as it happens in the 1DET mechanism. Accordingly, in the present cases, the solvent relaxation coordinate X cannot represent the reaction coordinate for the PET process as the systems involve thermally non-equilibrated R states along X . In these cases, however, it is logical to assume that unlike the slow relaxing solvation along X , the relaxation along the intramolecular coordinate q of the ET systems, which is represented by the low frequency vibrational modes of the reacting systems, is unusually fast such that along q the population distribution of the R states always maintains a thermal equilibrium during the progress of the ET process. Accordingly, following photoexcitation, even if the R states remain in the non-equilibrium distribution along X for very long time, there is a quick thermal equilibration for R states along q , and this equilibration is maintained all along the progress of the ET reaction.^{18,88-98} Therefore, in these cases, the q coordinate effectively act as the reaction coordinate for the ET reaction instead of the solvent coordinate X that is supposed to be the effective reaction coordinate in conventional situations. The description of the ET reaction that involves the q coordinate as the effective reaction coordinate while the R states remain in the non-equilibrium distribution along X coordinate is commonly known as the two-dimensional ET (2DET) model. The theoretical description of this 2DET model has been proposed and elegantly analyzed by Sumi, Nadler and Marcus.^{18,99}

Figure 1.6 shows the conceptual picture of the 2DET model assuming that reorganizations along q and X coordinates are completely decoupled, where the transition state is represented by the curve “CC”. Physically, the coordinate q is represented by the changes in the bond lengths and bond angles for the reactants that accompanies with the progress of the ET reaction. As discussed earlier, the changes in the solvent polarization around the reactants are physically the representative of the coordinate X . In the 2DET model, when a reactant state R is prepared following photoexcitation, this R state is invariably formed with a non-equilibrium configuration along X coordinate, i.e. with $X \neq 0$, and because solvent relaxation along X is very slow, the R state maintains this non-equilibrium situation all along the ET reaction. Following photoexcitation, even though the R state is also formed initially with a $q \neq 0$, but immediately after excitation the system attends a thermal equilibrium along q , as the relaxation along q is very fast. According to the 2DET model, thus, the ET reaction is compelled to proceed along the fast relaxing q coordinate, with an excess energy remaining in the system due to $X \neq 0$ configuration of the R state during the ET reaction. Therefore, in the 2DET model, one can visualize the ET reactions to occur along q , for different X coordinates, as arise due to non-equilibrium distributions of R along the X coordinate.

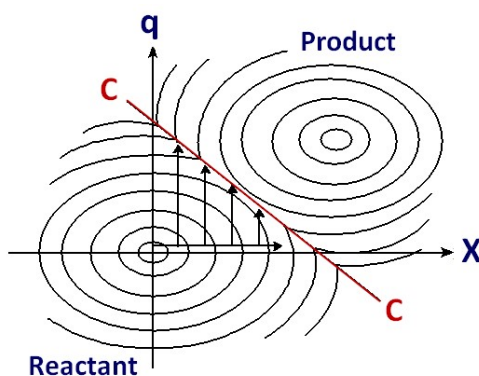


Figure 1.6. Conceptual presentation of the free energy contours for the reactant and product states, spanned by the solvent coordinate X and nuclear coordinate q (2DET model). Curve CC indicates the transition state.

For the presentation of the 2DET model in Figure 1.6, the contours for the free-energy surface of the R states are shown on one side and those of the P states are shown on the other side of the transition state curve, CC. In this figure, for simplicity, both X and q coordinates are considered in their normalized forms, which means that the (X, q) coordinates for the R and P states for their minimum energy configurations would be $(0, 0)$ and $(1, 1)$, respectively.¹⁸ A more informative presentation of the 2DET model for a PET reaction can be shown conceptually in Figure 1.7. In this presentation also, X represents the normalized solvent reorganization coordinate and q represents the normalized intramolecular reorganization coordinate. As indicated in this figure, as the first step, the photoexcitation produces the initial R state with $X = -X_g$ (cf. the free energy curves at the right half), which continues to oscillate along X (cf. double sided curved arrows), keeping the excess energy intact in the system, which is equal to $\lambda|X_g|^2$. This happens because solvent relaxation is very slow

and hence the system cannot dissipate its excess energy via solvent relaxation to attain the equilibrated R state along X , with $X = 0$ configuration, before the onset of ET reaction. Accordingly, following 2DET mechanism, the non-equilibrated R state (with $X = |X_g|$) proceeds for the ET reaction along the intramolecular reaction coordinate q and this particular situation is represented by the upper blue curve in the left half of Figure 1.7, while the solvent-equilibrated R state for this system as would have been expected for fast solvent relaxation can be represented by lower blue curve in the left half of Figure 1.7.

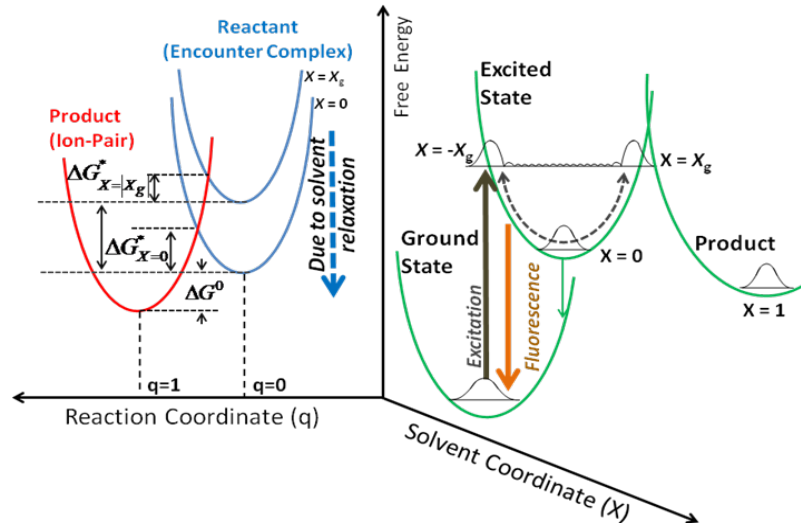


Figure 1.7. Schematic presentation of the 2D-ET process using equilibrium and non-equilibrium free energy curves for the R state along solvent coordinate. Photoexcitation produces non-equilibrium R state with $X = -X_g$ and it continues to oscillate along X axis (*cf.* Free energy curves at the right half). The non-equilibrated R state undergoes ET reaction along intramolecular q coordinate (q) along with its excess energy, as represented by upper blue curve in the left half of the figure. The expected solvent equilibrated R state in a fast relaxation solvent system would have been represented by lower blue curve shown in the left half of the figure.

In 2DET model, since q and X coordinates are considered to be decoupled from each other, the free energies of the R and P states (G_R and G_P , respectively) are explicitly expressed in terms of these two coordinate systems. Considering both q and X coordinates in their normalized forms, the G_R and G_P for the concerned systems can be expressed as,^{18,88-97}

$$G_R(X, q) = \lambda_s X^2 + \lambda_i q^2 \quad (1.21)$$

$$G_R(X, q) = \lambda_s (X - 1)^2 + \lambda_i (q - 1)^2 + \Delta G^0 \quad (1.22)$$

where λ_i and λ_s are the intramolecular and solvent reorganization energy, respectively. As we have already discussed, in the 2DET model the ET reaction effectively occurs independently along the fast relaxing q coordinate for all possible non-equilibrium distributions of R state along X coordinate. Hence, for such a system, the effective ET rate constant ($k_{et,eff}$) will be the sum of all the X -dependent rate constants weighted by the non-equilibrium distribution $\{\rho(X)\}$ of the R state along

X, i.e. $k_{et,eff} = \sum k_{et}(X)\rho(X)$. For any given X coordinate, considering the ET reaction to be non-adiabatic in nature, the rate constant $k_{NA}(X)$ can be expressed as,

$$k_{NA}(X) = \frac{2\pi}{\hbar} V_{el}^2 (4\pi\lambda_s k_B T)^{-1/2} \exp\left(\frac{-\Delta G^*(X)}{k_B T}\right) \quad (1.23)$$

where $\Delta G^*(X)$ is the X dependent free energy of activation for the ET reactions, that occur through the intramolecular q coordinate, as schematically shown in Figure 1.7.

Using expressions 1.21 and 1.22 and assuming that high frequency vibrational modes are not participating in the reaction, the expression for the effective free energy of activation for any nonzero X configuration, say at $X = X_g$, would be given as,

$$\Delta G^*(X_g) = \frac{(\Delta G^0 + \lambda_i + (1 - 2|X_g|\lambda_s)\lambda_s)^2}{4\lambda_i} \quad (1.24)$$

As indicated from eq. 1.24, following the 2DET model, since the R state cannot attain and maintain a thermal equilibrium along X during the ET reaction occurring along q (cf. Figures 1.6 and 1.7; eq. 1.24), the effective free energy of activation $\Delta G^*(X_g)$ can incorporate only a fraction of λ_s in its manifestation than full λ_s , which can thus be considered as the effective solvent reorganization energy, $\lambda_{s,eff}$, under the given non-equilibrium solvent configuration, and would be expressed as,

$$\lambda_{s,eff} = \lambda_s - 2\lambda_s |X_g| \quad (1.25)$$

It is evident from eq. 1.25 that the $\lambda_{s,eff}$ for a 2DET reaction would be much lower than total λ_s for a typical 1DET reaction (cf. eq. 1.8 and 1.9). Following eq. 1.25, for 2DET reactions, the onset of Marcus Inversion (MI) is thus supposed to start at an exergonicity of $-\Delta G^0 = (\lambda_i + \lambda_{s,eff})$,^{18,88-98} while for conventional 1DET reactions, the onset of MI is expected to appear at $-\Delta G^0 = (\lambda_i + \lambda_s)$.^{9-12,14-16,26-30,34-55,100-115} Hence, it is evident that for the similar D-A systems, the onset of MI for the PET reactions following 2DET model, as one would expect to occur in a constrained media, should appear at a relatively lower exergonicity as compared that of the PET reactions following 1DET model, as are supposed to occur in the fast relaxing homogeneous solvent systems.^{38,112,116-129} Therefore, it is quite understandable that the constrained micro-heterogeneous media, where 2DET mechanism is expected to be applicable for the PET reactions, will effectively provide a more conducive reaction environment for the PET systems to realize the MI region quite easily than in the fast relaxing conventional homogeneous solvents, because inversion region would appear at much lower exergonicity region in the former situations than in the latter.^{38,112,116-129}

1.3. Photoinduced Processes

Photochemical science deals with the chemical and physiochemical processes that transpire through the involvement of electronically excited molecules, produced by the absorption of suitable radiation in the visible and near ultraviolet region of the electromagnetic spectrum. All these processes are in general termed as the photoinduced processes. Few important photoinduced processes are,

fluorescence and phosphorescence of the chromophoric molecules, nonradiative deexcitation of excited molecules, structural relaxation dynamics of flexible molecules in the excited state, solvent relaxation dynamics, photoinduced electron transfer reactions, excited state proton transfer processes, photodissociations, photoionizations, and so on. From extensive studies in different photoinduced processes it has been realized that the absorption of photon often makes some of the chemical and physiochemical reactions to take place very easily which are otherwise not feasible in dark. This is because the energy available from photoexcitation can meet the necessary energy for the initiation of such processes, which is otherwise not possible to be availed from thermal reaction bath in the case of the dark reactions. In other words, energy available from photoexcitation in general add favourably to the reacting systems to account for the overall energy changes that take place for the concerned chemical reaction. To understand the beneficial effects of photoexcitations toward the overall energy changes in the reacting systems, we can represent different situations of dark ET and PET reactions, as shown schematically in Figure 1.8. For case (a) in Figure 1.8, a kinetically slow, mildly exergonic dark ET reaction is presented, while the corresponding PET reaction, as initiated by the photoexcitation of any one of the reactants (D or A) in the system to overcome the associated activation barrier, leading the reaction to take place with orders of magnitude faster rate. For case (b) in Figure 1.8, the situation is such that the dark ET reaction cannot simply take place due to energetically up-hill condition for the product state, but the absorption of light by either D or A makes the corresponding PET reaction thermodynamically very feasible (negative ΔG^0 value) and thus would occur with a substantially fast rate.

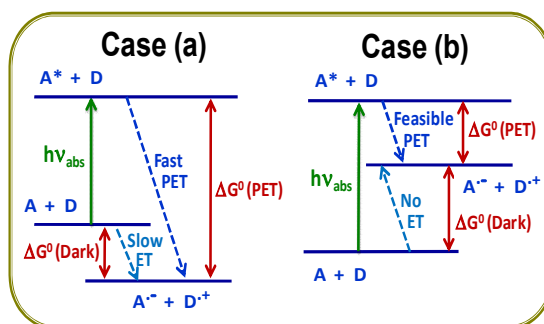


Figure 1.8: Schematics of the possible energetic situations for dark ET and PET reactions. While for case (a) the dark ET is mildly exergonic, for case (b) the dark ET is energetically not simply feasible. In both the cases, the PET is energetically much more favorable and would occur with orders of magnitude higher rates.

The absorption of electromagnetic radiation in the UV-vis region results in the transition of an electron from a lower to a higher electronic state, creating the excited state of the absorbing molecule. Such electronic transitions occur in the unusually fast time scales, typically in the range of $\sim 10^{-15}$ sec. The excited states thus produced following photoexcitation of suitable UV-vis light, can subsequently undergo various competitive relaxation processes, the important ones being the internal conversion (IC), intersystem crossing (ISC), radiative decay, nonradiative decay,

intramolecular reorganization, solvent reorganization, energy transfer processes, proton transfer reactions, electron transfer reactions, and so on. The schematic representations of the important intramolecular relaxation processes for the excited chromophoric molecules in the condensed phase are shown schematically in Figure 1.9 and such a conceptual presentation of the different relaxation processes of the excited molecules is commonly referred as the Jablonski diagram, named after the Polish physicist, Prof. Aleksander Jabłoński, who introduced such a presentation for the first time to describe the photoexcitation and subsequent relaxation of the electronically excited chromophoric molecules in a condensed phase.

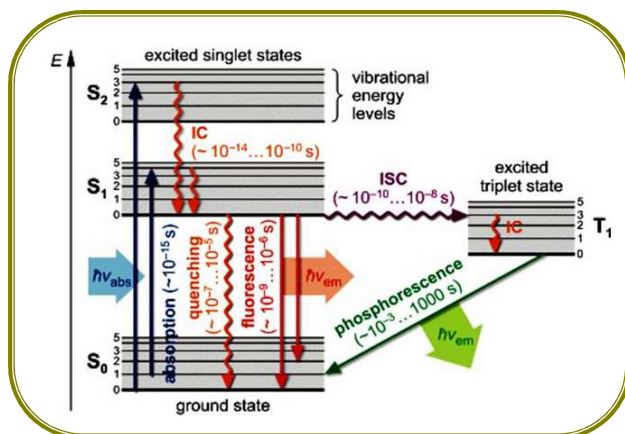


Figure 1.9. The Jablonski diagram, representing schematically the photoexcitation of a chromophoric system and its subsequent various important intramolecular relaxation processes. Abs - absorption; IC - internal conversion; ISC - intersystem crossing; Em - emission; S_i - i^{th} singlet state; and T_i - i^{th} triplet state.

Different relaxation processes as mentioned above for the electronically excited molecules can occur over quite a wide range of time scales, from femtoseconds to milliseconds. The typical time scales of different relaxation processes, as are also indicated in the Jablonski diagram in Figure 1.9, are basically determined by the rapidity with which the concerned nuclear or electronic rearrangements can take place to cross over the associated transition states. In photochemical science, there are many elementary processes that occur in unusually fast time scales and to understand the details of these fast and ultrafast processes it is necessary to monitor the concerned short lived excited states or transient species formed following the absorption of the excitation light. With the advent of various fast and ultrafast time-resolved spectroscopic techniques, it has now become quite easy to study the dynamics of various ultrafast elementary processes, even when the processes occur with the time constants in the sub-picosecond time scales.

1.4. Energetics of Photoinduced Electron Transfer Processes

As we have discussed before, the possibility of a photoinduced reaction is increased very significantly as compared to the related dark reaction, as the energy of photoexcitation favorably supports the free energy change of the concerned chemical reaction (cf. Figure 1.8). In this regard,

as we consider the photoinduced electron transfer (PET) reactions, it is important to note that the photoexcitation of either the donor (D) or the acceptor (A) can effectively increase the electron donating power of D and the electron accepting power of A, as compared to the donor and acceptor properties of the respective molecules in their ground states.²⁹ Accordingly, for many D-A pairs, where ET reactions are not feasible when both D and A molecules are in the ground states, they can undergo very efficient ET reactions when either D or A are promoted to their excited states following photoexcitation. Another important aspect with PET reaction is that the process can be instantaneously triggered by exciting the sample with a fast or ultrafast light pulse and accordingly the progress of the reaction can be followed easily in real time following the initiation of the process by photoexcitation, making it possible to explore the details of the kinetics and dynamics of the concerned reactions. Accordingly, extensive research has been devoted on PET reactions to understand the mechanistic and kinetic details of the processes under various reaction conditions.

The critical factors that determine the success of the PET reactions are the suitability of the donor (D) and acceptor (A) molecules in regard to their electrochemical and photochemical properties. These properties of the reactant molecules must not only comply with the exergonicity (ΔG^0) of the ET reaction, but should also have sufficiently long lifetimes in the excited states such that the quenching of their excited states can take place quite substantially due to the participation of the ET process. In the energetic terms, the feasibility of an ET reaction in a D-A pair is determined by the overall free energy change (ΔG^0) for the system, which would be dependent on the redox potentials of D and A molecules. Additionally, a work term for the stabilization of the ion-pair state (D^+A^-) produced through the ET reaction in the dielectric medium is also needed to be considered while estimating the ΔG^0 value. Further, for a PET reaction, the excitation energy provided to either D or A is also needed to be considered favorably in the ΔG^0 calculation. Considering all these, the ΔG^0 value for a PET reaction involving neutral D and A molecules can be given by the well known Rehm-Weller equation as,^{29,130}

$$\Delta G^0 = E(D^+/D) - E(A/A^-) - E_{00} - \frac{e^2}{\epsilon_s r} \quad (1.26)$$

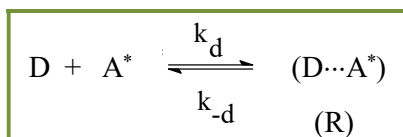
where $E(D^+/D)$ and $E(A/A^-)$ are the reduction potentials of D^+ and A, respectively, E_{00} is the 0-0 energy of the excited reactant (either D or A) involved in the PET reaction, and $e^2/\epsilon_s r$ is the coulomb interaction term representing the electrostatic stabilization energy for the ion-pair state formed in the ET process, where ϵ_s is the static dielectric constant of the medium and r is the centre to centre distance between the two ions (D^+ and A^-) in the ion-pair state.

1.5. Predicted Kinetics of PET Reactions under Diffusive Condition

Photoinduced electron transfer (PET) reactions are usually carried out in solution phase under a diffusive condition, whereby either an excited acceptor (A^*) is interacted with a ground state donor

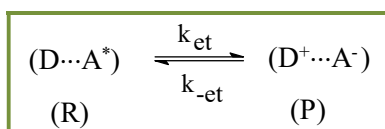
(D) or vice versa. Following photoexcitation thus, the progress of the PET reaction, say between A^* and D, in the solution under diffusive condition, can be visualized in terms of the following three sequences of the reaction steps.²⁹

1) In step 1, the reactants (D and A^*) undergo mutual diffusion to come within the interaction sphere and thus to form the encounter complex ($D\cdots A^*$), also called the precursor complex, which in all practical purposes is the reactant state (R), which we have discussed so far while dealing with Marcus ET theory. Under diffusive condition, both formation and dissociation of the encounter complex maintain equilibrium in the solution phase, which can suitably be represented as,



where, k_d is the rate constant for the diffusion mediated formation of the encounter complex and k_{-d} is the rate constant for the diffusion mediated dissociation of the encounter complex.

2) Once the encounter complex is formed, transfer of electron can take place within this assembly, producing the ion-pair state ($D^+\cdots A^-$), which is called either the successor complex or for all practical purposes, the product state (P), that we have indicated earlier in dealing with the Marcus ET theory. In real systems, since reverse ET can also take place logically to convert the product state into the reactant state, this reversible step of the PET process can be represented as,



where k_{et} and k_{-et} are the rate constants for the forward ET and reverse ET steps, respectively.

3) The ion-pair state produced through forward ET reaction (k_{et}) can disappear not only via reverse ET (k_{-et}) process but also involving some other prominent processes for its disappearance, which might include, (i) charge recombination reaction (CR; rate constant k_{CR}) to produce both D and A in their ground states, (ii) ion dissociation reaction (ID; rate constant k_{ID}) to produce the solvent separated D^+ and A^- ions, and (iii) a suitable radial reaction (RR; rate constant k_{RR}) leading to the formation of some stable products. Considering all these disappearance processes collectively as the product formation channel for the ion-pair state, and assuming all of them as the first order or pseudo-first order processes, we can represent the overall ion-pair disappearance processes as,



Following the above sequences of the processes and applying a steady-state condition for the studied system, i.e. assuming $d[A^*]/dt = 0$ and $d[D\cdots A^*]/dt = 0$, the concerned bimolecular

quenching constant k_q , which represents the effective rate constant for the bimolecular ET process under the diffusive condition, can be expressed as,²⁹

$$k_q = \frac{k_d}{1 + \left(\frac{k_{-d}}{k_{et}} \right) \left(1 + \frac{k_{-et}}{k_{et}} \right)} = \frac{k_d}{1 + \frac{k_d}{Kk_{et}} \left(1 + \frac{k_{-et}}{k_{et}} \right)} \quad (1.27)$$

where $K = (k_{diff}/k_{-diff})$, is the equilibrium constant for the diffusion mediated formation of the encounter complex (R). In most PET systems, the back ET (k_{-et}) is mostly an energy uphill process (positive ΔG^0 value), while the concerned CR is an energy downhill process (negative ΔG^0 value). Moreover, in conventional solvents of high polarity and low viscosity, the ion-dissociation process (k_{ID}) also becomes significantly prominent, causing the contact ion-pair state ($D^+ \cdots A^-$) to dissociate into solvent separated ions. Thus, even if the contribution of the radial reaction (k_{RR}) might not be contributing very significantly in the PET systems, still one can reasonably assume that $k_P > k_{-et}$ and accordingly the simplified form of k_q can be expressed as,²⁹

$$k_q = \frac{k_d}{1 + \frac{k_d}{Kk_{et}}} \quad (1.28)$$

Following diffusion mediated formation (k_{diff}) and dissociation (k_{-diff}) of the encounter complex (R), the equilibrium constant K can be expressed as,

$$K = \frac{4\pi N_A r_{DA}^2 \delta r}{1000} \exp\left(-\frac{w_c}{RT}\right) \quad (1.29)$$

where, N_A is Avogadro's number, r_{DA} is the contact distance between D and A^* , δr is the distance beyond r_{DA} over which ET is feasible (reaction zone) for the interacting ($D \cdots A^*$) pairs, and w_c is the work done to bring the D and A^* species at a distance r_{DA} from infinity. In PET reactions involving either or both D and A as neutral species, w_c can simply be considered as zero, because there is no electrostatic interaction involved. Further, for all practical purposes, the δr value for ET reactions can be considered as $\sim 2 \text{ \AA}$. Therefore, from eq. 1.29, the K value for neutral reactants can roughly be considered as $\sim 1 \text{ mol}^{-1} \text{ dm}^3$.^{10,29}

1.5.1. Correlations of the Quenching Constants with the Free Energy Changes for Bimolecular PET Reactions under Diffusive Condition

In bimolecular PET studies, the experimental condition is kept such that the reactant that would be excited, says acceptor (A), is in exceptionally low concentration, typically few μM , and the other reactant, which is donor (D) in this case and acts as the quencher for the excited A^* , is also in the reasonably lower, typically in the tens of mM concentrations, so that the overall reaction proceeds exclusively through the formation of the diffusion mediated encounter complexes, without the presence of any preexisting ($D \cdots A$) pairs in the ground state within the encounter distance ($r = r_{DA} + \delta r$). The quenching constant (k_q) values thus obtained from such studies are effectively the

measures of the rate constants for the observed bimolecular PET reactions under diffusive condition. For such PET reactions, correlation of the k_q values with the exergonicity ($-\Delta G^0$) of the reactions surprisingly do not follow the Marcus Inversion (MI) behavior as predicted from Marcus ET theory (Section 1.2 and Figure 1.2), but in general display a trend that k_q initially increases asymptotically with $-\Delta G^0$ at the lower exergonicity region and subsequently saturates to a diffusion-controlled limit as $k_q \approx k_d$, at the higher exergonicity region. Such correlation is commonly known as the Rehm-Weller behavior, after the names of the scientists who first reported such a unique behavior.¹³⁰ A qualitative presentation of the k_q vs ΔG^0 plot for bimolecular PET reactions displaying Rehm-Weller behavior under diffusive condition is shown in Figure 1.10. To understand the difference of such a behavior from the typical MI behavior, a conceptual inverted bell shaped curve predicted from Marcus ET theory is also shown in Figure 1.10 for a qualitative comparison of the two behaviors, while correlating the observed ET rates with the exergonicity of thereactions.

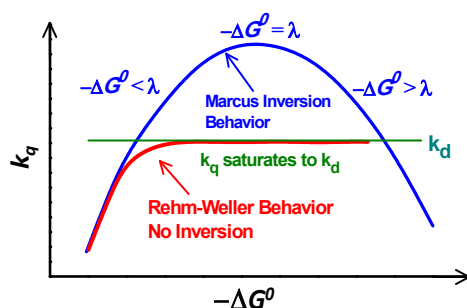


Figure 1.10. Qualitative presentation of the k_q vs ΔG^0 correlation for PET reactions under diffusive condition displaying the Rehm-Weller behavior is shown. Conceptual inverted bell shaped Marcus inversion behavior for the k_q vs ΔG^0 correlation expected from Marcus ET theory is also shown for a comparison.

That k_q vs $-\Delta G^0$ correlations for bimolecular PET reactions under diffusive condition follow the Rehm-Weller behavior in general than the MI behavior had been quite puzzling initially for quite long time, but was realized eventually to be accountable well within the framework of the Marcus ET theory. In the study of Rehm-Weller,¹³⁰ however, to account the saturation of k_q to the k_d value at the higher exergonicity region, the authors considered that k_{et} in eq. 1.28 involves a free energy of activation in its expression such that k_q is effectively expressed as,

$$k_q = \frac{k_d}{1 + \left(\frac{k_d}{K}\right) \frac{1}{\nu \exp(-\Delta G^* / RT)}} \quad (1.30)$$

where, ν is the usual pre-exponential factor associated with k_{et} as discussed before (cf. eq. 1.1) and ΔG^* is the free energy of activation, which was empirically expressed by Rehm and Weller as,

$$\Delta G^* = \left(\frac{\Delta G^0}{2}\right) + \left\{ \left(\frac{\Delta G^0}{2}\right)^2 + \left(\frac{\lambda}{4}\right)^2 \right\}^{1/2} \quad (1.31)$$

where, ΔG^0 and λ are the free energy change and the total reorganization energy for the ET reaction, respectively. To be noted that the Rehm-Weller expression for ΔG^* is markedly different than the quadratic relation proposed from Marcus ET theory (cf. eq. 1.8). As eq. 1.31 suggests, on increasing reaction exergonicity ($-\Delta G^0$), the ΔG^* value will decrease asymptotically, as qualitatively shown by Figure 1.11A. Due to such a change in ΔG^* , the k_q value initially increases in an asymptotic manner with the increasing reaction exergonicity and eventually saturates to k_d at the higher exergonicity region, displaying the typical Rehm-Weller behavior, as qualitatively shown in Figure 1.11B.

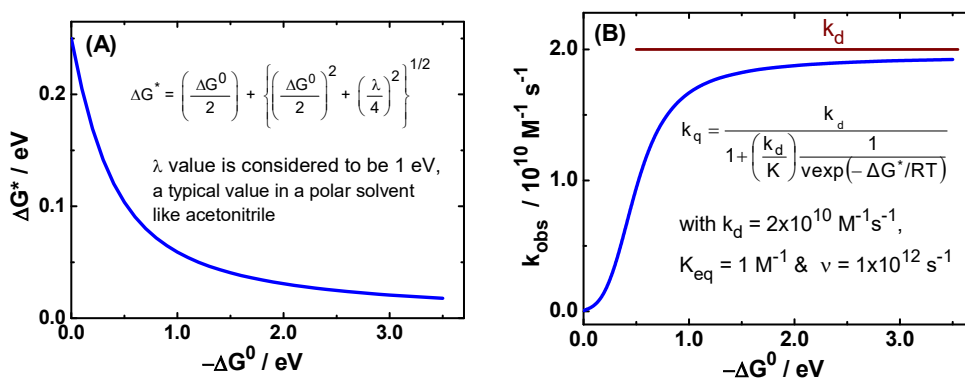


Figure 1.11: Conceptual presentations of (A) changes in the ΔG^* with reaction exergonicity ($-\Delta G^0$) and (B) the variations of k_{obs} values with reaction exergonicity as governed by Rehm-Weller relations (eqs. 1.37 and 1.38) for bimolecular ET reactions in polar solvent media.

As we have mentioned before, within the framework of Marcus ET theory, i.e. on considering ΔG^* as the quadratic function as given by eq. 1.8, the Rehm-Weller behavior shown by Figure 1.10, can also be obtained up to a certain exergonicity, as long as the intrinsic k_{et} in Step 2 discussed in Section 1.5 remains higher than k_d . On increasing the reaction exergonicity much higher, however, the situation will eventually be reached when intrinsic k_{et} will become lower again than the k_d value, due to the largely increased ΔG^* in these situations, as expected from Marcus ET theory (cf. eq. 1.8). Accordingly, in the exceedingly high exergonicity region, the k_q vs ΔG^0 plot would eventually display the MI behavior, which can qualitatively be represented as shown Figure 1.12. In the intermediate region of the reaction exergonicity, however, the MI behavior will always be masked by the diffusion controlled limit ($k_q \approx k_d$), displaying typically the Rehm-Weller kind of behavior. From the present discussion, we can infer that to obtain the true k_{et} vs. ΔG^0 plot that would display the MI behavior clearly for bimolecular ET reaction, we need to suppress the effect of the diffusion of the reactants on the observed reaction rates. To achieve this, Miller and coworkers designed their experiments by attaching various donor and acceptor groups by covalent bonds and thus could demonstrate the MI behavior very convincingly for the first time in 1984, following the intramolecular charge shift reactions in pulse radiolytically produced radical species in the thoughtfully constructed donor-spacer-acceptor (D-S-A) kind of bi-functional chemical systems that are suitable for intramolecular ET reactions.⁵⁷⁻⁵⁹

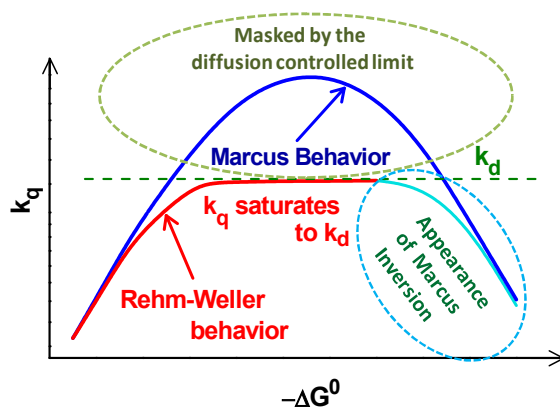


Figure 1.12. Qualitative presentation of the appearance of Marcus Inversion behavior for the bimolecular PET reaction under diffusive condition on making the reaction exergonicity ($-\Delta G^0$) exceedingly higher.

1.6. Solvation Dynamics

For chemical reactions in solution phase, the solvent molecules around the reacting species play very important role in influencing the dynamics of the reactions. Thus, it is very important to understand the solvent relaxation process to reveal the details of reaction dynamics in solution, especially those reactions that involve charge redistributions, e.g. electron transfer, charge transfer, proton transfer, etc. In most solvent relaxation studies, dynamic fluorescence Stokes' shift method has been realized as the most effective technique.¹³¹⁻¹⁴⁷ Since the dipole moment of the probe molecule changes instantaneously at the moment of photoexcitation, the solvent polarization around the excited probe starts responding to this dipole moment change, causing a time-dependent reorganization of the solvent molecules around the excited dye to achieve the equilibrium solvent polarization eventually for the new dipole. This solvent reorganization process thus causes a time-dependent energy relaxation for the whole system, which is reflected as the time-dependent shift in the fluorescence spectra of the probe (dynamic fluorescence Stokes' shift), as schematically shown in Figure 1.13, and carries the detailed information of the solvent relaxation dynamics for the studied system.^{45,46,51}

In the dynamic fluorescence Stokes' shift studies, a suitable probe dye in the concerned solvent is excited with an ultrafast light pulse and its fluorescence decays are sequentially measured at regular wavelength intervals, covering the whole steady-state (SS) emission spectrum of the dye.^{45,46,51} These fluorescence decays are uniformly fitted using a suitable function, normally as a tri-exponential function, to obtain the fitted decays $D(\lambda, t)$ for each of these wavelengths, which are then used to construct the time-resolved emission spectra (TRES), following the procedure given by Maroncelli and Fleming.^{45,46,51} Briefly, each of these fitted decays are first normalized relative to their respective integrated intensity to obtain the intensity normalized decays, $D_N(\lambda, t)$, as,

$$D_N(\lambda, t) = \frac{D(\lambda, t)}{\int_0^\infty D(\lambda, t) dt} \quad (1.32)$$

where $D(\lambda, t)$ is explicitly expressed as,

$$D(\lambda, t) = \sum_{i=1}^3 \{B_i(\lambda)\} \exp[-t / \{\tau_i(\lambda)\}] \quad (1.33)$$

Here, $\{B_i(\lambda)\}$ and $\{\tau_i(\lambda)\}$ are the pre-exponential factor and decay time, respectively, for the i^{th} component for the decay at wavelength λ . The obtained $D_N(\lambda, t)$ curves are subsequently used along with the SS emission intensities at each of the measuring wavelengths, $I_{SS}(\lambda)$, to calculate the time-dependent changes in the fluorescence intensity, $I(\lambda, t)$, at each of these wavelengths as,

$$I(\lambda, t) = D_N(\lambda, t) \times I_{SS}(\lambda) \quad (1.34)$$

Evidently, the plots of the $I(\lambda, t)$ parameter as a function of λ for different time delays represent the TRES of the probe, displaying the modulation of the emission spectra by the relaxation dynamics of concerned solvent. The TRES thus obtained following eq. 1.34 are in the wavelength scale and these spectra are in general converted to the wave-number ($\bar{\nu}$; energy) scale using the relation as,^{148,149}

$$I(\bar{\nu}, t) = \lambda^2 I(\lambda, t) \quad (1.35)$$

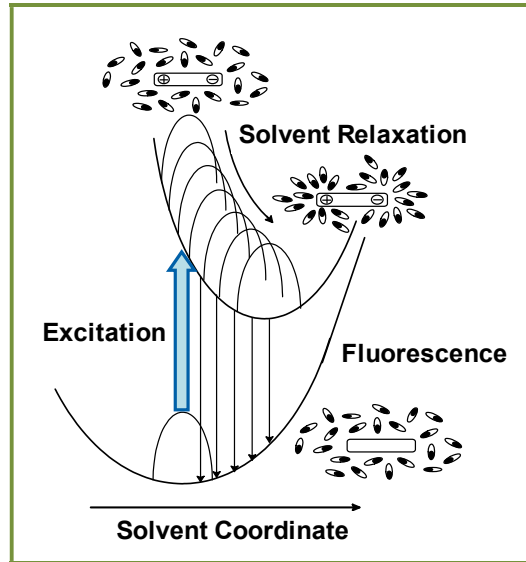


Figure 1.13. Conceptual presentation of dynamic fluorescence Stokes' shift caused by solvent relaxation process subsequent to the photoexcitation of the fluorescent probe in a polar solvent.

In actual experiments, since the fluorescence decays are practically possible to measure for limited number of wavelengths only, to obtain the smooth TRES for the studied system, the data points calculated following the aforementioned procedures are finally fitted using a log-normal line shape function, which is defined as,¹³⁰

$$I(\bar{\nu}) = a \exp \left\{ -\ln(2) \left(\frac{\ln[1 + 2b(\bar{\nu} - \bar{\nu}_p)/w]}{b} \right)^2 \right\}, \quad \text{when} \quad \{2b(\bar{\nu} - \bar{\nu}_p)/w\} > 1$$

$$= 0, \quad \text{when} \quad \{2b(\bar{\nu} - \bar{\nu}_p)/w\} \leq 1 \quad (1.36)$$

In the above expression, a is the amplitude, $\bar{\nu}_p$ is the wave-number for the emission peak position, w is the spectral width, and b is the asymmetry parameter for the line shape. In the log-normal fitting of the experimental data points all these parameters are used as the adjustable parameters to obtain smooth TRES for the studied system for their further utilization and analysis.

Following the smooth TRES obtained through log-normal fitting of the experimental data, the dynamic Stokes' shifts for these spectra are monitored in terms of the shifts in the emission maxima with time, $\bar{\nu}_{\max}(t)$. In most cases, these shifts are realized to follow a multi-exponential function as,

$$\bar{\nu}_{\max}(t) = \sum_{i=1}^n a_{si} \exp(-t / \tau_{si}) + \bar{\nu}_{\infty} \quad (1.37)$$

where a_{si} and τ_{si} are the pre-exponential factor and decay time, respectively, for the i^{th} solvent relaxation component, while $\bar{\nu}_{\infty}$ is the final position of the emission maxima at very long time. In most of these studies, for the convenience of presentation and analysis, the $\bar{\nu}_{\max}(t)$ values are in fact used to construct the normalized spectral shift correlation function, $C(t)$, as,

$$C(t) = \frac{\bar{\nu}(t) - \bar{\nu}(\infty)}{\bar{\nu}(0) - \bar{\nu}(\infty)} \quad (1.38)$$

whereby the $C(t)$ function is usually expected to decay following a multi-exponential function as,

$$C(t) = \sum_{i=1}^n a_{si} \exp(-t / \tau_{si}) \quad (1.39)$$

where a_{si} and τ_{si} are the parameter as defined before. Studies on the TRES are not only very useful to understand the solvent relaxation dynamics, but are also often essential to resolve the spectral characteristics of multiple emissive species present or formed in the solution. In many of the studies, the TRES are often normalized to unit area under each of the respective spectra to obtain the time-resolved area normalized emission spectra (TRANES), which are realized to provide the intriguing features of the emissive species in the system more conveniently than given by TRES as such.

1.7. General Micellar Characteristics of Block Copolymers (Pluronics and Tetronics) in Aqueous Solutions

Self-assembled surfactant aggregates have always been an active research area because of their technological importance and wide range applications. Over last few decades, considerable research has been devoted in understanding the phenomena related to the self-assembling of various surfactant systems, especially their micellization process. These studies were motivated mainly from the following facts. Firstly, the aqueous solutions of the surfactants forming micellar aggregates of characteristic size, shape and surface properties are quite easy to prepare and accordingly these surfactant solutions can be used suitably as the model systems to investigate various processes concerning physicochemical phenomena of the colloidal systems. Secondly, there are considerable similarities of the surfactant aggregates like micelles and vesicles with the biological lipid

membranes, and accordingly studies involving such surfactant aggregate can be considered as the model systems to understand many intriguing insights of the complex biological systems. Lastly, the surfactant aggregates like micelles, vesicles, etc. can be used as the unique reaction media to modulate various chemical reactions, which are certainly not possible to achieve by using homogeneous solvent systems as the reaction media.

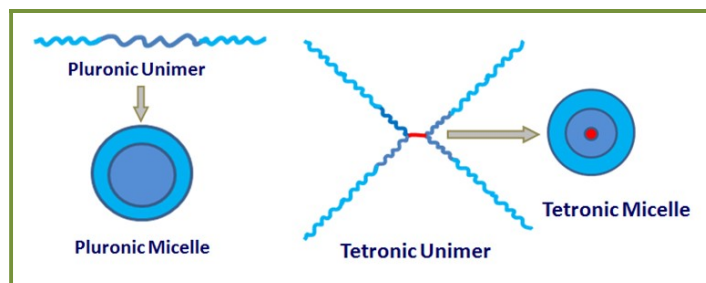


Figure 1.14. Representative structures of the Pluronic and Tetronic block copolymers and the conceptual presentation of the micelles formed by these copolymers in aqueous solution.

Among various surfactants, two important classes of block copolymer based surfactant systems that are constituted by the unique arrangements of the polyethyleneoxide $\{(EO)_n\}$ and polypropyleneoxide $\{(PO)_m\}$ blocks, and are commercially available under the trade names of Pluronics® and Tetronics®, have attracted considerable research interests for the last two decades, mainly because of their interesting thermo-responsive behavior in solution, and also because of their wide range of applications in detergents, lubricants and as emulsifiers. Pluronics are basically the linear *Triblock Copolymers* made up of two $(EO)_n$ blocks connected to a $(PO)_m$ block from both ends, having a general formula as, $(EO)_n-(PO)_m-(EO)_n$.^{150,151} Similarly, tetronics are essentially the *Star Block Copolymers*, made up of four $(PO)_m-(EO)_n$ type of copolymer chains connected through their $(PO)_m$ ends to a central ethylene diamine group, giving rise to an X-shaped structure, with a general formula as, $[(EO)_n-(PO)_m]_2-[N(CH_2)-(CH_2)N]-[(EO)_n-(PO)_m]_2$.¹⁵²⁻¹⁵⁸ Typical structures of the pluronic and tetronic series of the block copolymers and also the type of the micellar structures formed by these copolymers in aqueous solution are conceptually shown in Figure 1.14. Due to their unique behavior in aqueous solution, and also due to their low toxicity and bio compatability, both pluronics and tetronics have found their importance in different pharmaceutical applications. These block copolymers have also been used extensively in nanotechnology to provide templates for the synthesis of various nano-structured materials. Further, because solubilizations of different reactants are enhanced within the surfactant aggregates, these systems have also found important uses in altering the rates and mechanisms of various chemical reactions very effectively, which are having many academic and applied significance. Among block copolymers, the tetronics having their unique star shaped structure along with the presence of their central ethylene diamine group have displayed many superior multi-stimuli responsive properties as compared to their counterparts like

Pluronics. Accordingly, the tetronic copolymers have attracted a lot of diversified studies in recent years involving their aggregates in aqueous solutions.¹⁵⁶⁻¹⁶⁰

In spite of the absence of ionic head groups, pluronics and tetronics can form their micelles in aqueous solution, quite alike the conventional surfactant systems.¹⁵²⁻¹⁵⁸ In the block copolymers, their (PO)_m blocks are quite soluble in water at lower temperatures, typically below ~288 K, but they become quite hydrophobic and insoluble at elevated temperatures, because of the diminishing hydrogen bonding of the PO units with the water molecules. In contrast, the (EO)_n blocks of these copolymers remain quite hydrophilic for a wide range temperature, typically for about 273 to 373 K, even though the solubility of the (EO)_n block also decreases slightly with the increase in temperature, albeit with a much reduced rate as compared to the (PO)_m block. Due to such differential solubilities of the (PO)_m and (EO)_n blocks, a block copolymer in aqueous solution undergoes micellization above a certain temperature, called the “*Critical Micelle Temperature (CMT)*”, whereby the core of these micelles are formed mainly through the aggregation of the (PO)_m blocks while the corona layer of these micelles is constituted predominantly by the hydrated (EO)_n blocks of the copolymer. To be mentioned here that for a given temperature, an aqueous solution of a block copolymer will display its micellization provided its concentration in the solution is above a certain value, referred as the “*Critical Micelle Concentration (CMC)*” of the copolymer. Important to note that the *CMT* and *CMC* are the two important parameters for the block copolymer systems to characterize their association properties in aqueous solution. With the knowledge of the *CMT* and *CMC* values of a block copolymer, one can suitably make its aqueous solution with required micelle concentration in the system just by adjusting the total copolymer concentration and the temperature of the solution.

It is generally observed that above *CMT* or *CMC* a surfactant solution exhibits quite characteristic and sudden changes in many of its physicochemical properties, e.g. interfacial tension, equivalent conductivity, turbidity, self-diffusion coefficient, solubilization, viscosity, etc., which can be used suitably to determine the *CMT* and *CMC* values. These parameters can also be estimated following the temperature and surfactant concentration dependent changes in the photophysical properties of a chromophoric probe dye solubilized in the surfactant solution.¹⁶¹⁻¹⁶⁵ The *CMT* and *CMC* values for aqueous solutions of large number of block copolymer systems are reported in the literature.^{162,166,167} From these reports, it is generally observed that the copolymers with larger (PO)_m blocks usually display a lower *CMT* and also a lower *CMC* as compared to those with smaller (PO)_m blocks. For the characterization of the micelles, along with *CMT* and *CMC* values, other important parameters to know are the aggregation number (N_{agg}) of the micelle, its hydrodynamic radius (r_h), and also its core radius (r_{core}). All these micellar parameters for different block copolymer systems in aqueous solution are also reported in the literature.^{118,162,166,167} As a general trend, it is observed that the N_{agg} value increases with an increase in the (PO)_m blocks and a decrease in the (EO)_n blocks of the copolymer systems. The N_{agg} value is also found to increase in general on increasing the

temperature or salt concentration in the block copolymer solution.¹⁶⁸⁻¹⁷⁰ Interestingly, however, in many triblock copolymers systems, e.g. F68, P85, P104, P123, and F127, the increase in N_{agg} with temperature does not accompany with any significant change in the hydrodynamic radius (r_h) of these micelles. Such a typical observation has been attributed to temperature dependent dehydration of $(EO)_n$ blocks and the consequent reduction in the corona thickness of the micelles such that the r_h value remains more or less unchanged.

For star block copolymers especially, there exists some steric constraints among their four $(EO)_n$ -(PO)_m arms. Accordingly, a very compact packing of these copolymers in their micelles is not possible and accordingly the micelles of these star block copolymers are in general relatively more hydrated than the corresponding triblock micelles. Further, due to the presence of the central ethylene diamine group, the star block copolymers can undergo protonation at the acidic pH region. Due to this protonation there develops a strong coulombic repulsion among the positively charged amine groups of the unimers as they approach each other, causing micellization of these copolymers to be more difficult in acidic pH as compared to the neutral or alkaline pH conditions.^{157,166,167}

In the present context, it is important to discuss briefly the unifying principle that assists the aggregation process of the surfactant systems, i.e. the commonly referred hydrophobic effect.^{171,172} The standard free energy change for the transfer of a hydrocarbon molecule from aqueous to the oil phase is largely negative, reflecting the fact that nonpolar molecule has extremely small solubility in water. Similar behavior is also expected for the hydrophobic tails of the surfactant molecules. The thermodynamics of micelle formation in aqueous solution shows the enthalpy change (ΔH) to be positive, suggesting that it is an endothermic process.¹⁷³ However, since the surfactant molecules undergo micellization spontaneously above CMC , it suggests that the free energy change ΔG for this process is negative.¹⁷³ Considering that $\Delta G = \Delta H - T\Delta S$, since ΔH is positive, it implies that ΔS for the micellization process should be largely positive. This can be rationalized considering a large solvent contribution towards ΔS for the micellization process.¹⁷³ When a monomeric surfactant molecule is dispersed in an aqueous solution, since its long tail is hydrophobic in nature, the water molecules around it are forced to form a clathrate cage to accommodate this molecule into the so formed void space. Formation of such a clathrate cage structure reduces the entropy of the system very largely. Once many such surfactant molecules are aggregated together to form the micelle, the individual molecules are no longer required to have the clathrate cage structure for the solvent and thus the water molecules that were earlier participated in the cage formation become free now, as the surfactant molecules are aggregated to form the micelle. Evidently thus, micellization of the surfactant molecules is associated with much less structural demands for the water molecules as compared to the solubilization of unimeric surfactant molecules in aqueous solution. Accordingly, during micellization, there is a large increase in entropy for the whole system, which is universally termed as the hydrophobic interaction, associated with the aggregation of hydrophobic molecules in an aqueous solution. From the discussion above, it is evident that micellization of the surfactant

systems in aqueous solution is effectively the entropy driven process, where ordering of surfactant molecules into the micelles is stabilized by the greater disorder introduced for the solvent molecules by destructing their cage structures that existed before around the surfactant monomers.¹⁷³

For different surfactant systems, their micellization and also the structures of the so formed micelles have been investigated extensively by using different experimental techniques, like, neutron scattering,^{166,167,174-178} X-ray scattering,¹⁷⁹ light scattering,^{162,166,167,177,179-181} absorption¹⁸² and fluorescence measurements.^{158,162,183-185} The general features of a micelle are schematically presented by using the “oil drop” model, as depicted originally by Prof. G.S. Hartley,¹⁸⁶ and is shown in Figure 1.15, considering the surfactant used is anionic in nature (–ve head group). In this scheme, although the packing of the surfactant chains is not presented accurately, yet the model describes the most general features of a micellar structure. Micelles are usually spherical in structure, with their radii approximately similar to the extended lengths of the hydrocarbon chains of the used surfactant systems. Packing of the hydrocarbon tails inside the micelle constitutes the liquid-like nonpolar micellar core region, where microviscosity has been estimated in the range of ~8 cP. The head groups of the aggregated surfactant molecules along with the entrapped water molecules as well as some bound counterions form the micellar Stern layer, with its width typically about few angstroms. Most of the counter ions of the aggregated surfactant molecules are dissociated from the micelle and are distributed into the Gouy-Chapman double layer, whose width can extend even up to several hundred angstroms.

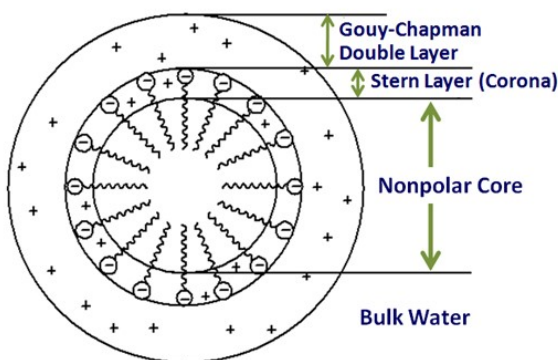


Figure 1.15. Schematic presentation of the Hartely’s “oil drop” model in describing the structure of an ionic (*anionic in this case*) micelle. For a nonionic micelle, there will not be any Gouy-Chapman layer and the charged Stern layer would be replaced by Palisade layer formed by the polar and hydrated head groups of the surfactant molecules.

For ionic micelles, due to the presence of the net charge on the Stern layer, a surface potential develops on the micelle, which is usually in the range of 50-100 mV. This potential slowly diminishes across the Gouy-Chapman layer, as the distance increases from the micellar surface. The charged double layer around the ionic micellar surface acts as an electrostatic barrier for the passage of the charged chemical species across the micellar surface and consequently assists to create a

spatial separation between the oppositely charged reactants and products existing in these micellar systems. For the micelles formed by the non-ionic surfactants, say block copolymer systems, even though there is no charged head group present in these surfactant molecules, their reasonably polar and hydrophilic head groups, namely the polyethylene oxide $\{(EO)_n\}$ groups, can easily form the hydrated corona layer of the micelle, similar to the Stern layer of the ionic micelles, which would face the bulk water outside, while the hydrophobic tails of these non-ionic surfactants, e.g. the dehydrated polypropylene oxide $\{(PO)_n\}$ groups of the block copolymers, would pack inside the micelle to form the hydrophobic core region of the micelle. To be mentioned here that while the hydrated and polar charged outer layer of an ionic micelle is termed as the “*Stern Layer*”, as indicated in Figure 1.15, the similar hydrated, polar and neutral outer layer of a nonionic micelle is commonly referred as the “*Palisade Layer*” of the micelle. For nonionic micelles, there is no Gouy-Chapman layer in their structures. Further, for the nonionic micelles, their size and shape often vary quite significantly depending upon the nature of the head groups, length of the hydrophobic tails of the surfactant molecules, concentration of the surfactant used, presence of the other additives in the solution and also on the experimental condition like the temperature of the solution.

The micelles formed by a surfactant system in aqueous solution are always in a dynamic equilibrium with the monomeric surfactant molecules present in the solution.^{171,187} There are two distinct processes, which occur in largely different time scales, and are directly associated with the equilibrium between the micelles and monomeric surfactants exist in the solution. The faster process, which occurs mostly in the microsecond time scales, is the exchange of the monomeric surfactants between the micelles and the bulk aqueous phase. The slower process, which occurs mostly in the millisecond time scales, is the complete dissolution of a micelle into its monomeric components. Interestingly, depending upon the solvent conditions, some surfactants may also form reverse micelle structures (microemulsions), e.g. in hydrophobic solvents containing a small amount of water into it. In these structures, the water molecules are dispersed as microdroplets inside the surfactant aggregates, where water droplets are surrounded by the shell of the polar surfactant head groups, while the long tails of these surfactant molecules are immersed into the bulk hydrophobic solvent present outside the aggregates. In these cases also the reverse micelles formed are always in a dynamic equilibrium with the monomeric surfactants coexist in the bulk solution.

Although numerous studies have been carried out to explore the structural and dynamical aspects of various surfactant aggregates, similar investigations on the aggregates formed especially by pluronic and tetronic systems are indeed very limited. Employing steady-state and time-resolved fluorescence anisotropy measurements, Dutt et al. have reported the rotational relaxation dynamics of the solubilized fluorescence probes in different pluronic micelles. Grant et al. have demonstrated using similar anisotropy measurements that a suitable molecular probe can be used as a local reporter to explore the microenvironments for the different regions of the block copolymer micelles. The solvent relaxation dynamics of the water molecules in different regions of pluronic micelles

have been reported by Bhattacharya, et al. and Kumbhakar, et al. following the standard dynamic Stokes' shift method. All these studies have indicated that the dynamical processes associated with the micelles formed by the pluronics (and understandably also by the tetronics) in aqueous solution are largely dependent on the EO to PO ratios of these block copolymer systems.

In many industrial applications, pluronic and tetronic systems are often used in combination with low molecular weight conventional ionic surfactants, as these mixed surfactant systems perform better in regard to the desired applications of the surfactant aggregates as compared to those of the pure surfactant systems.^{162,166,167,188-190} Considering such applications, many experimental studies have been carried out to explore the details of the solution behaviors of these mixed surfactant systems.^{162,166,167,188,191,192} In these cases, due to the presence of two surfactant systems of largely different chemical constitution and characteristics, they can lead to the formation of the microheterogeneous mixed surfactant assemblies with complex structures, whose properties and solution behavior are essential to be understood very explicitly to find their usefulness in different applications. Combination of pluronics with low molecular weight ionic surfactants, namely, sodium dodecyl sulfate (SDS), cetyltrimethylammonium chloride (CTAC), cetyltrimethylammonium bromide (CTAB), etc. have been studied quite extensively by using various experimental methods like, light scattering, neutron scattering, calorimetric studies, fluorescence measurements, and so on. According to these studies, use of the low molecular weight ionic co-surfactants in lower concentrations in combination with block copolymer systems, e.g. pluronics, results in the formation of typical supramolecular assemblies of the mixed surfactant systems, where the hydrocarbon chains of the small ionic surfactants are suitably incorporated and dissolved into the nonpolar poly PO core of the pluronic micellar structure, while the charged head groups of these small surfactants are protruded at the periphery of the pluronic micellar core, pointing towards the hydrated corona region of the pluronic micellar structure, as shown schematically in 1.16.

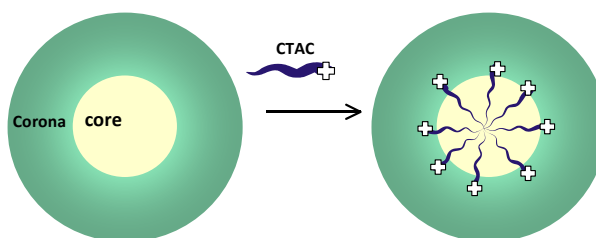


Figure 1.16. Schematic presentation of the mixed micellar assemblies formed on combining a low molecular weight conventional ionic surfactant with a block copolymer like a pluronic in aqueous solution. It is shown how a charged layer is developed with the pluronic micelle on incorporation of the ionic co-surfactants.

Interestingly, in these mixed micellar assemblies involving ionic co-surfactant in combination with a pluronic copolymer, there is the development of a charged layer within the pluronic micelle, for which the charge density can be altered systematically by changing the molar ratio of the ionic co-surfactant to the pluronic copolymer simply, offering a variety of applications

of such mixed supramolecular assemblies in different areas. Obviously, the utilization of a mixed surfactant-copolymer system in a specific application would largely depend on the physical and chemical properties of the dissolved solutes in these supramolecular assemblies. Since these mixed assemblies provide wide range of microenvironments in a single phase, solubilized molecules in these systems can also display wide range of physical and chemical properties depending on their position in these mixed micellar assemblies. Further, the location of the solutes in these mixed micellar systems can also be changed suitably by changing the ratio of the two surfactants and thereby it is possible to tune the physical and chemical properties of the solutes for their better utilizations.

1.8. Lanthanide Ions as Electron Acceptors in PET Studies

The lanthanides [Lanthanum (La) to Lutetium (Lu)] are quite distinctive among the chemical elements, that resemble extremely closely to each other in regard to their chemical properties, especially towards their oxidation states.^{193,194} This is readily described by the electronic configuration of the lanthanide atoms, $\text{Ln}(0) [\text{Xe}] 4f^{0-14} 5d^{0-1} 6s^2$; where La(0) and Lu(0) have $5d^1$ electron while rest of the Ln(0) have $5d^0$ electron, as well as that of their stable trivalent ions in aqueous solution, $\text{Ln(III)} \{[\text{Xe}]4f^{0-14}\}$, determined by the various degrees of stabilization experienced by the 4f, 5d, and 6s orbitals upon sequential ionization of the concerned lanthanide elements.¹⁹⁵ The 4f–4f electronic transitions in lanthanides being parity-forbidden, the lanthanides are having very low molar absorption coefficients (typically $<3 \text{ M}^{-1} \text{ s}^{-1}$) and they display characteristic narrow-line emissions, mostly in the visible to near infrared region.¹⁹⁶ Since the trivalent state is the most common oxidation state of the lanthanide ions, and because different Ln(III) ions display wide range of reduction potentials, determined by the varying degrees of stabilizations of the electronic configurations for the resultant Ln(II) ions, the redox behaviours of the Ln(III) ions are very interesting to study. This is especially relevant in regard to their electron accepting abilities in photoinduced electron transfer (PET) processes involving suitable electron rich species. The intricate details of these PET processes have not been elaborately explored till now, and these informations are anticipated to have both academic and applied consequences.¹⁹⁷⁻²¹¹

Electron transfer (ET) studies involving Ln(III) ions have in general gained considerable research interest due to the relevance of such species in the areas like geo-mitigation,²¹²⁻²¹⁶ luminescence sciences,^{196,198,203,204,217-219} optoelectronics,²⁰⁵⁻²⁰⁷ biotechnology,¹⁹⁹⁻²⁰² bio-sensing,^{199-202,220,221} bio-imaging,^{200-202,220,221} and many others.²²²⁻²²⁸ Besides the fascinating optical properties of the Ln(III) ions, they are also viewed as quite efficient redox species. The redox chemistry of the lanthanide ions and their consequent interactions with various electron donating agents have a strong bearing towards their migration behaviour in the geological environments, when leached out accidentally from spent nuclear fuels.^{213,215,216} It is found that trivalent lanthanide ions encompass a wide range of reduction potentials and act as are very good oxidizing agents, especially in aqueous

media.^{196,229-233} It is therefore interesting to explore if these ions could play divergent roles in the PET processes involving suitable electron rich species. In literature, limited attention has only been paid on the ET interactions of Ln(III) ions with different organic and inorganic electron donating species.^{199,201,203-207,197,222-228,234} Photophysical and photochemical studies are foreseen as the useful tools to realise the photoinduced redox reactions of lanthanide ions with various electron transfer agents present in the geological environments, which might be convenient in designing strategies to control the migration of the concerned metal ions in the geoenvironment. Also the studies on the bimolecular PET reactions involving Ln(III) ions in aqueous media have demonstrated the possible involvement of the unique mechanism of multichannel ET, where Ln(III) ions can provide multiple accepting channels for the electron from the excited donor molecules, suggesting many academic and applied prospects for the PET processes involving Ln(III) ions as the electron acceptors.¹⁹⁷

1.9. Motivation and Objective of the Present Thesis

Though electron transfer (ET) simply implies the transfer of an electron from a donor to an acceptor moiety, the overall ET process is in general very complicated, because the kinetics of the process is cooperatively controlled by large number of energetic and dynamic parameters in a complex manner. These factors include the redox characteristics of the donor and acceptor systems, their electronic coupling strengths, energy associated with intramolecular reorganization in the donor-acceptor system coupled with the ET reaction, energy involved in the intermolecular reorganization of the solvent system around the interacting donor-acceptor pairs, dynamics of both intramolecular and solvent reorganization processes, and so on. Understanding the detailed insights of these parameter associated with the ET processes under different experimental conditions, especially those under restricted solvent environments, e.g. in microheterogeneous systems, is undoubtedly an extremely challenging task, and has attracted enormous research interests for quite sometime, from both academic and applied viewpoints. The understandings of such studies are very important as they have direct consequences in processes like photosynthesis, solar energy conversion, photovoltaics, and so on. In these processes, the primary step is essentially the photoinduced ET (PET) reaction, initiated by the excitation of a reactant through its absorption with a suitable light photon, which subsequently opens up a sequence of chemical reaction steps to eventually produce the energy rich final products.^{8,9,26,29,42,43}

Research on PET reactions in restricted microheterogeneous media, like micelles, have gained considerable attention in the last two decades, owing to the fact that in many practical applications of ET reactions, e.g., solar energy conversion and its storage, photovoltaics, photocatalysis, sensing, etc. these reactions are needed to be carried out in various microheterogeneous environments.^{4,38,127,235,236} The advantage of microheterogeneous media is that it provides an opportunity to spatially separate the primary products of the ET reactions, i.e. the two

oppositely charged radical ions (D^+ and A^-), and thus increasing the lifetime of these primary products, through the reduction in their energy wasting charge recombination process, and thereby enhancing the availability of these energy rich species for subsequent reactions and specific applications.²³⁷⁻²⁴¹ Among various microheterogeneous media, micellar systems have attracted the major interests of the researchers as the models for constrained reaction media. These model systems are useful in understanding the effect of the topology of the microheterogeneous environments on the outcome of chemical reactions and also to explore if the kinetics and energetic of the reactions can be modulated appreciably by manipulating the microscopic environments of the microheterogeneous systems. To be mentioned in this context that the micellar media have been used very extensively to control the PET reactions, modulating their energetic and kinetics in very intriguing manners.^{117,118,236} It is understood from such studies that with appropriate selection of the micelle, it is possible to either enhance or inhibit the effective PET rate as compared to that expected in a homogeneous media.²⁴²⁻²⁴⁷ Further, the studies on ET and other biologically important reactions in micellar media have many academic and applied importance, due to the structural resemblance of the micelles with various biological membranes.²⁴⁸⁻²⁵⁰ Although PET reactions in conventional homogeneous solvents are reported quite elaborately, similar studies on PET reactions in microheterogeneous media are indeed very limited.

As discussed in the earlier sections, the most remarkable outcome of Marcus outer sphere ET theory is the parabolic dependence of the ET rate on the exergonicity ($-\Delta G^0$) of the ET reaction, referred as the Marcus Inversion (MI) behavior.^{10-12,14-19} The theoretically predicted MI behavior for the ET rates had generated lot of controversy for many years, mainly due to the lack of finding any experimental evidence for such an intriguing behavior. Presently, however, there are many experimental evidences depicting the presence of MI on correlating the observed ET rates with the exergonicity of the ET reactions.^{29,57,105,236} It is interesting to point out, however, that in most of the cases, where MI behavior has been observed very clearly, the ET reactions had been carried out involving either chemically bound donor and acceptor moieties, i.e. for the intramolecular charge separation (CS) reactions,^{57-59,251-259} or in the ET reactions that involve interacting radical ions (D^+ and A^-) in their physical contact, i.e. for the charge recombination (CR) reactions in the contact ion pairs (D^+/A^-).²⁶⁰⁻²⁶³ For both of the above types of ET reactions, the separation between the two reacting species (i.e. between D and A in the case of CS and between D^+ and A^- in the case of CR) effectively remains unchanged during the progress of the reaction, which in other words suggests that there is no change in the donor and acceptor positions during the ET reaction, as often caused by the diffusion of the reactants in the reaction media. For bimolecular ET reactions, however, as the donor and acceptor positions are changed continuously by the mutual diffusion of the reactants in the reaction medium, the finding of MI behavior is not only very rare, but also in cases where even if it is observed, the extent of inversion is so weak that the behavior is not as convincing as in the cases of intramolecular CS reactions or in the CR reactions involving contact ion pairs.²⁶⁴⁻²⁷²

In section 1.5.1, we have discussed how the correlation of the observed ET rates (k_q) with the reaction exergonicity ($-\Delta G^0$) for bimolecular PET processes under diffusive conditions follow the Rehm-Weller type of behavior,¹³⁰ where the observed ET rate, which is estimated conveniently in the form of the bimolecular quenching rate constant, k_q , increases initially with $-\Delta G^0$ at the lower exergonicity region, but saturates eventually to the diffusion-controlled limiting value (k_d) at the higher exergonicity region, instead of displaying the MI behavior, as predicted from Marcus ET theory. As it is understood, such a behavior mainly arises due to the influence of the mutual diffusion of the reactants (donors and acceptors) on the observed k_q value. While at the lower exergonicity region the k_q increases asymptotically with $-\Delta G^0$, because the formation rate of the encounter complex through diffusion of the reactants is faster than the intrinsic ET rate (cf. section 1.5.1), at reasonably higher exergonicity region, however, the intrinsic ET rate becomes very fast, faster than the diffusional rate of the reactants. Under this situation, the encounter complex formation through reactants' diffusion becomes the rate determining step, causing the saturation of k_q to its limiting value of bimolecular diffusion-controlled rate constant, k_d .²⁹ In this context, Tachiya and Murata had made a judicial distinction between the MI behavior and Rehm-Weller behavior for the observed ET kinetics based on the mechanistic differences of the two situations of these ET processes.²⁷³ In Marcus ET theory, the first order rate for the donor-acceptor pair separated by a fixed distance is considered as the actual ET rate (k_{et}) and accordingly the observed rate constant k_{et} is correlated with $-\Delta G^0$, which is predicted to follow the MI behavior. In the Rehm-Weller model, however, as considered by Tachiya and Murata,²⁷³ the observed rate constant (k_q) for bimolecular reaction is determined not only by the diffusion of the donors and acceptors in the solution but also by the distance dependent first order ET rate constant, $k_{et}(r)$, in the encounter complexes formed, where the latter effect is quite dependent on the exergonicity of the reaction. Based on this consideration, Tachiya and Murata had calculated the diffusion mediated second order reaction rate constants (k_q) corresponding to the Rehm-Weller model of the ET process, suitably incorporating the $k_{et}(r)$ effect on the bimolecular ET rate. From their calculations, the authors could show that even though the k_q vs $-\Delta G^0$ correlation displays a kind of saturation at the reasonably higher exergonicity region, as realized to be the typical Rehm-Weller behavior, the k_q vs $-\Delta G^0$ correlation, however, shows an inversion like behavior, as expected from Marcus ET theory, if the exergonicity of the reaction is made exceedingly high, typically $\sim 2\text{eV}$ or more.²⁷³ According to these authors thus, it is possible to observe the MI region for the observed rate constants of bimolecular PET reaction under diffusive condition, if the reaction exergonicity is made beyond the point where inversion behavior eventually overtakes the Rehm-Weller behavior, as conceptually demonstrated in Figure 1.12.

It is understandable from the discussion made so far that there are two main reasons that prohibit the observation MI behavior for bimolecular PET reactions; they are, (i) diffusion of the reactants in the solution, and (ii) the lack of availability of the suitable donor-acceptor series that can provide very high reaction exergonicity, much higher than the total reorganization energy (λ) for the

concerned ET process, to surmount the exergonicity region over which the Rehm-Weller behavior is normally exhibited. In regard to the diffusional intervention of the bimolecular PET reactions, it is visualized that the constrained reaction media, e.g. micelles, can provide a suitable reaction condition to facilitate the PET reaction to occur effectively under non-diffusive condition and thus favoring the observation of the MI behavior even for the bimolecular PET reactions. As the micelles are formed through the aggregation of the surfactant molecules in a well defined manner, their internal structures are reasonably stiff, where the dissolved reactant molecules are forced to remain entangled with the surfactant chains, causing the movements of these reactants inside the micelles to be highly restricted.^{169,274-282} To represent it in another way, we may consider that the microviscosity inside the micellar phase is very large such that the diffusion of the reactants in these media is reduced very largely and accordingly the bimolecular PET reactions are effectively conditioned to occur under a non-diffusive condition, involving only those donor-acceptor pairs that are already pre-existed within the reaction distance at the moment of the photoexcitation process. This makes the overall reaction to be faster than the diffusion process and can be visualized as equivalent to an intramolecular PET reaction. Evidently, the bimolecular PET reaction in the constrained reaction media like micelles would differ largely as compared to the diffusion mediated bimolecular reactions in the conventional low viscosity homogeneous solvents. In a constrained media, since the bimolecular PET reaction effectively occurs similar to an intramolecular PET reaction, alike the intramolecular PET, the MI behavior is also expected to be observed quite easily for bimolecular PET reactions carried out in constrained reaction media.

Considering the other factor that inhibits the observation of MI for bimolecular PET reactions in conventional solvent, i.e. the extremely high reaction exergonicity, much higher than λ , which is difficult to achieve in most cases due to the lack of the suitable donor-acceptor series. This limitation can also be surmounted quite substantially in the constrained media like micelles, due to the extremely slow solvent relaxation dynamics in these media. For a bimolecular PET reaction, the total reorganization energy λ is mainly contributed by the solvent reorganization energy λ_s , with a minor contribution arising from the intramolecular reorganization energy λ_i . It is well known that the motion of the solvent molecules in constrained media, e.g. micelles, is retarded by several order of magnitudes, as compared to that in homogeneous solvents.^{137,138,140-143,283} Hence, in constrained media, the solvent relaxation process can effectively be slower as compared to the observed ET rate, and under this situation, the solvent reorganization will not contribute completely to assist the ET reaction in these media. With the given circumstances, thus, the effective solvent reorganization energy, $\lambda_{s,eff}$, contributed to the ET reaction, will be just a fraction of the total λ_s , and accordingly the effective total reorganization energy, λ_{eff} , will be much less than the total λ , as otherwise contributed in conventional low viscosity homogeneous solvents (cf. section 1.2.4). In the constrained media, as λ_{eff} becomes less than λ , the Marcus inverted region is understandably shifted at a relatively lower exergonicity region as compared to that in the conventional solvents. Consequently, micellar media

would be the very favorable reaction media that would support the observation of the MI behavior for bimolecular ET reactions to be realized quite easily.

The objective and motivation of the present thesis is to explore the details of the above mentioned aspects of the bimolecular PET reactions in constrained media like micelles, constituted by using the surfactant systems like tetronics and pluronics, either in their pure forms, or in combination with other conventional surfactants or suitable additives, that helps in modulating the micellar microenvironments. Present thesis elaborately describes various important photophysical phenomena that have been investigated to acquire a better understanding of the ET reactions between different donor-acceptor pairs in the studied micelles as well as in simple aqueous solution. The main objective for the present work has been to determine if the Marcus Inversion behavior can indeed be observed for bimolecular PET reactions under the conditions where the reactions are carried out under the constrained condition of the micellar environments. In the present study, the effect of the changing poly ethyleneoxide $\{(EO)_n\}$ and poly propyleneoxide $\{(PO)_m\}$ blocks of the studied star block copolymer (tetronic) micelles on the kinetics and energetics of the PET processes in these micellar media has also been investigated quite extensively. With the aim to find a possible modulation of the PET kinetics, mixed micellar systems composed of tetronics polymers as the base material and ionic liquids as the additives have also been investigated extensively, in respect to the modulations in the micellar characteristics and their effects on the the PET reactions carried out in these constrained media. Along with the nanosecond and sub-nanosecond studies, ultrafast ET kinetics have also been investigated in selective systems to consolidate the observed phenomena, especially the Marcus Inversion behavior, in various time scales. As solvent relaxation dynamics often play a significant role in the ET reactions, wherever possible, solvent relaxation dynamics have also been explored in the present study for the micellar media used to investigate the PET reactions. With the experience gained from the PET studies in micellar media, the studies have also been extended to understand the complex PET reactions of the lanthanide ions with organic donors under diffusive reaction conditions, considering the possible multichannel electron accepting property of the lanthanide ions, an intriguing aspect that is hardly reported in the literature. While the instruments and methodologies used in the present study are provided in the forthcoming Chapter 2 with all the necessary details, the experimental results obtained for the different parts of the present study and their interpretations and inferences have been systematically presented and discussed in the subsequent Chapters 3 to 6 of the present thesis, making the presentation as comprehensive as possible. Finally, the summary of the present work and the future prospects of the research carried out in this study have been given briefly in the concluding Chapter 7.

CHAPTER-2

INSTRUMENTS AND METHODS

2.1. Introduction

This chapter provides the brief descriptions of the various experimental techniques used in the present study to carry out the research work pertaining to the present thesis. To understand the mechanism and kinetics of photoinduced electron transfer (ET) and charge transfer (CT) processes and also to explore the static and dynamic characteristics of different microheterogeneous systems used in the present work, various steady-state and time-resolved absorption and fluorescence measurements have been carried out in the present study. Basic principles of these photophysical instruments and methods, namely, UV-vis spectrophotometer, steady-state (SS) spectrofluorimeter, time-correlated single photon counting spectrometer (TCSPC), femtosecond fluorescence up-conversion system, nano second laser flash photolysis setup and zeta potential measurement instrument, have been provided in this chapter with the necessary details, as presented sequentially in the following sections.

2.2. Ground State Absorption Measurements

Any photochemical process is initiated by absorption of light by the concerned chemical system. Therefore it becomes important to have a prior knowledge on the optical absorption characteristics of the studied chemical system. Optical absorption spectroscopy in the ultraviolet to visible (UV-vis) region is a very important technique to obtain information about the ground-state absorption characteristics of a chemical system, namely, the wavelength ranges of its absorption bands, absorption peak positions, as well as the strengths of different absorption bands, as given by the extinction coefficient values at different wavelength positions. The characteristics of the absorption bands of a chemical system in the UV-vis spectrum are determined by the nature of the electronic transitions involved and also on the interaction of the concerned electronic states with the solvent microenvironment around the chromophoric moiety of the chemical system. Hence UV-vis absorption spectroscopy provides an opportunity to characterize many intricate details of the chromophoric systems along with their surrounding microenvironments. Alteration in the polarity, polarizability and hydrogen bonding characteristics of the solvents can often induce very significant changes in the absorption spectra of chromophoric systems.²⁸⁴⁻²⁸⁷ Ground state complexation of the chromophoric unit with other reactants present in the chemical system can also influence the absorption characteristics of the concerned chromophore. Therefore, this simple photochemical instrument in the form of ground state UV-vis absorption spectrometer can provide a variety of information in regard to the nature of the chromophoric systems, their ground-state interactions with surrounding environments, their interactions with other reactants present in the studied chemical systems, and so on, which are very useful before proceeding for the other photochemical or photophysical studies involving the concerned chromophoric systems. Needless to say that the

measurements of the UV-vis absorption spectra and thus to get the knowledge of the ground state absorption characteristics of the chemical systems and accordingly to adjust the optical density and/or concentration of the absorbing species in the experimental solutions are the essential prerequisites before carrying out the other photochemical studies meaningfully, to obtain the desired results in the convincing manner.

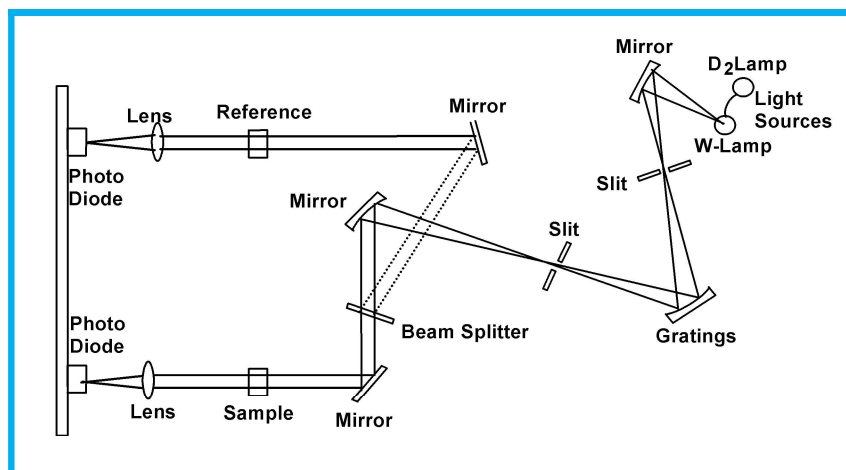


Figure 2.1. Schematic presentation of the double beam UV-vis absorption spectrophotometer used in the present study.

The absorption characteristics of the dissolved chromophoric species in a solution for a given wavelength of the light beam is defined by the absorbance (A) value of the solution, which is directly proportional to the concentration (C) of the absorbing species and its molar extinction coefficient (ϵ_λ) at the concerned wavelength, λ , and is expressed as,²⁸⁴⁻²⁸⁷

$$A = \log\left(\frac{I_0}{I}\right) = \epsilon_\lambda Cl \quad (2.1)$$

where I_0 and I are the intensities of the incident and transmitted light, respectively, at wavelength λ , and l is the optical path length in the solution along which the light beam passes through. In a typical UV-vis absorption spectrometer, the sample is kept in a quartz cuvette of 1 cm path length. For substantially concentrated solutions, thinner quartz cells are usually used with typical path lengths of either 0.1 or 0.2 cm. In our study, a Jasco make (Tokyo, Japan) UV-vis spectrophotometer (model V-650) was used to carry out all ground-state absorption measurements for the studied chemical systems. The spectrophotometer can record absorption spectra for the wavelength range of 200-1100 nm. It uses two light sources, one W-lamp covering from 1100 nm down to 350 nm and a D₂ lamp covering from 350 nm down to 200 nm. It is a double beam spectrophotometer and it uses two Si-photodiodes as the light detectors. Wavelength resolution for the present spectrophotometer is 0.2 nm and the lowest absorbance measurable by this instrument is ~ 0.005 . Figure 2.1 shows the schematic presentation of this double beam UV-vis spectrophotometer used in the present study.

2.3. Steady-State Fluorescence Measurements

Emission of light from excited molecules during their electronic transition from the excited state to the ground state of same multiplicity is termed as the fluorescence emission of the chromophoric system. The steady-state (SS) spectrofluorimetric measurement is a very important technique to obtain information about the fluorescence characteristics of a chemical system, namely, the wavelength ranges of its fluorescence bands, its emission peak positions (emission maxima), the shape of the fluorescence spectra and so on, which are in general very sensitive to the solvent environment around the chromophoric system and are also influenced very significantly by the interaction of the chromophoric system in its excited state with various quencher systems present in the solution.^{284,286,287} Fluorescence spectroscopy is a very simple but extremely powerful technique to investigate various photochemical processes that occur in the excited singlet state of the chromophoric molecules. In the present study a Hitachi make (Tokyo, Japan) spectrofluorimeter (model V-650) was used to carry out all SS fluorescence measurements (fluorescence intensity, excitation spectra or emission spectra) for the studied chemical systems. This instrument uses a 150 watt continuous powered high pressure xenon lamp as the excitation source and a Hamamatsu make R-928F photomultiplier tube (PMT) as the photodetector. The sample is excited typically in a 1 cm x 1 cm suprasil quartz cuvette, and the emitted fluorescence is collected and measured in the perpendicular direction with respect to the direction of the excitation beam. The wavelength range covered in the present instrument is 220 to 800 nm. The schematic presentation of the steady-state spectrofluorimeter used in the present study is shown in Figure 2.2.

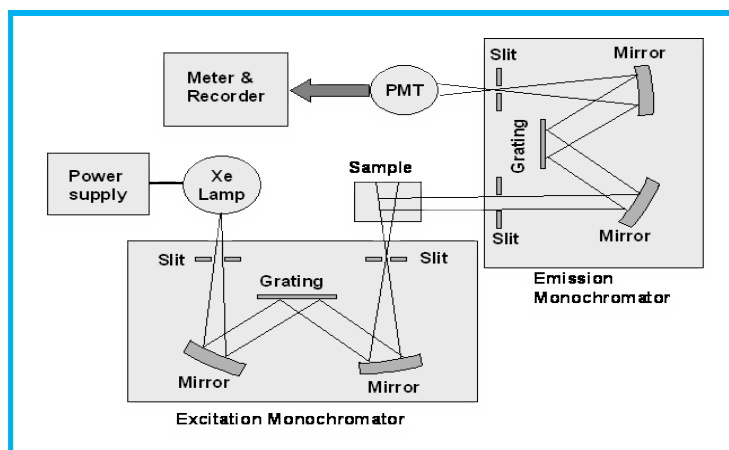


Figure 2.2. Schematic presentation of the steady-state fluorescence spectrometer used in the present study.

2.3.1. Correction of the Emission Spectra

The emission spectra recorded with a spectrofluorimeter are often distorted due to the wavelength dependent responses of the different components used in the instrument, e.g. excitation source, monochromator, PMT, etc. Therefore, it is important to know the wavelength-dependent responses of the detection system as a whole to correct the observed emission spectra from the instrument. In

the present work, spectra of the standard quinine sulfate solutions were recorded and compared with the known spectrum of this fluorophore²⁸⁸ as given in the unit of photon/nm, to get the correction factors for the overall wavelength dependent responses of the instrument. Accordingly, the measured emission spectra for the studied chemical systems were multiplied by the above correction factors for each wavelength to obtain the corrected emission spectra for the studied systems. In the normal measurements, the emission spectra are recorded in the wavelength domain, represented as $I(\lambda)$. In some applications, these emission spectra in the wavelength domain are converted to the respective frequency domain spectra, $I(\nu)$, by using the following standard relation.^{148,149}

$$I(\nu) = \lambda^2 I(\lambda) \quad (2.2)$$

2.4. Time-resolved Fluorescence Measurements

Time-resolved (TR) fluorescence measurements are carried out to understand the characteristics of the fluorescence intensity decay with time and consequently to estimate excited state lifetime, also called the fluorescence lifetime, of the excited molecules. These measurements are very crucial to understand the kinetics and dynamics of various photoinduced processes involving excited chromophoric molecules. Irradiation of a fluorophoric system with an ultra-short light pulse results in the creation of an initial population (n_0) of the excited fluorophores instantaneously in the system. Following this, the excited fluorophores participate in different radiative and nonradiative deexcitation processes to cause the time-dependent decay of the excited molecules. Therefore, the decay rate for the population of the excited molecules can be expressed as,^{284-287,289-292}

$$\frac{dn(t)}{dt} = -(k_r + k_{nr})n(t) \quad (2.3)$$

where $n(t)$ is the number of the excited molecules present at time t following the excitation pulse and k_r and k_{nr} are the decay rate constants for the radiative and nonradiative deexcitation processes of the excited fluorophores. Solving eq. 2.3, one can have,

$$n(t) = n_0 \exp\{-(k_r + k_{nr})t\} \quad (2.4)$$

Though in a real system it is difficult to know the exact number of the excited molecules, however, considering that the fluorescence intensity observed at any time t is proportional to the number of excited molecules, $n(t)$, existed at that time, we can suitably convert eq. 2.4 into the form of a time-dependent fluorescence intensity decay, often called simply the fluorescence decay of the sample, which can be expressed as,

$$I(t) = I_0 \exp(-t / \tau_f) \quad (2.5)$$

where I_0 is the intensity at time zero and τ_f is referred as the fluorescence lifetime of the studied sample, which is related to the k_r and k_{nr} values of the concerned chromophoric system as,

$$\tau_f = \frac{1}{k_r + k_{nr}} \quad (2.6)$$

The above mentioned fluorescence decays of the samples are suitably recorded using different TR fluorescence measurement techniques, and the τ_f values of the studied chromophoric systems are estimated following adequate analysis of the observed fluorescence decays.

In the recording of the fluorescence decay, if the width of the excitation light pulse is extremely narrow (δ -pulse) and the response time of the detection system is also unusually fast, the fluorescence lifetime of the studied sample can be obtained by fitting the observed intensity decay profile as an exponential function simply, as given by eq. 2.5.^{284-287,289,290} In the cases, however, where the fluorescence lifetime of the sample is significantly short such that neither the excitation light pulse can be considered as the δ -pulse nor the response time of the detection system can be considered to be unusually fast, both the excitation pulse width and the response time of the instrumental setup will distort the observed intensity decay profile significantly as compared to the true fluorescence decay of the sample. Under such situations, the observed decay profiles are required to be fitted following a reconvolution analysis procedure to estimate the τ_f values of the samples, as will be described in the latter part of this section. In the present context, an important point to be mentioned that since the fluorophores are excited in very large numbers in the system by using an excitation pulse and because each of these excited fluorophores randomly spend different lengths of times before giving its emission (or deexcitation), the τ_f value estimated from the analysis of the observed fluorescence intensity decay is truly the measure of the statistical average of the times that the ensemble of the excited molecules spend in the excited state.

Considering the time scales of the excited molecules and depending on the methodologies used for the concerned TR measurements, there are various experimental techniques available to record the fluorescence intensity decay profiles of the studied chemical systems. Among various TR fluorescence measurements techniques, the widely used one is the “Time-Correlated Single Photon Counting (TCSPC)” technique, applied extensively in the nanosecond to picosecond time domains. In the present study, a TCSPC spectrometer obtained from Horiba Jobin Yvon IBH, UK (model Data Station Hub), was used to measure the fluorescence decays of the investigated samples. For a part of the present study, where the investigated samples were anticipated to undergo ultrafast fluorescence decays, faster than picoseconds, their fluorescence intensity decays were recorded using the ultrafast fluorescence up-conversion technique, useful to record fluorescence decays in the sub-picosecond to femtosecond timescales. In the following section we discuss the essential details of both TCSPC and up-conversion techniques as used in the present study.

2.5. Time-Correlated Single Photon Counting (TCSPC) Technique

2.5.1. Basic Principles of TCSPC Technique

The principle of the TCSPC technique is based on the consideration that the time-dependent changes in the fluorescence intensity for an ensemble of molecules excited by a δ -pulse is equivalent to the

probability distribution for the emission of a photon from a single excited molecule as a function of time subsequent to its excitation.²⁸⁹⁻²⁹² Accordingly, the TCSPC technique relies on the stringent experimental condition that only a single emission photon would be detected effectively for each excitation pulse such that the distribution of the number of detected photons following large number of excitations as a function of time represents the time-dependent emission probability of a single photon from an excited molecule and hence the fluorescence decay of the studied sample.

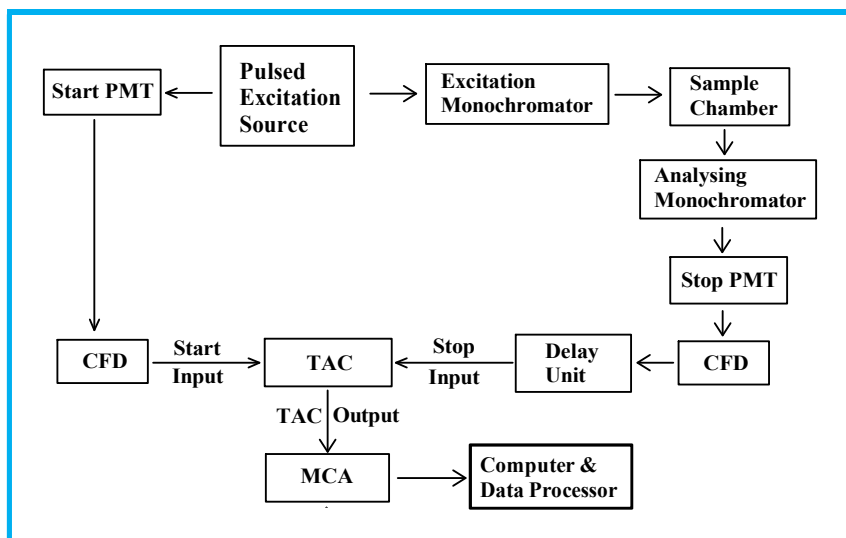


Figure 2.3. A schematic diagram showing different components of a typical TCSPC spectrometer. The abbreviations are: PMT - Photomultiplier tube, CFD – Constant fraction discriminator, TAC – Time to amplitude converter, MCA – Multichannel analyzer.

The schematic diagram of a typical TCSPC set up is shown in Figure 2.3. According to this figure, the major part of the light pulse from a pulsed excitation source is used to excite the sample while a small part of the light pulse is directed to a “start PMT” to create an electrical start pulse, which is directed to the “START input” of the “Time to Amplitude Converter (TAC)”, after passing through a “Constant Fraction Discriminator (CFD)”, which modulates the electric pulse adequately for the TAC unit to recognize its arrival time very precisely. As the start pulse arrives, a linear charging process becomes operational in the TAC and it continues till the arrival of a stop pulse within a pre-set range of time, called the “TAC range”, or otherwise gets automatically discontinued and discharged, if no stop pulse arrives within the pre-set TAC range. The part of the light pulse that excites the sample effectively produces the emission photons. On receiving one such emission photon by the “stop PMT”, an electrical stop Pulse is produced, which is directed to the “STOP input” of TAC after passing through a CFD, for the precise recognition of its arrival time by the TAC. As mentioned before, the arrival of this stop pulse terminates the linear charging of the TAC and the total charge thus accumulated in the TAC generates the “TAC output” pulse having its amplitude proportional to the time difference (Δt) between the arrivals of the START and the STOP pulses at the TAC unit. The TAC output is finally fed into the Multichannel Analyzer (MCA), after

passing it through an Analog-to-Digital Converter (ADC), where a numerical value is generated, which is proportional to the pulse height of the TAC output, and accordingly select a corresponding memory channel of the MCA unit to add a count into that address.²⁸⁹⁻²⁹³

To record a fluorescence decay following TCSPC technique, the whole process discussed above, i.e. from the pulsing of the excitation source to the adding of a count in an appropriate MCA channel, is repeated for extremely large number of times. Accordingly, a histogram of counts is generated in the MCA, where distribution of counts against MCA channel represents the time-dependent probability of a single photon emission by an excited molecule, and accordingly the fluorescence decay of the studied sample, provided the counting rate in the measurement is kept $\leq 2\%$ of the pulsing rate for the excitation light source.²⁸⁹⁻²⁹² This restricted count rate of $\leq 2\%$ effectively means that out of 100 excitation pulses, only about 2 pulses can effectively produce an emission photon for its detection by the stop PMT (hence counted by the MCA), while the rest of about 98 pulses are just not able to produce any emission photon for the detection by the used stop PMT. Such a stringent condition of $\leq 2\%$ count rate is necessary to ascertain that under no situation an excitation pulse can produce more than one photon for its detection by the stop PMT so that the observed histogram of counts in MCA corresponds the true probability distribution of single photon emission and accordingly represents the true fluorescence decay of the studied sample. From experience, it is realized that with count rate $> 2\%$, there arises a small possibility that an excitation pulse can in some occasions produce more than one photons for the stop PMT, of which, only the first photon is counted in the TCSPC method but the second and the other subsequent photons are missed to be counted in the MCA due to incomplete TCSPC sequences. Accordingly, the histogram recorded in the MCA does not represent the correct probability distribution of single photon emission and hence not the true fluorescence decay of the studied sample.²⁸⁹⁻²⁹²

2.5.2. Important Components of a TCSPC Spectrometer

The important components that are integral to a typical TCSPC instrument are briefly discussed below. In our present study, a new generation of the TCSPC instrument, as obtained from Horiba Jobin Yvon IBH, UK, Model Data Station Hub, was used for the TR fluorescence measurements in the sub-nanosecond to nanosecond time domains. In this new generation instrument, some of the components, as are discussed below in general, are avoided for an improved data acquisition strategy. While discussing the typical TCSPC components, concerned changes incorporated in the used IBH instrument are also indicated explicitly for the completeness of the present discussion.

(a) Pulsed Excitation Source: Different high frequency pulsed light sources can be used as the excitation light sources in the TCSPC measurements. In the earlier version of TCSPC instruments, H₂, D₂ or N₂ filled nanosecond flash lamps with repetition rates typically in the tens of kHz range, were used as the excitation light sources. In the new generation TCSPC instruments, including the

IBH instrument used in our study, high frequency (typically 1 MHz) light emitting diodes (LEDs) and diode lasers are commonly used as the excitation sources. In our IBH instrument, on using the diode laser excitation and employing a special PMT based detection module (TBX4 from IBH), the instrument response function (IRF) for the spectrometer is found to be about 190 ps at the full width at half maximum (FWHM). With LEDs as the excitation sources, however, the IRF for the present TCSPC setup is reasonably broad, typically about 1.2 ns (FWHM). In our TCSPC instrument, we also have an MCP-PMT based detector assembly and using this detector in combination with a diode laser excitation, the IRF for our TCSPC setup narrows down to about 100 ps (FWHM).

(b) The Start and the Stop PMTs: In the earlier version of the TCSPC instruments, where nanosecond flash lamps were used as the excitation sources, a part of the excitation light is directed to the “start PMT” to generate the electrical “START” signal for the TAC unit. Since the part of the light directed towards start PMT is quite substantial in intensity, an ordinary PMT with medium gain and low transit time is sufficient to act as the start PMT. Importantly, in the new generation TCSPC instruments, the electric pulses synchronized with the pulsing of the light sources (LEDs or diode lasers) are directly used as the START signals for TAC and thus avoids the use of a start PMT.

In the TCSPC measurement, since each individual photon emitted by the sample needs to be detected by the stop PMT to generate the electrical “STOP” signals for TAC, the stop PMT must be of very high gain. To achieve such high gain, it is required to increase the number of dynodes in the PMT, which in effect increases the transit time and also the transit time spread quite substantially, reducing the time resolution of the TCSPC measurements. Accordingly, in the TCSPC instruments, specially designed PMTs that are having very high gain but not compromised much on transit time are being used. In our TCSPC setup, a peltier cooled detection module (model TBX4 from IBH), which is based on a specially designed high gain Hamamatsu PMT having spectral responses in the 300 to 800 nm region, was used to detect the photons emitted from the studied sample.

(c) Constant Fraction Discriminator (CFD): In the TCSPC measurements, the electrical pulses obtained from the PMT (either START or STOP) are required to be routed through a CFD to achieve two important goals. The first is to improve the signal to noise ratio (S/N) for the measurement by discarding the low amplitude spurious signals, by assigning an appropriate threshold voltage in the CFD. PMT signals having amplitudes higher than the threshold will only be processed to generate the adequate input signals for the TAC. Since the TCSPC measurement is based on the time difference between START and STOP inputs to the TAC unit, the exact timing for the arrival of these pulses to the TAC unit is very essential to be recognized. The second purpose of using the CFD is to achieve the above mentioned goal. For this purpose the PMT signals having amplitudes higher than the threshold value are modulated in a unique manner to generate the zero-crossing pulses such that the zero-crossing points become independent of the original pulse heights and thus can be used accurately for the timing information for the arrival of the START and STOP

pulses to the TAC unit. Thus, the timing error associated to a leading edge discriminator in regard to the heights of the PMT pulses can suitably be eliminated by using a CFD in the TCSPC setup.

(d) Variable Delay Unit: In a TCSPC setup, a “Variable Delay Unit” is used to regulate the arrival of the STOP pulse such that even for the fastest STOP pulse it will reach the TAC unit only after the related START pulse reaches the TAC. Accordingly, a suitable delay time is introduced in the delay unit in the path of the STOP pulse to ascertain that the fluorescence decay (as MCA histogram) of the sample is collected in the appropriate region of the MCA channels, leaving some initial and final channels available for the monitoring of the background counts.

(e) Time-to-Amplitude Converter (TAC): As mentioned before, in a TCSPC setup the role of the TAC unit is to generate a voltage pulse that is proportional to the time delay between the arrivals of the START and STOP pulses in the TAC unit. The TAC functioning in a TCSPC setup is qualitatively shown in Figure 2.4.^{289,291,294-296} In the TAC unit, on receiving the START pulse and following a short preset delay, the timing capacitor of the unit starts charging linearly receiving charges from a constant current source. This process continues till a STOP pulse is received by the TAC within the preset “TAC range”, which terminates this charging and generates an output “TAC pulse” whose height is proportional to the time difference between the arrivals of the START and STOP pulses, i.e. $V_{TAC} \propto \Delta t$. In the cases, where a STOP pulse is not received within the TAC range, the charging process is auto terminated and the capacitor gets auto discharged but without giving any TAC pulse but rather to reset the TAC for the next START pulse. The TAC pulse produced on receiving a STOP pulse within the TAC range is routed to the MCA through an ADC unit whereby the TAC signal is converted into a numerical value to select an appropriate MCA channel to add a count into that address. These sequences are repeated for extremely very large number of times to obtain a statistically reliable histogram of counts to represent the fluorescence decay of the sample. In a TCSPC setup, different TAC ranges like 50, 100, 200 or 500 ns are suitably selected depending on the studied sample to record the fluorescence decay within the available MCA channels.

In a TCSPC measurement, since the counting rate is kept exceptionally low ($\leq 2\%$), in more than 98% of the occasions, even though the START pulse arrives at the TAC and the charging process gets initiated, there is no emission photon to generate the STOP pulse that would stop the the TAC charging and thus would add up a count in the MCA. Such cases of non-fruitful TAC charging would cause unnecessary fatigue to the timing capacitor of this unit, especially when the pulsing rate of the excitation source is very high, say 1 MHz, as in the cases of the typical LED or diode laser sources. To avoid this undue taxing for TAC, in the modern TCSPC instruments the measurement sequence is applied in the reverse mode whereby the stop PMT signal is used as the START input for the TAC while the synchronized electric pulse from the excitation source is used as STOP input for TAC. In the MCA channels, the fluorescence decay is thus recorded in its reverse form, which is then converted into its normal form using an appropriate electronic operation

(reversing) for the further inspection and analysis. To be mentioned here that in our TCSPC setup the TAC, ADC and MCA units are integrated into a single PC card. A dedicated PC set along with the controlling software from IBH is used to record, display and store the the fluorescence decays of the samples. Suitable analysis software is also obtained from IBH to fit the measured decay curves.

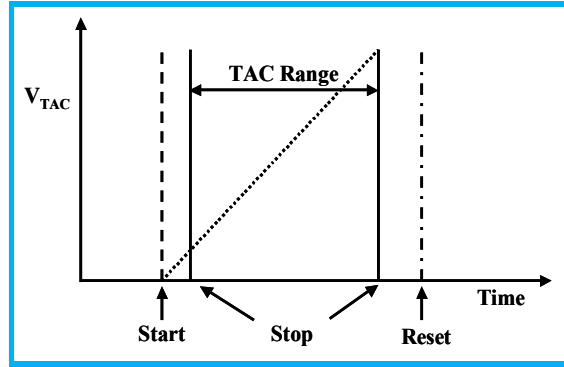


Figure 2.4. Conceptual presentation of how a TAC unit works. Start is the arrival of the START pulse that initiates TAC charging. Stop is the arrival of a STOP pulse that terminates TAC charging. TAC range is the time interval for which arrivals of the STOP pulses are processed for TCSPC measurement. Reset is the auto-discharge of TAC if no STOP pulse arrives within TAC range.

(f) Multichannel Analyzer (MCA): The function of MCA in the TCSPC setup is to store the time-correlated information between the START and STOP pulses, in the form of the counts in the appropriate channels, as determined by the heights of the TAC output pulses. Thus is done by using an ADC in combination with the MCA, as we have mentioned earlier. To measure a fluorescence decay curve, the MCA in the TCSPC instrument is used in its conventional Pulse Height Analysis (PHA) mode, whereby the TAC output pulses are sorted in accordance to their heights, and accordingly the counts are added in the appropriate MCA channels. In the TCSPC measurement, however, if one requires the recording of the time-resolved emission spectra (TRES) of the studied sample, the MCA needs to be used in its Multichannel Scaling (MCS) mode. In this mode of operation, for a pre-selected time duration, only those TAC output pulses are counted for which the pulse heights fall within a small pre-defined voltage range, say from V_{TAC} to $(V_{TAC} + \Delta V)$, and the total count thus obtained are stored in a single MCA channel. The above sequence of measurements are repeated and synchronized with the step-wise changes in the measuring emission wavelengths, covering the whole spectral range of the sample studied. The histogram thus obtained is the TRES for the time delay equal to the pre-defined voltage V_{TAC} . Similar measurements are done with different pre-defined voltage V_{TAC} values to record a series of TRES for the studied sample.

2.5.3. Time Calibration of the MCA Channels in a TCSPC Spectrometer

In the TCSPC setup, since the fluorescence decays are recorded as the histograms in the MCA channels, it is essential to have the exact time calibration for the MCA channels to estimate the

fluorescence lifetimes of the studied samples. Time calibration of the MCA channels is carried out by using a number of accurately time calibrated delays at the variable delay unit in the path of the STOP pulses (cf. Figure 2.3).^{289,291,297} To do this MCA calibration, either the stop or the start signal is splitted into two, one is fed to the start input of the TAC and the other is passed through the precisely calibrated delay introduced in the delay unit before it is fed to the stop input of the TAC. In this case, since both the START and STOP inputs are originated from the same source, depending on the TAC range used and the precise delay introduced in the delay unit, counts are collected only at a specific single channel in the MCA. Accordingly, depending on the different values of the precisely calibrated delays in the delay unit, different MCA channels are selected to collect the counts, where the difference between the two consecutive selected channels is the representative of the corresponding time delays introduced in the delay unit. The histogram thus recorded in the MCA are analyzed suitably to estimate the time calibration for the MCA channels used in the TCSPC measurement.

2.5.4. Analysis of the Fluorescence Decays Recorded using TCSPC Measurement

In a TCSPC spectrometer, the light pulses used for the excitation of the samples always have a finite time width. Further, the overall detection system of the TCSPC spectrometer also has a finite response time. Thus, the fluorescence decay curve, $I(t)$, obtained experimentally through TCSPC measurement, is not the true fluorescence decay, $G(t)$, but a convolution of $G(t)$ caused by the instrument response function, $P(t)$, of the used TCSPC setup, also often called the excitation time profile. Considering that $P(t)$ is constituted of a large number of sequential δ -pulses, the observed decay curve, $I(t)$, can be expressed as the convolution integral of $G(t)$ and $P(t)$ as,^{289-293,298-300}

$$I(t) = \int_0^t P(t') G(t - t') dt' \quad (2.7)$$

Since both $I(t)$ and $P(t)$ are measured experimentally, eq. 2.7 can be used suitably to perform the convolution analysis to extract the true fluorescence decay $G(t)$ of the sample. In this analysis, a $G(t)$ function is first presumed, which is then convoluted using the experimental $P(t)$ following eq. 2.7 to calculate a fitted curve, $Y(t)$, which is compared with the experimental decay curve, $I(t)$.^{289-291,298,299} The variables in the presumed $G(t)$ function are iteratively changed in the analysis until the calculated $Y(t)$ matches nicely with the experimental $I(t)$ curve, representing a fit for the observed decay curve.

Considering that the fluorescence decay of a sample is usually exponential in nature (cf. eq. 2.5), in the convolution analysis, the $G(t)$ function is usually considered as a sum of exponentials as,

$$G(t) = \sum_i B_i \exp(-t/\tau_i) \quad (2.8)$$

where B_i is the pre-exponential factor and τ_i is the fluorescence lifetime for the i^{th} decay component. The success of a convolution analysis and thus the acceptance of the fit for an experimental decay are judged from the consideration of different statistical parameters, as are discussed below.

(a) Reduced Chi-square (χ_r^2) Value: The reduced chi-square (χ_r^2) value associated to a convolution analysis of an experimental decay is defined as,

$$\chi_r^2 = \frac{\sum_i W_i [Y(i) - I(i)]^2}{(n - p)} \quad (2.9)$$

where $Y(i)$ and $I(i)$ represent the counts at the i^{th} channel of the fitted and experimental curves, respectively, $W_i = 1/I(i)$, is the weighting factor of the count in the i^{th} channel, n is the number of data channels (MCA channels) used for the decay in the analysis and p is the degrees of freedom in the analysis, which is equal to the number of variables in the $G(t)$ function. For a perfect fit of an experimental decay using convolution analysis, the χ_r^2 value should expectedly be very close to unity. Form experience it is realized that a χ_r^2 values between 1.00 to 1.20 invariably represent very good fittings for the TCSPC based experimental fluorescence decays.²⁸⁹⁻²⁹³

(b) Distribution of the Weighted Residuals: To understand the goodness of a convolution analysis of a TCSPC based fluorescence decay, along with the χ_r^2 value, the other important statistical parameter considered very seriously is the distribution of the weighted residuals among the data channels used. For the i^{th} data channel, the weighted residual, $r(i)$, is defined as,

$$r(i) = \sqrt{W_i} [Y(i) - I(i)] \quad (2.10)$$

where $W_i = 1/I(i)$, is the weighting factor for the count in the i^{th} channel, while $Y(i)$ and $I(i)$ represent the counts in the fitted curve and the experimental decay, respectively, at the corresponding data channel. For a good fit, the $r(i)$ should be randomly distributed about the zero line for the whole region of the data channels for the decay curve used in the convolution analysis.

2.6. Fluorescence Up-conversion Measurements

Using TCSPC technique, even on employing a very fast detection module like the MCP-PMT setup, the shortest fluorescence lifetime measureable is only in the range of about few tens of picoseconds.^{289,291,301} Another fast technique sometimes used to measure fluorescence lifetime values in the similar time scale is the streak camera,^{289,291,301} where best time-resolution achieved can be in the range of ~ 10 ps. However, to measure the fluorescence lifetimes of the samples shorter than this range, i.e. in the sub-picosecond to femtosecond region, none of the above techniques can be useful. The best method to get ultra-short time-resolution, very similar to the width of the ultrafast laser pulses, is the nonlinear phenomena based techniques for time gating, as achieved through the use of the high energy ultrashort laser pulses.³⁰²⁻³⁰⁶ The frequency mixing techniques, especially the up-conversion method, first introduced by Mahr and Hirsch,³⁰⁵ is one of the most extensively used procedure to achieve ultrafast time-resolution in the fluorescence measurements. In this technique, the emission from the sample is mixed with a part of the ultra-short laser pulse in a nonlinear crystal to generate the sum frequency of the two light. As this mixing process takes place only during the

temporal overlap of the ultra-short laser pulse with the fluorescence emission, this technique provides a time-resolution quite comparable to the width of the ultra-short laser pulse, called the gate pulse in the process of fluorescence up-conversion technique.

2.6.1. Brief Description of the Present Fluorescence Up-conversion Setup

Figure 2.5 shows the schematic diagram of the femtosecond fluorescence up-conversion setup used in the present study. This setup uses a mode-locked Ti:sapphire oscillator (from CDP Inc. Russia) as the ultrafast laser source, which is optically pumped by a diode pumped solid state laser obtained from Coherent (Verdi, 5W at 532 nm). The Ti:sapphire laser operates with its fundamental wavelength at around 800 nm, having pulse width of ~ 50 fs, and repetition rate of 82 MHz. In the up-conversion measurements, depending on the sample to be studied, the fundamental laser light is converted either to its second harmonic (~ 400 nm) or third harmonic (~ 266 nm), passing the laser beam through a properly phase matched beta barium borate (BBO) crystals. The so produced higher harmonic light is separated from the residual fundamental light by using a dichroic mirror, whereby the higher harmonic light is used to excite the sample and the residual fundamental of the laser light is used as the gate pulse to up-convert the fluorescence obtained from the sample.^{307,308}

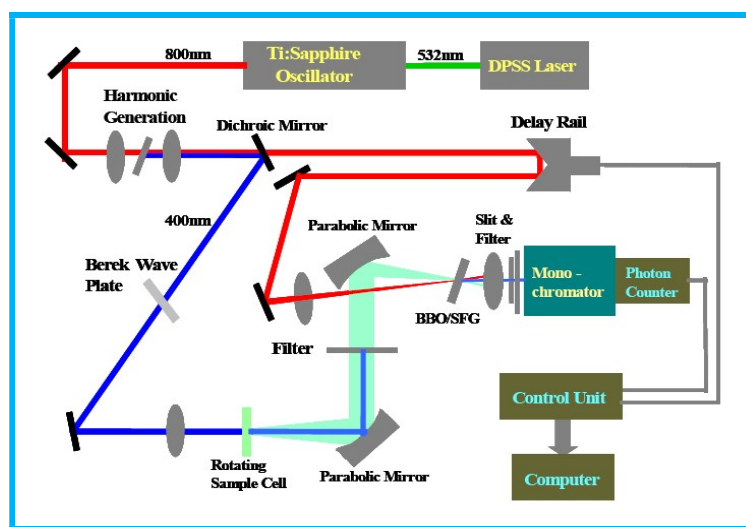


Figure 2.5. Schematic diagram of the femtosecond fluorescence up-conversion setup used in the present study. The functioning of different components are described in the main text below.

In the present setup, fluorescence from the sample is collected using two parabolic mirrors and the collected light focused into a phase-matched 0.5 mm BBO crystal. In this nonlinear crystal, the fluorescence is up-converted by using the fundamental laser light as the gate pulse, also focused into this crystal, both spatially and temporally, with regard to the focused fluorescence beam. To vary the delay of the gate pulse with respect to the excitation pulse, and thus to up-convert different time slices of the fluorescence decay of the studied sample, the gate pulse is made to pass through an optical delay rail. The emergent light beam from the BBO crystal after up-conversion is passed

through an appropriate band-pass filter to block the excitation and the gate beam first and subsequently the beam is passed through a double monochromator and the spectrally selected up-converted light is detected by using a PMT based photon counting setup. In these measurements, the intensity of the laser light is kept reasonably low to ensure the linear dependence of the fluorescence intensity of the sample with the excitation intensity and also avoid any adverse effect of photo-degradation of the sample during the measurement. Further, to minimize the photo-degradation of the studied samples, the samples are taken in a very small thickness (0.4-1.0 mm) rotating quartz cell, where sample cell is continuously rotated during measurement to avoid the localized heating of the sample and consequently to reduce the photo-degradation of the sample very significantly.

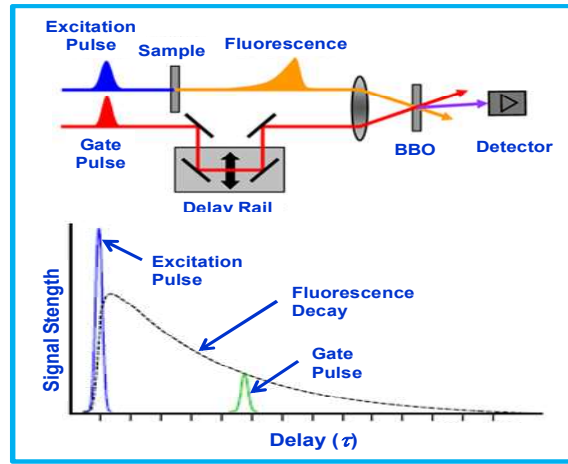


Figure 2.6. Schematic presentation of the spatial and temporal overlap of the fluorescence light and the gate pulse along with the working principle of the fluorescence up-conversion method.

At any given time delay (τ) of the gate pulse with respect to the excitation pulse, there will be the up-conversion of a small time-slice of the fluorescence decay as determined by the temporal overlap of the two light beams, as shown schematically in Figure 2.6. The intensity of this up-converted light, $I_{sum}(\tau)$, is determined by the correlation function of the fluorescence intensity, $I_f(\tau)$, and the time profile of the gate pulse, $I_{gate}(t)$, and would be expressed as,^{309,310}

$$I_{sum}(\tau) = \int I_f(\tau) I_{gate}(t - \tau) dt \quad (2.11)$$

As suggested from this equation, the sum frequency signal will be produced only when the fluorescence light and the gate pulse are temporality coincided into the non-linear crystal and the time dependent changes in the intensity of the sum frequency signal $I_{sum}(\tau)$ will represent the fluorescence decay of the concerned sample.

In the up-conversion instrument, the width of the gate pulse can in effect become the time resolution for the concerned measurement, though in reality the overall detection system would actually determine the achieved time resolution as displayed by the measured instrument response function (IRF), for which the full width at half-maximum (FWHM) is often somewhat higher than the width of the gate pulses used. In the present experimental setup, the instrument response

function (IRF) was independently measured following the cross correlation of the excitation pulse with the fundamental laser pulse. The IRF thus obtained show a Gaussian intensity profile with its FWHM typically about 220 fs. In the present experimental setup, to vary the excitation wavelength for the studied sample, the Ti-sapphire laser output was tuned adequately to some extent such that the second harmonic output is varied in the range of about 390 nm to about 430 nm. All the experiments in the present study were carried out at the magic angle condition to avoid any influence of the rotational relaxation process of the fluorophore on the measured fluorescence decay. Measured kinetic traces from the up-conversion measurements were suitably analyzed following convolution method, as we have discussed before in regard to the analysis of the TCSPC data.

2.7. Fluorescence Anisotropy Measurements

In a homogeneous solution, the ground-state fluorophores are all oriented randomly. When such a sample solution containing isotropically orientations chromophoric molecules is irradiated with a polarized light beam, due to preferential excitation of the molecules having transition dipoles oriented along the polarization axis of the light beam, an anisotropic distribution of the excited chromophoric molecules is created in the solution, which can be detected easily through the fluorescence anisotropy measurement. To be mentioned here that the irradiation of an isotropic solution by a polarized light beam also creates an anisotropic distribution in the ground state of the molecules in the solution. We, however, do not consider this ground state anisotropy, as our interest is to carry out fluorescence anisotropy only, which depends solely on the anisotropic distribution of the chromophoric molecules in the excited state.

As mentioned above, the origin of fluorescence anisotropy is the selective excitation of the suitably oriented chromophores in the solution, which can be apprehended better from the following discussion. From quantum chemistry, it is known that both absorption and emission processes are associated with the corresponding transition dipoles, oriented very specifically in the structural framework of the chromophoric molecule. Though in some molecular systems the absorption and emission transition dipoles may coincide with each other, in general, however, they can be oriented at different directions making an angle β between the two. On using a plane polarized excitation light beam, the probability of the absorption process for the chromophoric molecules in the light path having their absorption transition dipoles oriented at an angle θ with respect to the electric field of the excitation light beam is proportional to the function, $\cos^2\theta$. Accordingly, the probability of absorption is maximum when $\theta = 0^\circ$ and it is zero when θ is 90° .^{284,289,291,311} Obviously thus, as the plane polarized light beam passes through the isotropic solution, an ensemble of excited state population is created in the system that is highly anisotropic in nature, which can be conceptually shown as in Figure 2.7. Similar to the absorption process, the probability of an excited molecule to emit a photon with the electric field vector making an angle θ with the emission transition dipole of

the molecule is again proportional to the function $\cos \theta$. Thus, due to orientation selective excitation and emission processes, the fluorescence obtained from a homogeneous solution following its excitation by a polarized light would be highly polarized or anisotropic in nature.

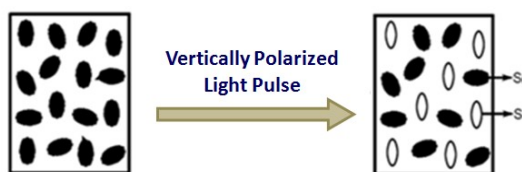


Figure 2.7. Creation of the anisotropic distribution of the chromophoric molecules in the excited state (and also in the groundstate) as the isotropic ground state system is irradiated with a vertically polarized excitation light pulse.

In the case of a dilute solution, where excitation energy transfer among chromophoric molecules cannot contribute in the depolarization process of the excited species, the decay in the fluorescence anisotropy of the sample occurs mainly through the rotational relaxation of the excited molecules. In this situation, the fluorescence anisotropy measurement can provide the information about the average angular displacement of the excited fluorophores at a given time subsequent to their excitation and this angular displacement is determined directly by the rate of the rotational diffusion of the excited molecules in the given system. Since the rotational diffusion of a molecule in a solution is dependent on the size and shape of the chromophoric unit along with the viscosity of the medium or the rigidity of the local microenvironment, from the discussions above it is clear that the fluorescence anisotropy measurements can be applied suitably to gather information regarding the local microenvironments of the complex systems like surfactant aggregates, supramolecular complexes, supramolecular systems, and many others.

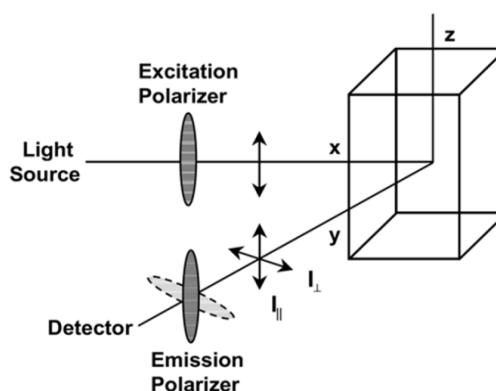


Figure 2.8. Schematic presentation of the methodology of fluorescence anisotropy measurement, keeping the electric vector of the plane polarized excitation light oriented along z-axis and recording the I_{\parallel} and I_{\perp} signals keeping the emission polarizer oriented parallel and perpendicular to the polarization of the excitation light.

Fluorescence anisotropy can be investigated using both steady-state (SS) and time-resolved (TR) fluorescence measurements. In SS measurement, the sample is continuously irradiated with a

constant intensity vertically polarized light beam and the fluorescence spectra are recorded for both parallel and perpendicular orientations of the emission polarizer with respect to the polarization plane of the excitation light. Similarly, in the TR measurement, the sample is irradiated with a vertically polarized pulsed light source and the fluorescence decays are collected for both parallel and perpendicular polarizations with respect to the polarization plane of the excitation light. The measurement strategy mentioned above is conceptually represented by Figure 2.8, where the electric vector of the excitation light is oriented along z-axis and the emission signals for the parallel (\parallel) or perpendicular (\perp) polarizations are recorded as I_{\parallel} and I_{\perp} , respectively, keeping the emission polarizer oriented parallel and perpendicular to the polarization of the excitation light, respectively.

In the SS fluorescence anisotropy study, the parameters I_{\parallel} and I_{\perp} represent the SS emission intensity for the parallel and perpendicular polarizations of the emission light, respectively. In this case, the SS or the average fluorescence anisotropy, $\langle r \rangle$, is expressed as

$$\langle r \rangle = \frac{I_{\parallel} - GI_{\perp}}{I_{\parallel} + 2GI_{\perp}} \quad (2.12)$$

where G is the correction factor to nullify the polarization bias of the setup for detection of the light with parallel and perpendicular polarizations. Similarly, in the TR fluorescence anisotropy study, the parameters I_{\parallel} and I_{\perp} represent the TR emission intensity for the parallel and perpendicular polarizations of the emission light, and can be explicitly written as $I_{\parallel}(t)$ and $I_{\perp}(t)$, respectively. Thus, in the TR fluorescence anisotropy study, the fluorescence anisotropy decay is expressed as,

$$r(t) = \frac{I_{\parallel}(t) - GI_{\perp}(t)}{I_{\parallel}(t) + 2GI_{\perp}(t)} \quad (2.13)$$

where G is having the same meaning as mentioned before. In actual experiments, the G factor is estimated independently by keeping the excitation polarizer orientated horizontally, i.e. the electric vector of the excitation light along y-axis, and measuring the fluorescence intensities by keeping the emission polarizer oriented along the vertical (I_{HV}) and horizontal (I_{HH}) directions, respectively, whereby the G factor is given by the intensity ratio as,

$$G = \frac{I_{HH}}{I_{HV}} ; \quad \text{for SS fluorescence anisotropy} \quad (2.14)$$

$$\text{and, } G = \frac{\int I_{HH}(t)dt}{\int I_{HV}(t)dt} ; \quad \text{for TR fluorescence anisotropy} \quad (2.15)$$

To be noted here that the G factor is not a fixed parameter for an instrument but its value is strongly dependent on the measuring emission wavelength. As indicated in eq. 2.12 and 2.13, fluorescence anisotropy is a dimensionless quantity. It is also important to mention here that the denominators in eq. 2.12 and 2.13 actually represent the total emission intensity for the sample.^{284,289,291,311} Thus, the $\langle r \rangle$ or $r(t)$ values in eq. 2.12 and 2.13 are actually the normalized emission anisotropies in the respective cases. Accordingly, the measured fluorescence anisotropy is always independent of the emission strengths of the studied samples.

It is rather simple to correlate the TR fluorescence anisotropy with the SS fluorescence anisotropy, because the average of the time-resolved anisotropy weighted by the intensity decay of the sample provides us the measure of $\langle r \rangle$ obtained from the SS measurement, i.e.^{284,289,291,311}

$$\langle r \rangle = \frac{\int_0^\infty I(t)r(t)dt}{\int_0^\infty I(t)dt} \quad (2.16)$$

For a fluorophore showing single exponential fluorescence anisotropy decay with reorientation time τ_r , the TR anisotropy can be expressed as,

$$r(t) = r_0 \exp(-t/\tau_r) \quad (2.17)$$

where r_0 is the initial anisotropy i.e. the anisotropy at $t = 0$, immediately after the δ -pulse excitation. Using this equation for $r(t)$ and substituting $I(t)$ from equations 2.5, we can use eq. 2.16 to obtain the $\langle r \rangle$ value as,

$$\langle r \rangle = r_0 \left(\frac{\tau_r}{\tau_r + \tau_f} \right) \quad (2.18)$$

where τ_r and τ_f are the time constants for the rotational correlation time and fluorescence lifetime, respectively. It is to be noted here that the eq. 2.18 is valid only if both the intensity decay and the anisotropy decays follow the single exponential functions. For many cases, however, both intensity and anisotropy decays are difficult to be considered as the single exponential functions. In these cases the intensity and anisotropy decays are often expressed as the multi-exponential functions, where bi-exponential functions are most commonly used in majority of the systems.³¹²⁻³¹⁵ Thus, a bi-exponential fluorescence decay is often displayed by a probe dye solubilized in two different environments in a microheterogeneous medium, e.g. as the bound and free dyes in a micellar solution. In these cases the fluorescence decay is expressed as,

$$I(t) = a_1 \exp(-t/\tau_{f1}) + a_2 \exp(-t/\tau_{f2}) \quad (2.19)$$

where τ_{f1} and τ_{f2} are the two lifetime values associated with the two decay components and a_1 and a_2 are their respective pre-exponential factors. Similarly for TR fluorescence anisotropy, a bi-exponential decay can be expressed as,³¹²⁻³¹⁵

$$r(t) = r_0 [\beta_1 \exp(-t/\tau_{r1}) + \beta_2 \exp(-t/\tau_{r2})] \quad (2.20)$$

where τ_{r1} and τ_{r2} are the two time constants (rotational correlation times) associated with the two anisotropy decay components and β_1 and β_2 are the fractional fluorescence contributions arising from the two emitting components or species, respectively. More complex nature of the $I(t)$ and $r(t)$ decays are also occasionally encountered in some specific cases. Though consideration of multi-exponential functions for such decays are often found to be quite suitable to correlate the experimental results, in some cases, however, the functional forms of the decays are indeed very complex, which are beyond the scope of our present discussion. It is however important to mention here that in many of such cases the analysis and interpretation of the observed results are often done

with limitations, especially employing some kind of modeling for the studied systems, where additional information from other supporting measurements is essential to carry out such analysis.

2.8. Time Resolved Transient Absorption Measurements

Photochemically induced transient species like electronically excited molecules, radical intermediates, photodissociation and photoionization products, etc. can be generated in sufficiently high concentrations using very intense short duration light flashes and these species can be investigated and monitored as a function of time using a suitable detection method, e.g. transient absorption technique, as demonstrated by Norrish and Porter in 1949,^{316,317} for which the authors were awarded with Nobel Prize in Chemistry in the year 1967. This methodology as demonstrated initially by Norrish and Porter using high intensity light flashes to create substantial concentrations of short lived transient species in the solution for their easy detection is commonly referred as the "Flash Photolysis Technique". The advanced version of this technique where flash light source is replaced by the high energy fast and ultrafast laser sources to create the transient species in the sample, the technique is recognized specifically as the "Laser Flash Photolysis Technique".

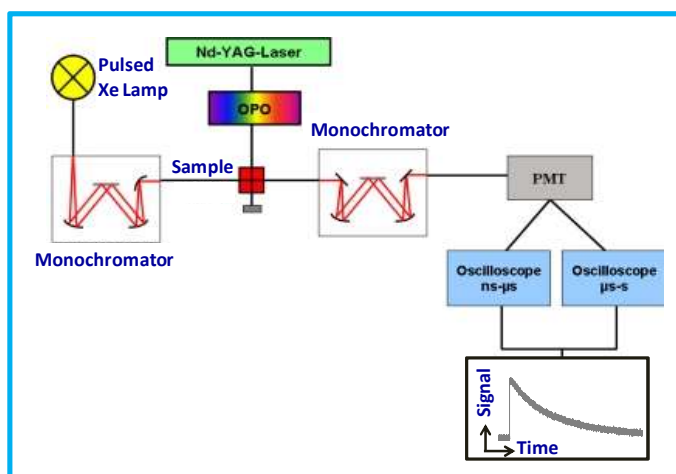


Figure 2.9. Schematic diagram of the nanosecond laser flash photolysis instrument used in the present study.

In a Laser Flash Photolysis Technique, the samples are excited by using a high energy short duration light pulse obtained typically from a nanosecond or picoseconds laser source. The transient species thus produced in the solution are in general detected following the absorption of light by these species from a probe light beam, recorded either in the "Kinetic Spectrophotometry" mode or in the "Time-Resolved Transient Absorption Spectroscopy" mode, depending on the experimental arrangements used in the measurement. While in the kinetic spectrophotometry, the time-dependent absorbance changes of the transient species (i.e. the transient decays) are recorded following the laser excitation, using a suitable digital oscilloscope, in the time-resolved (TR) transient absorption spectroscopy, the transient absorption spectra are recorded directly as a function of the time delay relative to the laser excitation of the sample, using a suitable spectrographic arrangement, mostly

made up of diode array detectors or charge coupled devices (CCDs). In the present work, a nanosecond Laser Flash Photolysis (LFP) setup, Model LP 920, obtained from Edinburgh Instrument, UK, was used for the transient absorption studies. In this LFP setup, a diode pumped picosecond Nd:YAG laser (Model PL 2251c, Ekspla, Lithuania) is used as the primary laser source and depending on the sample to be investigated, a suitable higher harmonic of the Nd-YAG laser (eg. 532, 355 or 266 nm) is produced by using the nonlinear conversion method and used for the excitation of the studied sample. In our present work, the 3rd harmonic (355 nm, 8 mJ, 35 ps) of the Nd:YAG laser was used for the excitation of the studied chemical systems. In the present LFP setup, a pulsed xenon lamp is used as the probe light source and transient signals are recorded in the form their kinetic traces following the kinetic spectrophotometric method. The transient kinetic traces recorded at different monitoring wavelengths are subsequently used to construct the time-resolved transient absorption spectra of the transient species produced in the studied system following its excitation with the intense picosecond laser pulse. A schematic presentation of the Laser Flash Photolysis (LFP) setup used in the present study is shown in Figure 2.9.

2.9. Zeta Potential Measurements

Zeta potential values are the indirect measures of the net charges present on the surfaces of the nanoparticle (NP) systems, which are in the present cases the surface active micellar aggregates. In the present study, the zeta potential measurements were carried out using the instrument model Zetasizer Nano, obtained from Malvern Instruments Ltd., UK. The zeta-potential values were estimated following Henry's equation on the experimental data obtained through electrophoretic light scattering studies, also known as the laser Doppler electrophoresis studies or the phase analysis light scattering studies.³¹⁸

CHAPTER-3

TUNING PHOTOINDUCED ELECTRON TRANSFER REACTIONS IN TETRONIC STAR BLOCK COPOLYMER MICELLES

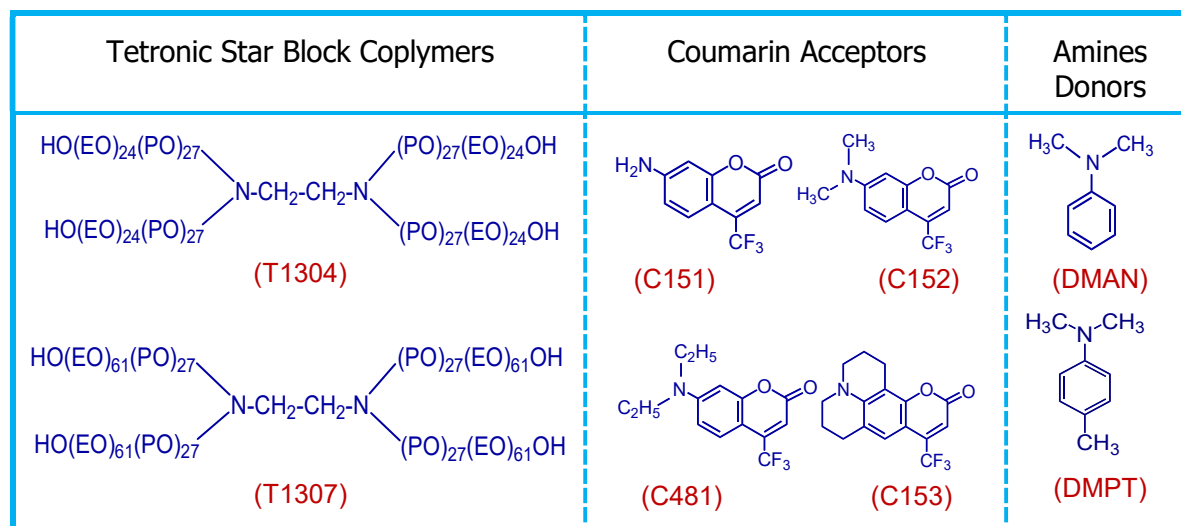
3.1. Introduction

In Chapter 1 we have discussed the chemical constitution and the general micellar characteristics of block copolymer systems made up of the polyethylene oxide (PEO) and polypropylene oxide (PPO) blocks, with specific references to pluronics and tetronics block copolymers (cf. Section 1.7). In the present study, the characteristics of the micelles formed by two tetronic copolymers, namely, tetronic 1304 (T1304) and tetronic 1307 (T1307), have been investigated extensively following different photophysical studies and these so characterized T1304 and T1307 micelles have been used as the constrained reaction media to investigate the photoinduced electron transfer (PET) reactions using suitable coumarin dyes as the electron acceptors and aromatic amines as the electron donors. The micellar assemblies formed by various block copolymers have wide range of applications in pharmaceutical industries, cosmetics, targeted drug delivery mechanisms, catalysis, micro-reactor systems, and many others.³¹⁹⁻³²⁹ While the linear pluronic copolymers, constituted of PEO and PPO blocks with the general formula as $(EO)_n-(PO)_m-(EO)_n$, have been investigated quite extensively, in regard to their self-assembly formations,³³⁰⁻³³⁶ the star shaped tetronic copolymers, constituted of the similar PEO and PPO blocks with general formula as $[(EO)_n-(PO)_m]_2-[N(CH_2)-(CH_2)N]-[(EO)_n-(PO)_m]_2$, are the relatively new entrants in the subject area, and have attracted a lot of research interests in recent years owing to many favorable properties of their self assembled systems as compared to those of the other block copolymer systems.^{151,156-158,160,337-339} It has been realized that due to steric constraints among the four $(EO)_n-(PO)_m$ arms, the tetronic copolymers form relatively more hydrated micelles than the corresponding pluronic copolymers.^{151,156-158,160} It is also revealed that the tetronic micelles have relatively slower rate of dissociation than pluronics and thus can retain the loaded drugs in these micelles for relatively longer times.^{151,340,341} Further, due to the presence of the central diamine moiety in the tetronics, the micellar assemblies of these copolymers are quite sensitive towards solution pH.^{156,157,160} Therefore, the tetronic aggregates are suggested to have better prospects in drug delivery and related applications, where possible stimuli responsive behaviour of these micelles can be useful in loading and unloading the drugs.^{157,327}

Micellar assemblies are known to modulate the kinetics, dynamics, mechanism and energetic of the chemical reactions very significantly. To understand these modulations correctly, it is important to know the micellar characteristics in detail, namely how these micelles are formed, what are the typical physiochemical properties (e.g. micropolarity, microviscosity, etc.) for the microenvironments inside these micelles, how the presence of different additives or the changes in the solution conditions and experimental parameters changes the behavior of these micelles, and so on. Since the microenvironments of the tetronic micelles are not well characterised, in the present study we applied various photophysical measurements to characterise the studied micellar systems quite elaborately before using these micelles as the reaction media to understand their effects in modulating the mechanism, energetic and kinetics of the studied PET reactions. With varying sizes

of the PEO and PPO blocks of pluronic and tetronic copolymers, their micellar microenvironments and thus the course of the chemical reactions in these micellar systems can be modulated very largely, leading to many potential uses in chemical, biological and industrial applications.^{151,156-158,160,337-339}

Chart 3.1. Chemical structures of T1304 and T1307 star block copolymers used to prepare the micellar systems and the coumarin acceptors and aromatic amine donors used for PET studies.



In the present chapter we discuss the characterization of the micellar microenvironments of two structurally related star block copolymers, tetronic 1304 (T1304) and tetronic 1307 (T1307), as investigated using various photophysical measurements. The chemical structures of the two tetronic copolymers are shown in Chart 3.1. Interesting to note that both T1304 and T1307 copolymers have the same $(\text{PO})_m$ block length but their $(\text{EO})_n$ block sizes are largely different.^{153,162,166,342} We have selected these two copolymer systems with the anticipation that the micellar microenvironments of these two copolymers would be substantially different to allow us to understand how the changing micellar characteristics is responsible in modulating the course of the PET reactions. In the present study, a fluorescent probe dye, namely, coumarin-153 (C153), has been used as the local reporter for the micellar microenvironments,^{235,343-347} and thereby we have estimated the micropolarity, microviscosity and solvation dynamics in the corona region of the studied tetronic micelles, following the changes in the absorption, steady-state (SS) emission and time-resolved (TR) fluorescence characteristics of the dye. To the best of our knowledge, this is the first report so far to explore the physicochemical characteristics of the studied starblock copolymer micelles, investigated especially following photophysical measurements. Subsequent to the characterisation of these micellar systems, we subsequently investigated the effectiveness of these micelles to understand the modulations in the kinetics and energetics of bimolecular PET reactions carried out in these micelles using a series of coumarin dyes as the electron acceptors and two aromatic amines, namely, *N,N*-dimethylaniline (DMAN) and *N,N*-dimethyl-*p*-toluidine (DMPT), as the electron

donors. The chemical structures of these coumarin acceptors and aromatic amine donors are also shown in Chart 3.1 along with those of T1304 and T1307 copolymers, for their quick references.

Basic aspects of Marcus' outer sphere ET theory have already been discussed in Chapter 1 with the necessary details.^{10-12,29,100} The most important feature of the Marcus ET theory is the prediction of the inverted parabolic nature of the ET rate constants (k_{et}) with the changing exergonicity ($-\Delta G^0$) of the reactions, commonly referred as the Marcus Inversion (MI) behaviour. Interestingly, the theoretically predicted MI behaviour is realized to remain mostly obscured for bimolecular PET reactions, especially in conventional low viscosity homogeneous solvents under diffusive condition, mainly due to the influence of the reactant diffusions on the observed reaction rates. In these cases, as the diffusion mediated formation of the precursor complex is the rate determining step, the diffusion process dictates the maximum observable rate constant k_q for the bimolecular PET reaction to become at the most equal to the diffusion controlled rate constant k_d , and thus masking the intrinsic ET rate constant k_{et} completely within the observed k_q value, even though intrinsic k_{et} might be very high in the higher exergonicity region.^{29,264,266,267,271,273} Unlike in conventional low viscosity solvents, in constrained surfactant assemblies (e.g., micelles, reverse micelles, vesicles, etc.), however, the reactant molecules are strongly entangled with the surfactant chains resulting their mutual diffusion drastically retarded. In these cases, therefore, the bimolecular PET reactions are compelled to occur mostly under non-diffusing condition, involving mainly those pre-existing donor-acceptor pairs where the reactants are already within the interaction zone (i.e. reaction sphere) at the point of photoexcitation of the sample.^{127,161,236,347-351} In such constrained microheterogeneous media therefore the kinetics and mechanism of the bimolecular PET reactions are expected to display quite different behaviour than observed in conventional homogeneous solvents. In fact in the literature, bimolecular PET reactions in different constrained media have shown to display the MI behaviour quite easily, though for the similar PET systems no MI could be observed in low viscosity and polar conventional homogeneous solvents.^{127,161,236,347-351} With these perspectives, in the present study bimolecular PET reactions have been carried out in the micellar media formed by the two tetronic copolymers, T1304 and T1307, using different coumarin dyes as the electron acceptors and two aromatic amines as the electron donors, as are shown in Chart 3.1. Since the microenvironments of these tetronic micelles are not very well characterized in the literature, in this study we have first characterised the microenvironments of T1304 and T1307 micelles elaborately following various photophysical measurements, and subsequently we carried out the PET reactions in these micelles to understand various modulations induced by these constrained media on the studied PET reactions, especially in regard to the observation of the MI behavior for the studied PET reactions. In the present context, we have also investigated the effect of the added salt, NaCl, in tuning the PET reactions in tetronic micellar media, because such tuning of chemical reactions can have many applied implications.

3.2. Materials and Methods

The T1304 and T1307 starblock copolymers (cf. Chart 1) were received as the gifts from BASF Corp., Parsippany, NJ, USA. The laser-grade coumarin dyes, coumarin-153 (C153), coumarin-152 (C152), coumarin-481 (C481) and coumarin-151 (C151), were obtained from Exciton, USA, and were used as received. The aromatic amines, *N,N*-dimethylaniline (DMAN) and *N,N*-dimethyl-*p*-toulidine (DMPT) were obtained from Sigma, and were vacuum distilled just before use. Nanopure water, having a conductivity of $<0.1 \mu\text{S cm}^{-1}$, was obtained from a Millipore Gradient A10 system and used for solution preparations. Organic solvents used in the present study were of spectroscopic grade and obtained from Spectrochem, India.

Experiments were carried out in aqueous 5% (w/v) T1304 and T1307 solutions that correspond to the two copolymer concentrations as 4.76 mM and 2.78 mM, respectively. To start with, 10% (w/v) stock solutions of the copolymers were first prepared, taking the required amounts of the copolymers gravimetrically (using a microbalance from Citizon, India) in a sealed container, adding some water to these samples, and keeping the mixtures overnight under refrigeration for complete dissolution. The total volumes of these solutions were subsequently adjusted to make the stock solutions exactly 10% (w/v) for the respective cases. Subsequently, these stock copolymer solutions were diluted to prepare 5% (w/v) copolymer solutions for the experimental measurements. In the present study, concentrations of the coumarin dyes were always kept quite low, less than 5 μM , which is much smaller than the concentrations of the micelles present in the experimental solutions (typically $\sim 130 \mu\text{M}$ for T1304 and $\sim 60 \mu\text{M}$ for T1307). Accordingly, it is ascertained that only a small fraction of the micelles are actually occupied with a dye molecule and majority of the micelles free from any dye molecule inside. Accordingly, in these experimental solutions, the probability micelle containing more than one dye molecules inside can be considered to be just negligible.^{127,161,347,352-354} All the measurements in the present study were carried out at 30°C, which is above the CMT of both T1304 and T1307 systems in their 5% (w/v) solutions.^{162,166,342} Further, at this temperature, different dimensional parameters for both T1304 and T1307 micelles are well reported in the literature,^{162,166,342} making these values very useful in analysing, correlating and interpreting the results obtained in the present study.

Experimental details of ground state absorption, SS emission, and TR fluorescence studies have already discussed in Chapter 2. In the present study a 406 nm pulsed diode laser (~ 100 ps, 1 MHz) was specifically used to carryout TR fluorescence measurements, whereby instrument response function (IRF) for the TCSPC setup is found to be ~ 190 ps at FWHM. For fluorescence decay measurements, magic angle configuration (at 54.7° orientation of the emission polarizer relative to vertically polarized excitation) was used to avoid the effect of rotational orientation of the dyes on the observed decay traces. These decays were fitted following convolution analysis, the details of which are discussed before in Chapter 2, Section 2.5.4. TR fluorescence anisotropy measurements were carried out following the method discussed in Chapter 2, Section 2.7. For

salvation dynamic studies, the procedure given by Maroncelli and Fleming³⁵⁵ was applied as discussed in Chapter 1, Section 1.6. In these cases, the wavelength dependent fluorescence decays of the probe dye (C153) were fitted as a tri-exponential function and the fitting parameter were used to construct the TR emission spectra (TRES) and the dynamic Stokes' shift correlation function, $C(t)$, which was eventually analysed suitably to estimate the relaxation times for the studied systems.³⁵⁵

3.3. Results and Discussion

3.3.1. Characterization of the Microenvironments in T1304 and T1307 Micelles

3.3.1.1. Micropolarity Estimations in T1304 and T1307 Micellar Systems: In order to estimate the micropolarity in the T1304 and T1307 micellar systems, C153 dye was used as the solvatochromic fluorescent probe.^{161,235,343-347} Using this probe, the SS fluorescence spectra were recorded in different conventional solvents of varying polarity (dielectric constant, ϵ)⁵⁷ along with those in the studied T1304 and T1307 micelles, as are shown in Figure 3.1A for a comparison. It is evident from this figure that the emission maximum (λ_{max}) of the dye undergoes a red shift as the polarity of the solvent is increased. Comparison of the emission spectra in T1304 and T1307 micelles with those in other conventional solvents clearly indicate that the spectra in the studied micelles appear in between the spectra obtained in ethyl acetate (EA, $\epsilon = 6.02$) and methanol (MeOH, $\epsilon = 32.7$) solvents, and resemble quite closely with that observed in *n*-decanol (DeOH, $\epsilon = 8.10$) solvent. With these initial observations, the emission spectra of C153 dye were subsequently recorded in a series of EA-MeOH solvent mixtures with varying co-solvent compositions, ensuring a systematic polarity change of these mixed solvents in sufficiently small steps, covering especially the polarity around that of DeOH solvent. From the observed spectra, a calibration curve was constructed by plotting the emission maxima ($\bar{\nu}_f$, in wavenumbers) of the spectra against the Lippert-Mataga solvent polarity parameter, Δf , defined as,^{118,119,148,347,356}

$$\Delta f = \left(\frac{\epsilon - 1}{2\epsilon + 1} - \frac{n_r^2 - 1}{2n_r^2 + 1} \right) \quad (3.1)$$

where, ϵ and n_r are the static dielectric constant and refractive index of the solvent used. While for the pure solvents the ϵ and n_r values were obtained from reported literature,³⁵⁷ for the mixed solvent systems, the effective ϵ and n_r values were estimated using the following relations,^{92,127,347,356-360}

$$\epsilon_{eff} = f_{EA}\epsilon_{EA} + f_{MeOH}\epsilon_{MeOH} \quad (3.2)$$

$$n_{r,eff}^2 = f_{EA}n_{r,EA}^2 + f_{MeOH}n_{r,MeOH}^2 \quad (3.3)$$

where f_i , ϵ_i and n_i represent the volume fraction, dielectric constant and refractive index of the concerned co-solvent, respectively.

The calibration curve obtained by correlating the $\bar{\nu}_f$ values against the Δf values of the solvents is quite a linear in nature, as shown in Figure 3.1B. Using this calibration curve, the ϵ

values for the localization sites of C153 dye in T1304 and T1307 micelles are estimated as about 7.2 and 11.3, respectively, assuming n_r value in the micellar systems quite similar to that of water ($n_r = 1.33$).^{125,127,361-364} Understandably, for the micellar systems, the core regions are quite nonpolar in nature, quite similar to those of the hydrocarbon solvents, while the outer aqueous phase is highly polar in nature. Therefore, the estimated ε values in the two tetronic micelles indicate that the probe dye preferentially resides in the corona region of these micelles where the micropolarities are in the intermediate region. That the estimated ε value is significantly higher in T1307 micelle than in T1304 micelle suggests that the corona layer of the former micelle is relatively more hydrated than the latter. This observation corroborates nicely with the larger (EO)_n block size in T1307 copolymer than T1304, responsible for the formation of the corona regions of the studied tetronic micelles.

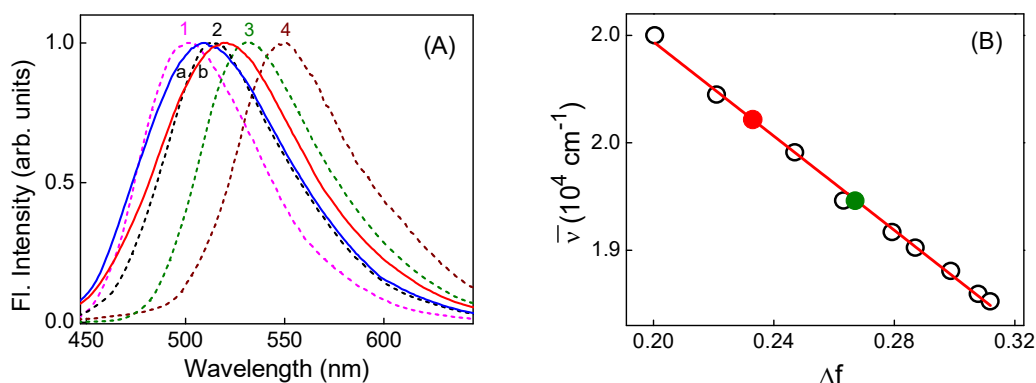


Figure 3.1. (A) Normalized fluorescence spectra of C153 dye; The dotted lines (1-4) are in EA, decanol, MeOH and water, respectively. The solid lines (a-b) are in 5% (w/v) T1304 (blue) and T1307 (brown) micelles, respectively. (B) Calibration plot (open circles) for the solvent polarity function (Δf) obtained through emission maxima (in cm^{-1}) of C153 dye in different EA-MeOH solvent mixtures; green and red closed circles represent T1307 and T1304 micelles, respectively.

3.3.1.2. Microviscosity Measurements in T1304 and T1307 Micelles: As discussed in Chapter 2, Section 2.7, fluorescence anisotropy studies, especially the TR fluorescence measurements, can provide valuable information regarding the microviscosity of the local microenvironments of the complex microheterogeneous systems.^{127,128,235,277,365} In the present study, to understand the microviscosity at the localization site of the fluorescence probe C153 in the T1304 and T1307 micelles, the fluorescence anisotropy decay traces of the probe dye were recorded in these micelles and observed results are shown in Figure 3.2.

In both T1304 and T1307 micelles, the fluorescence anisotropy decay traces for the probe dye follow the bi-exponential function as,

$$r(t) = r_{01} \exp(-t/\tau_{r1}) + r_{02} \exp(-t/\tau_{r2}) \quad (3.4)$$

where τ_{r1} and τ_{r2} are the two rotational relaxation times and r_{01} and r_{02} are their respective initial anisotropies. Using the fitted parameters, the average rotational relaxation times, $\langle \tau_r \rangle$, were estimated using the following relation,

$$\langle \tau_r \rangle = A_{r1}\tau_{r1} + A_{r2}\tau_{r2} \quad (3.5)$$

where A_{r1} and A_{r2} are the rotational relaxation time weighted relative contributions for the respective components (cf. Section 2.7 in Chapter 2). The anisotropy decay parameters estimated for C153 dye in T1304 and T1307 micelles are listed in Table 3.1.

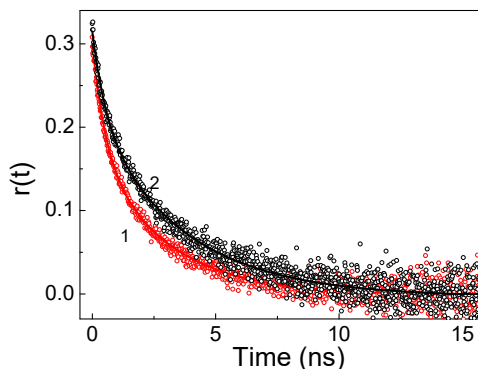


Figure 3.2. Fluorescence anisotropy decays (open circles) of C153 dye in (1) 5% (w/v) T1307 and (2) 5% (w/v) T1304 micelles. Continuous curves represent their respective bi-exponentials fits.

Table 3.1. Anisotropy decay parameters for C153 probe in T1304 and T1307 micellar systems.

Micellar media	τ_{r1} (ns) ^a	$(r_{0,1})^b$	A_{r1} (%) ^c	τ_{r2} (ns)	$(r_{0,2})^b$	A_{r2} (%) ^c	$\langle \tau_r \rangle$ (ns)	τ_w (ns)	η_m (cP) ^d
T1304	0.55	0.10	6.3	3.58	0.22	93.7	3.39	1.54	58
T1307	0.55	0.17	9.0	2.96	0.09	91.0	2.74	1.48	47

^aError limit in τ_{r1} and τ_{r2} values are ± 0.03 ns; ^bError limit in $r_{0,1}$ and $r_{0,2}$ values are ± 0.01 ;

^c $A_{ri}(\%) = A_{ri} \times 100$; ^dCalculated following eq. 3.9

For a probe dye dissolved in the corona region of a micelle, there exist three different motions that can contribute to the overall fluorescence anisotropy decay for the probe dye. These motions are: (i) the wobbling motion of the probe at the solubilization site in the micelle, (ii) the lateral diffusion of the probe along the spherical shell constituting the micellar corona, and (iii) the rotational motion of the whole micelle containing the probe dye. Considering the correlations of the above three motions, it is suggested that a probe dye dissolved in the corona region of a micelle would effectively experience a two-step model for its overall rotational relaxation process and accordingly the fluorescence anisotropy decay would follow a bi-exponential function,^{274,275} as has been established very convincingly in many previous studies carried out in different conventional and pluronic micellar systems.^{128,235,277,348,365} According to the two-step model, the two rotational relaxation times, τ_{r1} and τ_{r2} , as estimated experimentally from the fluorescence anisotropy decay for a probe dye in a micellar system, would be explicitly given as,

$$\frac{1}{\tau_{r1}} = \frac{1}{\tau_w} + \frac{1}{\tau_{r2}} \quad (3.6)$$

$$\frac{1}{\tau_{r2}} = \frac{1}{\tau_L} + \frac{1}{\tau_M} \quad (3.7)$$

where τ_W , τ_L and τ_M are the independent rotational correlation times for: (i) the wobbling motion of the dye at its localization site, (ii) the lateral diffusion of the dye in the corona region, and (iii) the rotation of the whole micelle, respectively. Using the experimentally observed τ_{r1} and τ_{r2} values and applying eq. 3.6, the τ_W values for the wobbling motions of the C153 dye in the corona regions of T1304 and T1307 micelles are estimated to be ~ 1.54 ns and ~ 1.48 ns, respectively. For the τ_M values representing the rotation of the whole T1304 and T1307 micelles in the solution, we can use the Stokes-Einstein-Debye (SED) relation, whereby the correlation time τ_M is expressed as,^{277,365-367}

$$\tau_M = \frac{4\pi r_M^3 \eta}{3k_B T} \quad (3.8)$$

where η is the viscosity of bulk water, k_B is Boltzmann's constant, T is the absolute temperature, and r_M is the radius of the micelle. Thus, using eq. 3.8, the τ_M values for T1304 and T1307 micelles are estimated as ~ 304 ns and ~ 320 ns, respectively. Since these τ_M values are much higher than the experimentally observed τ_{r2} values (cf. Table 3.1), we can assume from eq. 3.7 that $\tau_L \approx \tau_{r2}$. While the similar τ_{r1} and τ_W values both in T1304 and T1307 micelles suggest that the wobbling motion of the probe dye in these micelles are quite similar, the significantly higher τ_{r2} and τ_L values in T1304 micelle than in T1307 micelle suggest that the lateral diffusion of C153 dye is comparatively more retarded in the former micelle than in the latter. These results are in accordance with the results obtained from the micropolarity measurements, as discussed in the previous section, indicating that the corona layer of T1304 micelle is relatively less hydrated than the T1307 micelle.

Using the average rotational correlation times, $\langle \tau_r \rangle$, and the hydrodynamic volume of the probe C153 dye, V_h , the microviscosity values, η_m , in the corona regions of the studied T1304 and T1307 micelles were estimated following the Stokes-Einstein-Debye (SED) relation relation as,^{168,169,277,361,365-369}

$$\langle \tau_r \rangle = \frac{\eta_m V_h}{k_B T} \quad (3.9)$$

Calculating the hydrodynamic volume V_h of the probe dye following Edward's volume addition method,³⁷⁰ which is obtained to be about 245 \AA^3 , the microviscosity values (η_m) in the corona region of T1304 and T1307 micelles are estimated as ~ 58 cP and ~ 47 cP, respectively. Relatively lower η_m value in the T1307 micelle than in T1304 micelle is directly in accordance with the higher degree of hydration for the corona region of the former micelle than the latter.

3.3.1.3. Solvation Dynamics Studies in T1304 and T1307 Micelles: Solvation dynamics in T1304 and T1307 micelles were investigated through dynamic Stokes' shift studies, following the procedure discussed in Chapter 1, Section 1.6. Figures 3.3A and B show the representative fluorescence kinetic traces for the probe dye C153 in 5% (w/v) T1307 and T1304 micelles,

respectively, recorded at 10 nm intervals, covering the whole spectrum of the dye (450-650 nm) in these micelles. As it is indicated, the kinetic traces are quite fast at the shorter monitoring wavelengths but, the traces gradually become slower and also start accompanying with an initial growth component, as the monitoring wavelength is slowly increased. These observations clearly indicate the presence of the time-dependent Stokes' shifts in the emission spectra of the probe dye in the studied micellar systems.

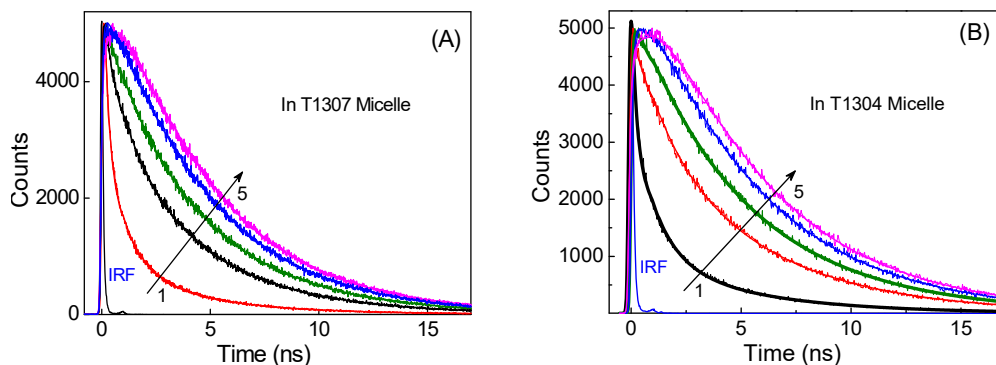


Figure 3.3. Fluorescence kinetic traces for C153 dye in **(A)** 5% (w/v) T1307 and **(B)** 5% (w/v) T1304 micelles. Traces (1-5) are for 460, 500, 520, 550, 600 nm, respectively. IRF represents the instrument response function. Samples were excited with 406 nm pulsed diode laser source.

The time-resolved emission spectra (TRES) for the probe dye in the two micelles were constructed following the procedure discussed in Section 1.6, Chapter 1, and the representative TRES obtained in T1307 and T1304 micelles are shown in Figure 3.4A and B, respectively. It is clearly indicated from Figure 3.4A and B that the TRES in both T1307 and T1304 micelles undergo significant extent of dynamic Stokes' shifts, because the spectra gradually move towards longer wavelength region as the delay time is steadily increased relative to the photoexcitation of the dye.

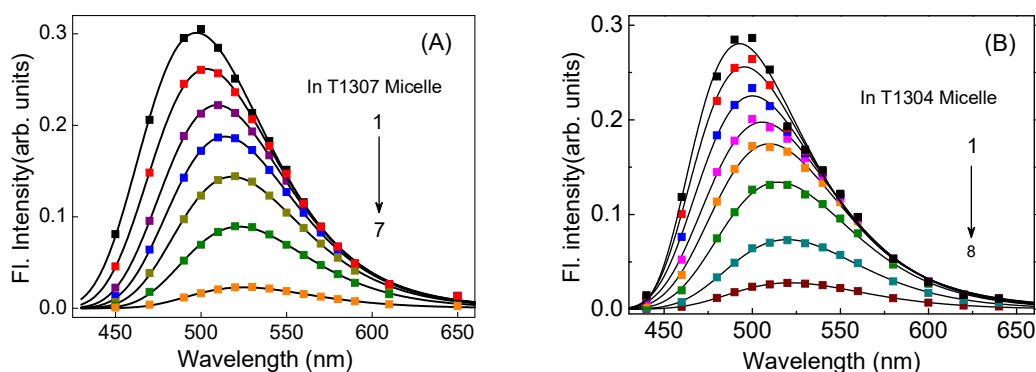


Figure 3.4. Time-resolved emission spectra (TRES) of C153 dye in **(A)** 5% (w/v) T1307 and **(B)** 5% (w/v) T1304 micelles. In panel A, the time delays for spectra 1 to 7 are: 0.05, 0.20, 0.50, 1.00, 2.00, 4.00, and 10.00 ns, respectively, and in panel B, the time delays for spectra 1 to 8 are: 0.05, 0.10, 0.20, 0.40, 0.80, 2.00, 5.00, and 10.00, respectively. The symbols in the spectra are the calculated data points for the TRES and the continuous curves through these data represent their respective lognormal fits.

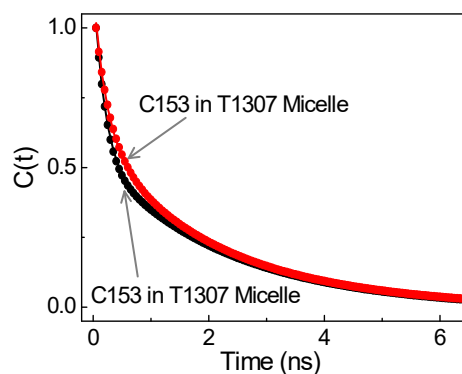


Figure 3.5. Normalized spectral shift correlation functions, $C(t)$, for the probe dye C153 solubilized in the corona region of T1307 (red) and T1304 (black) micelles.

Using the TRES constructed for the studied micellar systems and following the procedure discussed in Section 1.6, Chapter 1, the normalized spectral shift correlation function, $C(t)$, were constructed for two studied micelles, as are shown in Figure 3.5. In both the cases, the $C(t)$ curves are seen to fit well with a bi-exponential function given as,

$$C(t) = a_{s1} \exp(-t/\tau_{s1}) + a_{s2} \exp(-t/\tau_{s2}) \quad (3.10)$$

where τ_{s1} and τ_{s2} are the two solvent relaxation times and a_{s1} and a_{s2} are their respective pre-exponential factors. Using the fitted parameters, the average solvent relaxation times, $\langle \tau_s \rangle$, were estimated using the following relation,

$$\langle \tau_s \rangle = A_{s1}\tau_{s1} + A_{s2}\tau_{s2} \quad (3.11)$$

where A_{s1} and A_{s2} are solvation time weighted relative contributions of the respective components (cf. Section 2.7 in Chapter 2). The decay parameters obtained from the analysis of the $C(t)$ curves in the T1304 and T1307 micelles, which represent the solvent relaxation processes at the corona region (the solubilization sites of the probe) of the two respective micelles, are listed in Table 3.2.

Table 3.2. Parameters related to solvent relaxations in T1304 and T1307 micelles estimated following dynamic Stokes' shifts for C153 dye in the concerned systems.

Systems	A_{s1} (%) ^a	τ_{s1} (ns) ^b	A_{s2} (%) ^a	τ_{s2} (ns) ^b	$\langle \tau_s \rangle$ (ns)	$\Delta \bar{\nu}_{\text{expected}}^{\text{sol}}$ (cm ⁻¹)	$\Delta \bar{\nu}_{\text{obs}}^{\text{sol}}$ (cm ⁻¹)	Missing %
T1304	8.7	0.19	91.3	2.34	2.15	2930	1172	60
T1307	8.1	0.22	91.9	2.10	1.95	3027	1073	65

^a: $A_{si}(\%) = A_{si} \times 100$;

^b: Error limit in τ_{s1} and τ_{s2} values are ± 0.03 ns;

As indicated from Table 3.2, in both the micelles, the faster solvation component τ_{s1} is almost in the similar range but the slower solvation component τ_{s2} is significantly longer in T1304 micelle than in T1307 micelle. In the present context it is important to recollect the solvation dynamics results reported in the literature for neat poly EO solvents.^{371,372} From these studies, it is

realized that the faster solvation components (τ_{s1}) in poly EO solvents arise mainly due to the cooperative local dynamics of EO units and accordingly this component is almost insensitive to the molecular weight or size of the poly EO chains.^{371,372} Following these reports, the similar range of the τ_{s1} values for both T1304 and T1307 micelles is inferred to the segmental motions of the local EO units in the micelles around the probe dye, which are expectedly quite independent of the poly EO block lengths in the two block copolymers used. From the studies in neat poly EO solvents, it is however reported that unlike the τ_{s1} component, the slower τ_{s2} component is a function of the poly EO chain size of the solvents, and its value increases on increasing the chain length, due to the consequent increase in the bulk viscosity of the neat poly EO solvents.^{371,372} In the present study, the slower τ_{s2} component is, however, found to show an opposite trend, appearing to be shorter in T1307 micelle than in T1304 micelle, though the size of the poly EO blocks are longer in the former copolymer than the latter (cf. Chart 3.1). It is thus evident that unlike in neat poly EO solvents, the τ_{s2} values in the studied tetronic micelles are not determined by the bulk solution viscosity but possibly related to the intriguing structural differences of the two micellar systems considered.

In the micellar corona region, the slower solvation components are reported to arise mainly due to the exchange of thermodynamically bound water (i.e. the water molecules hydrogen bonded to the surfactant chains; the poly EO blocks in the present cases) with the mechanically trapped water (i.e. the water molecules trapped and intermolecularly hydrogen bonded among themselves, but not with the surfactant chains).^{139,168,170,235,361,373} In the micropolarity and microviscosity determinations, we have encountered before that due to longer poly EO blocks in T1307 system, this micelle undergoes a higher degree of hydration for its corona region as compared to T1304 micelle (cf. Section 3.3.1.1 and Section 3.3.1.2). Accordingly, it is anticipated that in T1307 micelle there is a much larger amount of mechanically trapped water as compared to that in T1304 micelle. Therefore, the observation that the τ_{s2} component is faster in T1307 micelle than in T1304, even though T1307 polymer has a higher molecular weight, certainly indicate that due to the presence of higher extent of entrapped water, the exchange of the thermodynamically bound water with the mechanically trapped water is more facile in T1307 micelle than in T1304 micelle, resulting the slower component of the solvation process relatively faster in former micelle than latter.

From Table 3.2 it is interestingly observed that in both the micelles the relative contribution A_{s1} for the faster solvation component is very small as compared to the relative contribution A_{s2} for the slower solvation component. Since the TCSPC spectrometer used in the present study for the dynamic Stokes' shift measurements has a finite time resolution (IRF with FWHM ~190 ps), it is anticipated that smaller contribution of A_{s1} in the experimental $C(t)$ curves could be due to the missing of a significant part of the initial dynamic Stokes' shifts arising due to solvation components faster than the time-resolution of our TCSPC setup. To estimate these initial missing parts of the dynamic Stokes' shifts in the present study, we adopted a standard procedure to estimate the total

expected dynamic Stokes' shifts ($\Delta\bar{\nu}_{\text{expected}}^{\text{sol}}$) for the studied micellar systems, as given by Fee and Maroncelli,¹³⁴ and compared these values with the experimentally observed dynamic Stokes' shift ($\Delta\bar{\nu}_{\text{obs}}^{\text{sol}}$) values. Thus, following Fee and Maroncelli,¹³⁴ the $\Delta\bar{\nu}_{\text{expected}}^{\text{sol}}$ values in the studied micelles were estimated as the difference between the conventional Stokes' shifts (shift in energy for the steady-state emission spectra with respect to its ground state absorption spectra of the probe) in the concerned micellar system and that in a selected nonpolar solvent, cyclohexane in the present study, where dielectric solvent relaxation is justifiably considered to be negligible. The $\Delta\bar{\nu}_{\text{expected}}^{\text{sol}}$ values thus estimated for the probe dye in the studied T1304 and T1307 micellar systems are listed in Table 3.2 along with the $\Delta\bar{\nu}_{\text{obs}}^{\text{sol}}$ value estimated experimentally from the dynamic Stokes' shift studies. As indicated from Table 3.2, the $\Delta\bar{\nu}_{\text{obs}}^{\text{sol}}$ values are indeed much lower as compared to the estimated $\Delta\bar{\nu}_{\text{expected}}^{\text{sol}}$ values in both the micelles, suggesting that a significant part of the fast solvation dynamics, faster than the time resolution of our present TCSPC setup, could not be detected in the present study both in T1304 and T1307 micelles.

It is interesting to note from Table 3.2 that the extent of the missing solvation contribution is only marginally higher in T1307 micelle than in T1304 micelle, even though the corona region of the former micelle has a much higher micropolarity ($\varepsilon = 11.3$) than the latter ($\varepsilon = 7.2$). This intriguing observation is possibly related to the underlying mechanisms of the solvation process in the micellar media. In the literature, the exceptionally fast solvation components in the micellar systems, which would expectedly be the main contributors for the missing dynamic Stokes shifts in the present experiments, are suggested to arise mainly due to the combined effects of the segmental motions of surfactant chains and the inertial motions of the entrapped water molecules in the micellar corona region.^{139,170,235,278,279,368,373} In the present study, since the missing dynamic Stokes' shifts are very similar for both T1307 and T1304 micelles, we infer that in the studied tetronic micellar systems the segmental motions of the poly EO blocks in the corona region are mainly responsible for the exceptionally fast solvation components, with only a minor contribution arising from the inertial motions of the entrapped water molecules. Our interpretation is apparently supported by the fact that the τ_{sl} values are quite similar for both T1307 and T1304 micelles, and is also corroborated by the results reported in neat poly EO solvents,^{371,372} suggesting that the faster solvation components (τ_{sl}) in these solvents are quite insensitive to the size of the poly EO chains.

3.3.2. Photoinduced Bimolecular Electron Transfer Studies in Tetronic Micelles

3.3.2.1. Ground State Absorption and Steady-State Fluorescence Studies: Ground state absorption spectra and steady-state (SS) fluorescence spectra of the coumarin dyes as the electron acceptors (cf. Chart 3.1) were recorded in 5% (w/v) T1307 and T1304 micellar solutions both in the absence and in the presence of varying concentrations of the aromatic amine donors (quenchers), DMAN and

DMPT (cf. Chart 3.1), to understand the ground state and excited state interaction of the studied acceptor-donor systems. Figure 3.6A shows the ground state absorption spectra for a representative dye C153 in T1307 micellar solution, in the absence and in the presence of a reasonably high concentration of DMAN donor. It is apparent from the results in Figure 3.6A that the absorption characteristics of the dye do not undergo any observable change on adding the amine donor in the solution. Very similar observations were also made with other coumarin dyes both in the micellar solutions, on addition of either DMAN or DMPT donors. It is evident from these results that both in T1307 and T1304 micelles the coumarin dyes in their ground states do not undergo any significant interaction with the added DMAN and DMPT donors.^{94,112,118-121,124,128,148,287,374,375}

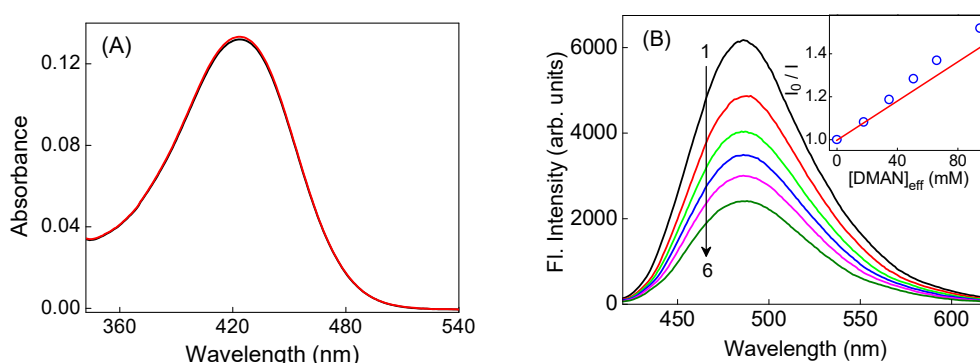


Figure 3.6. (A) Absorption spectra of C153 in 5% T1307 micelles in the absence (black) and presence (red) of 72.8 mM (effective concentration; *vide infra*) DMAN. (B) Steady-state fluorescence spectra of C151 in T1307 micelle in the presence of different effective concentrations (*vide infra*) of DMAN; (1-6)/mM: 0, 17.7, 34.6, 50.7, 66.1, and 94.8. Inset shows the Stern-Volmer plot for the studied C151-DMAN system in T1307 micelle.

Changes in the SS fluorescence spectra of the coumarin dyes shown in Chart 3.1 were also recorded in both T1307 and T1304 micellar media, sequentially increasing the concentration of the DMAN and DMPT quenchers in the solution, to understand the interactions of the studied dyes in their excited S_1 states with the added aromatic amine donors. For all the studied dyes, there is a systematic reduction in their SS fluorescence intensity with the increasing concentration of either DMAN or DMPT quenchers, both in T1307 and T1304 micellar media. The SS fluorescence quenching results for a representative dye C151 in T1307 micellar solution in the presence of gradually increasing concentration of DMAN donor are shown in Figure 3.6B. Observed SS fluorescence quenching results clearly indicate that there is a significantly strong interaction for the studied coumarin dyes in their excited S_1 states with the used DMAN or DMPT donors, both in T1307 and T1304 micellar solutions.^{94,112,118-121,124,128,148,287,374,375}

For all the coumarin-amine systems investigated in the present study, it is noticed that there is no noticeable change in the shape of the emission spectra, though the fluorescence intensity of the dyes decreases largely by the presence of the amine quenchers. It is thus indicated that the quenching interaction of the excited coumarin dyes with the amine donors does not involve any exciplex formation.^{94,112,118-121,124,128,148,287,374,375} It is known from the literature that the coumarin dyes

are efficient electron acceptors while the aromatic amines like DMAN and DMPT are very efficient electron donors.^{94,112,118-121,124,128,375} Based on these electron acceptor and electron donor properties of the coumarin dyes and the amine quenchers, and considering that the electron accepting ability of the coumarin dyes will be increased significantly in their excited states as compared to that in their ground state, the SS fluorescence quenching observed in the studied coumarin-amine systems in T1307 and T1304 micelles is attributed to the photoinduced ET (PET) interaction involving the ground state DMAN and DMPT as the electron donors and the excited state (S_1 state) coumarin dyes as the electron acceptors. In the present context it is to be mentioned that the central ethylene diamine groups of the tetronic copolymers, which are aliphatic amine by nature and are expected to behave in an analogous manner like the aliphatic hydrazine systems as compared to aromatic hydrazine systems,⁹³ no appreciable electron transfer interaction is expected for the excited coumarin dyes with the intrinsic diamine groups of the tetronic copolymers. Further, as we characterised in Section 3.3.1.1, the probe dye C153 and similarly the other dipolar coumarin dyes used in the present study reside mainly in the corona region of the studied T1307 and T1304 micelles. Accordingly, the coumarin dyes in the T1307 and T1304 micelles would be far away from the ethylene diamine groups in the tetronic copolymer micelles, as the latter will be situated at the interior of the micellar cores. Therefore no PET interaction is expected for the excited coumarin dyes with the diamine groups of the tetronic copolymer micelles used in the present study.

As we have mentioned above and also established in Section 3.3.1.1, the studied coumarin dyes (cf. Chart 3.1) being dipolar in character, they preferentially solubilize in the corona region of the studied T1307 and T1304 micelles where micropolarity values are estimated be in the intermediate range ($\epsilon = 11.3$ and 7.2 in the respective cases). Similarly, considering the fact that the aromatic donor molecules, DMAN and DMPT, are also reasonably dipolar in character and are quite insoluble in the water phase, it is reasonable to assume that these donors cum quencher amines will also reside preferentially in the corona region of the studied micelles, as their micropolarities in this region are in the intermediate range. Considering this preferential solubilization of the reactants in the micellar corona region, the effective concentration of the used quencher in the corona layer of the studied micelles were estimated by using the relevant relation as,^{118,124,127,236}

$$[Q]_{eff} = \frac{N_{agg}[Q]_t F}{V_{corona} \{ [copolymer]_t - CMC \}} \quad (3.12)$$

where N_{agg} is the aggregation number for the concerned copolymer in the micelle, $[Q]_t$ is the total quencher concentration used with respect to the total bulk solution, V_{corona} is the volume of the corona layer per mole of the concerned micelle, $[copolymer]_t$ is the total copolymer concentration used in the solution (4.76 mM for T1304 and 2.78 mM for T1307), CMC is the critical micelle concentration concerned copolymer (0.095 mM for T1304 and 0.556 mM for T1307), and F is the correction factor applied based on the relative partitioning of the used quencher between the micellar phase and the aqueous phase outside micelle.

In the present study, the factor F was estimated using the relation $F = P/(1+P)$, where P is the octanol/water partition coefficient of the concerned amine. For DMAN and DMPT quenchers, the “log P ” values are reported to be 2.31 and 2.81, respectively³⁷⁶ and accordingly the F values in the two cases are estimated to be 0.995 and 0.998, respectively. In respect to eq. 3.12, to estimate the V_{corona} values, the dimensions of the T1304 and T1307 micelles, as reported in the literature, were utilized in the present study. Thus, for T1304 micelle, the average micellar radius and average core (nonpolar) radius were considered as ~ 69.9 Å and ~ 44.9 Å, respectively,^{162,166,342} whereby the thickness of the corona layer is estimated as ~ 25 Å and accordingly the volume of the corona layer is calculated as $\sim 1.05 \times 10^6$ Å³ per T1304 micelle and ~ 632.4 dm³ per mole of the T1304 micelles. Similarly, for T1307 micelle, the average micellar radius and average core (nonpolar) radius were considered as ~ 71.1 Å and ~ 38 Å, respectively,^{162,166,342} resulting the thickness of the corona layer as ~ 33.1 Å. Accordingly, for T1307 micelle, the V_{corona} value is calculated as $\sim 1.27 \times 10^6$ Å³ per micelle and ~ 764.9 dm³ per mole of the concerned micelles. The various micellar parameters used in the present study for T1304 and T1307 systems are listed in Table 3.3.

Table 3.3. Parameters for the T1304 and T1307 micellar systems used in the present study.^a

Micellar Systems	MW	CMC (mM)	CMT (°C)	N _{agg}	R _h (Å)	R _c (Å)
T1304	10500	0.095	20.8	36	69.9	44.9
T1307	18000	0.556	23.4	26	71.1	38.0
T1307+1M NaCl	18000	0.055	20.5	42	79.6	44.7
T1307+2M NaCl	18000	0.021	11.6	43	75.4	45.1

^a Taken from ref. 162,166 and 342. MW: Molecular weight; CMC: Critical micelle concentration; CMT: Critical micelle temperature; N_{agg}: Aggregation number; R_c: Core radius; R_h: Hydrodynamic radius.

The SS fluorescence quenching for the coumarin dyes by DMAN and DMPT quenchers was analyzed following the standard Stern-Volmer (SV) relationship as,^{94,112,118-121,124,128,148,287,374,375}

$$\frac{I_0}{I} = 1 + K_{SV} [Q]_{\text{eff}} = 1 + k_q \tau_0 [Q]_{\text{eff}} \quad (3.13)$$

where I_0 and I are the fluorescence intensity for the studied dye in the absence and in the presence of the quencher, $[Q]_{\text{eff}}$ is the effective quencher concentration in the micellar corona layer and K_{SV} is the SV quenching constant, which is more explicitly expressed as “ $k_q \tau_0$ ”; where k_q is the bimolecular quenching constant for the studied coumarin-amine systems and τ_0 is the fluorescence lifetime of the studied dye in the absence of any quencher. For the representative C151-DMAN pair in T1307 micellar medium, the observed SV plot is shown in the inset of Figure 3.6B, while the main panel of the figure represents the SS fluorescence quenching results for the same system. As indicated from this SV plot, there is a mild positive deviation for the experimental data at the higher quencher

concentrations from the expected SV linearity as expected from eq 3.13. To be mentioned that such positive deviations in SV plots were observed for all the studied coumarin-amine pairs, both in T1304 and T1307 micellar media.

Since in the ground state absorption studies (cf. Figure 3.6A) there is no indication of any ground state complex formation between the coumarin dyes and the amine donors, the positive deviations in the SV plots evidently indicate that the SS fluorescence quenching in the studied coumarin-amine systems in T1304 and T1307 micellar media would be certainly associated with a significant extent of transient quenching, occurring in the fluorophore-quencher encounter pairs that pre-exist within the reaction zone before the photoexcitation of the dyes, as are also attributed earlier in the literature to rationalize the similar quenching results obtained in different micellar media involving conventional surfactant systems.^{94,118,119,121,124,128,236} Such transient quenching occurs in the micellar media because there is large restriction in the diffusional motion of the reactant molecules and accordingly the formation of the fluorophore-quencher encounter pairs through their mutual diffusion is not that feasible. Evidently thus, most of the quenching interactions in the micellar media are needed to occur involving the pre-existing fluorophore-quencher pairs within the reaction zone. In the micellar corona region, as the effective volume available for the solubilization of the fluorophore (acceptor) and quencher (donor) molecules is quite small and because both the fluorophore and quencher molecules are preferentially solubilised with this corona region, it is quite expected that at the near vicinity of an excited fluorophore there could already be a quencher molecule present at the moment of fluorophore excitation. This is in fact highly anticipated because with the kind of bulk quencher concentrations used ($[Q]_t$ as given by eq. 3.12) to carry out the quenching experiments the concerned effective quencher concentration ($[Q]_{eff}$ as given by eq. 3.12) becomes significantly high making the transient quenching process to be highly feasible in the micellar media, though with the similar $[Q]_t$ concentration range no transient quenching is expected while the fluorescence quenching studies are carried out in conventional low viscosity homogeneous solvents. Considering the positive deviations observed in the SV plots obtained from SS fluorescence quenching studies, the k_q values for the concerned coumarin-amine systems could be estimated only approximately in the T1307 and T1304 micelles using the initial slopes of the SV plots, which are designated as the $k_{q(SS)}$ values in the present context. The representative $k_{q(SS)}$ values obtained for the studied coumarin-DMAN systems in both T1307 and T1304 micelles are listed in Table 3.4 along with the corresponding k_q values obtained from the time-resolved fluorescence quenching studies ($k_{q(TR)}$) for their direct comparison, as presented and discussed in the next section.

3.3.2.2. Time-Resolved Fluorescence Quenching Measurements: To understand the kinetic details of the fluorescence quenching process for the coumarin dyes by the DMAN and DMPT quenchers in the T1307 and T1304 micellar solutions, we carried out detailed time-resolved (TR) fluorescence quenching measurements for the studied fluorophore-quencher pairs in the concerned micellar

media, following the changes in the fluorescence decay characteristics of the dyes at their respective emission maxima in the presence of varying concentrations of the amine quenchers used. Representative decay traces for C151 dye in T1307 micelle in the presence of varying concentration of DMAN are shown in Figure 3.7. Very similar observations were also made for fluorescence decays of the dyes for all the other coumarin-amine pairs in both the micellar media.

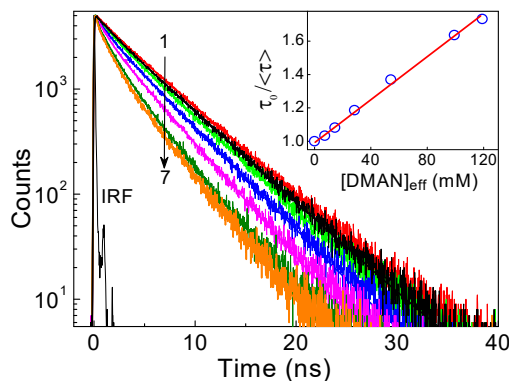


Figure 3.7. Fluorescence decay traces of C151 in 5% T1307 solution in the presence of different effective concentrations of DMAN quencher; For decays 1-7, $[DMAN]_{eff} = 0, 7.4, 14.5, 28.4, 54.2, 99.3$ and 119.2 mM, respectively. IRF is the instrument response function. Inset shows the corresponding Stern-Volmer plot following eq. 3.14.

As indicated from Figure 3.7, the fluorescence decays of the dyes gradually become faster as the quencher concentration is systematically increased in the solution. Following reconvolution analysis (cf. Section 2.4, Chapter 2), it is found that while in the absence of the quenchers the fluorescence decays fit well with a single exponential function, in the presence of the quenchers the decays become non-single exponential in nature. For the studied concentration range of the quenchers used, the decays could satisfactorily be fitted using a bi-exponential function as,

$$I(t) = a_1 \exp(-t/\tau_1) + a_2 \exp(-t/\tau_2) \quad (3.14)$$

where τ_1 and τ_2 are the two decay time constants (fluorescence lifetimes) and a_1 and a_2 are their respective pre-exponential factors. For these bi-exponential decays, the average fluorescence lifetime ($\langle\tau\rangle$) values for the dyes were evaluated using the relation as (cf. Section 2.7, Chapter 2),

$$\langle\tau\rangle = A_1\tau_1 + A_2\tau_2; \quad \text{where} \quad A_1 = \frac{a_1\tau_1}{a_1\tau_1 + a_2\tau_2} \quad \text{and} \quad A_2 = \frac{a_2\tau_2}{a_1\tau_1 + a_2\tau_2} \quad (3.15)$$

The $\langle\tau\rangle$ values thus estimated for the coumarin dyes with the varying concentrations of the quenchers in the studied micellar media were effectively used to evaluate the kinetics of the observed PET reactions in the concerned coumarin-amine systems. Thus, for the estimation of the bimolecular quenching constants for the studied coumarin-amine systems from the TR fluorescence quenching results, the reduction in the $\langle\tau\rangle$ values were correlated with the changing $[Q]_{eff}$ values of the amine quenchers used following the standard SV relationship as,^{94,112,118-121,124,128,148,287,374,375}

$$\frac{\tau_0}{\langle \tau \rangle} = 1 + K_{SV} [Q]_{eff} = 1 + k_q \tau_0 [Q]_{eff} \quad (3.16)$$

where all the parameters have their usual meaning as mentioned before with respect to eq. 3.13 . The related SV plot obtained for the representative C151-DMAN pair in T1307 micelle is shown in the inset the Figure 3.7 along with the observed fluorescence decays recorded for the same system as shown in the main panel of Figure 3.7. As indicated from the inset of Figure 3.7 the observed SV plot for the studied system is quite linear in nature, as was expected from eq. 3.16. Similar linearity in the SV plots was also observed for all the coumarin-amine pairs studied, both in T1307 and T1304 micelles, at least for the concentration range of the quenchers used in the present TR fluorescence quenching measurements.

Table 3.4. The list of the $k_{q(SS)}$ and $k_{q(TR)}$ values for Coumarin-DMAN pairs in T1307 and T1304 micelles.

Used Micelle	PET System	$k_{q(SS)}, (10^8 \text{ M}^{-1}\text{s}^{-1})$	$k_{q(TR)}, (10^8 \text{ M}^{-1}\text{s}^{-1})$
T1307	C151-DMAN	37.73	18.16
	C152-DMAN	52.51	46.03
	C481-DMAN	66.54	43.50
	C153-DMAN	22.93	12.80
T1304	C151-DMAN	23.33	13.19
	C152-DMAN	31.67	28.35
	C481-DMAN	27.81	19.12
	C153-DMAN	14.39	9.11

The linearity observed in the SV plots from the TR fluorescence quenching measurements is certainly an interesting finding, because for these fluorophores-quencher systems the SV plots obtained from SS fluorescence quenching studies in the two micellar media clearly showed positive deviations from the otherwise expected linear correlation (cf. eq. 3.13). For the TR fluorescence measurements in the present study, since the time resolution of the used TCSPC setup is not exceptionally high due to the finite width of the IRF (~190 ps at FWHM), it is anticipated that the ultrafast transient quenching components, occurring faster than the time resolution of the present instrument, are just remained undetected in the measured fluorescence decays for the studied coumarin-amine systems in the concerned micellar media. Accordingly, in the observed TR results, the fluorescence quenching contributions are expected to be arising mainly from the relatively slower quenching components, while contribution of the unusually fast transient quenching

components is effectively missed, causing the resultant $\tau_0/\langle\tau\rangle$ versus $[Q]_{\text{eff}}$ plots to be effectively linear in nature, at least for the concentration range of the quenchers used in the present study.

In the present work, since the observed SV plots from TR fluorescence quenching studies displayed satisfactory linear correlations as given by eq. 3.16, the k_q values for the studied coumarin-amine pairs in T1304 and T1307 micelles were obtained very conveniently using the slopes of these SV plots and the k_q values thus estimated are designated specifically as the $k_{q(TR)}$ values in the present context. The representative $k_{q(TR)}$ values obtained in the present study for the coumarin-DMAN systems in both T1307 and T1304 micelles are listed in Table 3.4 for their comparisons with the corresponding $k_{q(SS)}$ values obtained from the SS fluorescence quenching studies discussed in the previous section. As indicated from Table 3.4, for any coumarin-amine pair, either in T1304 or in T1307 micelle, the $k_{q(TR)}$ value obtained from TR fluorescence quenching study is always lower than the $k_{q(SS)}$ value obtained from the SS fluorescence quenching study.

Table 3.5. Various parameters related to PET process for coumarin-DMPT and coumarin-DMAN systems in T1304 and T1307 micellar media.

Used Micelle	Dyes	Donors	τ_0 (ns)	$k_{q(TR)} (10^8 \text{ M}^{-1}\text{s}^{-1})$	E_{00} (dye) (eV)	ΔG^0 (eV)
T1304	C151	DMPT	5.47	11.71	2.88	-0.54
		DMAN		13.19		-0.48
	C152	DMPT	3.09	27.92	2.82	-0.42
		DMAN		28.35		-0.36
	C481	DMPT	3.17	21.31	2.82	-0.39
		DMAN		19.12		-0.33
	C153	DMPT	5.02	16.14	2.66	-0.20
		DMAN		9.11		-0.15
T1307	C151	DMPT	4.98	11.50	2.84	-0.61
		DMAN		18.16		-0.55
	C152	DMPT	1.91	63.66	2.77	-0.48
		DMAN		46.03		-0.42
	C481	DMPT	2.00	62.85	2.78	-0.45
		DMAN		43.50		-0.39
	C153	DMPT	4.35	25.08	2.63	-0.27
		DMAN		12.80		-0.22

The higher $k_{q(SS)}$ values for the studied coumarin-amine systems in both T1304 and T1307 micelles are apparently due to the additional contributions arising from the unusually fast transient quenching components in the SS measurements, which are understandably kept away with in the $k_{q(TR)}$ values estimated from the TR quenching studies, due to the limited time resolution of our TCSPC setup. In the present study, since SV plots obtained from TR quenching studies showed linear correlations very convincing following eq. 3.16, the $k_{q(TR)}$ values were estimated more accurately from these SV plots as compared to the $k_{q(SS)}$ values obtained from the initial slopes of the positively deviated SV plots obtained from the SS quenching studies. Therefore, these more accurately estimated $k_{q(TR)}$ values were in effect considered as the measures of the observed reaction rate constants for the concerned bimolecular PET processes in different coumarin-amine systems in the two tetronic micellar media. Accordingly thus, these $k_{q(TR)}$ values were used for the further correlations of the observed bimolecular rate constants with the energetic of the PET reactions in the studied systems with reference to the Marcus outer sphere ET theory, as are discussed in a forthcoming section. The $k_{q(TR)}$ values obtained for all the coumarin-DMAN and coumarin-DMPT pairs both in T1307 and T1304 micelles are listed in Table 3.5 along with the other relevant photophysical and energetic parameters related to the concerned PET processes in the studied systems, for their quick references.

3.3.2.3. Calculation of Free Energy Changes and Correlations with observed PET Rates: The free energy changes (ΔG^0) for the PET reactions in the studied coumarin-amine systems in the two tetronic micellar media can be estimated using the Rehm-Weller relation as,^{130,148}

$$\Delta G^0 = E(D^+ / D) - E(A / A^-) - E_{00} - \frac{e^2}{\epsilon_s r} \quad (3.17)$$

where E_{00} is the 0–0 transition energy between the S_0 and S_1 states of the coumarin dyes, $E(D^+/D)$ and $E(A/A^-)$ are the reduction potentials for the concerned amine donors and coumarin acceptors, respectively, e is the electronic charge, ϵ_s is the static dielectric constant at the localization site of the donor-acceptor pairs in the micellar media and r is the separation between the interacting donor-acceptor pair in the micelles studied. In the above equation, the last term is the solvent stabilization energy for the contact ion-pair ($D^+ \cdots A^-$) state produced in the PET reaction. For simplicity, the r values in the present cases were considered as equal to the sum of the radii of the concerned donor and acceptor systems used.

Since the redox potential values of the coumarin dyes especially could not be estimated reliably in the studied tetronic micellar media due to their limited solubility of the micelles, in the present study, therefore, we utilized both the $E(D^+/D)$ and $E(A/A^-)$ values as obtained from the reported literatures in acetonitrile solution,^{375,377} subsequent to their appropriate corrections for changing the reaction medium from acetonitrile to the tetronic micellar systems, applying the empirical relations suggested by Prof. W. R. Fawcett.^{92,378,379} As given by Prof. Fawcett, the

solvation energies for an anion (A^-) and a cation (D^+) in a solvent of static dielectric constant, ϵ_s , can empirically be expressed as,

$$G_s^0(A^-) = -\frac{N_0 z_i^2 e^2}{8\pi\epsilon_0} \left(1 - \frac{1}{\epsilon_s}\right) \left(\frac{1}{r_i + (1/A_p)}\right) \quad (3.18)$$

$$G_s^0(D^+) = -\frac{N_0 z_i^2 e^2}{8\pi\epsilon_0} \left(1 - \frac{1}{\epsilon_s}\right) \left(\frac{1}{r_i + (1/B_p)}\right) \quad (3.19)$$

where N_0 is the Avogadro's number, z_i is the number of charge units on the concerned ion, e is the amount of charge of an electron, ϵ_0 is the permittivity of the free space, r_i is the radius of the concerned ion expressed in nm, A_p is the Fawcett's solvent acidity parameter defined by eq. 3.20 and B_p is the Fawcett's solvent basicity parameter defined by eq. 3.21.

$$A_p = 1.29 E_T(30) - 33.3 \quad (3.20)$$

$$B_p = 10.14 + 0.108 D_n \quad (3.21)$$

In the expressions of A_p and B_p , the parameter $E_T(30)$ represents the solvent polarity in the $E_T(30)$ scale and the parameter D_n represents the donor number of the solvent medium, as defined specifically by Dimroth, et al. and Gutmann, et al., respectively.^{380,381}

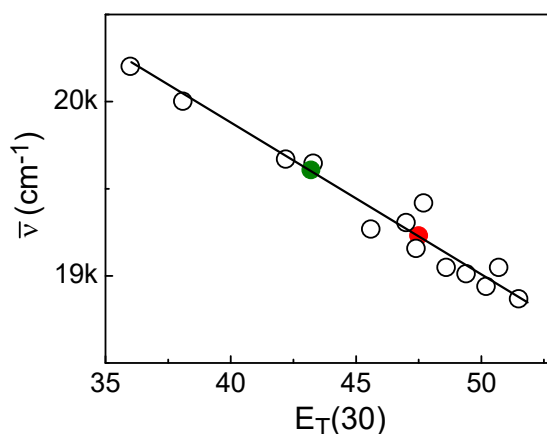


Figure 3.8. Calibration plot (black) for the fluorescence maxima (in cm^{-1}) of C153 against the solvent polarity function, $E_T(30)$, in MeOH-Toluene solvent mixtures and some pure solvents.^{380,383} Data points corresponding to the emission maxima of C153 in T1304 (green) and T1307 (red) micelles are superposed on the calibration plot.

According to Prof. Fawcett,^{92,378,379} the A_p and B_p values, as obtained by using eq. 3.20 and 3.21, are empirically assigned the dimension of nm^{-1} for their uses in eq. 3.18 and 3.19, respectively, to calculate the $G_s^0(A^-)$ and $G_s^0(D^+)$ values. For the studied T1304 and T1307 micellar systems, the concerned $E_T(30)$ and D_n values are not available in the literature. In the present study, the D_n values for both T1304 and T1307 micelles were considered to be similar to the reported D_n value in DeOH solvent.³⁸² The rationale behind this consideration is that the SS fluorescence spectra of the coumarin dyes in the studied tetronic micelles resemble quite closely with those in DeOH solvent (cf. Section

3.3.1.1 and Figure 3.1A). For the studied T1304 and T1307 micelles, the $E_T(30)$ values were estimated independently, following the construction of a calibration curve from the changing fluorescence maxima of the probe dye C153 in different neat solvents and also in several toluene-methanol solvent mixtures, for which $E_T(30)$ values are well reported in the literature. The calibration curve thus obtained in the present study is shown in Figure 3.8 and the $E_T(30)$ values estimated for T1304 and T1307 micelles are found to be about 43.2 and 47.4, respectively.

For the calculations of the $G_S^0(A^-)$ and $G_S^0(D^+)$ values, we considered the radii of the A^- and D^+ ions to be the same as the concerned acceptor and donor systems, respectively, and these radii were estimated following the widely used Edward's volume addition method.³⁷⁰ Finally, the $E(D^+/D)$ and $E(A/A^-)$ values for the studied donors and acceptors in the acetonitrile (ACN) solutions were corrected in the following manner to estimate the $E(D^+/D)$ and $E(A/A^-)$ values of these systems in the studied micellar media.

$$E(D^+ / D) = E(D^+ / D)_{ACN} - G_S^0(D^+)_{ACN} + G_S^0(D^+)_{micelle} \quad (3.22)$$

$$E(A / A^-) = E(A / A^-)_{ACN} + G_S^0(A^-)_{ACN} - G_S^0(A^-)_{micelle} \quad (3.23)$$

Different energy parameters estimated for the studied donors and acceptors based on Fawcett's empirical relations are listed in Table 3.6 for their ready references. Subsequent to the estimations of the $E(D^+/D)$ and $E(A/A^-)$ values for donors and acceptors in the two tetronic micelles, and obtaining the concerned E_{00} values for the coumarin dyes in these micellar media considering them equivalent to the intersecting wavelengths of their peak normalized excitation and emission spectra in the studied micelles, the ΔG^0 values were eventually calculated for each of the donor-acceptor pairs in the two tetronic micellar media using eq. 3.17. The ΔG^0 values thus calculated for different coumarin-amine pairs in T1304 and T1307 micelles are specifically listed in Table 3.5 along with the related $k_{q(TR)}$ values obtained from the TR fluorescence quenching studies, for a direct correlation of these two parameters in different PET systems.

The correlations of the bimolecular quenching constants, $k_{q(TR)}$, obtained from the TR fluorescence studies, with the ΔG^0 values for the coumarin-amine pairs in the two tetronic micellar media (cf. Table 3.5) are shown in Figure 3.9. It is evidently indicated from this figure that the $k_{q(TR)}$ value increases gradually with $-\Delta G^0$ at the lower exergonicity ($-\Delta G^0$) region, representing the normal Marcus region for the concerned ET systems. The $k_{q(TR)}$ value, however, decreases clearly with $-\Delta G^0$ at the higher exergonicity region, exhibiting the intriguing Marcus Inversion (MI) behaviour for the studied ET systems in the tetronic micellar media, as predicted from the famous Marcus ET theory (cf. eqs. 1.8 and 1.14). Since observation of MI behaviour for bimolecular PET reactions remains obscured in conventional low viscosity homogeneous solvents due to diffusional influence on the observed reaction rates,^{26,29,42,44,105,130,268,270,272,273,384-387} the appearance of the MI behavior for the studied bimolecular PET reactions in T1304 and T1307 micellar media clearly suggests that the constrained micellar microenvironment enforces both the diffusional rates of the

reactants and the solvent relaxation dynamics to occur with significantly slower rates, causing the studied bimolecular PET reactions to proceed in accordance with the Marcus ET theory. In acetonitrile, where solvent viscosity (η) is ~ 0.37 cP, the diffusion-controlled bimolecular rate constant k_d for the similar coumarin-amine systems is reported to be about $1.5 \times 10^{10} \text{ dm}^3 \text{ mol}^{-1} \text{ s}^{-1}$.³⁷⁵ As we have seen in Section 3.3.1.2, the microviscosity values estimated for the corona regions of T1304 and T1307 micelles are ~ 58 cP and ~ 47 cP, respectively. Accordingly, the expected k_d values ($k_d \propto 1/\eta$) in these two micellar systems are estimated to be about 9.6×10^7 and $11.8 \times 10^7 \text{ dm}^3 \text{ mol}^{-1} \text{ s}^{-1}$, respectively, which are evidently lower than the observed $k_{q(TR)}$ values for the studied ET systems (cf. Table 3.4). It is thus evident that the bimolecular PET reactions for the studied coumarin-amine systems in the T1304 and T1307 micellar media indeed occur following a non-diffusive reaction condition.^{161,347}

Table 3.6. Calculated electrochemical properties of the donors (DMAN and DMPT) and acceptors (coumarin dyes) systems in T1304 and T1307 micellar media.

Used Micelle	Redox species	$E(A/A^-)_{ACN}$ (V) ^a	$E(D^+/D)_{ACN}$ (V) ^a	$G_s^0(X)_{ACN}$ (eV) ^b	$G_s^0(X)_{micelle}$ (eV) ^b	$E(A/A^-)_{micelle}$ (V)	$E(D^+/D)_{micelle}$ (V)
T1304	C151	-1.565		-1.837	-1.605	-1.80	
	C152	-1.626		-1.734	-1.516	-1.84	
	C481	-1.660		-1.653	-1.447	-1.87	
	C153	-1.685		-1.630	-1.426	-1.89	
	DMAN		0.76	-1.750	-1.599		0.91
	DMPT		0.70	-1.691	-1.543		0.85
T1307	C151	-1.565		-1.837	-1.740	-1.66	
	C152	-1.626		-1.734	-1.641	-1.72	
	C481	-1.660		-1.653	-1.564	-1.75	
	C153	-1.685		-1.630	-1.542	-1.77	
	DMAN		0.76	-1.750	-1.694		0.82
	DMPT		0.70	-1.691	-1.634		0.76

^aThese $E(A/A^-)_{ACN}$ and $E(D^+/D)_{ACN}$ values are against SCE, obtained from ref. 375 and 377.

^b $G_s^0(X)$ stands for $G_s^0(A^-)$ or $G_s^0(D^+)$ for the concerned acceptor donor systems, respectively.

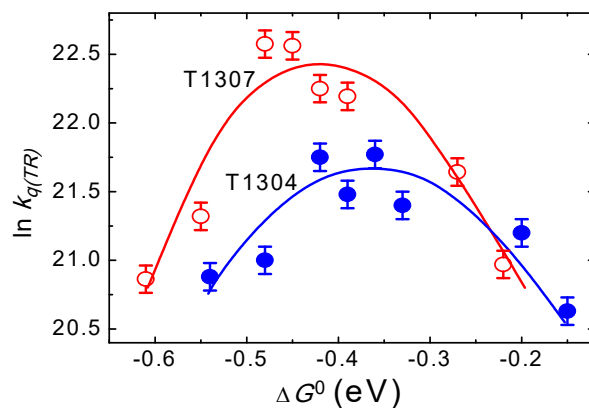


Figure 3.9. The $\ln(k_{q(TR)})$ versus ΔG^0 plots for the PET reactions in the coumarin-amine systems studied in T1304 and T1307 micellar media. Continuous curves are drawn just as a visual guide for correlations among the data points. In both the micelles, MI behaviour is clearly indicated.

As discussed in Section 3.3.1.1, the dielectric constant (ϵ) for the corona regions of T1304 and T1307 micelles are in the range of about 7-12. Thus, using eq. 1.11, the solvent reorganization energy, λ_s , for the studied micellar media are be estimated to be ~ 1 eV. Accordingly, from Figure 3.9, it is intriguingly noticed that the onset of MI in both T1304 and T1307 micelles appears at the exergonicity values ($-\Delta G^0 \sim 0.4$ eV) that are exceedingly lower than the values expected from the conventional Marcus ET theory, i.e. $-\Delta G^0 = \lambda = \lambda_s + \lambda_i$ (cf. Figure 1.2 shown in Chapter 1). This observation thus suggests that unlike the complete solvent relaxation, as applicable to the conventional ET theory, the PET reactions in the studied micellar systems certainly need occur with a non-equilibrium solvent reorganization around the reactant states.^{18,161,347} This proposition is also supported by the fact that the τ_s values for the studied micellar systems (cf. Table 3.2) are almost in the range of the observed $k_{q(TR)}$ values (cf. Table 3.4), indicating clearly that both PET and solvent relaxation processes in these cases occur quite in the similar time scales. Under such a situation, following photoexcitation of the coumarin dyes, the concerned reactant states, i.e. $D^{\bullet\bullet}A^*$ (cf. Chapter 1, Section 1.5) cannot attend the thermally equilibrated solvent configurations around them during the ET reactions, and accordingly the ET processes occurring in these systems cannot be treated adequately following the conventional Marcus ET theory. With such a non-equilibrium solvent configurations for the $D^{\bullet\bullet}A^*$ states, the ET processes would eventually occur involving the intramolecular reorganization coordinate (q) as the effective reaction coordinate, keeping the non-equilibrium distributions along the solvent reorganization coordinate (X) to be remained as it is. This theoretical model that visualizes and explicitly considers this intriguing PET mechanism in restricted salvat media is commonly kown as the two-dimensional ET (2D-ET) theory, as we have discussed with the necessary details in Section 1.2.4, Chapter 1.^{18,88-98}

Comparing the PET results obtained in T1304 and T1307 micellar systems, several interesting differences may be noticed quite evidently. Thus, even though the $k_{q(TR)}$ versus ΔG^0 correlations in both the micellar systems show the MI behaviour, the ET rates are in general

relatively higher in T1307 micelle than in T1304 micelle. Additionally, in T1307 micelle, the onset of the MI evidently appears at a relatively higher exergonicity ($-\Delta G^0 \sim 0.45$ eV) than in T1304 micelle ($-\Delta G^0 \sim 0.41$ eV). As we have discussed in Sections 3.3.1.1 and 3.3.1.2, the micropolarity is significantly higher and microviscosity is moderately lower in T1307 micelle than in T1304 micelle. Since the PET reactions in the present micellar media occur under a non-diffusive condition, small differences in the microviscosity are not expected to cause any significant change in the PET processes (i.e. in the relative rates and on the onset of MI) for the two micellar media used. We thus infer that the changes in the micropolarity for the two micelles are the main reason for the differences in the ET characteristics observed in T1304 and T1307 micellar media. Accordingly, in T1307 micelle, the higher micropolarity for its corona region (due to more hydration of larger PEO blocks) causes this micellar system to be relatively more conducive for the PET reactions, resulting the $k_{q(TR)}$ values in this micelle to be in general higher than those in the T1304 micelle. This is expected because higher polarity provides better stabilization for the ion-pair (D^+/A^-) states produced in the ET reactions and thus assists the reactions to occur favourably. The higher micropolarity in T1307 micelle also causes a higher contribution of the λ_s value towards the ΔG^* value of the concerned PET reaction (cf. eq 1.24), as the PET reactions in the studied systems occur under the 2D-ET mechanism (cf. Chapter 1),^{18,99} leading the onset of MI in the present micelle to appear at a relatively higher $-\Delta G^0$ value as compared to that in the T1304 micelle.

3.3.2.4. Salt Effect on the Micellar micropolarity and ET Kinetics: To substantiate that the differences in the ET characteristics observed in T1307 and T1304 micelles are due to micropolarity differences in these two micelles, we also investigated the salt effects involving T1307 micelle as the typical case study and using NaCl as the added salt. As reported in the literature, added salt acts as a dehydrating agent for the block copolymer micelles, increasing the hydrophobic characteristics of their PEO and PPO blocks.^{177,388-390} Thus, in the presence of NaCl salt, the T1307 solution is reported to display significantly lower *CMC* and *CMT* values as compared to those in the absence of the salt.³⁴² In the present study it is further observed that there is a gradual blue-shift in the emission spectra for the probe dye C153 in T1307 micelle on increasing the NaCl concentration, as are shown in Figure 3.10A. Following these results and using the same calibration plot as shown in Figure 3.1 and is also reproduced in Figure 3.10B, the ϵ values for the T1307 micelle in the presence of 0, 1 and 2M NaCl concentrations are estimated to be about 11.3, 10.2 and 8.5, respectively, evidently indicating that the micropolarity for the corona region of the micelle decreases systematically on increasing the concentration of the NaCl salt.

To understand the changes in the microviscosity for the corona region of T1307 micelle in the presence of NaCl salt, time-resolved fluorescence anisotropy measurements were carried out as discussed in Section 3.3.1.2. Anisotropy decays observed in the present cases are shown in Figure 3.11A and the corresponding anisotropy decay parameters are listed Table 3.7A. Observed results

clearly indicate that in accordance with the dehydrating effect of the added salt,^{177,388-390} the presence of the increasing concentrations of the NaCl salt gradually increases the microviscosity for the corona region of the studied T1307 micelle.

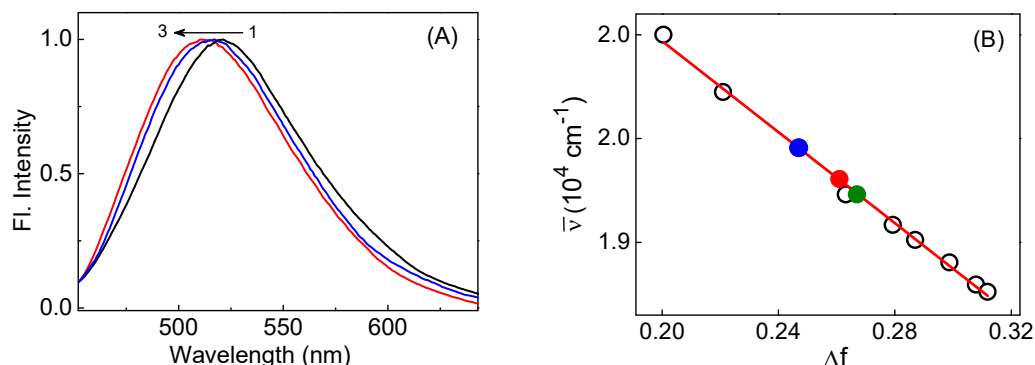


Figure 3.10. (A) Normalized fluorescence spectra of C153 in 5% w/v T1307 in the presence of 0, 1 and 2 M NaCl concentrations. (B) Calibration plot for solvent polarity (Δf) estimation, as reproduced from Figure 3.1B. The data points represented by green, red and blue closed circles correspond to the T1307 micelle in the absence of any salt and in the presence of 1M and 2M NaCl, respectively.

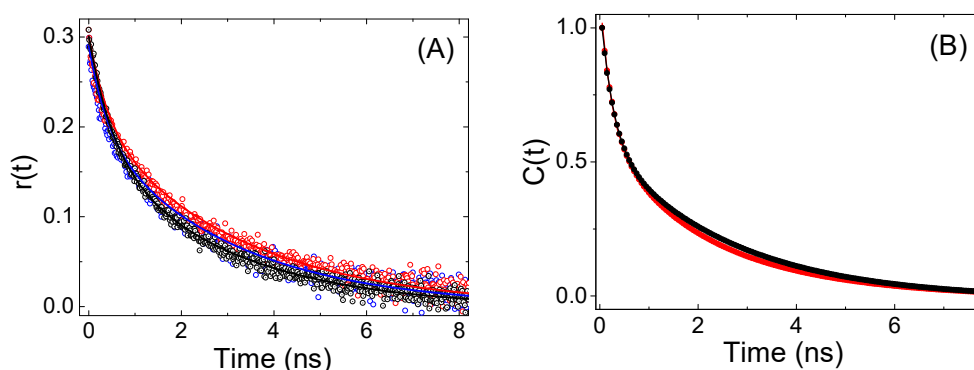


Figure 3.11. (A) Fluorescence anisotropy decay traces of C153 in 5% w/v T1307 in the presence of 0 M (black), 1 M (blue), 2 M (red) NaCl, respectively. (B) Normalized spectral shift correlation functions, $C(t)$, for C153 in 5% T1307 in the absence (black) and presence (red) of 2M NaCl. *Note:* The $C(t)$ curve in the presence of 1M NaCl was almost the same as that in the absence of NaCl.

To understand the changes in the solvent relaxation dynamics in the corona region of T1307 micelle in the presence of NaCl salt, the dynamic Stokes' shift studies were also carried out, as discussed in Section 3.3.1.3. The normalized spectral shift correlation functions observed in the present cases are shown in Figure 3.11B and the corresponding solvent relaxation parameters are listed Table 3.7B. Considering all the observed results, it is unambiguously indicated that the addition of NaCl salt effectively reduces the hydration characteristics of the T1307 micelle, causing the corona region of the micelle to become relatively less polar and hence to be relatively less conducive for the PET reactions carried out in this micellar media.

Table 3.7. Decay parameters for time-resolved fluorescence anisotropy and solvent relaxation process for the probe dye C153 in 5% w/v T1307 in the presence varying NaCl concentrations.

(A) Parameters for Fluorescence Anisotropy Decay							
Micellar System	τ_{rl} (ns)	$r_{0,l}$	A_{rl} (%)	τ_{r2} (ns)	$r_{0,2}$	A_{r2} (%)	$\langle\tau_r\rangle$ (ns)
T1307	0.55	0.09	9	2.96	0.17	91	2.74
T1307+ 1M NaCl	0.55	0.06	7	3.20	0.14	93	3.01
T1307+ 2M NaCl	0.58	0.07	7	3.40	0.15	93	3.20
(B) Parameters for Solvent Relaxation Dynamics							
Micellar System	τ_{sl} (ns)	A_{sl} (%)		τ_{s2} (ns)	A_{s2} (%)		$\langle\tau_s\rangle^a$ (ns)
T1307	0.22	8.10		2.10	91.90		1.95
T1307+ 2M NaCl	0.26	8.07		2.56	91.92		2.37

Table 3.8. List of the PET parameters and the free energy changes for the coumarin-amine systems in T1307 micelle at different NaCl concentrations.

Dyes	$[NaCl]$ (M)	τ_0 (ns)	E_{00} (eV)	$E(A/A^-)$ (V)	$k_{q(TR)} (10^8 M^{-1}s^{-1})$		$E(D^+/D)$ (V)		ΔG^0 (eV)	
					DMAN	DMPT	DMAN	DMPT	DMAN	DMPT
C151	0	4.98	2.84	-1.66	18.16	11.50	0.82	0.76	-0.55	-0.61
	1	5.12	2.84	-1.70	16.11	13.42	0.84	0.77	-0.52	-0.59
	2	5.09	2.85	-1.75	14.87	11.37	0.87	0.81	-0.49	-0.54
C152	0	1.91	2.77	-1.72	46.03	63.66	0.82	0.76	-0.42	-0.48
	1	2.31	2.79	-1.75	40.17	45.74	0.84	0.77	-0.41	-0.48
	2	2.44	2.81	-1.80	35.88	34.00	0.87	0.81	-0.39	-0.44
C481	0	2.00	2.78	-1.75	43.50	62.85	0.82	0.76	-0.39	-0.45
	1	2.49	2.79	-1.78	39.62	48.06	0.84	0.77	-0.38	-0.44
	2	2.69	2.80	-1.82	33.34	32.60	0.87	0.81	-0.35	-0.40
C153	0	4.35	2.63	-1.77	12.80	25.08	0.82	0.76	-0.22	-0.27
	1	4.33	2.64	-1.80	12.90	16.54	0.84	0.77	-0.20	-0.27
	2	4.41	2.66	-1.85	9.65	14.57	0.87	0.81	-0.18	-0.24

^aThe $E(A/A^-)_{ACN}$ and $E(D^+/D)_{ACN}$ values are against SCE.

The PET kinetics for the coumarin-DMAN and coumarin-DMPT pairs in T1307 micelle in the presence of varying NaCl concentrations were performed following TR fluorescence quenching studies as described in Section 3.3.2.2. Representative SV plots for C151-DMAN pair in the absence and presence of two different NaCl concentrations are shown in Figure 3.12A. Similar observations were also made for the other coumarin-amine pairs in T1307 micelle with the changing NaCl concentration. Observed results clearly indicate that the slopes of the SV plots gradually decrease on increasing the NaCl concentration, suggesting a gradual decrease in the ET rate in the presence of the added salt. The kinetic and energetic parameters for the present PET systems in T1307 micelle at different NaCl concentrations were determined following the procedures discussed in Sections 3.3.2.2 and 3.3.2.3. Concerned $k_{q(TR)}$ and ΔG^0 values as estimated in the present cases are listed in Table 3.8. For completeness, the calculated electrochemical properties for the studied donors (DMAN/DMPT) and acceptors (coumarin dyes) in the T1307 micelle at different NaCl concentrations are also listed in Table 3.9. Finally, the correlations of the $\ln(k_{q(TR)})$ values with the ΔG^0 values as obtained for different coumarin-amine pairs in the T1307 micelle in the presence of different NaCl concentrations are depicted in Figure 3.12B for a comparison.

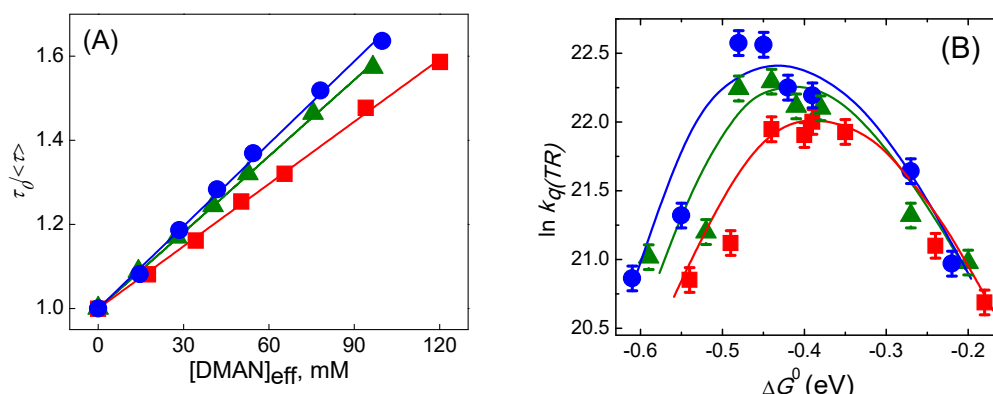


Figure 3.12. (A) Stern-Volmer plots from TR fluorescence quenching of C151 by DMAN in 5% T1307 micelle in the presence of 0 M (blue, circle), 1 M (green, triangle) and 2 M NaCl (red, square), respectively. (B) The $\ln(k_{q(TR)})$ versus ΔG^0 plots for the coumarin-amine pairs in T1307 micelle in the presence of different NaCl concentrations; 0 M (blue, circle), 1 M (green, triangle), and 2 M (red, square), respectively. The MI behaviour is clearly indicated in all the cases.

As clearly indicated from Figure 3.12B, MI behaviour is very evidently displayed by the studied PET systems in T1307 micellar medium in the presence of all the NaCl concentrations used. Interestingly, the onset of the MI for the observed correlations in the present cases slowly shifts toward lower exergonicity along with a reduction in the $k_{q(TR)}$ values, as the NaCl concentration is increased in the T1307 micellar solution. These results corroborate nicely with the fact that with the addition of a salt the polarity of the micellar microenvironments undergoes a reduction due to the progressive dehydration of the micellar phase. Furthermore, since the solvent relaxation rate becomes slower on addition of the salt (cf. Table 3.7B), the contribution of λ_s towards ΔG^* of the

PET reaction also reduces accordingly (cf. eq 1.24) and thus the onset of MI gradually shifts toward the lower exergonicity. From the observed results it is clearly indicated that the changes in the microenvironment for micellar medium that one achieved on replacing the polar T1307 micelle by the relatively less polar T1304 micelle can also be realized effectively just by adding a suitable concentration of NaCl salt into the T1307 micellar solution, without requiring the tetronic system to be changed. In brief, thus, it can be realized from present results that the modulations both in regard to the onset of Marcus inversion and the observed PET rates can be achieved quite suitably through the tailoring of the micellar microenvironments, either by changing the tetronic copolymers as such or by adding a suitable dehydrating or hydrating agent in any tetronic micelle, which can be schematically represented as shown in Figure 3.13. This kind of control of the chemical processes in the micellar systems through the modifications of the micellar microenvironments is definitely an interesting finding and would possibly find prospective applications in many practical areas.

Table 3.9. Calculated electrochemical properties of the donor (DMAN/DMPT) and acceptors (coumarin dyes) in T1307 micelles in the presence of different NaCl concentration.

(A) Electrochemical Properties of the Acceptor Systems					
Chemical Syatem	Electro-chemical Parameter	Solvent Systems			
		ACN	T1307	T1307 + 1 M NaCl	T1307 + 2M NaCl
C151	$G_S^0(A^-)$ (eV)	-1.837	-1.740	-1.705	-1.653
	$E(A/A^-)$ (V) ^a	-1.565	-1.66	-1.70	-1.75
C152	$G_S^0(A^-)$ (eV)	-1.734	-1.641	-1.609	-1.561
	$E(A/A^-)$ (V) ^a	-1.626	-1.720	-1.75	-1.80
C481	$G_S^0(A^-)$ (eV)	-1.653	-1.564	-1.534	-1.489
	$E(A/A^-)$ (V) ^a	-1.660	-1.750	-1.78	-1.82
C153	$G_S^0(A^-)$ (eV)	-1.630	-1.542	-1.513	-1.468
	$E(A/A^-)$ (V) ^a	-1.685	-1.77	-1.80	-1.85
(B) Electrochemical Properties of the Donor Systems					
DMAN	$G_S^0(D^+)$ (eV)	-1.750	-1.694	-1.675	-1.638
	$E(D^+/D)$ (V) ^a	0.76	0.82	0.84	0.87
DMPT	$G_S^0(D^+)$ (eV)	-1.691	-1.634	-1.616	-1.581
	$E(D^+/D)$ (V) ^a	0.700	0.76	0.77	0.81

^aThe $E(A/A^-)$ and $E(D^+/D)$ values in ACN (against SCE) were obtained from ref. 375 and 377.

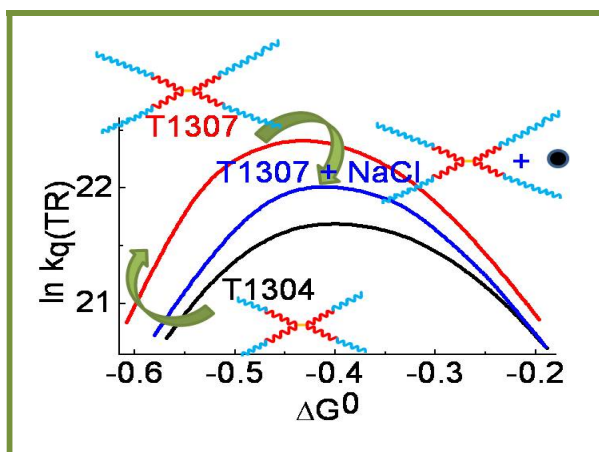


Figure 3.13: Pictorial representation on the modulation of the PET kinetics achieved by using either the different tetronic micellar systems or the concentration of suitable salt as the additive in a single copolymer micelle.

3.4. Conclusion

In the present study, the microenvironments of T1304 and T1307 tetronic star block copolymer micelles have been characterized extensively using steady-state (SS) and time-resolved (TR) fluorescence studies, fluorescence anisotropy measurements and solvent relaxation dynamics studies involving C153 as the fluorescent probe dye. It is revealed from the elaborate study that the T1307 micelle is more polar, less viscous and more hydrated in nature as compared to the T1304 micelle. These findings corroborate nicely with the larger PEO block lengths of T1307 copolymer as compared to that of the T1304 copolymer. Bimolecular PET studies involving a series of 7-amino coumarin derivatives as the electron acceptors and the aromatic amines DMAN and DMPT as the electron donors have also been carried out in detail in T1307 and T1304 micellar media following both SS and TR fluorescence quenching studies. The SS fluorescence quenching results show positive deviations in the constructed Stern-Volmer (SV) plots, while TR fluorescence quenching results show the expected linearity in the SV plots. Thus, the slopes of the SV plots from the TR fluorescence quenching studies were suitably used to estimate the bimolecular quenching rate constants, $k_{q(TR)}$ for different donor-acceptor pairs in the studied micellar media. Interestingly, Marcus Inversion (MI) is clearly observed in both T1304 and T1307 micellar media on correlating the $k_{q(TR)}$ values with the concerned exergonicity ($-\Delta G^0$) of the ET reactions. Moreover, in both the micelles, the onset of the MI appears at a much lower exergonicity than one can anticipate from the consideration of the conventional Marcus ET theory. Such a shift in the onset of MI towards lower exergonicity suggests the involvement of 2D-ET mechanism in the present PET systems in the micellar media. Interestingly it is found that the $k_{q(TR)}$ values are higher and the onset of MI appears at a relatively higher exergonicity in the T1307 micelle as compared to those in T1304 micelle. These results are attributed to the larger PEO blocks and consequently to the higher hydration and

higher micropolarity at the corona region of the T1307 micelle than the T1304 micelle. Sequential changes in the micellar microenvironments and in the observed ET kinetics are also found in T1307 micelle with the changing concentration of NaCl salt as an additive in the experimental solution, demonstrating that the kinetics as well as the onset of MI for the PET reactions can be modulated suitably either by changing the constitution of the tetronic copolymer system or just by changing the concentration of the salt in a single tetronic micelle. Such intriguing modulations in the energetic and kinetics of the PET reactions in the micellar media are not only very appealing from the academic view points but would expectedly find prospective uses in many applied areas.

CHAPTER-4

IONIC LIQUIDS AS CO-SURFACTANTS FOR TETRONIC MICELLES IN MODULATING PHOTOINDUCED ELECTRON TRANSFER PROCESS

4.1. Introduction

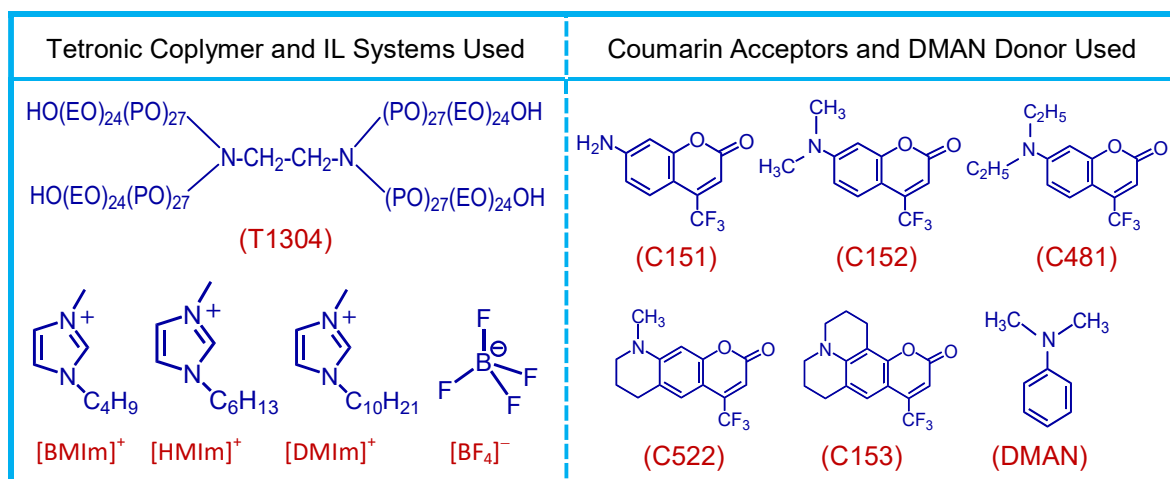
In Chapter 3, we have investigated bimolecular PET reactions in the micelles of two star-block copolymers, namely, tetronic 1304 (T1304) and tetronic 1307 (T1307), correlating the results with the differential microenvironments of the two micellar systems.³⁴⁷ Our study revealed that between T1304 and T1307 micelles, the corona region of the latter is more hydrated, more polar and less viscous than the former.³⁴⁷ Accordingly, in T1307 micelle, the PET rates were observed to be significantly higher and the onset of MI was seen to appear at a relatively higher exergonicity as compared to those in T1304 micelle. Additionally, it was observed that addition of NaCl can cause significant dehydration of T1307 micelle such that the ET kinetics in this micelle could be tuned significantly by changing the salt concentration in the solution.³⁴⁷ Since characteristics of the micelles are extremely important in tuning PET reactions, in the present study our endeavor was to understand the influence of ionic liquids (IL) as the co-surfactants for T1304 tetronic copolymer micelles in tuning the bimolecular PET reactions in the so formed mixed micellar assemblies.

ILs are environmentally benign salts that are in the liquid state at normal temperatures and are composed of either organic-organic or organic-inorganic types of cation-anion combinations, where the close packing of the ions are hindered due to their large and irregular size and shape. Resembling the molten salts, the ILs display many unique properties like low vapor pressure, non-flammability, high ionic mobility and excellent chemical stability, and accordingly various ILs have been explored extensively for their widespread utilizations as the popular “green solvents”.^{391,392} Among ILs, the ones having hydrophobic alkyl chains as the substituents, usually at their organic cationic parts, are known to display properties quite similar to the conventional surfactants, especially in regard to their aggregation and surface active properties. Such ILs having hydrophobic alkyl chains in their structures are designated as the surface active ILs (SAILs).³⁹³⁻³⁹⁵ In fact, it is observed that the SAIL systems often display more effective surface activity than many other conventional surfactants in different applications.^{396,397} Being biologically friendly in general, ILs can be considered as the preferred co-surfactants than the conventional co-surfactants like SDS, TX100, CTAC, etc. used in modifying the microenvironments of different block copolymer micelles through the formation of the mixed micellar systems, that have wide applications in different areas.^{118,176,179,197,396,397} Interestingly, however, unlike conventional surfactant–block copolymer based mixed micellar systems, very limited studies are reported in the literature using ILs as the co-surfactants for the mixed micellar assemblies.

The effects of alkyl chain lengths, anionic counterparts and concentrations of various pyridinium based ILs on the pluronic P123 micelles have been reported by Vekariya et al.³⁹⁸ observing a systematic decrease in the micellar size and aggregation number in the presence of ILs as the additives. The effect of the 1-alkyl-3-methylimidazolium ($[C_nMIm]^+$; n is the carbon number

of the alkyl chain) based ILs on the TX100 micelles have also been reported by Thakkar et al. al.,³⁹⁹ where hydrophilic counter anions were seen to cause a decrease but the hydrophobic counter anions caused an increase in the micelle size. Pillai et al.¹⁶⁶ have also investigated the microstructural changes for the T1304 star block copolymer micelles by the presence of $[C_n\text{MIm}]^+$ based ILs with various counteranions and observed quite analogous results in regard to the micellar size and aggregation number. All these studies, however, missed to give attention to the physicochemical characteristics of the studied mixed micelles, like the micropolarity, microviscosity, solvent relaxation dynamics, and so on, which are very important parameters in modulating the chemical reactions like the PET processes. Additionally, to the best of our knowledge, there is no report so far in relation to the studies on bimolecular PET processes in the tetronic-IL mixed micellar assemblies. In the present study, thus, we have investigated the PET reactions involving various coumarin dyes as electron acceptors and *N,N*-dimethylaniline (DMAN) as the electron donor, using a number of T1304-IL mixed micellar assemblies, where a series of $[C_n\text{MIm}][\text{BF}_4]$ ILs are used as the co-surfactants.

Chart 4.1. Chemical structures of the T1304 star block copolymer, the $[C_n\text{MIm}][\text{BF}_4]$ series of ILs, the coumarin dyes and the DMAN donor used in the present study



Selection of the T1304- $[C_n\text{MIm}][\text{BF}_4]$ mixed micelles in the present study is based on the consideration that the necessary structural parameters of these mixed micelles are well reported in the literature. Along with the PET studies, we have also carried out elaborate characterization of the micropolarity, microviscosity, and solvent relaxation dynamics in these mixed micellar systems, to correlate the energetics and kinetics of the PET processes adequately, especially in reference to the Marcus ET theory and Marcus Inversion (MI) behavior for the observed ET rates. The $[C_n\text{MIm}][\text{BF}_4]$ series of ILs used in the present study have varying 1-alkyl chains (C_n) with n values equal to 4, 6 and 10, and we use their abbreviations as [BMIm][BF₄], [HMIm][BF₄], and [DMIm][BF₄], respectively, where the alphabets B, H, and D signify the 1-butyl, 1-hexyl and 1-

decyl chains, respectively. In this study we try to understand the role of these ILs in affecting the microenvironments of the so formed mixed micellar systems and thus to modulate the kinetics and energetics of PET reactions, having immense academic and applied implications. Chemical structures of T1304 copolymer, IL systems, coumarin dyes, and DMAN donor are shown in Chart 4.1 for their quick visualizations.

4.2. Materials and Methods

The sources of the T1304 star block copolymer, coumarin dyes, DMAN donor, nanopure water and organic solvents used in this study were the same as mentioned in Chapter 3. The $[C_n\text{Mim}][\text{BF}_4]$ series of ILs were obtained from Prof. Anil Kumar of CSIR-National Chemical Laboratory, Pune, India, and used as received. All the experimental solutions were prepared in 5% (w/v) T1304 solution following the procedure discussed in Chapter 3. Requisite weights of the ILs (cf. Chart 4.1) were added to 5% (w/v) T1304 solution to prepare the desired mixed micellar systems keeping the concentration of the ILs always constant at 30 mM for all the experimental solutions. The dye concentrations used were about 5 μM , which is much lower than the typical micelle concentration present in the solution ($\sim 130 \mu\text{M}$) and thus only a small fraction of the micelles can actually get occupied by single dye molecules and the fraction of the micelles hosting more than one dye molecules can be considered to be just negligible.^{127,161,347,352-354}

Experimental details for the ground state absorption, steady-state (SS) emission, and time-resolved (TR) fluorescence measurements are the same as discussed in Chapter 2. As in Chapter 3, the fluorescence lifetime measurements, fluorescence anisotropy studies and dynamic Stokes' shift studies in the present work were also carried out using a 406 nm pulsed diode laser as the excitation source in the TCSPC setup, for which the width of the IRF is found to be ~ 190 ps at FWHM.¹⁴⁸ Similar to the study in Chapter 3, the C153 dye was used as the fluorescence probe to estimate various physiochemical parameters of the studied mixed micellar systems. All the experiments were carried out at 30 °C, which is far above the CMT of the 5% (w/v) T1304 solution used in the present study.

4.3. Results and Discussion

4.3.1. Ground State Absorption and Steady-State Fluorescence Studies

Ground state absorption measurements were carried out for all the coumarin-DMAN pairs (cf. Chart 4.1) in both pure T1304 micelle and in different T1304-IL mixed micelles. In all the cases, the absorption spectra of the studied coumarin dyes are not affected any significantly by the presence of the DMAN donor. Representative results for C153-DMAN pair in pure T1304 micelle are shown in the inset of Figure 4.1A. Observed results suggest that in all the micellar media there is no significant interaction for the ground state coumarin dyes with the DMAN donor.

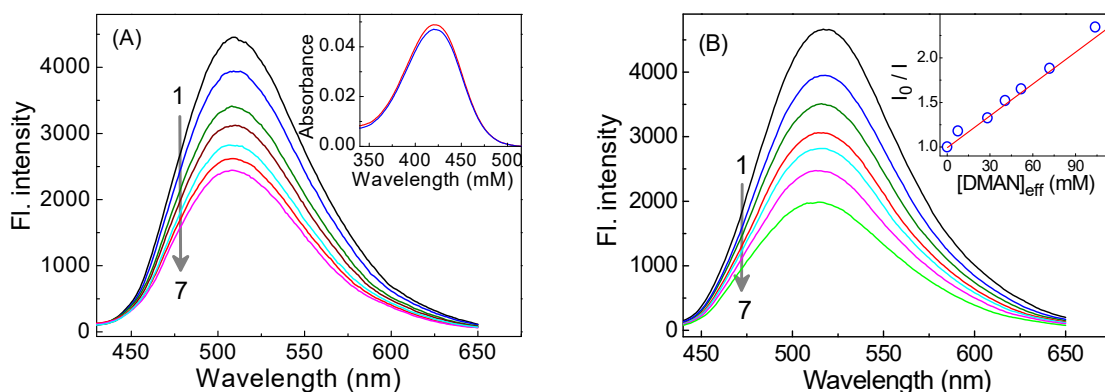


Figure 4.1. (A) Fluorescence quenching of C153 dye in T1304 micelle by DMAN. For (1-7) $[DMAN]_{eff}/mM$ are: 0, 22.9, 43.7, 62.7, 80.1, 96.1 and 110.9 mM, respectively. Inset shows the absorbance spectra of the dye in the absence (blue) and presence (red) of 110.9mM DMAN. (B) Fluorescence quenching of C153 in T1304-[DMIm][BF₄] mixed micelle by DMAN; for (1-7) $[DMAN]_{eff}/mM$ are: 0, 7.6, 28.3, 40.6, 51.9, 71.8 and 103.8 mM, respectively. Inset shows the SV plot obtained for C153-DMAN pair in the studied mixed micelle.

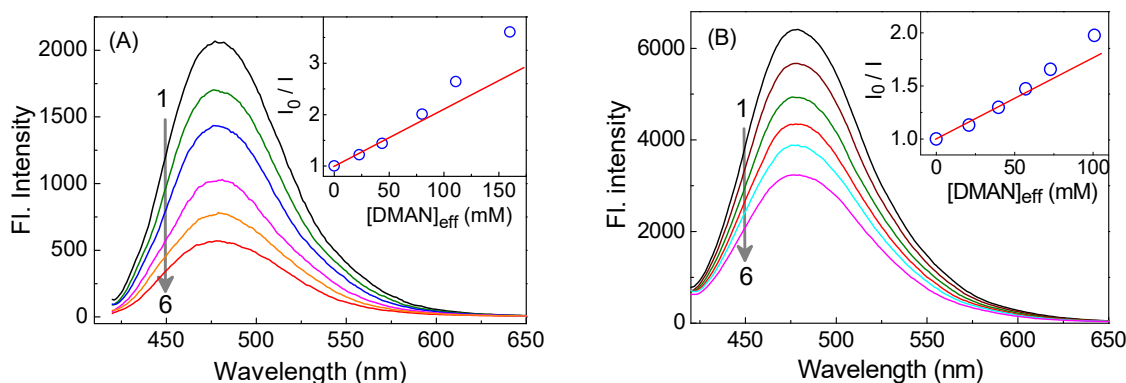


Figure 4.2. (A) Fluorescence quenching of C151 dye in T1304 micelle by DMAN. For (1-6) $[DMAN]_{eff}/mM$ are: 0, 22.9, 43.7, 80.1, 110.9, 160.2 mM, respectively. (B) Fluorescence quenching of C151 dye in T1304-[BMIm][BF₄] mixed micelle by DMAN. For (1-6) $[DMAN]_{eff}/mM$ are: 0, 20.8, 39.8, 57.0, 72.9, 100.9 mM, respectively. In both the panels, the Insets show the SV plots for the C151-DMAN pair in the respective micellar assemblies.

To understand the interaction of the excited coumarin acceptors with DMAN donor in the studied micellar media, SS fluorescence measurements were carried out for all the coumarin-DMAN systems both in the absence and presence of 30 mM ILs (cf. Chart 4.1) in 5 % (w/v) T1304 micellare solutions. In all the cases, the fluorescence intensity undergoes a systematic decrease on increasing the DMAN concentration in the solution, indicating a strong interaction of the excited (S_1) coumarin dyes with the DMAN donor in all the micellar systems. Representative results for C153-DMAN pair in pure T1304 micelle and in T1304-[DMIm][BF₄] mixed micellar system are shown in Figure 4.1A and B, respectively, while those for the C151-DMAN pairs in pure T1304 micelle and T1304-[BMIm][BF₄] mixed micelle are shown in Figure 4.2A and B, respectively.

As discussed in Chapter 3 (cf. Section 3.3.2.1), the SS fluorescence quenching for the coumarin-DMAN systems in different micellar media were also correlated with the estimated effective quencher concentrations $[Q]_{\text{eff}}$ in the corona regions of the studied micelles (cf. eq 3.12), following the standard Stern-Volmer (SV) relation (cf. eq. 3.13). To be mentioned in this respect that in the estimation of the $[Q]_{\text{eff}}$ values, the required dimensional and aggregation parameters for the studied micelles were either obtained from the literature reports or estimated independently in the present study, and the concerned parameters are listed in Table 4.1.¹⁶⁶ The SV plots obtained for different coumarin-DMAN systems in pure T1304 micelle and T1304-IL mixed micelles in general display a mild positive deviation from the otherwise expected linearity from SV relation (cf. eq. 3.13, Chapter 3), as the $[Q]_{\text{eff}}$ concentration is increased in the solution. Typical such SV plots corresponding to the SS fluorescence quenching results shown in Figures 4.1B, 4.2A and 4.2B are displayed in the insets of their respective panels. The positive deviations observed in the SV plots from the SS fluorescence quenching studies suggest that in these micellar media there is a reasonable extent of transient quenching effect on the observed quenching in different fluorophore-quencher pairs, as we have indicated before in Chapter 3, and also reported earlier for the PET reactions in other micellar systems.^{38,116,119,127,236,347-349,400,401} Because the SV plots from SS quenching studies follow a mild positive deviation in the present cases, the apparent bimolecular quenching constant values, $k_{q(SS)}$, could be estimated only from the initial slopes of these plots and are listed in Table 4.2 along with the corresponding $k_{q(TR)}$ values obtained from TR fluorescence quenching studies as are discussed in the next section.

Table 4.1. The micellar dimensional and aggregation parameters and the estimated micro-polarities in the corona region of the studied pure T1304 and T1304-IL mixed micellar systems.^a

Micellar System	CMC (mM)	R_c (Å)	R_h (Å)	N_{agg}	ϵ	$E_T(30)$ (kcal mol ⁻¹)	D_n
T1304	0.095	44.9	69.9	36	7.2	43.4	31.0
T1304-[BMIm][BF ₄]	0.095	45.6	71.4	35	7.7	44.1	31.0
T1304-[HMIm][BF ₄]	0.095	45.3	71.1	34	8.0	44.6	31.0
T1304-[DMIm][BF ₄]	0.095	38.7	64.9	20	11.2	47.5	31.0

^a R_h , R_c , N_{agg} values were obtained from ref. 166. The CMC values and the micropolarity parameters (ϵ and $E_T(30)$) for these systems were estimated in the present study, as discussed latter. The D_n values for all micelles were considered to be similar to the reported D_n value in DeOH solvent.³⁸²

In the present study, since the CMC values for the concerned T1304-IL mixed micelles are not available in the literature, we independently measured the CMC values in these cases following the T1304 concentration dependent shifts in emission spectra of the probe dye C153, both in the

absence and in the presence of the 30 mM ILs listed in Chart 4.1. In aqueous solution, C153 shows its emission peak at ~ 550 nm. As the small aliquots of concentrated T1304 stock solution (10% w/v) were gradually added to the aqueous solution of C153 dye, a significant blue shift was observed initially for the emission peak of the dye, which was, however, subsided largely at higher T1304 concentration regions. Accordingly, two distinct linear kind of correlations for the fluorescence maxima (λ_{fl}) of the dye as a function of T1304 concentrations could be drawn in all the cases and the intersecting points of these correlations are considered as the *CMC* values in the respective cases. Typical such results both in the absence and in the presence of 30 mM [DMIm][BF₄] as the co-surfactant are shown in Figure 4.3. Similar correlations were also obtained in the presence of the other ILs used in this study (cf. Chart 4.1). The *CMC* values estimated in different cases are listed in Table 4.1. Interestingly the *CMC* values obtained in different cases are found to be very similar (cf. dashed vertical line in Figure 4.3), which is about 0.1 wt % or 0.095 mM T1304 in the solution.

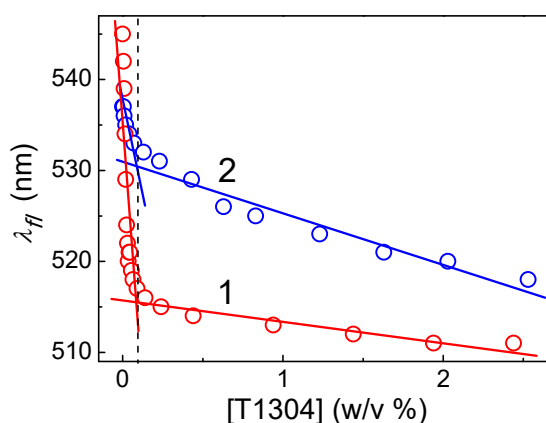


Figure 4.3. Changes in the fluorescence maxima of C153 dye on addition of different concentrations of T1304; (1) Starting with aqueous solution of only dye, and (2) starting with aqueous solution of the dye containing 30 mM [DMIm][BF₄]. The intersecting points indicate the *CMC* values in the respective cases, which are incidentally found to be quite similar (as shown by the dashed vertical line).

4.3.2. Time-Resolved Fluorescence Quenching Measurements

The fluorescence decays of the coumarin dyes were recorded both in the absence and in the presence of varying quencher concentrations in all the studied micellar media. As the representative results, fluorescence decays recorded for the C153-DMAN system in the pure T1304 micelle and in the T1304-[DMIm][BF₄] mixed micellar system are shown in Figures 4.4A and B, respectively. Similar time-resolved (TR) results were also obtained for the other coumarin-DMAN systems in all the micellar media. As indicated from Figure 4.4, the fluorescence decays of the dyes gradually become faster as the quencher concentration is systematically increased in the solution. It is observed in the absence of the quencher, the fluorescence decays in all the cases fit well with a single-exponential function, giving the lifetime values, τ_0 , as are listed in Table 4.2. In the presence of the DMAN quencher, however, the decays become distinctly non-single-exponential in nature and could be

fitted adequately using a bi-exponential function (cf. eq. 3.14). In these cases, the average lifetime values, $\langle \tau \rangle$, were estimated using eq. 3.15, as discussed previously in the Chapter 3, and it is observed that $\langle \tau \rangle$ values for the studied coumarin-DMAN systems undergo a gradual decrease as the DMAN concentration is systematically increased in the solution. Similar to the TR quenching results reported in Chapter 3 (cf. section 3.3.2.2), for all the present cases also, the $\langle \tau \rangle$ values correlate quite linearly with the changing $[Q]_{\text{eff}}$ values in the micellar corona region, as expected from the standard SV relationship given by eq. 3.16 in Chapter 3. Typical such SV plots obtained for C153-DMAN pair in T1304 and T1304-[DmIm][BF₄] micelles are shown in the insets of Figures 4.4A and B, respectively. The $k_{q(\text{TR})}$ values for different coumarin-DMAN pairs in the studied micelles were estimated suitably using the slopes of these linear SV plots (cf. section 3.3.2.2, Chapter 3) and the $k_{q(\text{TR})}$ values thus obtained in different cases are listed in Table 4.2.

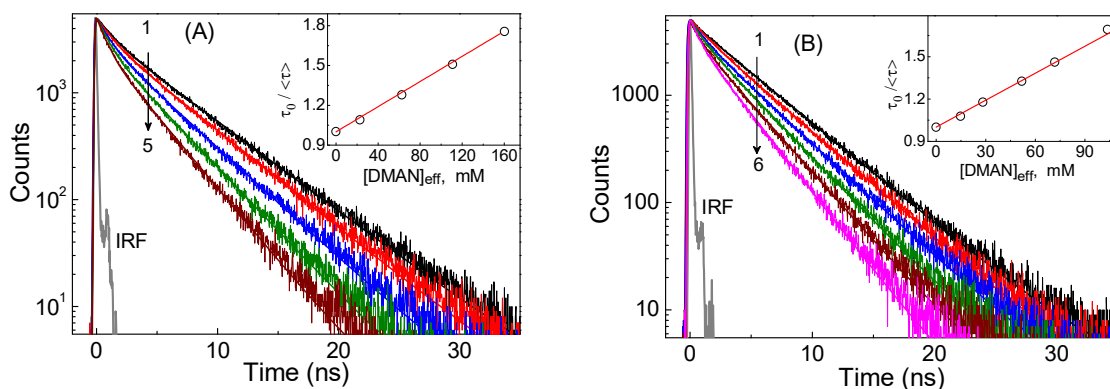


Figure 4.4. Fluorescence decays of C153 in (A) T1304 micelle and (B) in T1304-[DmIm][BF₄] mixed micelle in the presence of varying DMAN concentrations. $[\text{DMAN}]_{\text{eff}}/\text{mM}$ for traces 1 to 5 in panel (A) are: 0, 22.9, 62.7, 110.9, 160.2, respectively, and for traces 1 to 6 in panel (B) are: 0, 14.8, 28.3, 40.6, 71.8, 103.8 mM, respectively. IRF is the instrument response function.

As it is observed from Table 4.2, the $k_{q(\text{TR})}$ values estimated from the TR fluorescence quenching studies are always lower than the respective $k_{q(\text{SS})}$ values estimated from the previously discussed SS fluorescence quenching measurements. It is thus evident from the observed results that for the quenching interactions of the studied coumarin-DMAN systems in the micellar media investigated in the present study there is always a presence of significant extent of transient quenching contributions in the SS results especially, which apparently remained undetected in the TR quenching results, due to the limited time-resolution of the present TCSPC setup (IRF ~ 190 ps). Since the $k_{q(\text{TR})}$ values were estimated very accurately using the linear SV plots from the TR fluorescence quenching results, these values were subsequently used to correlate with the free energy changes (ΔG^0) of the PET reactions following the Marcus ET theory, as discussed with necessary details in Chapter 1.^{10-12,14-19}

Table 4.2. Various energy parameters for PET reactions involving coumarin acceptors and DMAN donor in pure T1304 micelle and in T1304-IL mixed micellar assemblies.

Micellar System	Coumarin Dye	τ_0 (ns)	$k_{q(SS)}$ ($10^8 \text{ M}^{-1} \text{ s}^{-1}$)	$k_{q(TR)}$ ($10^8 \text{ M}^{-1} \text{ s}^{-1}$)	$E(A/A^{\cdot-})$ (V)	$E(D^+/D)$ (V)	E_{00} (eV)	ΔG^0 (eV)
T1304	C151	5.47	23.33	13.19	-1.80	0.91	2.88	-0.48
	C152	3.09	31.67	21.31	-1.84		2.82	-0.36
	C481	3.17	27.81	19.12	-1.87		2.82	-0.33
	C522	5.14	30.33	16.11	-1.86		2.76	-0.28
	C153	5.02	14.39	9.11	-1.89		2.66	-0.15
T1304 + [BMIm][BF ₄]	C151	5.45	14.90	12.67	-1.77	0.90	2.88	-0.50
	C152	3.01	38.54	23.51	-1.82		2.82	-0.38
	C481	3.15	45.67	24.32	-1.85		2.81	-0.34
	C522	5.12	30.46	17.44	-1.84		2.75	-0.29
	C153	5.04	15.58	9.17	-1.87		2.66	-0.16
T1304 + [HMIm][BF ₄]	C151	5.55	25.04	14.57	-1.76	0.89	2.87	-0.50
	C152	3.05	53.44	29.72	-1.81		2.81	-0.38
	C481	3.04	66.04	35.91	-1.83		2.82	-0.35
	C522	5.19	35.45	24.51	-1.83		2.75	-0.30
	C153	4.95	23.66	12.8	-1.86		2.66	-0.18
T1304 + [DMIm][BF ₄]	C151	5.39	28.01	15.66	-1.67	0.82	2.87	-0.58
	C152	2.50	56.08	35.59	-1.72		2.81	-0.46
	C481	2.40	66.67	43.29	-1.75		2.81	-0.42
	C522	4.89	34.76	30.54	-1.75		2.75	-0.37
	C153	4.48	27.68	14.47	-1.78		2.65	-0.24

4.3.3. Correlations of the Observed PET Rates with the Free Energy Changes (ΔG^0) of the PET Reactions in the Studied Micellar Media

The ΔG^0 values for the PET reactions involving excited (S_1) coumarin acceptors and DMAN donor in the studied micelles were estimated following the Rehm-Weller relation as given by eq. 3.17 in Chapter 3. Since the redox potential values for the coumarin acceptors could not be estimated

reliably using cyclic voltametric measurements, due to the limited solubility of the studied dyes in the used micellar media, in the present study we utilized the redox potentials for both the acceptor dyes and donor DMAN systems, namely the $E(A/A^-)$ and $E(D^+/D)$ values, in acetonitrile solutions, as reported in the literatures, introducing however the appropriate corrections for these values due to the changes in the reaction medium from acetonitrile (ACN) to the studied micellar systems. The concerned methodology of these correction, referred as the Fawcett's corrections,^{92,378,379} has been elaborately discussed previously in Chapter 3 (cf. Section 3.3.2.3).

Table 4.3. Calculated electrochemical properties of the acceptor (coumarin dyes) and donor (DMAN) systems in acetonitrile (ACN) solvent and in T1304 and T1304+IL micellar media.

(A) Electrochemical Properties of the Acceptor Systems						
Acceptor	Electro-chemical Parameter	Solvent Systems				
		ACN	T1304	T1304 + [BMIm][BF ₄]	T1304 + [HMIm][BF ₄]	T1304 + [DMIm][BF ₄]
C151	$G_S^0(A^-)$ (eV)	-1.837	-1.605	-1.629	-1.643	-1.735
	$E(A/A^-)$ (V) ^a	-1.565	-1.800	-1.770	-1.760	-1.670
C152	$G_S^0(A^-)$ (eV)	-1.734	-1.516	-1.539	-1.551	-1.637
	$E(A/A^-)$ (V) ^a	-1.626	-1.840	-1.820	-1.810	-1.720
C481	$G_S^0(A^-)$ (eV)	-1.653	-1.446	-1.467	-1.480	-1.560
	$E(A/A^-)$ (V) ^a	-1.660	-1.870	-1.850	-1.830	-1.750
C522	$G_S^0(A^-)$ (eV)	-1.677	-1.467	-1.489	-1.501	-1.583
	$E(A/A^-)$ (V) ^a	-1.653	-1.860	-1.840	-1.830	-1.750
C153	$G_S^0(A^-)$ (eV)	-1.630	-1.426	-1.447	-1.459	-1.538
	$E(A/A^-)$ (V) ^a	-1.685	-1.890	-1.870	-1.860	-1.780
(B) Electrochemical Properties of the Donor Amine						
DMAN	$G_S^0(D^+)$ (eV)	-1.750	-1.599	-1.615	-1.624	-1.691
	$E(D^+/D)$ (V) ^a	0.760	0.910	0.900	0.890	0.820

^a $E(A/A^-)$ and $E(D^+/D)$ values in ACN against SCE were obtained from ref. 375.

To incorporate the aforesaid Fawcett's corrections,^{92,378,379} we needed the micropolarity parameters like dielectric constant (ϵ) and $E_T(30)$ values for the studied micellar systems. These micropolarity parameters for the corona region of the studied micelles were estimated following the

SS fluorescence characteristics of the probe dye C153 (cf. Figure 4.5A, B and C), as discussed elaborately earlier in Chapter 3 (cf. Sections 3.3.1.1 and 3.3.2.3). In the present context, the required donor numbers (D_n) for the studied micellar systems were considered to be similar to that of the decanol solvent ($D_n = 31.0$),^{380,382,402} and the justification for this consideration is similar to that as discussed earlier in Chapter 3 (cf. Section 3.3.2.3). Different electrochemical parameters estimated for the studied coumarin and DMAN systems in different micellar media following Fawcett's corrections are listed in Table 4.3.^{92,378,379} The subsequently estimated ΔG^0 values for the concerned PET systems following the standard Rehm-Weller relation (cf. eq. 3.17, Chapter 3) are listed in Table 4.2 along with the concerned $k_{q(SS)}$ and $k_{q(TR)}$ values to understand their direct correlations.

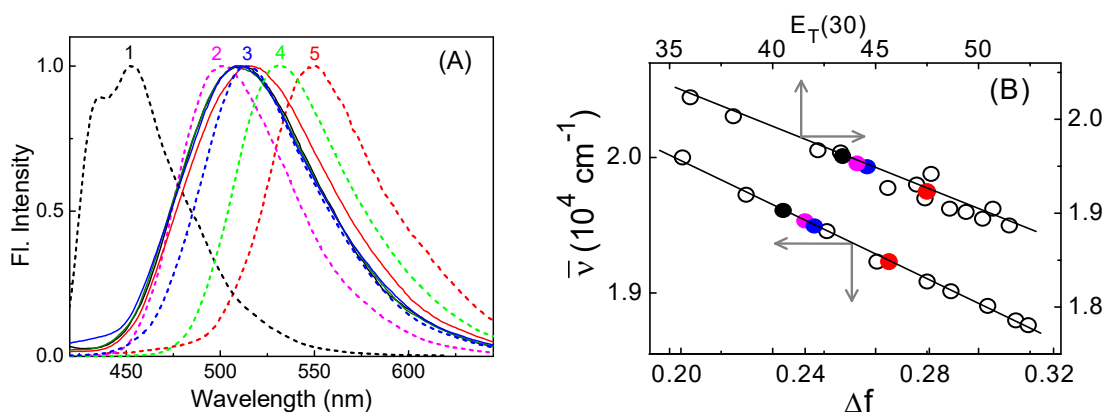


Figure 4.5. (A) Emission spectra for C153 dye; Dotted lines in different conventional solvents: cyclohexane(1), ethyl acetate(2), decanol(3), methanol(4) and water (5), while solid lines in the studied micelles: T1304 (black), T1304-[BMIm][BF₄] (green), T1304-[HMIm][BF₄] (blue), T1304-[DMIm][BF₄] (red). (B) and (C) Calibration plots for Δf and $E_T(30)$ values, respectively; open circles are calibration data and solid circles are the data for the studied micellar systems: T1304 (black), T1304-[BMIm][BF₄] (magenta), T1304-[HMIm][BF₄] (blue), T1304-[DMIm][BF₄] (red).

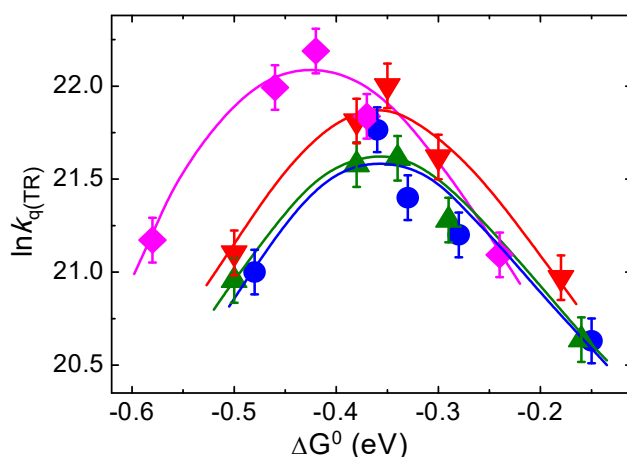


Figure 4.6. Plots of $\ln(k_{q(TR)})$ versus ΔG^0 for PET reactions in T1304 (blue), T1304-[BMIm][BF₄] (olive), T1304-[HMIm][BF₄] (red) and T1304-[DMIm][BF₄] (magenta) micelles. The curves through the data points in the respective micelles have been drawn as a visual guide for the observed correlation.

The correlations of the $k_{q(TR)}$ values with the ΔG^0 values for different coumarin-amine pairs in the pure T1304 micelle and in the T1304-IL mixed micellar systems are shown in Figure 4.6 for their direct comparison. From this figure, it is apparent that the $k_{q(TR)}$ values increase with $-\Delta G^0$ at the lower exergonicity ($-\Delta G^0$) region but evidently decrease with $-\Delta G^0$ at the higher exergonicity region, displaying clearly the Marcus Inversion (MI) behavior in all the cases, as discussed earlier in Chapter 1. The MI in the present study indicates that the T1304 micelle and T1304-IL mixed micellar systems provide very conducive reaction environments for the unique MI behavior to be observed easily for the studied bimolecular PET reactions. The correlations in Figure 4.8 further indicate that with the addition of the ILs as the co-surfactants in T1304 micellar system induces quite significant changes on the ET rates as well as on the exergonicity ($-\Delta G^0$) value for the onset of the MI behavior as compared to those in the pure T1304 micelle. It is also clearly indicated that with the increasing chain lengths for the $[C_nMIm]^+$ cations in the ILs used, there is a gradual increase in the $k_{q(TR)}$ values along with a systematic shift for the onset of the MI towards the higher exergonicity region for the studied PET systems.

As can be seen from Figure 4.6, the onset of the MI in pure T1304 micelle appears at an exergonicity of ~ 0.36 eV and the onset shifts to an exergonicity of ~ 0.45 eV in the case of T1304-[DMIm][BF₄] mixed micellar system. However, these exergonicity values for the onset of the MI are invariably much lower than one would expect considering the fast solvent relaxation and the consequent thermal equilibration of the solvent polarizations around the reacting donor-acceptor pairs. As mentioned in Chapter 1, such a situation arises when solvent relaxation process is significantly slower such that the ET reactions need to proceed along the intramolecular coordinate keeping the reactant state in the thermally non-equilibrated conditions along the solvent coordinate, which is described explicitly in the two-dimensional ET (2DET) theory.^{18,93,94,403} To investigate this aspect further and to comprehend the reasons behind the IL induced modulations in the ET rates on their correlations with the exergonicity values, we also estimated the microviscosity and the solvent relaxation dynamics in the corona region of the studied micellar systems and the relevant discussions are presented in the following sections.

4.3.4. Time-Resolved Fluorescence Anisotropy Studies: Microviscosity Estimations

The microviscosity (η_m) measurements for present micellar systems were carried following the TR fluorescence anisotropy studies, as discussed earlier in Chapter 3 (cf. Section 3.3.1.2). Observed fluorescence anisotropy decay traces for the probe dye (C153) in different micellar systems are shown in Figure 4.7. The anisotropy decay parameters as estimated from the analysis of these decays and also the subsequently calculated average rotational correlation times $\langle \tau_r \rangle$ of the probe dye (C153) in different micellar systems (cf. Section 3.3.1.2, Chapter 3) are listed in Table 4.4. It is evident from Figure 4.7 and Table 4.4 that the anisotropy decays are in general faster in T1304-IL

mixed micelles as compared to the pure T1304 micelle, suggesting that the probe dye in the micellar corona region experiences a reduced microviscosity as the ILs are incorporated as the co-surfactants into the T1304 micelle. Moreover, it is found that all the τ_{r1} , τ_{r2} and $\langle\tau_r\rangle$ values in the studied micellar systems undergo a gradual decrease, as the alkyl chain lengths for the $[C_n\text{MIm}]^+$ cations of the ILs are increased systematically. Observed results suggest that the ILs that are having longer alkyl chains for the $[C_n\text{MIm}]^+$ cations are incorporated more preferably into the T1304 micelle, which in turn causes the corona region of the so formed mixed micelles to be gradually less viscous as compared to that of the pure T1304 micelle.

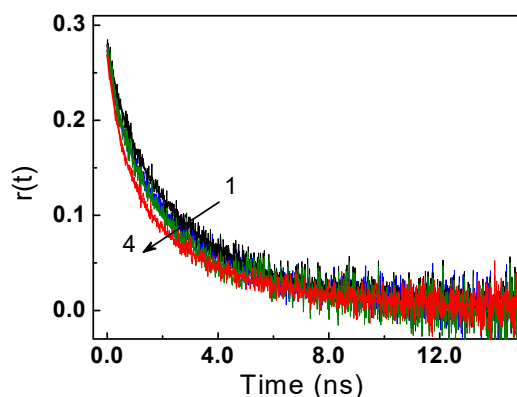


Figure 4.7. Fluorescence anisotropy decay traces of C153 in (1) T1304, (2) T1304-[BMIm][BF₄], (3) T1304-[HMIm][BF₄] and (4) T1304-[DMIm][BF₄] micellar media at 30 °C. The concentration of T1304 in each case is 5% (w/v) and the concentrations of the ILs are 30 mM.

Table 4.4. Anisotropy decay parameters of C153 in pure T1304 and T1304-IL micellar media.

Medium	τ_{r1} (ns) ^a	$(r_{0,1})^b$	$A_{r1}(\%)^c$	τ_{r2} (ns) ^a	$(r_{0,2})^b$	$A_{r2}(\%)^c$	$\langle\tau_r\rangle$ (ns)	$\eta_m(\text{cP})^d$
T1304	0.55	0.10	6.3	3.58	0.22	93.7	3.39	58
T1304+ [BMIm][BF ₄]	0.54	0.12	8.8	3.47	0.19	91.2	3.21	55
T1304 + [HMIm][BF ₄]	0.52	0.10	6.5	3.30	0.21	93.5	3.09	53
T1304 + [DMIm][BF ₄]	0.50	0.10	8.8	2.92	0.16	91.2	2.71	46

^aError limit in τ_{r1} and τ_{r2} values are ± 0.03 ns; ^bError limit in $r_{0,1}$ and $r_{0,2}$ values are ± 0.01 ;

^c $A_{ri}(\%) = A_{ri} \times 100$; ^dCalculated following eq. 3.9

Applying the Stokes-Einstein-Debye (SED) relation and considering the hydrodynamic volume V_h of the dye as 245 Å³ (calculated using Edward's volume addition method),³⁷⁰ the η_m values in the corona regions were calculated using eq. 3.9 in Chapter 3, and the values thus estimated for different micellar systems used in the present study are listed in Table 4.4. As it is indicated from this table, while the η_m value for the pure T1304 micelle is ~58 cP, the value reduces

to ~46 cP in T1304-[DMIm][BF₄] mixed micelle that is having the longest alkyl chain length IL. Such decrease in the η_m values for the T1304-IL mixed micellar systems as compared to the pure T1304 micelle clearly suggests that with the incorporation of the ILs into the T1304 micelle there is a significant increase in the hydration for the micellar corona region, which also corroborates nicely with the increased micropolarity for the T1304 micelle with the incorporation of these ILs, as we have already discussed before (cf. Section 4.3.3).

4.3.5. Solvent Relaxation Dynamics Studies in the Investigated Micellar Media

Solvent relaxation dynamics in the corona region of the studied micellar media were explored following the dynamic Stokes shift studies using C153 as the fluorescence probe. In all the micelles, the fluorescence kinetic traces for the probe dye display much faster decay at the shorter wavelengths and an initial growth followed by a relatively slower decay at the longer wavelengths, clearly indicating the occurrence of dynamic Stokes' shifts in these cases due to solvent relaxation dynamics. Representative kinetic traces in T1304-[DMIm][BF₄] mixed micelle covering the entire emission spectrum (450 nm-650 nm) of C153 dye are shown in Figure 4.8. Time resolved emission spectra (TRES) were constructed following the procedure discussed in Chapter 1 (cf. Section 1.6) and in all the cases the TRES show a reasonable red shift in the emission maxima with the increasing delay time following the photoexcitation process. Representative TRES for C153 dye in T1304-[DMIm][BF₄] mixed micelle is shown in Figure 4.8B. From the TRES, the normalized spectral shift correlation functions $C(t)$ were also constructed in all the studied micelles following the procedure given in Chapter 1 (cf. Section 1.6) and are shown in Figure 4.9 for their comparison.

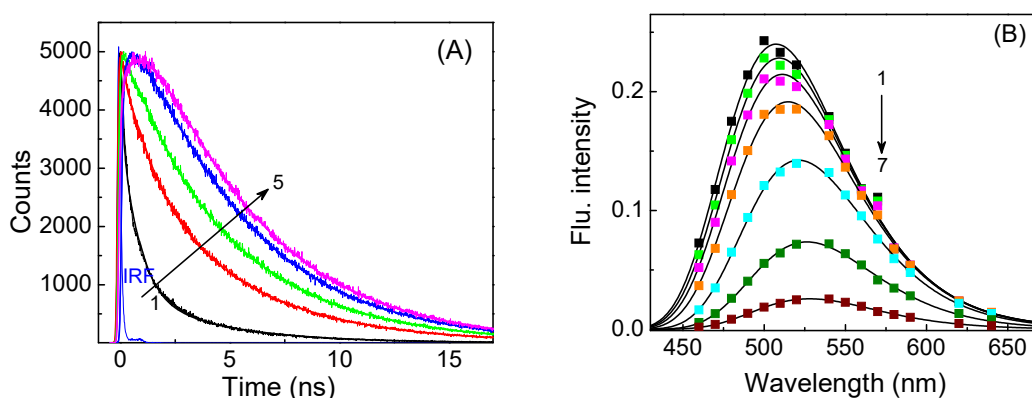


Figure 4.8. (A) Fluorescence kinetic traces for C153 dye in T1304-[DMIm][BF₄] mixed micelle monitored at different emission wavelengths, (1-5/nm): 460, 500, 520, 550, 600, respectively. (B) The TRES for C153 dye in T1304-[DMIm][BF₄] mixed micelle constructed at different time delays following the photoexcitation of the dye, (1-7/ns): 0.05, 0.2, 0.4, 0.8, 2.0, 5.0 and 10.0, respectively. The symbols are the experimental data points and the continuous curves are the lognormal fits to the data points at the respective time delays.

Alike most other micellar systems, in the present cases also the $C(t)$ curves fit adequately with a bi-exponential function (cf. Section 3.3.1.3, Chapter 3) and the decay parameters thus

estimated are listed in Table 4.5. In the present cases, since the time resolution of the used TCSPC setup is limited (FWHM of IRF ~ 190 ps), in the present context we also estimated the anticipated total dynamic Stokes' shifts ($\Delta \bar{\nu}_{\text{expected}}^{\text{sol}}$) and the initial missing percentage of the Stokes' shifts in the present systems, estimated following the procedure discussed in Chapter 3 (cf. Section 3.3.1.3), and the values of these parameters thus obtained in different micelles are also listed in Table 4.5. Observed results suggest that a large part of the initial dynamic Stokes' shifts are missed in the current measurements using the present TCSPC setup. Based on these results we infer that the $C(t)$ curves constructed in the present study actually represent the slower parts of the solvation relaxation process in the studied micelles, which effectively decays with a bi-exponential function.

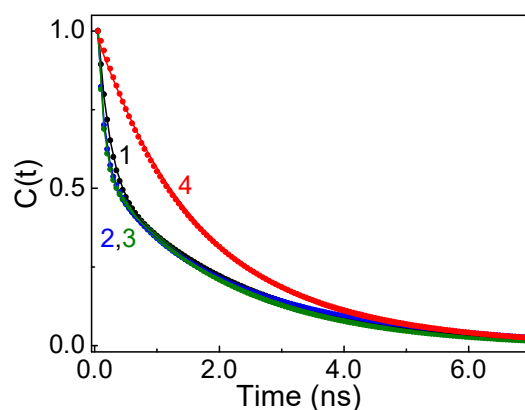


Figure 4.9. Normalized spectral shift correlation functions, $C(t)$, for C153 in (1) T1304, (2) T1304-[BmIm][BF₄], (3) T1304-[HmIm][BF₄] and (4) T1304-[DmIm][BF₄].

Table 4.5. Solvation times and their relative contributions as obtained from bi-exponential analysis of the normalized spectral shift correlation function $C(t)$ in pure T1304 and T1304-IL mixed micellar media.

Medium	A_{s1} (%) ^a	τ_{s1} (ns) ^b	A_{s2} (%) ^a	τ_{s2} (ns) ^b	$\langle \tau_s \rangle$ (ns)	$\Delta \bar{\nu}_{\text{expected}}^{\text{sol}}$ (cm ⁻¹)	$\Delta \bar{\nu}_{\text{obs}}^{\text{sol}}$ (cm ⁻¹)	Missing %
T1304	9	0.19	91	2.30	2.11	2930	1172	60
T1304 + [BmIm][BF ₄]	7	0.13	93	2.27	2.12	2930	1172	60
T1304 + [HmIm][BF ₄]	6	0.10	94	2.05	1.93	2930	1131	61
T1304 + [DmIm][BF ₄]			100	1.72	1.72	3184	784	75

^a: $A_{si}(\%) = A_{si} \times 100$; ^b: Error limit in τ_{s1} and τ_{s2} values are ± 0.03 ns;

From the results in Figure 4.9 and Table 4.5, it is evident that in the presence of the ILs as the co-surfactants, the solvation process becomes faster in the T1304 micelle and the effect is apparently stronger on increasing the alkyl chain lengths of the used ILs. Thus, both τ_{s1} and τ_{s2}

values decrease gradually and the relative contribution of τ_{s1} systematically reduces with a concomitant increase in the relative contribution of τ_{s2} component, as we move from pure T1304 micelle (no IL added) to T1304-[BMIm][BF₄] and T1304-[HMIm][BF₄] mixed micellar systems. Interestingly, in the T1304-[DMIm][BF₄] system, we could not detect any τ_{s1} component and the $C(t)$ curve effectively fitted with a single-exponential function, apparently suggesting that in this case the contribution of τ_{s1} is reduced so drastically that this component as a whole becomes completely undetected in the constructed $C(t)$ curve from the measurements carried out using the TCSPC setup having a limited time resolution. This is undoubtedly supported by the much larger missing percentage of the initial Stokes' shifts in the T1304-[DMIm][BF₄] mixed micelle as compared to those in other micelles. Observed solvent relaxation dynamics results clearly suggest that with the incorporation of the ILs as the co-surfactants into the T1304 micelles there is a significant increase in the hydration for the micellar corona region, which also corroborates nicely with the increased micropolarity and decreased microviscosity in these cases as we have discussed before (cf. Section 4.3.3 and 4.3.4). Despite the pronounced effects of the added ILs on the solvent relaxation dynamics for the studied micelles, a comparison of the $\langle\tau_s\rangle$ values (cf. Table 4.5) with the observed $k_{q(TR)}$ values (cf. Table 4.2) reveals that in all these cases the average solvent relaxation rates ($\langle\tau_s\rangle^{-1}$) are quite in the similar range as that of the observed PET rates ($k_{q(TR)}$), indicating that during the PET reactions in the present cases, the solvent configuration around the reactant state, as created at point of photoexcitation of the coumarin dyes, cannot undergo a complete thermal equilibration, as normally presumed in the conventional Marcus ET theory.^{10-12,14-19} Accordingly we infer that the 2DET mechanism^{18,93,94,403} is actually applicable to the PET reactions investigated in the present study using T1304 micelle and T1304-IL mixed micelles as the reaction media.

4.3.6. Modulations of Marcus Inversion (MI) Behavior by the Presence of ILs as the Co-surfactants in T1304 Micelles

Comparing the $k_{q(TR)}$ versus ΔG^0 correlations for the PET reactions in pure T1304 micelle and T1304-IL mixed micelles, as are shown in Figure 4.6, it is evident that the $k_{q(TR)}$ value for any particular donor-acceptor pair increases quite substantially as the [C_nMIm][BF₄] series of ILs are added to the T1304 micellar solution. Similarly, for the $k_{q(TR)}$ versus ΔG^0 correlations as whole in different micelles, the onset of the MI gradually also shifts significantly toward higher exergonicity ($-\Delta G^0$), as these ILs are added in the micellar solution. It is also interestingly seen from Figure 4.6 that both the aforesaid effects become gradually more pronounced as the alkyl chain length (C_n) of the [C_nMIm][BF₄] series of ILs is increased systematically. For the PET reactions involving similar coumarin-aromatic amine systems in low viscosity conventional homogeneous solvents, e.g acetonitrile (ACN; $\eta = 0.37$ cP),³⁵⁷ the bimolecular diffusion-controlled rate constant k_d is reported to be $\sim 1.5 \times 10^{10} \text{ dm}^3 \text{ mol}^{-1} \text{ s}^{-1}$.^{375,404} Therefore, based on the estimated microviscosities (η_m) in the

corona regions of the studied micellar systems (η_m ranging between 46 to 58 cP; cf. Table 4.4) and considering that k_d values are inversely related to the viscosity (i.e. $k_d \propto 1/\eta$), the expected k_d values in the the studied micelles are estimated to be in the range of $\sim 9.6 \times 10^7$ to $\sim 12.1 \times 10^7 \text{ dm}^3 \text{ mol}^{-1} \text{ s}^{-1}$. These values are certainly much lower than the observed $k_{q(TR)}$ values for the PET processes in the studied coumarin-DMN pairs in the present micellar media (cf. Table 4.2), indicating that the bimolecular PET in the studied micellar systems definitely occurred under a non-diffusive reaction condition, involving mainly those pre-existing acceptor-donor pairs that are within the reaction zone at the point of photoexcitation of the coumarin dyes. From this observation it is also anticipated that in the studied micellar media the appearance of the MI behavior in the $k_{q(TR)}$ versus ΔG^0 correlations is presumably the consequence of this non-diffusive nature of the bimolecular PET reactions in the micellar media, because under such a situation the observed reaction would effectively behave like an intramolecular ET process.^{38,116,119,127,236,347-349,400,401,405,406} With the addition of the ILs in the studied T1304 micellar solution, even though there is a reasonable decrease in the η_m values for the concerned mixed micelles (cf. Table 4.4), these microviscosity changes cannot adequately account the observed facts like the appearance of the onset of MI at an exceptionally lower exergonicity than usually expected, i.e. at $-\Delta G^0 = \lambda$, and the large modulations taken place in the $k_{q(TR)}$ versus ΔG^0 correlations, as the ILs are added in the T1304 micellar solution, because in the present cases the $k_{q(TR)}$ values are always higher than the expected k_d values, as we have discussed above. Accordingly to get a better insight of the reasons behind the observed changes in the $k_{q(TR)}$ versus ΔG^0 correlations by the presence of the ILs in the studied T1304 micellar solution, we explored the solvent relaxation dynamic process in the present micellar systems, because the PET process in any reaction medium is intricately related to the relaxation dynamics of the surrounding solvent.^{18,88-98}

As we have discussed in Section 4.3.5, the average solvent relaxation rate constants ($\langle \tau_s^{-1} \rangle$) and the observed PET rate constants ($k_{q(TR)}$) are apparently in the similar range, indicating that the PET reactions in the studied micellar systems actually occur involving a thermally non-equilibrated solvent configuration for the reactant (R) state, as this R state is created through the photoexcitation of the concerned coumarin dyes. Since the thermally equilibrated solvent configuration for the R state is the presumption in the development of the conventional Marcus 1DET theory (cf. eq. 1.14), it is apparent that the observations made with PET processes in the studied micellar systems cannot be accounted suitably by using this 1DET model, even though this theoretical model is otherwise seen to be very successful in rationalizing various findings associated with the PET reactions in low viscosity conventional solvents, where solvent relaxation dynamics is exceptionally fast.^{9-12,14-16,26-30,34-55,100-115} In our present cases, since the average solvent relaxation dynamics is significantly slow, we infer that the PET reactions in the studied micellar systems effectively occur following the 2DET mechanism, a theoretical model that has been designed to correlate the ET reactions occurring with the involvement of non-equilibrium solvent polarizations around the reactant states, as we have discussed previously in Section 1.2.4 in Chapter 1.^{18,93,94,403}

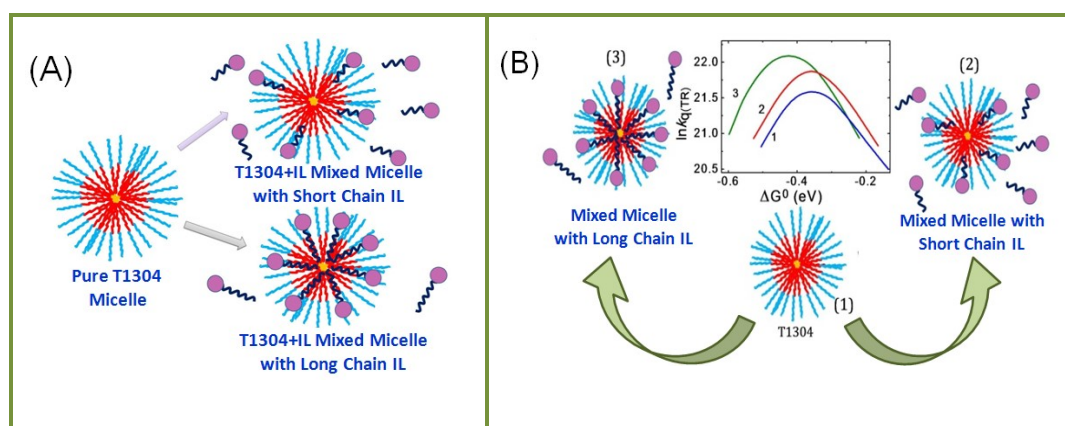
As indicated from Figure 4.6, the $k_{q(TR)}$ values in the T1304-IL mixed micelles are considerably higher as compared to those in pure T1304 micelle. Observed results with the micropolarity and microviscosity determinations clearly suggested that in the T1304-IL systems the added ILs actually participate as the co-surfactants through their inclusion into the existing T1304 micelles in the solution, ensuing the formation of the new T1304-IL mixed micellar systems, for which the micropolarity increases significantly (cf. Table 4.1) and the microviscosity decreases considerably (cf. Table 4.4) for the corona region of the resultant mixed micelles. Accordingly, the solvent environment around the R state for the PET process in the corona regions of these mixed micelles become more conducive for the ET reaction as compared to that in the pure T1304 micelle. Evidently thus, the observed rate constant for the PET reaction ($k_{q(TR)}$) becomes significantly higher in the T1304-IL mixed micelles than in the pure T1304 micellar medium. With the same perspective, since the micropolarity gradually increases (and also microviscosity decreases) for the T1304-IL mixed micellar systems on increasing the alkyl chain length of the [CnMIm][BF₄] series of the ILs as the co-surfactants, the $k_{q(TR)}$ value is also expected to increase along this series of the ILs used, as we have indeed observed experimentally (cf. Figure 4.6). Present results can be rationalized with the consideration that the IL cations with longer hydrophobic chains can enter more deeply and get entangled more proficiently at the nonpolar core of T1304 micelle, resulting a stronger binding of the longer alkyl chain ILs with the resultant micelle, whereby the cationic head groups of these ILs are suitably placed into the moderately polar corona region, causing an increase in the hydration for the corona region of the so-formed mixed micellar assemblies.

Table 4.6. List of the zeta potential values for T1304 micelles and T1304-ILmixed micellar systems.

Micellar System	T1304	T1304+[BMIm][BF ₄]	T1304+[HMIm][BF ₄]	T1304+[DMIm][BF ₄]
ζ (mV)	−4.27	−3.27	−1.97	0.58

The proposition for the incorporation of the used ILs into the T1304 micelles to form the mixed micellar assemblies is clearly supported by the measured zeta potential (ζ) values for these micellar systems, as are listed in Table 4.6. As it is indicated, while the ζ value for pure T1304 micelle is estimated to be about −4.27 mV, which is quite similar to the ζ values reported for other copolymer micelles,^{407,408} for the T1304-IL mixed micellar systems the ζ value gradually becomes less negative and eventually turns to be positive, as the IL is changed from [BMIm][BF₄] to [HMIm][BF₄] to [DMIm][BF₄]. Measured trend in the ζ values clearly indicate that as the alkyl chain length for the substituent in the IL cation increases, the incorporation of the IL into the T1304 micelle becomes more favorable and accordingly more numbers of these ILs are incorporated into the resultant mixed micellar assemblies, on keeping the IL concentration same (30 mM) in all the

cases. This proposition of the differential constitutions of the T1304-IL mixed micelles as a function of the changing alkyl chain lengths of the ILs used in this study can be conceptually presented as in Scheme 4.1A. Understandably, as the number of IL molecules incorporated into the mixed micelles is more for the longer alkyl chain length ILs, they can induce a larger hydration and higher increase in the micropolarity for the corona region and subsequently can result a higher rate constant for the observed PET reaction. Accordingly, the $k_{q(TR)}$ values in the studied micellar systems are seen to follow the order, T1304-[DMIm][BF₄] > T1304-[HMIm][BF₄] > T1304-[BMIm][BF₄] > $k_{et}(T1304)$ (cf. Figure 4.6). Present observations effectively suggest that the use of the tetrionic-IL based mixed micellar systems can render a possible tuning the bimolecular PET reactions, not only in regard to the shifting in the commencement of MI behavior along the exergonicity scale but also in the tuning the observed PET rates quite significantly through the use of ILs of varying alkyl chain lengths as the co-surfactants. The above effects can conceptually be demonstrated as shown in Scheme 4.1B. Such tunings in micellar microenvironments and in the PET reactions using tetrionic-IL based mixed micellar systems are expected to find prospective utilizations in many applied areas.



Scheme 4.1. (A) Schematic representations of the T1304+IL mixed micelles formed on addition of ILs of differential chain lengths. (B) Conceptual presentation for the tunings in the micellar microenvironments and in the PET reactions using tetrionic-IL based mixed micellar systems.

4.4. Conclusion

Bimolecular PET reactions between a series of 7-aminocoumarin dyes as electron acceptors and DMAN as the electron donor have been investigated following both SS and TR fluorescence quenching studies using pure T1304 micelle and T1304-IL mixed micellar systems as the constrained reaction media, where 1-alkyl-3-methylimidazolium tetrafluoroborate ([C_nMIm][BF₄]) type of IL series has been used as the co-surfactants in combination with T1304 star block copolymer micelle. Both SS and TR studies show significant fluorescence quenching for the coumarin dyes by the DMAN quencher in all the micelles studied. While the Stern-Volmer (SV) plots from the SS fluorescence quenching results show a positive deviation from the expected linearity, indicating the substantial contributions arising from the ultrafast transient quenching

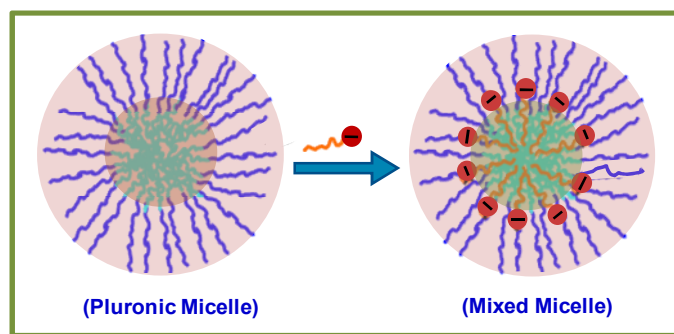
effects in the observed SS quenching results, the SV plots from TR fluorescence quenching results show expected linearity, indicating negligible contribution arising from the ultrafast transient quenching. Accordingly, TR fluorescence quenching results were used to estimate the bimolecular quenching constants ($k_{q(TR)}$) for different coumarin-DMAN pairs in the studied micellar media. Micropolarity, microviscosity and solvent relaxation dynamics in the corona regions of the studied micelles were also investigated following SS fluorescence and TR fluorescence anisotropy and dynamic Stokes' shift studies using coumarin 153 as the probe. Observed results indicate that the ILs with longer alkyl chain lengths influence the micellar microenvironments more effectively, causing an increased hydration for micelle and accordingly an increased micropolarity, reduced microviscosity and faster solvent relaxation dynamics in the micellar corona region. It is proposed that the ILs with longer alkyl chain lengths are incorporated in greater numbers into the T1304 micelles to form the T1304-IL mixed micellar assemblies, and accordingly the presence of more number of cationic head groups of the ILs present in the micellar corona region, causing this region to be gradually more hydrated as compared to the pure T1304 micelle or the T1304-IL mixed micelles having shorter alkyl chain length ILs. Correlations of the $k_{q(TR)}$ values with the reaction exergonicities ($-\Delta G^0$) in different micellar media display clear Marcus Inversion (MI) behaviors, and interestingly the onsets of the MI in all the cases are seen to arise at much lower exergonicity values as compared to that expected following conventional Marcus 1DET theory. Since the average solvent relaxation rates and observed PET rates are found to be quite in the similar range in the studied systems, it is suggested that the PET reaction in the present micellar systems follow the 2DET mechanism, a theoretical model designed for the ET reactions that occur involving non-equilibrium solvent polarization for the reactant states (cf. Section 1.2.4, Chapter 1). In T1304-IL mixed micelles, it is further noticed that the $k_{q(TR)}$ value gradually increases and the onset of MI systematically shifts towards higher exergonicity as the alkyl chain length for the co-surfactant ILs is increased systematically. The reason for these results is attributed to the gradually increasing hydration and enhanced micropolarity of the corona region of the studied mixed micellar systems as the alkyl chain length of the IL co-surfactants increases gradually along the IL series used in this study. Observed results clearly indicate that the constrained micellar microenvironments enforce the studied PET reactions to effectively occur following 2D-ET mechanism, than the conventional 1DET mechanism, and also demonstrate that the bimolecular PET reactions in such systems can be modulated to a substantial extent, both in terms of the observed PET rates and the onset of MI, just by varying the alkyl chain lengths of the ILs used as the co-surfactants in combination with the tetronic copolymer micelles, which are expected to find suitable uses in different applied areas.

CHAPTER-5

ULTRAFAST PHOTOINDUCED ELECTRON TRANSFER IN PLURONIC-SURFACTANT SUPRAMOLECULAR ASSEMBLIES

5.1. Introduction

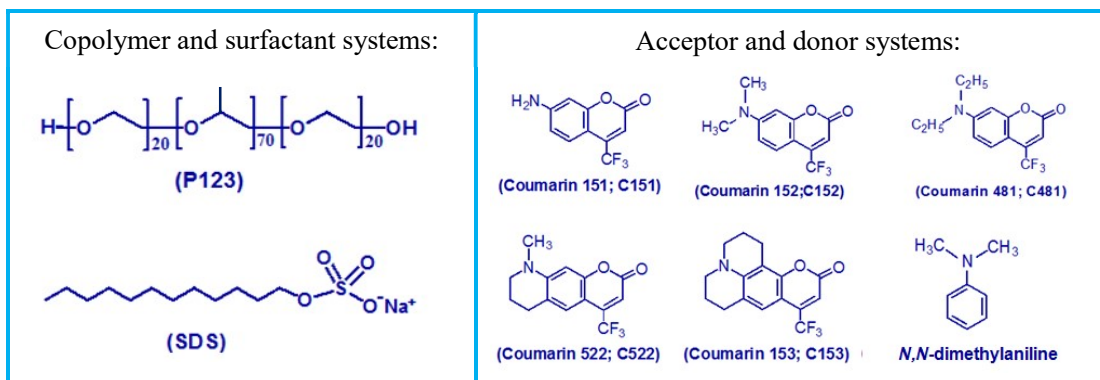
In the earlier chapters we have presented and discussed our results obtained on bimolecular photoinduced electron transfer (PET) studies in different tetronic based micellar media whereby we have seen that such constrained reaction media can provide us an opportunity to modulate the characteristics of the micellar microenvironments (e.g. polarity, viscosity, solvation dynamics, etc.) by using some easy means like addition of co-surfactants or salts. These modulations can in effect change the dynamics and energetics of the studied chemical reactions in these media very significantly, especially those of the PET reactions, finding their better utilizations in different areas like solar energy conversions, photovoltaics, biotechnology, sensor technology and many others.^{1-5,8,9,26,29,38,42,43,236,269,350,351,409-411} Micellar assemblies formed by triblock copolymers, commonly known as the pluronics, are the important micellar systems where the microenvironments of these micelles can be modulated very effectively just by the addition of different conventional surfactants as the suitable co-surfactants,^{118,179,412-414} as in these cases unique mixed micellar assemblies are formed which can change the course of the studied chemical reactions, especially that of the bimolecular PET reactions, very efficiently, bringing out many prospective applications for such systems.^{118,176,179,197,307,396,397,401,412,413,415-420} As suggested in the literature,^{118,412,413,416,421-423} on addition of a smaller co-surfactant system into a pluronic micellar solution, say the addition of the conventional surfactant like sodium dodecyl sulfate (SDS) into the solution of pluronic-123 (P123) micelles, as we have investigated in the present study, the smaller co-surfactant molecules are suitably incorporated into the larger P123 micelles resulting the formation distinct mixed micellar structure where the hydrophobic chains of the co-surfactants are mainly embedded into the core of the larger pluronic micelles (composed of poly-PO blocks mainly) while the ionic (or polar) head groups of the co-surfactants are placed in the hydrated corona region (composed of hydrated poly-EO blocks) of the resultant mixed micelles, as are conceptually presented in Scheme 5.1.^{179,307,414,416,418,424} Interestingly, in such mixed micellar assemblies, there is the development of a charged layer inside the micellar corona region, for which the charge density can be changed very efficiently by changing just the molar ratio of the co-surfactant to pluronic concentrations, commonly referred as the n -value of the concerned mixed micellar system, i.e. $n = [\text{co-surfactant}]/[\text{pluronic}]$.^{118,307,401,412,413,415-420} The developments of such charge layers inside the micellar assemblies and the consequent changes in the hydration characteristics for the corona region of the mixed micellar systems thus formed can affect the solubilization sites of different solutes in these micelles quite significantly, particularly those of the charged species,^{307,417,418} and accordingly these mixed micellar systems can offer tremendous opportunities for the tuning of different chemical reactions, particularly the PET reactions, which can find many useful applications in various applied areas.^{118,307,401,415-420}



Scheme 5.1. Schematic presentation of the formation of copolymer-surfactant mixed micellar aggregate on the addition of an ionic surfactant into a pluronic micellar solution.

Earlier studies on PET reactions in different micellar media, including those of pure pluronic copolymers and also those formed by the mixed pluronic-co-surfactant systems, have invariably shown that the quenching constants for the bimolecular PET reactions ($k_{obs} = k_{q(TR)}$) always follow the Marcus Inversion (MI) behavior with the changing exergonicity ($-\Delta G^0$),^{119-122,125,127,129,349,425-429} as predicted from the Marcus outer sphere ET theory.^{10-12,29,100} It is however interestingly found that the observed MI in such cases do not fulfill the conditions that emanate from the conventional one-dimensional ET (1DET) theory, because in the constrained micellar media the solvent relaxation dynamics is essentially very slow, suggesting the involvement of thermally non-equilibrated solvent reorganizations around the reactant (R) and/or product (P) states as the ET reactions proceed in these constrained media.^{18,88-98} As discussed in the preceeding chapters, the PET reactions in the constrained media indeed do not follow the 1DET model but essentially take place following a two-dimensional ET (2DET) mechanism, an advanced ET theory formulated by Sumi and Marcus to accommodate those ET reactions that occur along with non-equilibrium solvent reorganizations around the R or P states.^{18,99} In the present study, we have investigated bimolecular PET reactions in different SDS-P123 mixed micellar systems of varying n -values ($n=[\text{SDS}]/[\text{P123}]$), using a series of 7-aminocoumarins as the electron acceptors and *N,N*-dimethylamine (DMAN) as the electron donor. As discussed in Section 1.7 in Chapter 1, the pluronic P123 is a tri-block copolymer, while the SDS used in this study as is a conventional surfactant containing an anionic head group and the chemical structures of these copolymer and surfactant systems along with those of the used coumarin acceptors and DMAN donor are shown in Chart 5.1 for their quick visualization. In the present study our objective has been to understand how the changing n -values for the SDS-P123 mixed micellar assemblies can affect the kinetics and energetics of the studied PET reactions in these constrained media, especially in regard to the appearance of the MI behavior and the applicability of the 2DET model in rationalizing observed PET results in the studied systems.

Chart 5.1. Chemical structures of the P123 tri-block copolymer and SDS surfactant and also those of the 7-aminocoumarin acceptors and DMAN donor used in the present study.



In regard to the present study, it is important to mention that the bimolecular PET reactions in the SDS-P123 mixed micellar assemblies were also investigated earlier from our group following the similar fluorescence quenching studies involving steady-state (SS) and conventional TCSPC based sub-nanosecond time-resolved (TR) measurements,⁴² as are used in the present investigation. We have discussed quite extensively in the earlier chapters that in the constrained media a major contribution towards the observed SS fluorescence quenching arises from the transient effect, i.e. from the ultrafast quenching occurring within the pre-existing donor-acceptor pairs where reacting donor and acceptor units are already within the interaction zone (i.e. reaction sphere) at the point of photoexcitation of the fluorophores molecule (acceptor).^{38,94,118-122,124,125,127-129,236,349,425-429} Therefore, it was realized that to get a better insight of these PET reactions it is essential to investigate these systems with an ultrafast sub-picosecond time resolution, as one can achieve by using the ultrafast fluorescence up-conversion technique. This has been the main goal of the present work to extend the PET study in the SDS-P123 mixed micellar assemblies involving up-conversion measurements with ultrafast (sub-picosecond) time resolution.^{117,118,197,401} Additionally, it is important to be mentioned here that in the earlier study from our group a 1 wt% of P123 solution was used to study all the PET reactions, where the typical concentrations of the micelles were in the range of about 18 to 33 μM , with the changing n -values between 0 to 2; considering the molecular weight of P123 copolymer as ~ 5800 , its CMC as $\sim 52 \mu\text{M}$, and the values for the aggregation number (N_{agg}) of the concerned micelles with different n -values ($n = 0$ to 2) are in the range of 50 to 90.¹¹⁸ Though the micellar concentration range between 18 to 33 μM was quite adequate to solubilize reasonable concentrations of the fluorophores and quenchers in these micelles to carry out the SS fluorescence quenching and the conventional TCSPC based TR fluorescence quenching studies,¹¹⁸ the fluorescence up-conversion measurements required to use much higher fluorophore and quencher concentrations to obtain reliable contributions of the ultrafast transient quenching components in the measured ultrafast kinetic traces. Accordingly, in the present study, we have used uniformly a much higher P123 concentration, i.e. 5 wt% P123 ($\sim 8.65 \text{ mM}$), to carry out different studies involving either SS quenching or TCSPC based quenching studies along with the up-conversion based ultrafast

fluorescence quenching studies as investigated additionally in the present work involving the different coumarin-DMAN systems in the SDS-P123 micellar media with their n -values varied from 0 to 2. In the present study, the concentrations of the micelles in the experimental solutions were about 5 times higher (i.e. in the range of about 90 to 187 μM for the n values from 0 to 2)¹¹⁸ than that used in the earlier study.⁴² Important to mention here that for $n = 2$ we needed to use an SDS concentration of ~ 17.2 mM, which is higher than the CMC of pure SDS in aqueous solution (~ 8 mM).^{118,187} In the present situation, however, the possibility of the pure SDS micelle formation in parallel to SDS-P123 mixed micellar systems is supposed to be very negligible, due to preferential formation of mixed micellar assemblies with the cooperative inclusion of large number of anionic SDS molecules into each of the P123 micelles and thus disfavoring the formation of pure SDS micelles in the studied solution.^{176,413} Accordingly, the results obtained from the present study conveniently represent the quenching processes involving the PET reactions in the SDS-P123 mixed micellar systems, as evidently investigated using either SS fluorescence quenching studies or the TR fluorescence quenching studies spanning over nanosecond to sub-nanosecond time resolutions.

5.2. Materials and Methods

The pluronic copolymer P123 and conventional surfactant SDS were obtained from Aldrich and used as received. Coumarin dyes, DMAN donor, nanopure water, and organic solvents used in this study were obtained from the same sources as mentioned in Section 3.2 in Chapter 3. A stock P123 solution with 10 % (w/v) copolymer concentration was first prepared by weighing the required amount of the copolymer sample in a container and adding some amount of water into it and keeping the mixture overnight under refrigeration for dissolution. The total volume of this solution was subsequently adjusted to make the stock solutions exactly 10% (w/v) with respect to the copolymer concentration. This stock solution was subsequently used to prepare all the experimental solutions, maintaining the P123 concentration always 5 % (w/v), but changing the concentration of the added SDS adequately to vary the n -values ($n = [\text{SDS}]/[\text{P123}]$) for the corresponding mixed micelles between 0 to 2. Coumarin concentrations in the experimental solutions were kept in the range of 5-15 μM , much lower than the actual micelle concentrations present in the solutions so that the fraction of the micelles containing more than one dye molecules into them can be considered to be negligible.^{127,161,347,352-354}

The experimental details for the ground state absorption, steady-state (SS) emission, and time-resolved (TR) fluorescence studies using TCSPC measurements are the same as given in Chapter 2 and 3. In the present study, the sub-picosecond ultrafast fluorescence measurements were also carried out using a femtosecond fluorescence up-conversion setup, for which the details are given in Section 2.6.1 in Chapter 2.^{116,413} In the up-conversion measurements, samples were taken in a rotating cell (0.4 mm path length) to avoid any photo-degradation and the measurements were carried out with magic angle polarization to avoid any effect of the rotational relaxation of the

fluorophores on the observed kinetic traces. Further, to obtain reliable data and also to examine the reproducibility of the measured kinetic traces, each measurement was repeated at least for three times and the data points in the recorded traces were averaged out to obtain the acceptable kinetic traces, which were analyzed subsequently following the standard re-convolution method.^{289-293,298-300} Typical IRF (cross correlation) for the present up-conversion setup is ~ 210 fs at FWHM.

5.3. Results and Discussion

5.3.1. Ground State Absorption and Steady-State Fluorescence Studies on the Interaction of Coumarin Dyes with DMAN Donor

To check whether the coumarin dyes in their ground state have any interaction with the DMAN donor, we carried out the absorption spectra of the dyes both in pure P123 micelle and in SDS-P123 mixed micelles with n values equal to 1 and 2 (henceforth referred as SDS-P123 ($n=1$) and SDS-P123 ($n=2$), respectively), both in the absence and presence of DMAN donor. Interestingly, the presence of the DMAN donor causes no observable change in the absorption spectra of the studied dyes, suggesting no ground state interaction of these dyes with the DMAN donor. Representative absorption results for C153 dye in pure P123 and in SDS-P123 ($n=2$) micelles are shown in Figure 5.1A and B, respectively. To be mentioned that the small increase in the absorbance at the blue edge of the spectra is due to small absorption contributions of DMAN quencher at this spectral region.

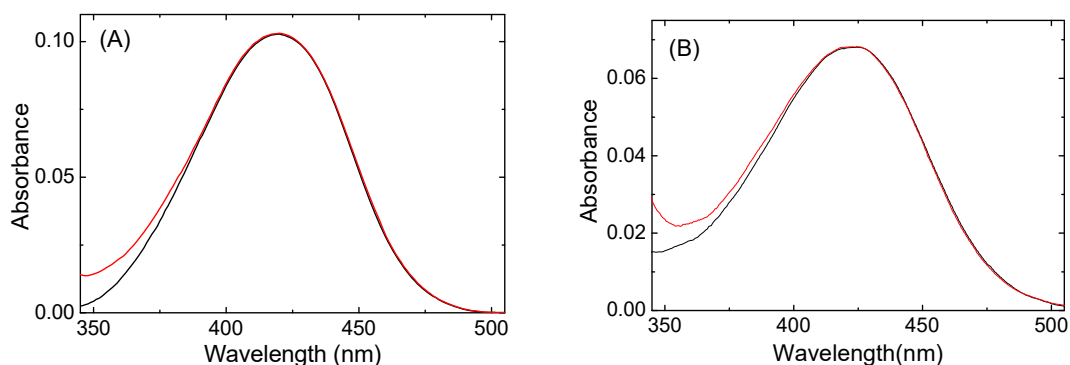


Figure 5.1. Absorption spectra of C153 dye (5 μ M) in the absence (black) and presence (red) of 75 mM effective DMAN concentration (cf. *vide infra*). **(A)** Absorption results in pure P123 micelle and **(B)** absorption results in SDS-P123 ($n=2$) mixed micellar system.

Steady-state (SS) fluorescence spectra of the coumarin dyes were recorded in pure P123 micelle and in SDS-P123 ($n=1$) and SDS-P123 ($n=2$) mixed micelles, in the presence of gradually increasing concentration of the DMAN donor, to understand the interaction of the coumarin dyes in their excited singlet (S_1) states with the DMAN quencher. In all the cases, there was a systematic decrease in the fluorescence intensity of the studied dyes with the increasing DMAN concentration. Representative results for the C153-DMAN pair in pure P123 micelle and in SDS-P123 ($n=2$) mixed

micelle are shown in Figures 5.2A and B, respectively. Observed results suggest a strong interaction of the excited (S_1) coumarin dyes with the ground state DMAN quencher. Interestingly, these SS fluorescence quenching do not accompany with any observable change in the shape of the observed emission spectra of the dyes, suggesting the absence of any exciplex formation in the present cases. As the excited coumarin dyes are known to behave as efficient electron acceptors and the DMAN quencher is well known as a strong electron donor,^{119,121,122,127,129,349,425-429} observed SS fluorescence quenching for the coumarin-DMAN pairs in the studied micellar systems are attributed to PET reactions involving S_1 states of the coumarin dyes and the ground state of the DMAN donor.

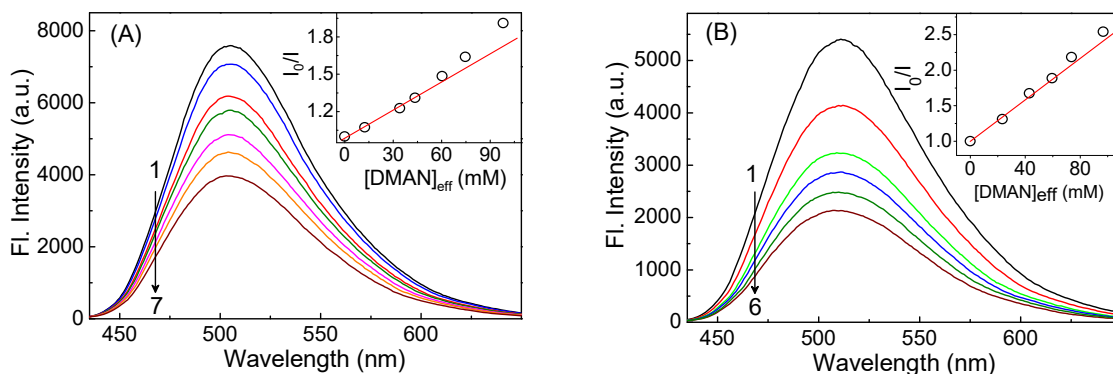


Figure 5.2. Changes in the SS fluorescence spectra of C153 (5 μ M) with the increasing effective concentration of DMAN quencher (cf. eq. 5.1). **(A)** Results in pure P123 micelle; $[DMAN]_{eff}/mM$ for (1-7) are: 0.0, 12.5, 34.1, 43.6, 60.4, 74.7, 98.1, respectively. **(B)** Results in SDS-P123 ($n=2$) mixed micelle; $[DMAN]_{eff}/mM$ for (1-6) are: 0.0, 23.5, 43.0, 59.6, 73.7, 96.8, respectively. Insets show the Stern-Volmer plots (cf. eq 3.13) for the corresponding SS fluorescence quenching displayed in the respective panels.

As discussed in Chapters 3 and 4 (cf. Section 3.3.2.1 and Section 4.3.1, respectively), in the present cases also, the observed SS fluorescence quenching results were correlated with the effective concentration of the DMAN quencher (referred as $[Q]_{eff}$), as it is present preferentially within the corona region of the studied micelles. To be mentioned also that the $[Q]_{eff}$ values were estimated similarly as given by eq 3.12 in Chapter 3. The micellar parameters that are essential for the estimations of the $[Q]_{eff}$ values and are also required in the subsequent correlations of the observed quenching results in the present study, were obtained either from the published literature¹¹⁸ or from the independent estimations carried out in the present work. These relevant parameters for the studied micellar systems are listed in Table 5.1. The $[Q]_{eff}$ values thus estimated in the present cases were used to correlate the observed SS quenching results for all the coumarin-DMAN pairs in the studied micellar assemblies following the standard Stern-Volmer (SV) correlation, as given by eq. 3.13 in Chapter 3.^{94,112,118-121,124,128,148,287,374,375}

Observed SV plots from SS quenching results are in general found to display a positive deviation from the expected linearity as expected from eq. 3.13. Representative of such SV plots obtained for the C153-DMAN pair in pure P123 micelle and in SDS-P123 ($n=2$) mixed micelle are

shown in the insets of Figures 5.2A and B, respectively. Recalling the similar positive deviations as were also observed in the SV plots for the SS fluorescence quenching studies in the tetronic-based micellar assemblies discussed in Chapter 3 and 4, we infer that in the present cases as well, the positive deviations in the SV plots arise due to the significant contributions of the ultrafast transient effects in the observed SS fluorescence quenching results. Because of these deviations of the SV plots from the expected linearity (cf. eq. 3.13), the SS fluorescence quenching results were avoided to estimate the bimolecular quenching constant (k_q) values for different coumarin-DMAN pairs in studied micellar assemblies, and the required k_q values in the present cases were effectively estimated from the time-resolved (TR) fluorescence quenching results, because these results show the expected linearity in the SV plots, as are discussed in the following section.

Table 5.1. Micellar dimensional and aggregation parameters and also the estimated micropolarities in the corona region of the studied SDS-P123 ($n=0-2$) micellar systems.^a

n -value	CMC (μM)	R_c (\AA)	R_h (\AA)	$N_{\text{agg}}(\text{P123})$	ε	$E_T(30)$ (kcal mol^{-1})	D_n
0	52	53.3	93.0	94	6.7	42.4	31.0
1	52	47.2	79.0	62	7.8	44.1	31.0
2	52	4.33	7.40	46	9.3	45.8	31.0

^a R_h , R_c N_{agg} values obtained from ref. 118. The ε and $E_T(30)$ values are estimated in the present study. The D_n values for all micelles were considered to be similar to the reported D_n value in DeOH solvent.³⁸²

5.3.2. Time-resolved Fluorescence Quenching Studies for Coumarin-DMAN Pairs in Micellar Media using Subnanosecond Time-Resolved TCSPC Measurements

The fluorescence decays of the studied coumarin dyes in pure P123 micelle and in SDS-P123 mixed micellar assemblies were recorded using subnanosecond time-resolved TCSPC measurements both in the absence and in presence of varying DMAN concentrations in the experimental solutions. In all the cases, it is observed that the fluorescence decays of the dyes gradually became faster as the quencher concentration is systematically increased in the studied micellar solutions. Moreover, it is found that while the fluorescence decays of the dyes in the absence of the quencher fit satisfactorily with a single-exponential function, in the presence of the DMAN quencher, however, the decays clearly become non-single-exponential in nature, and require to fit with a bi-exponential function (cf. eq. 3.14), for the used concentration range of the DMAN quencher. Representative fluorescence decays obtained for the C153-DMAN pair in pure P123 micelle and in SDS-P123 ($n=2$) mixed micellar assembly are shown in Figures 5.3A and B, respectively.

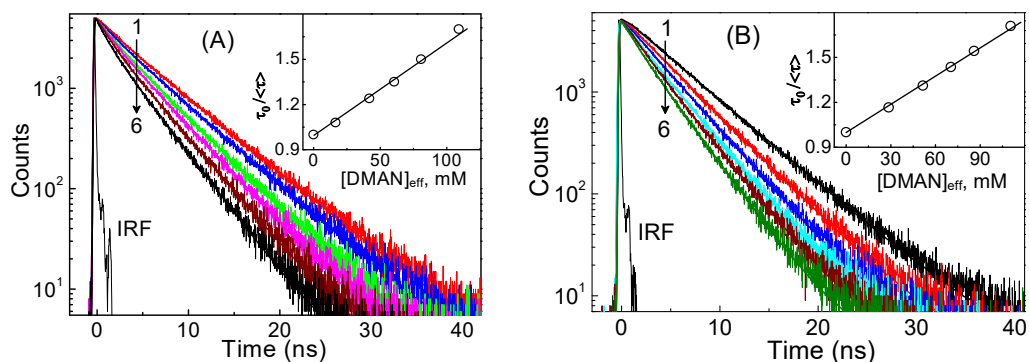


Figure 5.3. Fluorescence decays of C153 (5 μM) dye with the increasing concentration of DMAN quencher. **(A)** Results in pure P123 micelle; for (1-6) the $[\text{DMAN}]_{\text{eff}}/\text{mM}$ are: 0, 16.5, 41.9, 60.6, 80.8 and 109.1, respectively. **(B)** Results in SDS-P123 ($n=2$) mixed micelle; for (1-6) the $[\text{DMAN}]_{\text{eff}}/\text{mM}$ are: 0, 28.7, 51.6, 70.4, 86.0 and 110.6, respectively. IRF is the instrument response function. Insets in the respective panels show the corresponding SV plots (cf. eq 3.16, Chapter 3).

Table 5.2. Various parameters related to PET reactions between coumarin acceptors and DMAN donor in the SDS-P123 ($n=0-2$) mixed micellar systems.

n value	Dye	τ_0 (ns)	$k_{q(\text{TR})}$ ($10^8 \text{ M}^{-1}\text{s}^{-1}$)	$E(\text{C/C}^-)$ (V)	$E(\text{A}^+/\text{A})$ (V)	$E_{00}(\text{dye})(\text{eV})$	ΔG^0 (eV)
0	C151	6.16	8.91	-1.83	0.94	2.89	-0.454
	C152	4.38	17.08	-1.88		2.83	-0.338
	C481	3.86	16.76	-1.90		2.82	-0.298
	C522	5.96	15.54	-1.89		2.77	-0.254
	C153	5.61	11.02	-1.92		2.68	-0.134
1	C151	5.99	12.92	-1.77	0.90	2.88	-0.505
	C152	3.91	34.08	-1.82		2.82	-0.390
	C481	3.83	28.59	-1.85		2.82	-0.353
	C522	5.6	20.68	-1.84		2.76	-0.295
	C153	5.53	11.25	-1.87		2.67	-0.178
2	C151	5.83	12.30	-1.72	0.86	2.87	-0.534
	C152	3.52	46.38	-1.77		2.82	-0.421
	C481	3.47	40.28	-1.80		2.81	-0.379
	C522	5.57	26.14	-1.79		2.75	-0.326
	C153	5.24	12.05	-1.82		2.67	-0.214

In the presence of the DMAN quencher, as the fluorescence decays of the studied dyes fit with a biexponential function, the average fluorescence lifetime values, $\langle \tau \rangle$, in the present situations were estimated using eq. 3.15, as given in Chapter 3. It is observed that the estimated $\langle \tau \rangle$ values for all the coumarin-DMAN pairs in the studied micelles decrease systematically with an increase in the DMAN concentration. Interestingly, however, unlike the nonlinear SV plots obtained from SS fluorescence quenching results, the SV plots obtained from TR quenching results show the expected linear correlation (cf. eq. 3.16 in Chapter 3) in for all the cases studied.¹⁴⁸ Representative SV plots obtained from TR quenching studies involving C153-DMAN pair in pure P123 micelle and SDS-P123 ($n=2$) mixed micelle are shown in the insets of Figures 5.3A and B, respectively.

The reason behind the linear correlation observed in the SV plots from the TR fluorescence quenching studies is definitely due to the limited time resolution of the presently used TCSPC setup (IRF ~ 190 ps at FWHM) such that the ultrafast transient quenching effects remain mostly undetected in these measurements and accordingly the relatively slower quenching parts that are detected in the present TR studies effectively lead to the observed SV plots to show the expected linear correlation (cf. eq. 3.16, Chapter 3), at least for the range of the $[Q]_{\text{eff}}$ values used in the present study. Since the SV plots from the TR fluorescence quenching studies show the linearity as expected, the bimolecular quenching constant values for the studied coumarin-DMAN pairs in different micellar systems were suitably estimated from the slopes of these linear plots and the values thus obtained are designated as $k_{q(\text{TR})}$ values, as are listed in Table 5.2.

5.3.3. Correlation of the Bimolecular Quenching Constants with the Free Energy Changes of the ET Reactions

The free energy changes (ΔG^0) for the PET reactions in the studied coumarin-DMAN pairs in pure P123 micelle and in SDS-P123 mixed micellar assemblies were estimated following the Rehm-Weller relation as discussed in Chapter 3 (cf. eq. 3.17). Since in the studied micellar systems it was not possible to carry out reliable cyclic voltammetric measurements due to the limited solubility of the coumarin dyes, especially, the redox potential values for both the acceptor and donor systems ($E(\text{A}/\text{A}^-)$ and $E(\text{D}^+/\text{D})$, respectively) used in the present study were adopted as the values reported in acetonitrile (ACN) solution,³⁷⁵ and appropriate corrections were applied to these values to make them applicable for the changing reaction medium from ACN solvent to the studied micellar media. The correction method applied in the present cases is known widely as the Fawcett's correction,^{92,378,379} and the details of this method have already been given explicitly in Chapter 3 (cf. Section 3.3.2.3). For the incorporation of the concerned Fawcett's corrections, the required micropolarity parameters (e.g. the ϵ and $E_{\text{T}}(30)$ values for the corona region) of the studied micellar systems were estimated following the SS fluorescence studies using the probe dye C153, the details

of which are already discussed in Chapter 3 (cf. Sections 3.3.1.1 and 3.3.2.3). Relevant fluorescence results from these studies and the so constructed calibration plots for the estimations of the ε and $E_T(30)$ values are shown in Figure 5.4A and B, respectively. Estimated ε and $E_T(30)$ values for the studied micellar systems are listed in Table 5.1 along with other micellar parameters. To be mentioned here that to accomplish the Fawcett's corrections, we also needed to have the donor numbers (D_n) for the studied micellar systems, and these values were considered to be similar to the D_n value of decanol ($D_n = 31.0$),^{380,382,402} and the reason for this consideration is the same as discussed previously in Chapter 3 (cf. Section 3.3.2.3).

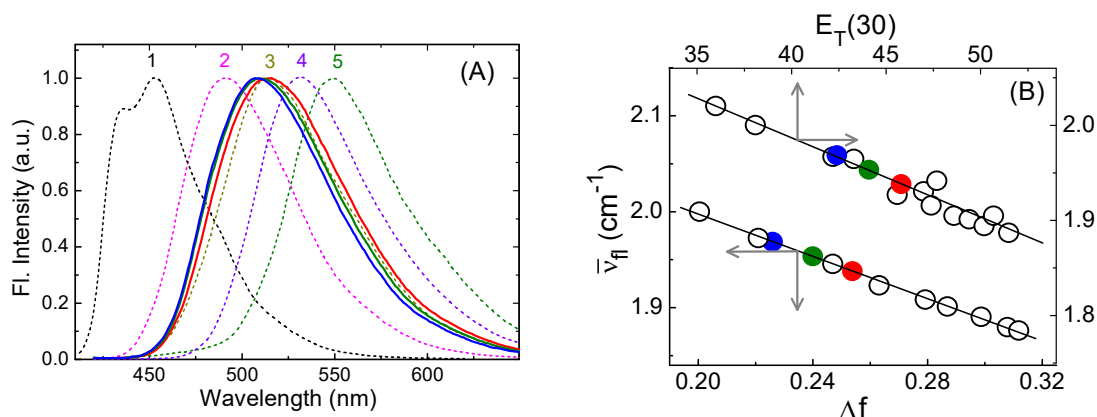


Figure 5.4. (A) Normalized fluorescence emission spectra of C153 dye (5 μM); Dotted spectra are for conventional solvents: (1) cyclohexane, (2) ethyl acetate, (3) decanol, (4) methanol and (5) water. Solid spectra for P123 (Blue), SDS-P123 ($n=1$) (Green), SDS-P123 ($n=2$) (Red) micelles. (B) Calibration plots for the Δf and $E_T(30)$ values; open circles are calibration data and solid circles are the data for the micellar systems: P123 (Blue), SDS-P123 ($n=1$) (Green), SDS-P123 ($n=2$) (Red).

Different electrochemical parameters obtained for the studied coumarin acceptors and DMAN donor in different micellar media studied following Fawcett's correction method are listed in Table 5.3,^{92,378,379} The ΔG^0 values estimated consequently for the PET reactions in the studied coumarin-DMAN systems in different micellar media using the corrected $E(A/A^-)$ and $E(D^+/D)$ values and applying the Rehm-Weller relation (cf. eq. 3.17, Chapter 3) are listed in Table 5.2 along with the concerned $k_{q(TR)}$ values estimated from the TR fluorescence quenching studies. Figure 5.5 shows the correlations of the $k_{q(TR)}$ values against the ΔG^0 values for different coumarin-DMAN pairs in the studied P123 micelle and SDS-P123 mixed micellar systems. It is evident from this figure that in all the micelles the $k_{q(TR)}$ versus ΔG^0 plots show very convincing Marcus Inversion (MI) behavior. Observed results clearly suggest that the constrained reaction conditions inside the used micellar media effectively make the investigated bimolecular PET reactions to display the unique MI behavior with the changing exergonicity ($-\Delta G^0$) of the PET reactions, though for the similar bimolecular PET reactions in the low viscosity conventional solvents the expected MI behavior is known to remain just indefinable or elusive.^{26,29,42,44,105,130,268,270,272,273,384-387} Drawing inferences from the results reported on the bimolecular PET reactions in various other constrained reaction media,

^{117,118,120,125,127,197,347,401} it can be suggested that the slow solvent relaxation and the reduced diffusion of the reactants in the studied micellar systems are indeed responsible to assist the investigated bimolecular PET reactions to follow the two-dimensional ET (2DET) mechanism and thus to display the interesting MI behavior,^{18,93,94,403} as we have observed in the present study.

Table 5.3. Calculated electrochemical properties for the donor (DMAN) and acceptors (Coumarin dyes) in the SDS-P123 systems.

(A) Electrochemical Properties of the Acceptor Systems					
Acceptor	Electrochemical Parameter	Reaction Media			
		ACN	P123 (n=0)	P123+SDS (n=1)	P123+ SDS (n=2)
C151	$G_S^0(A^-)$ (eV)	-1.847	-1.580	-1.639	-1.694
	$E(A/A^-)$ (V) ^a	-1.565	-1.83	-1.77	-1.72
C152	$G_S^0(A^-)$ (eV)	-1.744	-1.493	-1.548	-1.599
	$E(A/A^-)$ (V) ^a	-1.626	-1.88	-1.82	-1.77
C481	$G_S^0(A^-)$ (eV)	-1.663	-1.425	-1.476	-1.525
	$E(A/A^-)$ (V) ^a	-1.660	-1.90	-1.85	-1.80
C522	$G_S^0(A^-)$ (eV)	-1.687	-1.445	-1.497	-1.547
	$E(A/A^-)$ (V) ^a	-1.653	-1.89	-1.84	-1.79
C153	$G_S^0(A^-)$ (eV)	-1.639	-1.405	-1.455	-1.503
	$E(A/A^-)$ (V) ^a	-1.685	-1.92	-1.87	-1.82
(B) Electrochemical Properties of the Donor Amine					
DMAN	$G_S^0(D^+)$ (eV)	-1.761	-1.584	-1.625	-1.664
	$E(D^+/D)$ (V) ^a	0.760	0.94	0.90	0.86

^a $E(A/A^-)$ and $E(D^+/D)$ values in ACN against SCE were obtained from ref. 375.

As given in Table 5.1, the dielectric constant (ϵ) values for the corona regions of presently studied micellar systems are in the range of 6.7 to 9.3. Therefore, following eq. 1.11 in Chapter 1, and considering the acceptor and donor radii (r_A and r_D , respectively) as estimated using Edward's volume addition method,³⁷⁰ the solvent reorganization energy, λ_s , in the studied micellar media are estimated in the range of about 1.0 to 1.1 eV. Accordingly, from Figure 5.5, it is interestingly noticed that the onsets of the MI behaviors in all the studied micellar media appear at much lower exergonicity values ($-\Delta G_{MI}^0 \sim 0.3-0.4$ eV) than what we would expect on the basis of the conventional Marcus ET theory (the one dimension ET (1DET) theory), i.e. the onsets of MI at

$-\Delta G^0 = \lambda = \lambda_s + \lambda_i$, as discussed in Chapter 1 (cf. Section 1.2.1, eq. 1.9 and Figure 1.2).^{10-12,14-19} Based on these observations, we infer that similar to the tetronic copolymer based micellar systems, as discussed in Chapter 3 and 4, in the presently studied pluronic copolymer based micellar assemblies also the non-equilibrium solvent reorganization actually shifts the onset of the MI towards the lowering exergonicity region, as it has been described explicitly in the two-dimensional ET (2DET) theory (cf. Section 1.2.4, Chapter 1).^{18,88-97}

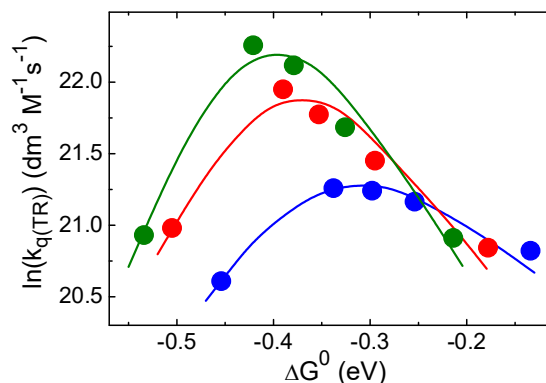


Figure 5.5. The $\ln(k_{q(TR)})$ versus ΔG^0 plots for the PET reactions in the coumarin-amine systems studied in SDS-P123 micellar aggregates; $n=0$ (blue), $n=1$ (red) and $n=2$ (green). Solid circles are the experimental data and the continuous curves are the guides to the eyes for the trends observed in the experimental results.

Comparing the $k_{q(TR)}$ versus ΔG^0 plots observed in pure P123 micelle and in SDS-P123 ($n=1$) and SDS-P123 ($n=2$) mixed micellar assemblies, as are shown in Figure 5.5, it is evident that the maximum $k_{q(TR)}$ values as well as the exergonicity values for the onset of the MI behaviors gradually increase quite significantly as the n values ($n=[\text{SDS}]/[\text{P123}]$) for the concerned SDS-P123 mixed micellar systems is increased systematically. These results thus suggest that the micellar microenvironments for the SDS-P123 mixed micellar systems can be tuned quite appreciably by changing the n values of these mixed micelles and accordingly by using these mixed micellar assemblies of varying n values it is possible to modulate the $k_{q(TR)}$ values as well as the $k_{q(TR)}$ versus ΔG^0 correlations for the studied PET reactions very significantly, which might find many useful applications in different applied areas involving different PET reactions.

5.3.4. Ultrafast Time-resolved Fluorescence Studies for Coumarin-DMAN Pairs in Different Micellar Media using Up-Conversion Measurements

In the subnanosecond TR fluorescence quenching studies discussed above in Section 5.3.2, the used TCSPC setup has a finite time resolution and thus the shortest decay time measureable in the above study is ~ 50 ps. It is thus evident that in the above measurements, it is not possible to detect the ultrafast transient quenching components associated with the studied PET reactions in the concerned micellar media. To explore these missing ultrafast transient quenching components, thus, we need to

extend the present investigation using the femtosecond fluorescence up-conversion measurements to record the ultrafast fluorescence kinetics traces for the coumarin-DMAN pairs in the studied micellar systems. The main aim of this ultrafast fluorescence up-conversion study is to establish unambiguously if the non-diffusive nature of PET reactions in the studied micellar media indeed prevails, and accordingly to eliminate any possible suspicion in regard to the MI behavior observed in the $k_{q(TR)}$ versus ΔG^0 correlations, apprehending it to be related by some means to the limited time-resolution of the TCSPC setup used in the previous measurements (cf. Figure 5.5).

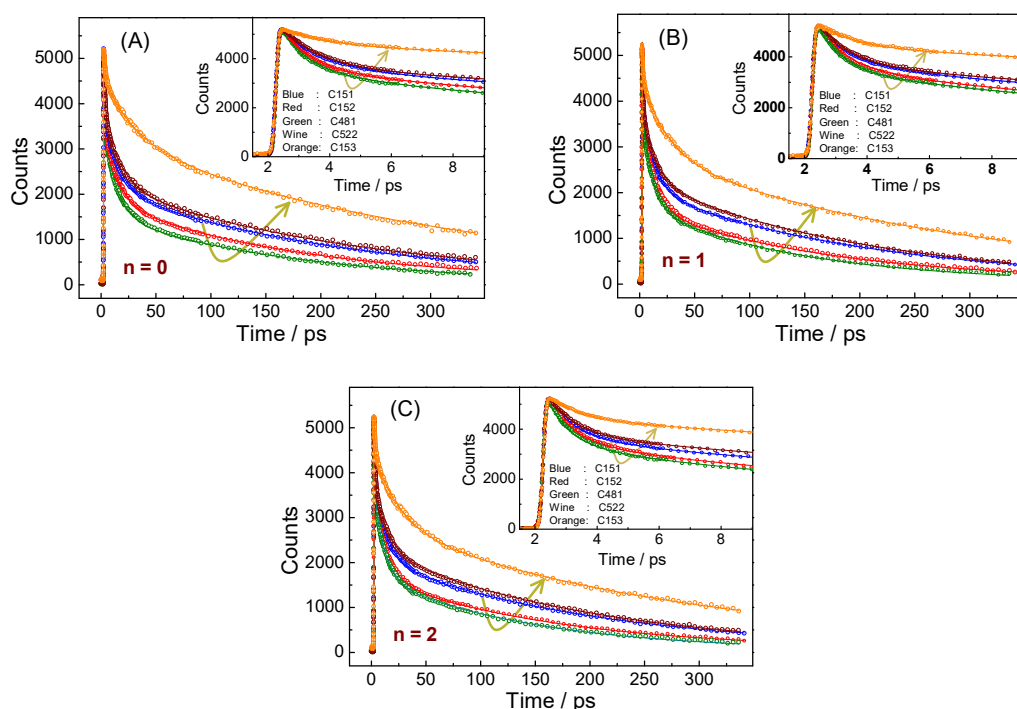


Figure 5.6. The ultrafast fluorescence kinetic traces recorded for the coumarin-DMAN pairs in (A) pure P123 ($n=0$) micelle, (B) in SDS-P123 ($n=1$) micelle and (C) SDS-P123 ($n=2$) micelle, respectively, using up-conversion measurements. The kinetic traces were recorded at the emission maxima of the concerned coumarin dyes. Insets show the initial parts of the kinetic traces after their suitable expansions. In all the cases, dye concentrations were typical about $15\mu\text{M}$ while the effective DMAN concentration was about 650 mM .

In the present fluorescence up-conversion study, to obtain the ultrafast fluorescence kinetic traces for the coumarin-DMAN pairs, the emission of the concerned coumarin dyes ($15\mu\text{M}$) were measured at their respective emission maxima both in the absence and in the presence of a fixed, about 650 mM , effective concentration of the DMAN quencher, in the studied micellar systems where the n -values for the molar concentrations of SDS to P123 were kept at 0, 1 and 2. The ultrafast fluorescence kinetic traces thus recorded for different coumarin-DMAN pairs in pure P123 micelle ($n=0$) and in SDS-P123 mixed micelles with $n=1$ and $n=2$ are shown in Figures 5.6A, B and C, respectively. As indicated from these results, the overall kinetic traces in all the cases are highly non-exponential in nature. Further, in all the cases, there is the substantially large contributions arising from the ultrafast fluorescence decays, which clearly indicate the appreciable involvements

of the ultrafast PET processes in the present systems occurring under the non-diffusing reaction condition, as are also reported in some earlier reported studies in similar constrained reaction media^{121,122,426} and also in the ultrafast PET studies carried out in suitable solvents using the latter directly as the electron donors for the excited chromophoric dyes.⁹¹⁻⁹⁵ Observed ultrafast kinetic traces in the present study were analyzed uniformly following a tri-exponential function to obtain their reasonably good fit,⁹¹⁻⁹⁵ and the kinetic parameters thus estimated in different cases are listed in Table 5.4.

Table 5.4. Fitting parameters from the tri-exponential analysis of the ultrafast fluorescence kinetic traces recorded for different coumarin-DMAN pairs in the studied micelles using up-conversion measurements.

n -value	Chemical systems	a_1	τ_1 (ps)	a_2	τ_2 (ps)	a_3	τ_3 (ps)
0	C151-DMAN	118.3	1.19	108.6	13.5	134.9	218.0
	C152-DMAN	134.7	0.93	117.8	12.0	116.4	174.6
	C481-DMAN	138.0	0.86	133.2	11.4	99.5	171.2
	C522-DMAN	120.6	1.20	102.2	16.2	142.4	237.1
	C153-DMAN	50.4	1.41	86.0	26.8	209.5	305.3
1	C151-DMAN	122.8	0.98	106.7	12.2	132.9	199.3
	C152-DMAN	130.6	0.85	133.0	10.6	106.1	166.6
	C481-DMAN	139.6	0.76	125.4	10.1	106.8	146.6
	C522-DMAN	126.7	0.95	100.6	12.4	146.8	203.0
	C153-DMAN	69.5	1.08	103.4	23.0	182.6	280.4
2	C151-DMAN	122.9	0.86	118.2	11.6	126.3	182.3
	C152-DMAN	138.4	0.80	124.9	9.99	104.5	148.6
	C481-DMAN	144.3	0.70	123.7	9.00	102.3	134.2
	C522-DMAN	121.4	0.84	109.6	11.7	143.6	181.3
	C153-DMAN	68.7	0.99	121.2	20.6	170.2	275.9

Correlations of the individual decay constants (τ_i^{-1}) with the ΔG^0 values for the PET reactions in the studied coumarin-DMAN pairs in different SDS-P123 micelles with changing n -values of 0, 1 and 2 for the SDS to P123 molar ratio are shown in Figures 5.7A, B and C, respectively. It is evident from this figure that all the the τ_i^{-1} versus ΔG^0 plots representing the three decay components of the

ultrafast decays obtained for the coumarin-DMAN pairs in different SDS-P123 micelles display very clear MI behavior. The observation especially that not only the faster τ_1 and τ_2 values, but also the slower τ_3 values, which is already in the sub-nanosecond time domain, also display very similar MI behavior with the changing ΔG^0 values (cf. Figure 5.7C), clearly substantiate our earlier inference that the bimolecular PET reactions in the constrained micellar media indeed occur under the non-diffusive conditions of the reacting donor-acceptor pairs. We infer that this non-diffusive nature of the bimolecular PET reaction is infact extended even up to the sub-nanosecond domain of the TR fluorescence quenching kinetics, as we have investigated using the convensional TCSPC based measurements, and accordingly the $k_{q(TR)}$ versus ΔG^0 plots obtained from such studies also to display the clear MI behavior, as are shown previously in Figure 5.5.

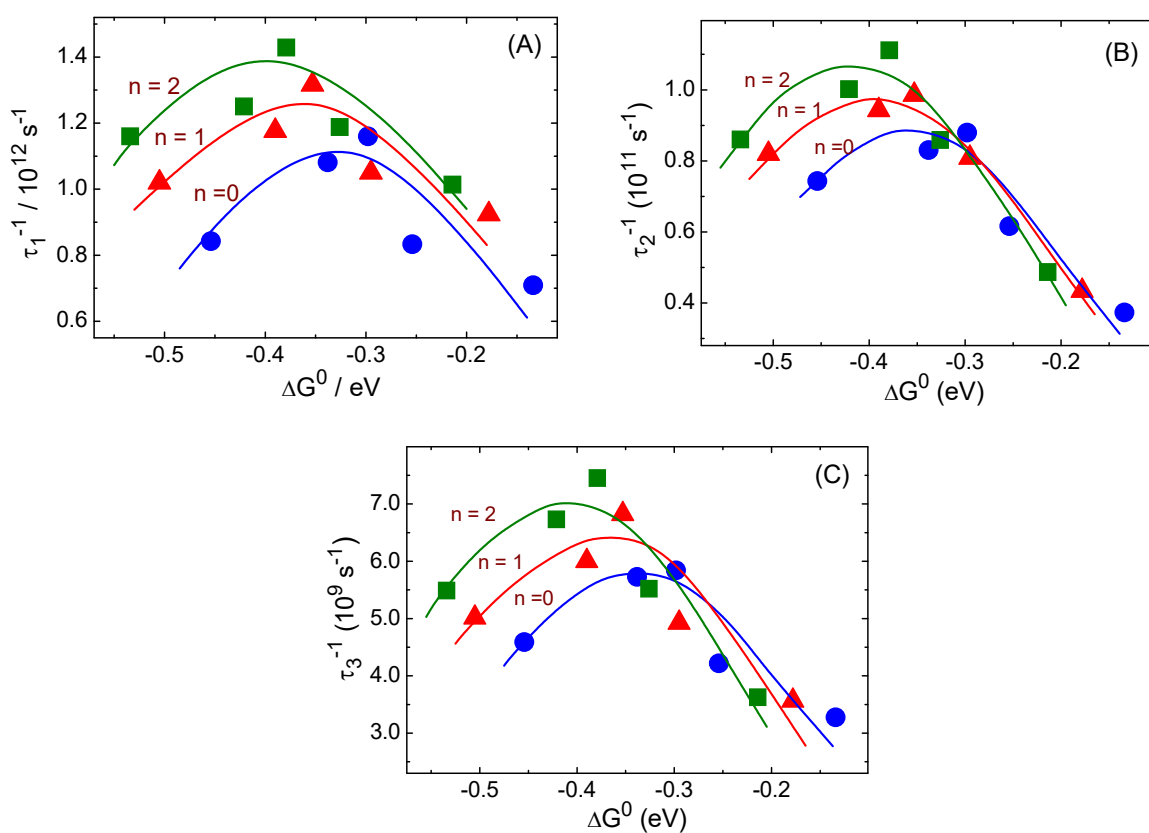
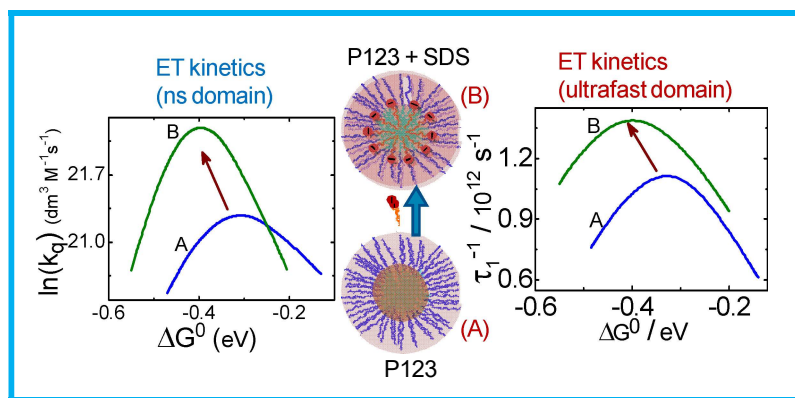


Figure 5.7. The τ_i^{-1} versus ΔG^0 plots for the coumarin-DMAN pairs in the SDS-P123 micellar systems of varying n -values for: (A) τ_1 component, (B) τ_2 component and (C) τ_3 component, respectively. Data points in blue, red and green represent the n -values equal to 0, 1 and 2, respectively. Continuous curves through the data points are just for the visual guide for the correlations. Observed MIs for all the decay components show a gradually increasing rate (τ_i^{-1}) and a sequentially shifting onset of MI towards higher exergonicity ($-\Delta G^0$) as the n -value increases.

In the present context, it is to be mentioned that even though we cannot assign any precise physical attributes to the three decay components, τ_1 , τ_2 and τ_3 , estimated from the ultrafast fluorescence decays, these components can however be grossly credited to the presence of different kinds of pre-existing donor-acceptor pairs, some are with the closest proximity to each other, to give

the ultrafast τ_1 component, and the others are with relatively larger separations but still the interacting donor-acceptor pairs are within the reaction zones at the point of the photoexcitation of the concerned chromophores, resulting the appearance of the intermediate components, τ_2 and τ_3 , in the observed in kinetic traces. Evidently, these differential separations of the interacting donor-acceptor pairs in the concerned bimolecular PET reactions mainly arise due to the extremely slow diffusion of the reactant molecules in the constrained micellar media, as these reactants are largely entangled with the surfactant chains of the micellare systems.^{38,117-121,125,129,197,236,347,349,401} Considering the non-diffusing nature of the investigated bimolecular PET reactions in the studied micellar assemblies, and recalling the earlier findings that the solvent relaxation dynamics in such micellar media are exceedingly slow,^{18,93,94,403} it is apparent to suggest that the PET reactions in the present cases indeed occur involving two-dimensional ET (2DET) mechanism,^{18,99} than the conventional 1DET mechanism, as applicable in the low viscosity conventional solvents.^{9-12,14-16,26-30,34-55,100-115}



Scheme 5.2. Modulation of ET kinetics from subnanosecond to subpicosecond time domain in P123-SDS mixed micellar media.

From Figure 5.7A, B and C, it is interestingly seen that for the PET reactions in the studied SDS-P123 micellar assemblies, the maximum values of the respective τ_i^{-1} components, as well as the exergonicity ($-\Delta G^0$) values for the onset of the observed MI gradually become higher as the n -value ($n=[\text{SDS}]/[\text{P123}]$) for the concerned mixed micellar systems is increased systematically. These changes corroborate nicely with the observations made with the $k_{q(TR)}$ versus ΔG^0 plots in different SDS-P123 mixed micelles with varying n -values (cf. Figure 5.5), clearly indicating that the incorporation of SDS co-surfactant into the P123 micelle modulates the kinetics and energetics of the studied bimolecular PET reactions quite largely, which can be conceptually represented by using the pictorial designs as shown in Scheme 5.2. Evidently, the modulations in the kinetics and energetics of the studied PET reactions are caused by the SDS induced changes in the micropolarity at the corona region of the used SDS-P123 mixed micelles, as we have discussed before in Section 5.3.3. Such modulations in the kinetics and energetic of the PET reactions achieved through the

simple alteration in the composition of the surfactant-pluronic mixed micellar systems are definitely very interesting findings and the concept demonstrated in this study is envisaged to find suitable application for the better utilization of the bimolecular PET processes in some applied areas.

5.4. CONCLUSION

In the present study, bimolecular photoinduced electron transfer (PET) reactions between a series of coumarin acceptors and the *N,N*-dimethylaniline (DMAN) donor have been investigated in different SDS-P123 mixed micellar assemblies, where SDS (sodium dodecyl sulfate) acts as the co-surfactant and P123 (pluronic 123) provides the basic micellar structure, to understand how the micellar characteristics as well as the energetics and kinetics of the concerned PET reactions in these mixed micellar systems are modulated by the changing n -values ($n = [\text{SDS}]/[\text{P123}]$) of the studied mixed micellar assemblies. It is observed that in all the studied SDS-P123 micellar systems, the quenching rate constants ($k_{q(\text{TR})}$) obtained from sub-nanosecond time-resolved (TR) fluorescence studies using TCSPC measurements, as well as the individual decay rate constants (τ_i^{-1}) estimated from the tri-exponential analysis of the ultrafast fluorescence kinetic traces recorded through femtosecond fluorescence up-conversion measurements, display the unique Marcus Inversion (MI) behavior. Observation of such MI behavior throughout the time scales of observations, from sub-nanosecond to sub-picosecond domains, inevitably suggests the involvement of the non-diffusive bimolecular PET reactions in the studied micellar assemblies. Further, the onsets of the MI in all the cases are found to appear at appreciably lower exergonicity ($-\Delta G^0$) values than what we expect from the estimated solvent reorganization energy (λ_s) and the convesional one-dimensions ET (1DET) theory, suggesting the non-applicability of this normal Marcus ET theory in the present cases investigated in the constrained micellar media. Recalling the reported literature results that the solvent relaxation dynamics in the micellar media are exceptionally slow, present results convincingly establish the applicability of the two-dimensional ET (2DET) mechanism in the present micellar systems, than the convesional 1DET mechanism which is otherwise applicable very suitably in low viscosity conventional solvents. In the present study, unique modulations are observed both in the kinetics and energetics of the PET reactions on changing the n -values of the studied SDS-P123 mixed micellar assemblies. Accordingly, the maximum reaction rate constants, either with regard to the $k_{q(\text{TR})}$ values (cf. Figure 5.5) or in terms of the τ_i^{-1} values (cf. Figure 5.7), and also the exergonicity values for the onsets of the MI in all these cases, gradually become increased in the studied systems as the n -values ($n=[\text{SDS}]/[\text{P123}]$) for the concerned SDS-P123 mixed micellar systems are increased systematically. It is revealed that, with the increasing n -values for the mixed micelles there is the systematic increase in the micropolarity for the corona region of these mixed micellar assemblies, which in turn modulates the kinetics and energetics of the studied PET reactions in these constrained media as have been observed experimentally. In addition to the noteworthy finding of the MI

behavior for the studied PET reactions in the used SDS-P123 mixed micellar systems, the significant modulations that could be achieved in the kinetics and energetics of these PET reactions simply by changing the compositions in terms of the SDS to P123 molar ratios (n -values) are very intriguing results and encouraging observations. These fascinating aspects of the modulations in the kinetics and energetics of the PET reactions through the use of the mixed micellar systems are predicted to find useful applications for the better utilizations of the PET reactions in different applied areas.

CHAPTER-6

LANTHANIDE (III) IONS AS MULTICHANNEL ACCEPTORS FOR PHOTOINDUCED ELECTRON TRANSFER REACTIONS

6.1. Introduction

In the previous chapters we have discussed bimolecular photoinduced ET (PET) processes in constrained micellar media using organic aromatic molecules both as the electron acceptors and donors, where the chromophoric acceptor dyes were used as the fluorophores and the aromatic amine donors were used as the quenchers to understand the PET kinetics following the associated fluorescence quenching process. In the present study, we have chosen inorganic trivalent lanthanide ions, Ln(III), as the unique acceptors that also act as the quenchers, in combination with a series of 4-methyl-aminocoumarin dyes used as the fluorescent donors to investigate the PET reactions following fluorescence quenching studies in homogeneous aqueous solution, distinctly different than the constrained micellar media used in the previous studies. The use of the Ln(III) ions in the present study has been with the consideration that in the literature extensive research have been devoted in understanding various intriguing behavior of the electron transfer (ET) processes involving these ions, because of the direct involvements of such ET reactions in many areas like geo-mitigation,²¹²⁻²¹⁶ luminescence sciences,^{196,198,203,204,217-219} optoelectronics,²⁰⁵⁻²⁰⁷ bio-sensing,^{199-202,220,221} bio-imaging,^{200-202,220,221} biotechnology,¹⁹⁹⁻²⁰² and many others.²²²⁻²²⁸

Table 6.1. Electronic configurations, reduction potentials, diffusion coefficients and hydrated radii of Ln(III) ions in aqueous solution.^{197,212,214,230-233}

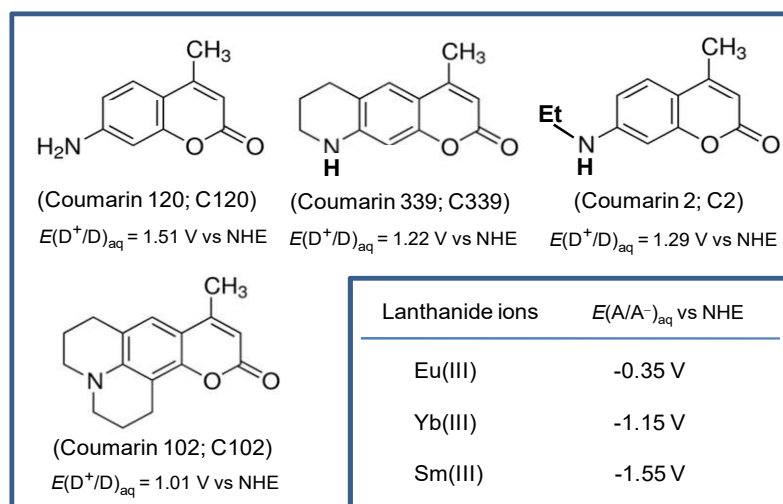
Ln(III)	Elect. Confn.; [Xe]4f ⁿ	$E(A/A^+)_{\text{aq}}$ vs. NHE; (V)	Diff. coeff.; (10 ⁶ , cm ² s ⁻¹)	$r_{A,\text{hydrated,Ln(III)}}$; (Å)
La(III)	4f ⁰	-3.10	6.29	3.896
Ce(III)	4f ¹	-3.20	6.26	3.915
Pr(III)	4f ²	-2.70	6.12	4.004
Nd(III)	4f ³	-2.60	6.18	3.965
Sm(III)	4f ⁵	-1.55	6.09	4.024
Eu(III)	4f ⁶	-0.35	5.85	4.189
Gd(III)	4f ⁷	-3.90	5.76	4.254
Tb(III)	4f ⁸	-3.70	5.64	4.344
Dy(III)	4f ⁹	-2.60	5.57	4.399
Ho(III)	4f ¹⁰	-2.90	5.65	4.337
Er(III)	4f ¹¹	-3.10	5.61	4.368
Tm(III)	4f ¹²	-2.30	5.71	4.292
Yb(III)	4f ¹³	-1.15	5.39	4.545

As listed in Table 6.1, the Ln(III) ions cover a very wide range of reduction potential values. Accordingly these inorganic ions have attracted enormous research interests to explore their divergent roles in various redox processes involving many suitable electron rich donor species.¹⁹⁷ In the literature, significant studies have been carried out on the interactions of Ln(III) ions with a variety of organic and inorganic electron donors.^{199,201,203-207,197,222-228,234} In addition to the extremely rich light absorption characteristics of the Ln(III) ions, owing to their various *f-f* electronic transitions, many of these trivalent ions are also very good oxidizing agents in aqueous solution, due to their favorable reduction potential values.^{196,229-233} It is reported in the literature that the 4-methyl-7-aminocoumarin dyes are reasonably good electron donors in their excited singlet (S_1) state to participate in the PET reactions involving suitable electron acceptors.^{122,430-433} In the literature, it has also been interestingly suggested that the bimolecular PET reactions involving Ln(III) ions in aqueous media are having the potential of supporting the multichannel ET process from an excited donor.¹⁹⁷ Accordingly, in the present study our endeavors have been to explore the intriguing details of the PET reactions involving Ln(III) ions as the unique electron acceptors and using a series of 4-methyl-7-aminocoumarin dyes as the electron donors, as have been discussed elaborately in the present chapter.

In the cases of a bimolecular PET reaction, the isolated donor and acceptor molecules in the solution first need to diffuse together to come very close to each other, i.e. within the reaction sphere to form the related precursor or encounter complex, in which the ET reaction actually takes place following an intrinsic ET rate as determined by the ET parameters associated with the concerned donor-acceptor pair. With this schematics, the PET reaction as a whole remains a diffusion mediated process, because the precursor complex formation is the prerequisite for the progress of such a bimolecular reaction (cf. Section 1.5, Chapter 1).¹⁴⁸ Keeping this diffusive nature of the bimolecular PET reactions in mind, it is expected that the intrinsic ET in the encounter complex can behave as the rate determining step for the overall bimolecular PET reaction only under the situations of reasonably lower exergonicity ($-\Delta G^0$) values where due to low driving force the intrinsic ET rate (k_{et}) is slower than the bimolecular diffusion controlled rate (k_d). For this lower exergonicity region thus, the observed rate constant (k_q or k_{obs}) for the bimolecular PET reaction would expectedly increase with the $-\Delta G^0$ value, because the propensity of the PET reaction is supposed to increase with the increasing exergonicity of the concerned process. However, as the $-\Delta G^0$ values for the bimolecular PET reactions are made to increase systematically to higher values, the intrinsic k_{et} also increases accordingly and beyond certain exergonicity this k_{et} surpasses the k_d value for the concerned solvent medium. Under this situation thus, the diffusion process (k_d value) takes over as the rate determining step for the overall reaction than the intrinsic ET process in the encounter complex, and accordingly at this high exergonicity region the observed rate constant k_q for the overall bimolecular PET reaction gets levelled-off to the k_d value, masking the effect of reaction exergonicity completely on the PET process. For the bimolecular PET reactions in conventional low viscosity homogeneous

solvents therefore, as the exergonicity of the reaction is gradually increased from the lower to the higher values, the observed k_q value initially increases asymptotically at the lower exergonicity region but reaches eventually to the diffusion limited k_d value and remains to be levelled-off there for the higher exergonicity region of the PET reactions. This unique behaviour, which is quite a general behavior observed on correlating the k_q values with the exergonicity of the PET reactions in conventional solvent systems, is commonly known as the Rehm-Weller behaviour (cf. Figure 1.10, Section 1.5.1, Chapter 1), named after the scientists who first observed and rationalized this trend.¹³⁰ In the present context, it is however anticipated that for the bimolecular PET reactions in the solution phase involving Ln(III) ions as the acceptors, there could be an intriguing change expected in the Rehm-Weller behaviour, because for most Ln(III) ions there exist multiple low lying electronic energy states,⁴³⁴⁻⁴³⁷ and these states can get accessed by the available exergonicity from the PET process which can thus open up the possibility of multichannel PET reaction in the studied systems,¹⁹⁷ modulating the Rehm-Weller correlation quite significantly.

Chart 6.1. The 4-methyl-7-aminocoumarin dyes and Ln(III) ions used in the present study along with their reduction potential values in aqueous solution against normal hydrogen electrode (NHE).^{122,197,229-233}



Interestingly, the sequence of the low lying electronic energy states for different Ln(III) ions are largely different, especially in regard to their energy spacings, and thus it is interesting to see how the kinetics and energetics of the PET reactions are affected by different Ln(III) ions, which is essential to understand the possible participation of multichannel PET process involving differential Ln(III) ions as the electron acceptors.¹⁹⁷ Apparently, the Ln(III) ions are very useful redox probes for their utilizations in the development of various lanthanide complex based analyte responsive sensor systems where PET reactions are involved either directly or indirectly in the concerned sensing mechanisms.¹⁹⁸⁻²¹⁰ To be mentioned, however, that the energetic and kinetic details of such PET reactions involving different Ln(III) ions as the electron acceptors are not reported very extensively in the literature, at least to the best of our knowledge.^{197,222,223,225,234} Accordingly in the

present study, bimolecular PET reactions have been investigated in detail in aqueous solution using suitable Ln(III) ions as the electron acceptors and the excited singlet (S_1) states of a series of 4-methyl-7-aminocoumarin dyes as the electron donors, following the steady-state (SS) and time-resolved (TR; sub-nanosecond to nanosecond) fluorescence quenching studies mainly, and substantiating the anticipated PET mechanisms in the present systems using nanosecond laser flash photolysis (LFP) experiments. In the present study, the used coumarin donor (D) and the Ln(III) acceptor (A) systems were selected based on their redox potential [$E(D^+/D)$ and $E(A/A^-)$, respectively] values such that the D-A pairs provide favorable free energy changes (negative ΔG^0 values) for the PET processes from the excited (S_1) coumarin dyes to the ground state Ln(III) ions, which can be monitored suitably following the SS and TR fluorescence quenching methods. The donor acceptor systems used in the present study are given in Chart 6.1 along with their reduction potential values for their easy reference.

6.2. Materials and Methods

Perchlorate salts of the trivalent lanthanide quenchers were obtained from Alpha Aesar and used without further purification. The laser-grade coumarin dyes, coumarin-120 (C120), coumarin-339 (C339), coumarin-2 (C2) and coumarin-102 (C102), were obtained from Exciton, USA. Nanopure water (cf. Section 3.2, Chapter 3) was always used to prepare the experimental solutions. In the absorption and fluorescence studies, coumarin concentrations were kept significantly low, in the range of 5-7 μM , to avoid any inner filter effect. For these experiments, two aqueous stock solutions were prepared, one containing only the coumarin dye and the other containing the coumarin dye plus the Ln(III) ion to be used, keeping the dye concentration the same in both the stock solutions. These two solutions were then mixed suitably to change the Ln(III) concentration systematically in whereby the coumarin concentration always remained unchanged. With this procedure thus, there was no dilution effect for the coumarin fluorophore in the experimental solution, and thus it was very convenient to correlate the observed changes in the absorption and fluorescence characteristics of the studied dye with the changing Ln(III) concentration in the dye solution.

Experimental details for ground state absorption, steady state (SS) fluorescence, time-resolved (TR) emission and nanosecond laser flashphotolysis (LFP) measurements are as mentioned and discussed in Chapter 2 and/or Chapter 3. Similar to the studies presented in the previous chapters, fluorescence decays were recorded at magic angle (54.7°) configuration, to avoid the effects of rotational relaxation of the probe dyes on the observed fluorescence kinetics. In the LFP studies, to obtain reasonable transient absorption signals, the coumarin concentrations were needed to keep somewhat higher such that the absorbance at the excitation wavelength (355 nm) was typically about 0.25 (dye concentrations about 15-20 μM). Transient absorption spectra were recorded for the nanosecond to microsecond time spans. The IRF of the present LFP setup is ~ 10 ns.

6.3. Results and Discussion

6.3.1. Interaction of the Ground State Coumarin Dyes with the Lanthanide Ions

To understand the interaction of the ground state coumarin dyes with the lanthanide ions $\{\text{Ln(III)}\}$, absorption spectra of the dyes were recorded in aqueous solution both in the absence and presence of varying concentrations of the Ln(III) ions used. In general, the absorption bands of the studied coumarin dyes undergo a small reduction in the absorbance values with the increasing concentration of the Ln(III) ions. Representative changes in the ground state absorption spectra for the dye, C102, in the presence of varying concentrations of Eu(III), Sm(III) and Yb(III) ions in aqueous solution are shown in Figure 6.1. To be noted in the present context that the coumarin dyes used in present study are reasonably good electron donating in nature.¹²² Similarly, the Ln(III) ions used in this work also have significantly good electron accepting ability.^{197,229-233} Accordingly, from the ground state absorption results, it is inferred that in the studied coumarin-Ln(III) systems there is the formation of small extent of ground state complexes, understandably through the weak charge transfer (CT) interaction between the coumarin donors and the Ln(III) acceptors used in the present study.^{148,197}

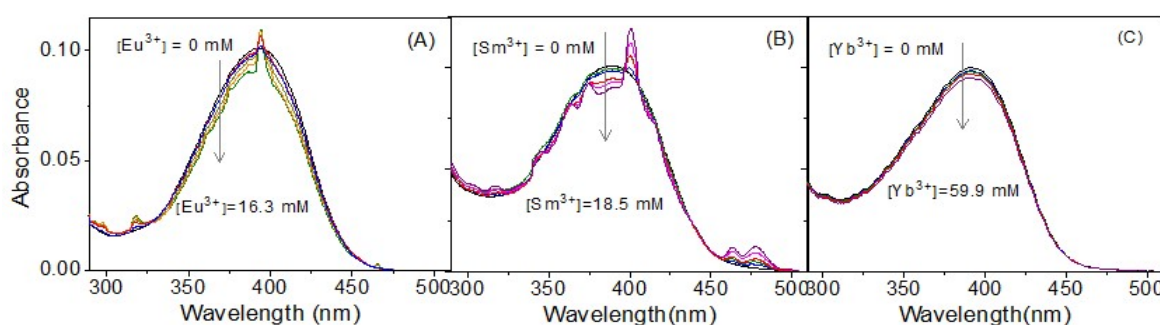


Figure 6.1. Changes in the absorption spectra for (A) C102-Eu(III), (B) C102-Sm(III) and (C) C102-Sm(III) systems with the gradually increasing concentration of the Ln(III) quenchers in aqueous solution. C102 concentration was $\sim 5 \mu\text{M}$.

6.3.2. Interaction of Excited (S_1) Coumarin Dyes with the Ln(III) Quenchers

6.3.2.1. Steady-state (SS) Fluorescence Quenching Study: To understand the excited (S_1) state interaction of the coumarin dyes with the Ln(III) quenchers, the SS fluorescence spectra of the dyes were recorded in aqueous solution both in the absence and presence of gradually increasing concentrations of the Ln(III) ions. In all the cases there was a systematic decrease in the fluorescence intensity for the broad emission spectra of the dyes with the increasing concentration of the Ln(III) ions. Evidently, the extent of this reduction in the fluorescence intensity was largely dependent on the coumarin-Ln(III) pairs used in the study. Representative SS fluorescence quenching results for the dye C102 in the presence of Eu(III), Sm(III) and Yb(III) ions in aqueous solution are shown in Figure 6.2.

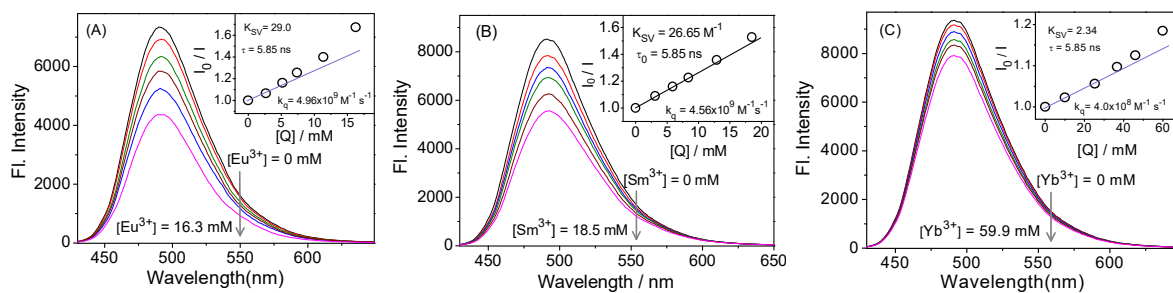


Figure. 6.2. Steady-state fluorescence quenching in (A) C102-Eu(III), (B) C102-Sm(III) and (C) C102-Sm(III) systems, with the gradually increasing concentration of the Ln(III) quenchers in aqueous solution. C102 concentration was $\sim 5 \mu\text{M}$. Insets show the respective Stern-Volmer plots, analyzed using eq. 6.1.

For the studied coumarin-Ln(III) systems, observed quenching in the SS fluorescence intensity do not accompany with any observable change in the shape for the emission spectra of the dyes. It is thus indicated that the fluorescence quenching in the present coumarin-Ln(III) systems does not possibly involve any appreciable exciplex formation, though a minute contribution from exciplex mechanism, as suggested by Inada et al.,²²² may not excluded completely for the present observations. To be noted however that in a highly polar solvent like water, as used in our present study, the exciplex formation is in general suggested to be highly unlikely in most donor-acceptor systems.²¹⁷ In the present study, since the coumarin dyes are reasonably good electron donating in nature and the Ln(III) ions are also having subatantially high electron accepting ability (cf. reduction potential values given in Chart 6.1),^{122,197,229-233} and also because the electron donating ability of the coumarin dyes increases substantially in their excited state than in the ground state,¹⁴⁸ it is inferred that the observed fluorescence quenching in the studied coumarin-Ln(III) systems is mainly due to the PET reaction between the excited (S_1) coumarin fluorophores and the ground state Ln(III) quenchers. Observed quenching results from the SS fluorescence studies in the present coumarin-Ln(III) systems were correlated using the standard Stern-Volmer (SV) relation as,¹⁴⁸

$$\frac{I_0}{I} = 1 + K_{SV}[Q] = 1 + k_q\tau_0[Q] \quad (6.1)$$

where I_0 and I are the SS fluorescence intensity in the absence and presence of the Ln(III) quencher (Q), $[Q]$ is the quencher concentration used, K_{SV} is the SV constant, k_q is the bimolecular quenching constant and τ_0 is the fluorescence lifetime of the coumarin dye in the absence of any quencher. Observed SV plots from the SS fluorescence quenching results are in general seen to display a positive deviation from the expected linearity. Representative SV plots obtained for C102 dye in the presence of Eu(III), Sm(III) and Yb(III) quenchers are shown in the insets of the respective panels in Figure 6.2A, B and C. The positive deviations observed in the SV plots for the present systems are attributed to the small extent of static quenching arising due to the small extent of ground state complex formation,¹⁴⁸ as indicated in the previous section from ground state absorption studies. The contribution of such static quenching over and above the dynamic fluorescence quenching of the

dyes by the Ln(III) quenchers causes the SV plots for such systems from SS fluorescence quenching to display positive deviations, resulting an overestimation of the k_q values, even on using the initial slopes of the concerned SV plots.¹⁴⁸ Accordingly, for the present systems, we relied on the time-resolved (TR) fluorescence quenching results to estimate the reliable k_q values, since the obtained SV plots in these cases were very linear in nature, as are discussed in the next section. In the present context, however, just for a comparison, the k_q values for different coumarin-Ln(III) systems as obtained from SS fluorescence quenching (represented as $k_{q(SS)}$, estimated using the initial slope of the SV plot) and TR fluorescencing quenching (represented as $k_{q(TR)}$, estimated using the linear SV plot; discussed elaborately in the next section), are listed together in Table 6.2. Evidently the $k_{q(SS)}$ values are always much higher than the corresponding $k_{q(TR)}$ values, suggesting the overestimation of the k_q values from the SS quenching results.¹⁴⁸

Table 6.2. Comparisons of the $k_{q(SS)}$ and $k_{q(TR)}$ values estimated for different coumarin-Ln(III) systems in aqueous solution.

Dyes	$(k_q / 10^9 \text{ M}^{-1}\text{s}^{-1})^a$	Eu(III)	Yb(III)	Sm(III)
C102	$k_{q(SS)}$	4.96	0.40	4.56
	$k_{q(TR)}$	2.45	0.20	1.76
C339	$k_{q(SS)}$	4.48	0.20	2.12
	$k_{q(TR)}$	3.34	0.05	0.69
C2	$k_{q(SS)}$	4.95	0.30	2.57
	$k_{q(TR)}$	2.67	0.09	0.66
C120	$k_{q(SS)}$	4.97	0.07	1.19
	$k_{q(TR)}$	2.99	0.01	0.35

^aError limits for $k_{q(SS)}$ and $k_{q(TR)}$ values are $\pm 10\%$ and $\pm 5\%$, respectively.

6.3.2.2. Time-resolved (TR) Fluorescence Quenching Study: The fluorescence decays of the coumarin dyes were recorded in aqueous solution in the absence and presence of varying concentrations of the Ln(III) quenchers, following the TR fluorescence quenching measurements. For all the coumarin-Ln(III) pairs, it is observed that the fluorescence decays of the coumarin dyes gradually became faster as the quencher concentration is systematically increased in the solution. Observed results thus indicate significant extent of dynamic interaction for the excited (S_1) coumarin dyes with the ground state Ln(III) quenchers, especially for the coumarin-Eu(III) and coumarin-Sm(III) systems, though for the coumarin-Yb(III) system, the observed TR fluorescence results indicate only a marginally faster decays for the dyes in the presence of the Yb(III) quencher, suggesting a relatively much weaker quenching interaction for the coumarin-Yb(III) system as

compared to the coumarin-Eu(III) and coumarin-Sm(III) systems. Representative TR fluorescence quenching results involving C339-Ln(III) system in aqueous solution are shown in Figure. 6.3.

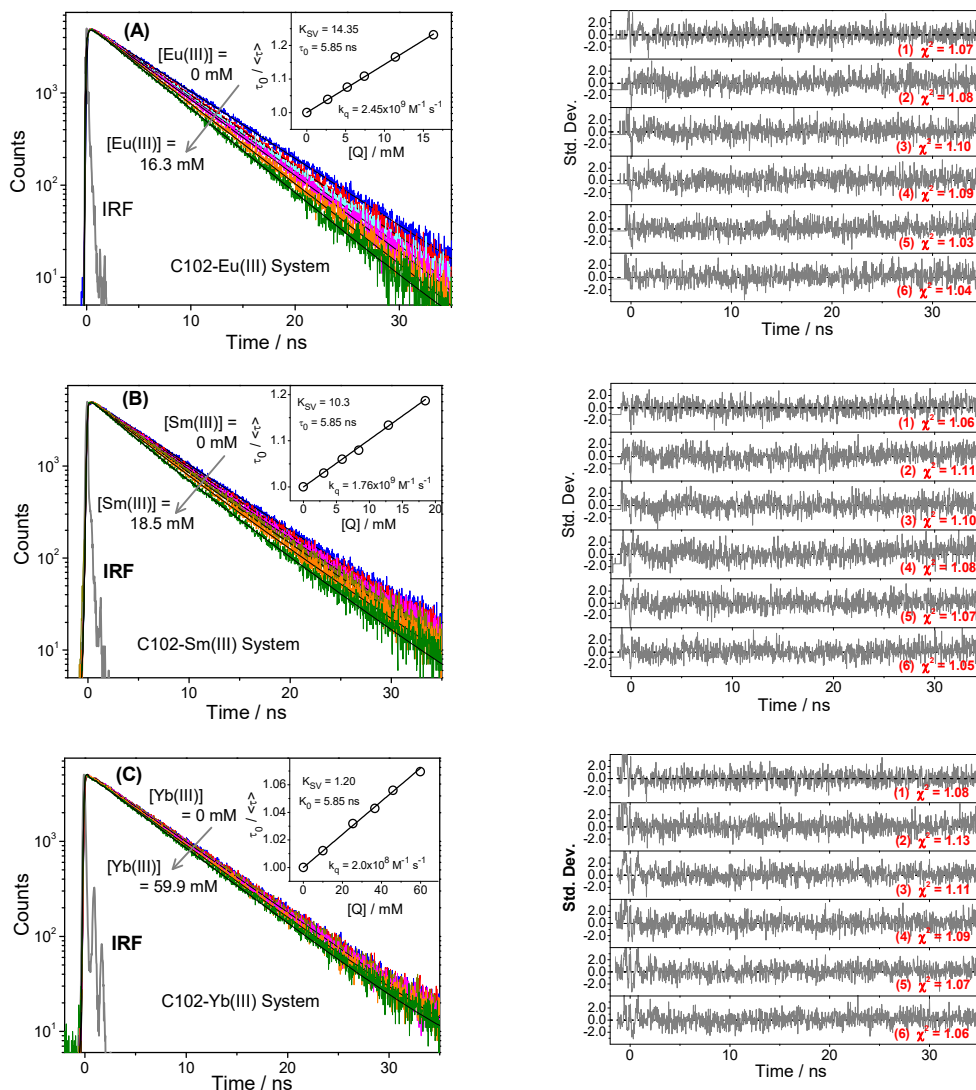


Figure. 6.3. Time-resolved fluorescence quenching as observed in (A) C102-Eu(III), (B) C102-Sm(III) and (C) C102-Yb(III) systems with the gradually increasing concentration of the Ln(III) quenchers in aqueous solution. C102 concentration was $\sim 5 \mu\text{M}$.

From the analysis of the fluorescence decays it is observed that while in the absence of the Ln(III) quenchers the observed decays for all the dyes fit very satisfactorily with a simple single-exponential function, for some of the coumarin-Ln(III) systems the observed fluorescence decays show mild bi-exponential nature (cf. eq. 3.14), although in the other cases the decays could also be fitted satisfactorily using a single-exponential function.⁶⁹ In the cases of bi-exponential decays, average fluorescence lifetime ($\langle \tau \rangle$) values were estimated following the relation as given in Chapter 3 (cf. eq. 3.15). For all the coumarin-Ln(III) systems, it is seen that the fluorescence lifetime values (average lifetimes in the case of bi-exponential decays) systematically decrease as the Ln(III) concentration is gradually increased in the experimental solution.

Table 6.3. Various parameters for the PET reactions between excited coumarin donors and ground state Ln(III) acceptors in aqueous solutions.

Dye	τ_0 (ns)	$E_{00}(\text{dye})$ (eV)	$E(D^+/D)$ (V), NHE	Ln(III)	$E(A/A^-)$ (V), ^s NHE	$k_{q(TR)}$ ($10^9 \text{ M}^{-1} \text{ s}^{-1}$) [#]	ΔG^0 (eV) ^s
C102	5.85	2.76	1.01	Eu(III)	-0.35	2.45	-1.42
				Yb(III)	-1.15	0.20	-0.62
				Sm(III)	-1.55	1.76	-0.22
C339	4.82	2.95	1.22	Eu(III)	-0.35	3.34	-1.4
				Yb(III)	-1.15	0.05	-0.60
				Sm(III)	-1.55	0.69	-0.20
C2	4.91	3.00	1.29	Eu(III)	-0.35	2.67	-1.38
				Yb(III)	-1.15	0.09	-0.58
				Sm(III)	-1.55	0.66	-0.18
C120	4.71	3.12	1.51	Eu(III)	-0.35	2.99	-1.28
				Yb(III)	-1.15	0.01	-0.48
				Sm(III)	-1.55	0.35	-0.08

[#]Error limit in the $k_{q(TR)}$ values is $\pm 5\%$. ^sError limit in the ΔG^0 values is $\pm 0.01 \text{ eV}$.

For the studied coumarin-Ln(III) systems, the reductions in the fluorescence lifetime values as function of the Ln(III) concentrations used were correlated using the standard Stern-Volmer (SV) relation as,¹⁴⁸

$$\frac{\tau_0}{\langle \tau \rangle} = 1 + K_{SV} [Q] = 1 + k_q \tau_0 [Q] \quad (6.2)$$

where all the parameters have their usual meaning as mentioned with respect to eq. 6.1. For all the coumarin-Ln(III) systems, the TR fluorescence quenching results provide very linear SV plots, at least for the concentration ranges of the Ln(III) ions used in the present study. Representative SV plots for the C102-Eu(III), C102-Sm(III) and C102-Yb(III) systems are shown in the insets of the respective panels in Figure 6.3A, B and C. The linearity of the SV plots in the present cases clearly suggest that unlike in the SS fluorescence quenching, there is no effect of the static quenching on the TR fluorescence quenching results.¹⁴⁸ The k_q values, designated here as $k_{q(TR)}$, were obtained for different coumarin-Ln(III) pairs suitably by using the linear SV plots and the values thus estimated are listed in Table 6.3 along with the corresponding $k_{q(SS)}$ values obtained from the SS fluorescence results for the studied systems. In the present study, considering the reasonably good electron

donating ability of the used coumarin dyes,¹²² and because the used Ln(III) ions are also quite good electron acceptors,^{197,229-233} the $k_{q(TR)}$ values estimated from the TR fluorescence quenching studies are considered as the observed reaction rate constants for the PET processes occurring in the studied coumarin-Ln(III) systems.¹⁴⁸

6.3.3. Laser Flash Photolysis Studies on Coumarin–Ln(III) Systems

As discussed in the previous sections, the SS and TR fluorescence quenching observed for the coumarin-Ln(III) systems were mostly attributed to PET process between the excited coumarin donors and the ground state Ln(III) acceptors. To ascertain this PET process, we carried out nanosecond laser flash photolysis (LFP) studies using selected coumarin-Ln(III) systems. Figure 6.4 shows the transient absorption spectra obtained for the C339 dye (25 μ M) in aqueous solution, both in the absence and presence of Eu(III) quencher (173 mM). The transient absorption spectra obtained either in the absence or in the presence of the Eu(III) quencher are qualitatively very similar, with the characteristic features to note are:- (i) a sharp absorption band at the shorter wavelength range, spanning over about 320 to 365 nm region, shown explicitly in the expanded form in Figure 6.5; (ii) a depleted absorption band in the intermediate wavelength region, spanning from about 365 nm to about 440 nm; and (iii) a broad absorption band at the longer wavelength region, spanning from about 540 nm to about 800 nm, shown explicitly in the expanded form in Figure 6.6.

In the present context, it is interesting to recall the work reported by Johnston and coworkers dealing with the LFP study of the structurally similar coumarin dyes using the same laser excitation as in our present study, i.e. 355 nm. In their study, the authors observed a significant extent of dye photoionizations producing both the dye cation radicals and hydrated electrons in the irradiated solution.^{432,438} Based on these results as reported by Johnston and coworkers^{432,438} and also considering the other literature reports,^{432,438-440} the coumarin cation radicals are indicated to have their transient absorptions mainly in the shorter wavelength region, typically in the range of about 350-400 nm. Following these literature reports, we infer that the sharp transient absorption band observed for our studied systems in the 320-365 nm region (cf. Figure 6.4 and 6.5) is mainly due to the C339^{•+} cation radical formed in the present systems. It is quite apparent from the observed results that the C339 dye experiences a small extent of direct photoionization on 355 nm laser excitation even in the absence of Eu(III) quencher, very similar to the observations made by Johnston and coworkers in their LFP study on the coumarin dyes.^{432,438} Interestingly, however, the intensity of this transient absorption band for the C339^{•+} cation radical increases by ~3 folds in the presence of Eu(III) quencher (cf. Figure 6.5A and B), unequivocally supporting the PET process in the studied C339-Eu(III) system. To be mentioned here that the transient absorptions bands observed in the present study either for the C339 dye alone or for the C339-Eu(III) system cannot be attributed to the triplet state of the studied dye, because the triplet quantum yields for the coumarin dyes are in general reported to be extremely low such that the direct formation of the triplet states of

these dyes through the intersystem crossing process in their excited S_1 states following their LFP studies is hardly observed in any of the reported literatures.^{356,441}

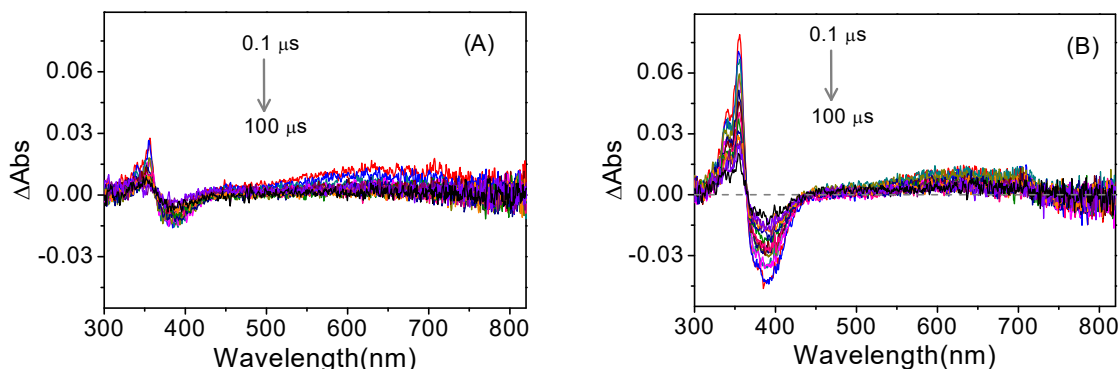


Figure 6.4. Transient absorption spectra for (A) C339 only and (B) C339-Eu(III) system in aqueous solution. In both the panels X and Y scales are kept same to appreciate the differences in the spectral features in the two cases. Dye and Eu(III) concentrations used in this study were 25 μ M and 173 mM, respectively.

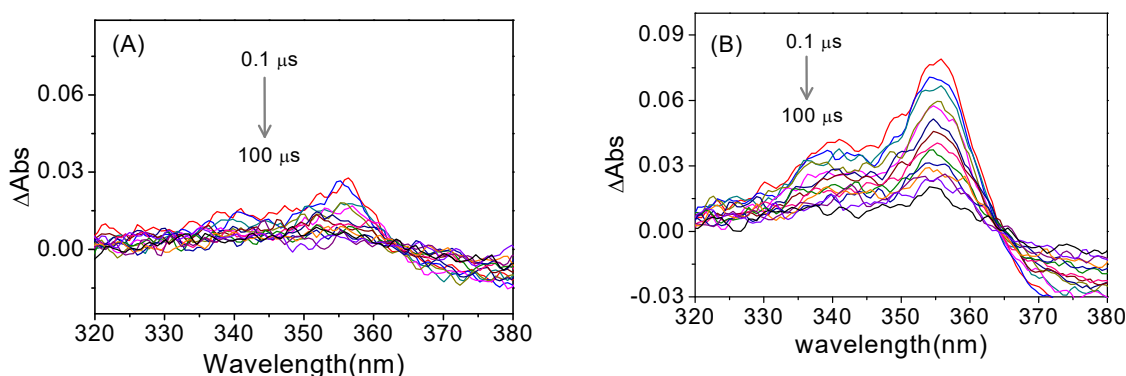


Figure 6.5. Shorter wavelength region of the transient spectra in Figure 6.4 shown in the expanded scales for (A) C339 only and (B) C339-Eu(III) system. In both the panels X and Y scales are kept same to appreciate the differences in the spectral features and absorbance values in two cases.

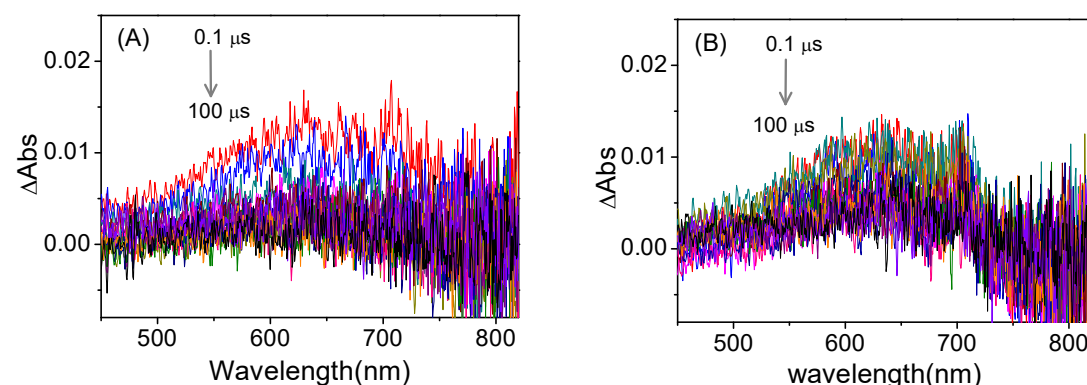


Figure 6.6. Longer wavelength region of the transient spectra in Figure 6.4 shown in the expanded scales for (A) C339 only and (B) C339-Eu(III) system. In both the panels X and Y scales are kept same to appreciate the differences in the spectral features and absorbance values in two cases.

The depleted transient absorption band in the intermediate wavelength region for both C339 dye and the C339-Eu(III) system (cf. Figure 6.4) are agreeably due to the disappearance of some of

the C339 dyes from the irradiated solution as they undergo either direct photoionization or the PET reaction with the Eu(III) quenchers, following their excitation by the laser light. Comparison of the results in Figure 6.4A and B indicate that the depletion of the dyes is ~ 3.5 fold higher in the presence of Eu(III) quencher than in the case of the dye alone. This results correlate nicely with the enhanced absorbance for the shorter wavelength transient band in the presence of Eu(III) quencher, attributed to the $C339^{\bullet+}$ cation radical (cf. Figures 6.4 and 6.5) and thus substantiates our inference that the excited (S_1) coumarin dyes undergo PET reaction with the ground state Ln(III) quenchers.

The transient absorption band in the longer wavelength region is observed to be very weak for both C339 alone and C339-Eu(III) system (cf. Figures 6.4 and 6.6). Besides, the absorbance for this longer wavelength transient band (540-820 nm) appears to be very similar for both C339 alone and C339-Eu(III) system. Since coumarin cation radicals do not have any appreciable absorption in this longer wavelength region,^{439,440} and because these dyes undergo some extent of direct photoionization with the 355 nm laser light, it is inferred that the longer wavelength transient absorption band is mainly due to the formation of small extent of hydrated electrons in the solution, as also reported previously by Johnston and coworkers following their LFP studies on similar coumarin dyes.^{432,438} Due to extremely weak nature, it is difficult to comment further on the characteristics of this longer wavelength transient absorption band observed for the studied system.

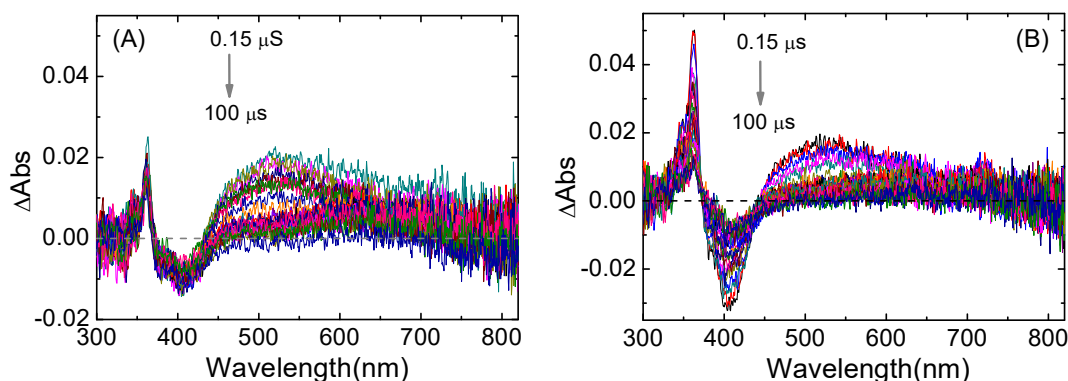


Figure 6.7. Transient absorption spectra for (A) C102 only and (B) C102-Eu(III) system in aqueous solution. In both the panels X and Y scales are kept same to appreciate the differences in the spectral features in two cases. Dye and Eu(III) concentrations used were 22 μ M and 138 mM, respectively.

In the present study, similar LFP studies were also carried out for C102 dye (22 μ M) both in the absence and presence of Eu(III) quencher (138 mM). The transient absorption spectra obtained in the present systems case are compared in Figures 6.7 for the whole spectral range. For a better understanding of the observed transient bands at the shorter and longer wavelength regions, the respective bands are plotted in the expanded forms and are shown in Figure 6.8 and 6.9, respectively. It is evident from the results shown in Figure 6.7 to Figure 6.9 that the LFP results obtained for the C102-Eu(III) system are very qualitatively similar to those obtained for the C339-Eu(III) system, as we have discussed just before and represented in the previous Figure 6.4 to Figure

6.6. The LFP results of C339-Eu(III) and C102-Eu(III) systems thus unequivocally establish the PET mechanism for the presently studied coumarin-Ln(III) systems.

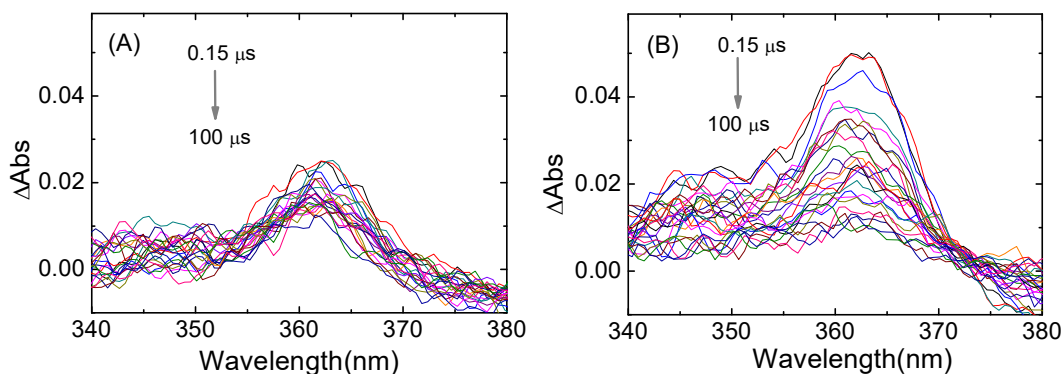


Figure 6.8. Shorter wavelength region of the transient spectra in Figure 6.7 shown in the expanded forms for (A) C102 only and (B) C102-Eu(III) system. In both the panels X and Y scales are kept same to appreciate the differences in the spectral features and absorbance values in two cases.

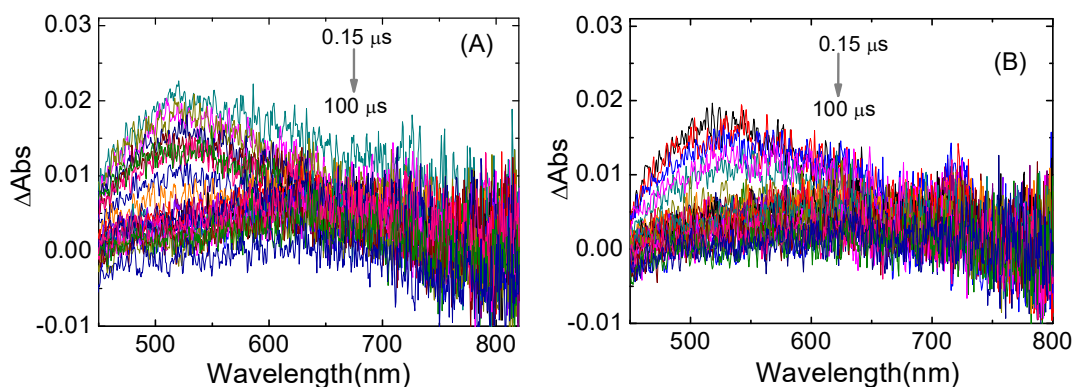


Figure 6.9. Longer wavelength region of the transient spectra in Figure 6.7 shown in the expanded forms for (A) C02 only and (B) C102-Eu(III) system. In both the panels X and Y scales are kept same to appreciate the differences in the spectral features and absorbance values in two cases.

The transient kinetic traces were independently recorded for C339 dye at 355 nm, i.e. the transient absorption band for the C339^{•+} cation, both in the absence and in the presence of Eu(III) and Sm(III) quenchers, and the observed kinetic traces are shown together in Figure 6.10 for their comparison. In all the cases, the transient decays are exceedingly slow, which are in accordance with the typical decay kinetics reported for different coumarin cation radicals.⁴⁴⁰ In brief, the LFP results obtained in the present study are in direct support to the PET mechanism suggested for the studied coumarin-Ln(III) systems in the aqueous solution.

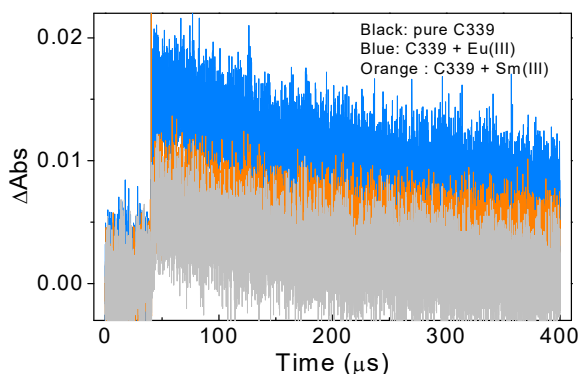


Figure. 6.10. Transient kinetic traces (at 355 nm) for C339 cation in the C339-Ln(III) systems. Dye concentration was 25 μM while Eu^{3+} and Sm^{3+} concentrations were 173 mM 133 mM, respectively.

6.3.4. Correlation of k_q Values with Free Energy Changes of PET Reactions

The ΔG^0 values for the PET reactions between excited (S_1) coumarin donors and ground-state Ln(III) acceptors in aqueous solution were estimated using the standard Rehm-Weller relation, the details of which have been discussed before in Chapter 3 (cf. eq. 3.17). As required for these estimations, the r_A and $E(A/A^+)$ values of the Ln(III) acceptors were obtained directly from the reported literatures (cf. Table 6.1),^{197,229-233} the r_D values of the coumarin donors were estimated by using the Edward's volume addition method,³⁷⁰ and the $E(D^+/D)$ values of these donors in aqueous solution were evaluated by applying the Fawcett's correction method on the reported $E(D^+/D)$ values of these dyes in acetonitrile (ACN) solution,^{92,378,379} a methodology which has been discussed elaborately in Chapter 3 (cf. Section 3.3.2.3). Different electrochemical parameters obtained for the studied coumarin dyes following Fawcett's correction method are listed in Table 6.4 and the correspondingly estimated ΔG^0 values for the studied coumarin-Ln(III) systems in aqueous solution following Rehm-Weller relation (eq. 3.17, Chapter 3) are listed in Table 6.3, which has been presented earlier in Section 6.3 to list the $k_{q(TR)}$ values for the concerned coumarin-Ln(III) pairs. Interesting to note from Table 6.3 that the ΔG^0 values for all the studied coumarin-Ln(III) systems are negative, suggesting the PET reactions in the present systems to be thermodynamically favorable. To be mentioned in the present context, however, that excluding the Eu(III), Yb(III) and Sm(III) ions, on using the other Ln(III) ions as the quenchers for the studied coumarin dyes, the ΔG^0 values for the concerned systems are estimated to be positive, as listed in Table 6.5 for a quick reference, suggesting the PET reaction in these latter coumarin-Ln(III) systems to be thermodynamic not feasible. In accordance with these ΔG^0 estimations, we in fact find in the present study that excluding the Eu(III), Yb(III) and Sm(III) ions, for the other Ln(III) quenchers there is no observable fluorescence quenching for the used coumarin dyes. In the present study, therefore, only the Eu(III), Yb(III) and Sm(III) ions were effectively used as the electron acceptors to investigate the PET reactions with the studied coumarin donors (cf. Chart 6.1) following the SS and time fluorescence quenching measurements.

Table 6.4. Electrochemical properties calculated for the coumarin dyes in aqueous solution based on the reported redox potential values in acetonitrile (ACN) solution.

Coumarin Donors	r_D (or r_i) (\AA) ^a	$E(D^+/D)_{\text{ACN}}$ (V), ^b SCE	$G_s^0 _{\text{ACN}}$ (eV) ^c	$G_s^0 _{\text{water}}$ (eV) ^c	$E(D^+/D)_{\text{water}}$ (V), SCE	$E(D^+/D)_{\text{water}}$ (V), NHE
C102	3.82	0.80	-1.488	-1.521	0.77	1.01
C339	3.58	1.01	-1.569	-1.604	0.98	1.22
C2	3.54	1.08	-1.583	-1.618	1.05	1.29
C120	3.31	1.30	-1.671	-1.708	1.26	1.51

^aObtained using Edward's volume addition method.³⁷⁰ The r_i values for the D^+ ions are considered to be the same as the r_D values of the concerned coumarin donors (D).

^bThese are the experimentally measured values in acetonitrile solution against SCE.²¹³

^cThe parameter G_s^0 is used for simplicity to represent the $G_s^0(D^+)$ values in the respective solvents.

Table 6.5. Calculated free energy changes (ΔG^0) for coumarin-Ln(III) systems following Rehm-Weller relation as given by eq. 3.17. Maximum error limit in the estimated values is about $\pm 0.01\text{eV}$

Coumarin-Ln(III) Systems	$\Delta G^0 / \text{eV}$			
	C102	C339	C2	C120
La(III)	1.33	1.35	1.37	1.47
Ce(III)	1.43	1.45	1.47	1.57
Pr(III)	0.93	0.95	0.97	1.07
Nd(III)	0.83	0.85	0.87	0.97
Pm(III)	0.83	0.85	0.87	0.97
Sm(III)	-0.22	-0.20	-0.18	-0.08
Eu(III)	-1.42	-1.40	-1.38	-1.28
Gd(III)	2.13	2.15	2.17	2.27
Tb(III)	1.93	1.95	1.97	2.07
Dy(III)	0.83	0.85	0.87	0.97
Ho(III)	1.13	1.15	1.17	1.27
Er(III)	1.33	1.35	1.37	1.47
Tm(III)	0.53	0.55	0.57	0.67
Yb(III)	-0.62	-0.60	-0.58	-0.48

As indicated from Table 6.1, the $E(A/A^{\cdot-})$ value is the least negative for Eu(III) ion, suggesting it to be the strongest acceptor for PET reaction. Obviously thus, the ΔG^0 values for the coumarin-Eu(III) systems are estimated to be substantially more negative than the coumarin-Yb(III) and coumarin-Sm(III) systems, causing the estimated $k_{q(TR)}$ values to be much higher for the former systems than the later two systems (cf. Table 6.3). The stronger electron accepting ability for Eu(III) ion is understandably due to the fact that the one electron reduction of this ion produces the divalent Eu(II) ion for which the electronic configuration in the 4f-shell becomes exactly half-filled, providing an additional stability for the resultant ion than in the other two cases.

It is also interesting to note from Table 6.1 that even though the $E(A/A^{\cdot-})$ value for the Sm(III) ion is the most negative among the three Ln(III) ions (i.e. Eu(III), Yb(III) and Sm(III) ions) used in the present study, yet this $E(A/A^{\cdot-})$ value is not as largely negative as observed for the rest of the Ln(III) ions. Accordingly, it is indicated that the Sm(III) ion has a relatively stronger electron accepting ability than the rest of the Ln(III) ions, excluding however the Eu(III), Yb(III) ions. The rationale behind this relatively stronger electron accepting ability for the Sm(III) ion is that the reduction of this ion leads to the formation of the divalent Sm(II) ion for which the 4f-shell attains an approaching half-filled configuration ($4f^6$). Accordingly thus, the reduction of the Sm(III) ion is not as difficult as that of the other Ln(III) ions, excluding certainly the Eu(III) and Yb(III) ions. Evidently thus, the estimated ΔG^0 values for the coumarin-Sm(III) systems are quite negative, making the concerned PET reactions thermodynamically very favorable, as supported by the reasonably high $k_{q(TR)}$ values obtained for these systems, as listed in cf. Table 6.3. That the $k_{q(TR)}$ values for the coumarin-Sm(III) systems are much lower than those of the coumarin-Eu(III) systems are in accordance with the relatively less negative ΔG^0 values for the former systems than the latter, as indicated from Table 6.3.

The one electron reduction of Yb(III) produces the corresponding divalent Yb(II) ion having a completely filled f-shell configuration ($4f^{14}$). Accordingly, the $E(A/A^{\cdot-})$ value for the Yb(III) ion is much less negative than that of the Sm(III) ion. Consequently, the ΔG^0 values for the studied coumarin-Yb(III) systems are considerably more negative than the ΔG^0 values for the coumarin-Sm(III) systems, as indicated from Table 6.3. Interestingly, however, the $k_{q(TR)}$ values obtained for the studied coumarin-Yb(III) systems are much lower than those of the corresponding coumarin-Sm(III) systems (cf. Table 6.3). These observations thus suggest that as an electron acceptor the Yb(III) ion behaves quite less efficiently as compared to the Eu(III) and Sm(III) ions for the studied PET systems. To obtain the underlying reason for this unusual behavior of the Yb(III) ion, the $k_{q(TR)}$ values for all the studied coumarin-Ln(III) systems were plotted against their respective ΔG^0 values, as are shown in Figure. 6.11. It is very evident from this figure that the $k_{q(TR)}$ values for all the coumarin-Ln(III) pairs do not fall into a common trend in regard to the changing ΔG^0 values for the studied PET systems and accordingly no generalized correlation, e.g. a single Rehm-Weller correlation, is not possible to be defined to account the ΔG^0 dependent changes in the $k_{q(TR)}$ values

for all the coumarin-Ln(III) systems used in the present study. Interestingly it is seen that while exergonicity ($-\Delta G^0$) values for the studied coumarin-Eu(III) systems follow the order, coumarin-Eu(III) > coumarin-Yb(III) > coumarin-Sm(III), the observed $k_{q(TR)}$ values for these studied systems intriguingly display quite contrasting order as, coumarin-Eu(III) > coumarin-Sm(III) > coumarin-Yb(III). These observations clearly indicate that the $k_{q(TR)}$ values for the coumarin-Yb(III) are unusually lower in spite of the fact that the exergonicity values for these systems are significantly higher than those of the coumarin-Sm(III) systems. Such an inconsistency in the correlations between $k_{q(TR)}$ and ΔG^0 values among different coumarin-Ln(III) systems definitely suggests that the propensity of the PET reactions in the present systems is not determined only by the ΔG^0 values of the PET reactions but is also influenced very strongly by an intrinsic factor associated with the used Ln(III) ions as the quenchers, causing the observed PET kinetics to change in a quite unusual manner than usually expected for the chemically related donor-acceptor pairs in the conventional low viscosity homogeneous solvents.^{130,260,264,375,416,442}

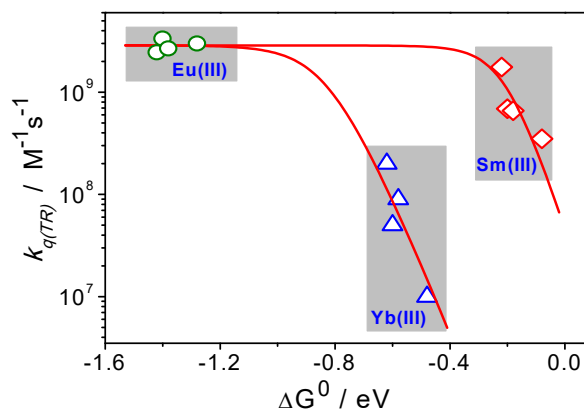


Figure 6.11. The k_q vs ΔG^0 plots for the PET reactions in the studied coumarin-Ln(III) systems in aqueous media. The k_q values are clubbed together independently for each of the Ln(III) ions, as indicated by the three different shaded boxes for the quenching data involving Eu(III), Yb(III) and Sm(III) ions as the quenchers.

For our studied coumarin-Ln(III) systems as the PET reactions are carried out under diffusive condition in aqueous solution, the progress of the overall reaction can be realized suitably by using the kinetic sequences as discussed elaborately in Section 1.5 in Chapter 1. For easy visualization these kinetic sequences are presented again in a consolidated manner in Scheme 6.1. According to this scheme, the observed rate constant for the bimolecular PET reaction would be the same as the observed quenching constant $k_{q(TR)}$ estimated from the TR fluorescence quenching study, which can be expressed explicitly as,^{29,30,148}

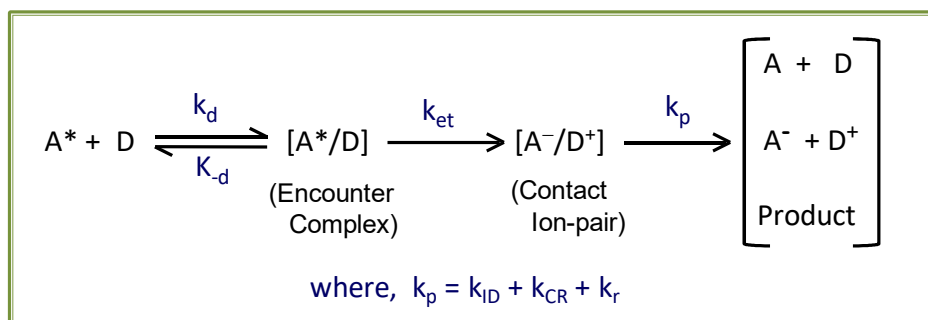
$$k_{q(TR)} = \frac{k_d}{1 + \frac{k_d}{K_{eq}k_{et}}} = \frac{k_d}{1 + \frac{k_d}{K_{eq} \nu \exp\left(\frac{-(\Delta G^0 + \lambda)^2}{4\lambda k_B T}\right)}} \quad (6.3)$$

where K_{eq} is the equilibrium constant for the encounter complex (D/A^*) formation, i.e. $K_{eq} = (k_d/k_{-d})$, and k_{et} is the intrinsic ET rate constant in the encounter complex, expressed explicitly by eq. 1.14 as discussed in Chapter 1. In the present context, however, considering the diffusive condition of the concerned PET reactions, the k_{et} function can be expressed in its simplified form where all the pre-exponential parameters in eq. 1.14 can be consolidated effectively into a single term which can be defined as the effective frequency factor, ν , for the concerned ET reactions, i.e.

$$\nu = \frac{2\pi}{\hbar} V_{el}^2 (4\pi\lambda k_B T)^{-1/2} \quad (6.4)$$

At the lower exergonicity region, since the product “ $K_{eq}k_{et}$ ” will be lower than the k_d value, eq. 6.3 suggests that the observed $k_{q(TR)}$ would increase asymptotically with the $-\Delta G^0$ values for the PET reactions. However, at the higher exergonicity region, since the “ $K_{eq}k_{et}$ ” value would become much higher than the k_d value, it is evident from eq. 6.3 that the $k_{q(TR)}$ will saturate to the limiting k_d value, making the observed bimolecular PET rate to be completely diffusion controlled.

Scheme 6.1. The overall kinetic scheme for the bimolecular PET reactions carried out under diffusive condition. Elementary steps in the scheme are as discussed in the section 1.5 in Chapter 1.



With the basic understandings as discussed above, we can now critically look into the $k_{q(TR)}$ vs ΔG^0 plots observed for different coumarin-Ln(III) systems in the present study. As indicated from Figure 6.11, while the coumarin-Sm(III) and coumarin-Yb(III) systems independently display quite systematic increase in their $k_{q(TR)}$ values with the increasing exergonicity ($-\Delta G^0$) in the respective PET reactions, the coumarin-Eu(III) systems apparently show the saturation of their $k_{q(TR)}$ values to the expected diffusion controlled limit (k_d) for the bimolecular reactions, possibly because of the extremely high exergonicity for the coumarin-Eu(III) systems as compared to the coumarin-Sm(III) and coumarin-Yb(III) systems (cf. Table 6.3). To be mentioned here that for the coumarin-Eu(III) systems, in spite of their $k_{q(TR)}$ values to reach apparently the saturation limit of k_d , the observed $k_{q(TR)}$ values for these systems distinctly display some fluctuations (cf. Figure 6.11), which are possibly arising due to the small differences in the ET parameters (e.g. V_{el} , λ_i , and so on) for different coumarin-Eu(III) systems (cf. Section 1.2.1 and 1.2.2 in Chapter 1). Accordingly, it is assumed that the average of the $k_{q(TR)}$ values for the studied coumarin-Eu(III) systems can be considered as a

reasonable measure for the k_d value applicable for all the coumarin-Ln(III) systems studied in the present work, irrespective of the Ln(III) quenchers used in the different PET systems.

For the coumarin-Sm(III) and coumarin-Yb(III) systems, though their ΔG^0 dependent changes in the $k_{q(TR)}$ values do not fall under a single Rehm-Weller kind of correlation, yet these changes for each of the coumarin-Ln(III) systems it is possible to be accounted independently using the relation given by eq. 6.3, albeit with the use of largely different reorganization energy (λ) values, considering this λ as well as the pre-exponential factor ν as the adjustable parameters, and assuming the k_d value similar to the average of the $k_{q(TR)}$ values obtained for the coumarin-Eu(III) systems, as discussed before. The correlation curves thus obtained for the coumarin-Sm(III) and coumarin-Yb(III) systems independently are presented in Figure 6.11 along with their respective experimental data. From these correlations, it is interestingly seen that even though the k_d and ν values appear to be quite similar for both the coumarin-Sm(III) and coumarin-Yb(III) systems, i.e. $k_d \sim 2.9 \times 10^9 \text{ M}^{-1} \text{ s}^{-1}$ and $\nu \sim 1.5 \times 10^{13} \text{ s}^{-1}$, the λ value is, however, estimated to be much higher for the latter systems ($\lambda \sim 2.3 \text{ eV}$) than the former ($\lambda \sim 1.3 \text{ eV}$). These results thus evidently suggest that in the normal Marcus region, where $k_{q(TR)}$ increases asymptotically with reaction exergonicity, the efficiency of the PET reaction is much lower for the coumarin-Yb(III) systems than the coumarin-Sm(III) systems. It is interesting to mention here that while for many donor-acceptor systems, especially those involving organic donor-acceptor pairs, the λ values are found to be mostly in the range of 1-1.3 eV,^{130,260,264,375,416,442} there are some limited donor-acceptor systems, especially those involving different Ln(III) ions as the electron acceptors, the λ values are sometimes reported to be significantly higher,^{222,227} quite similar to the λ value estimated in the present study for the coumarin-Yb(III) systems. From the observed results it seems quite apparent that the PET process involving Yb(III) ion as the electron acceptor is inherently associated with a much higher λ value as compared to the Sm(III) and Eu(III) ions used as the acceptors, making the overall PET process with the former quencher quite less efficient as compared to the latter two quenchers.

To understand the largely reduced propensity for the PET processes involving Yb(III) ion as the quencher as compared to the Sm(III) and Eu(III) ions, we considered the possible involvement of the low lying electronic energy states of the concerned Ln(III) ions as the electron acceptors, because these ions possess different sequences of these associated energy states,⁴³⁴⁻⁴³⁷ which can in some favorable situations support the multichannel PET reactions for studied PET systems. Though this aspect is not extensively reported in the literature, yet in one of the previous studies reported from our group,¹⁹⁷ it was evidently indicated that the Ln(III) ions as the electron acceptors can indeed involve some of their low lying electronic energy states to support multichannel PET process with some suitable electron donors, causing the concerned PET processes to occur with quite unusual propensity than expected for the commonly used organic donor-acceptor systems.^{130,260,264,375,416,442} Considering the similar multichannel PET processes for the present

coumarin-Ln(III) systems, it is likely that an excited coumarin dye can simply transfer an electron to any one of the accessible low lying electronic states of the interacting Ln(III) ion, and the higher energy ion-pair state thus formed in this PET reaction can subsequently cascade down the energy landscape through their non-radiative relaxation into the surrounding solvent bath.

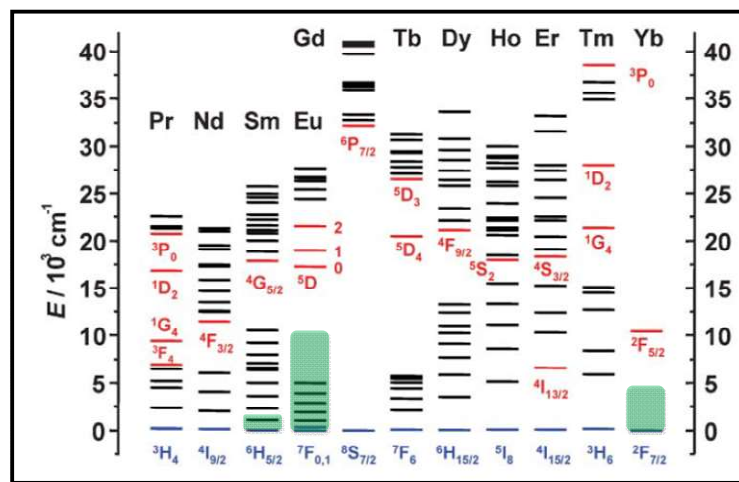


Figure 6.12. Potential energy diagram of the trivalent lanthanide aquo ions (reproduced from ref. 196, with permission from The Royal Society of Chemistry). The bars show the available energies in different cases to involve the higher energy state of the lanthanide ions in the PET reaction.

To understand the aforesaid multichannel PET mechanism in the studied coumarin-Ln(III) systems better, we show the relative energy states of different Ln(III) ions in Figure 6.12, as reported in the literature.¹⁹⁶ The average exergonicity values available from the PET reactions in the studied coumarin-Ln(III) systems involving Eu(III), Yb(III) and Sm(III) ions are also highlighted with the green bars in the respective cases in Figure 6.12. Noticeably, the available average exergonicity for the coumarin-Eu(III) systems is quite high to access a large number of the low lying energy states of the Eu(III) quencher, causing the PET reactions to occur very proficiently, with the $k_{q(TR)}$ values reaching effectively the diffusion controlled limit (k_d). For coumarin-Sm(III) systems, though the available exergonicity is quite small, yet it can access at least two of the low lying energy states of the Sm(III) ion, causing the PET reactions to occur with reasonably good proficiency (cf. Table 6.3 and Figure 6.12). Interestingly, for the coumarin-Yb(III) systems, though the available exergonicity is substantially higher than the coumarin-Sm(III) systems, yet this exergonicity cannot access any of the higher energy states of the Yb(III) ion, making the PET reactions to proceed only through the lowest energy state of the Yb(III) ion and thus causing the concerned PET precosses to occur with quite less profocency as compared to those with Sm(III) and Eu(III) ions (cf. Table 6.3 and Figure 6.12). Thus, involving the multichannel PET mechanism, we can at lease qualitatively justify why the coumarin-Yb(III) and coumarin-Sm(III) systems display largely different $k_{q(TR)}$ vs ΔG^0 correlations, resulting their independent Rehm-Weller correlations than a common Rehm-

Weller behaviour as normally observed with most of the chemically related donor-acceptor systems.^{130,260,264,375,416,442} As it is understandable, with the involvement of multichannel PET mechanism, the overall PET processes in such systems become very complicated to deal with, and accordingly these processes warrant very extensive research work to derive the exact correlations for the observed PET rates with the changing exergonicity of the reactions, especially within the framework of the Marcus ET theory. In any case, from the present study it is realized that the multichannel PET is apparently the main reason for the differential behaviours observed with the different coumarin-Ln(III) systems used in the present study.

It is interesting at this point to recall the work of Inada et al.,²²² where fluorescence quenching studies were carried out in acetonitrile solution using a series of aromatic hydrocarbons as the fluorophores and Eu(III) and Yb(III) ions as the quenchers. In their study, observed $k_{q(TR)}$ values (authors designated as k_q simply) displayed a common correlation with the changing ΔG^0 values for both dye-Eu(III) and dye-Yb(III) systems, apparently indicating no abnormality for the Yb(III) ion, as other wise observed in our present study. In the study of Inada et al., authors also investigated the back electron transfer (BET) reactions for the same dye-Ln(III) systems and the observed BET kinetics were correlated to estimate different ET parameters, which were subsequently used to construct a theoretical Rehm-Weller curve and compared with the experimental $k_{q(TR)}$ vs ΔG^0 plot. It was interestingly observed that the $k_{q(TR)}$ vs ΔG^0 plot for their studied dye-Ln(III) systems is shifted quite largely towards lower exergonicity ($-\Delta G^0$) region as compared to the theoretically obtained Rehm-Weller curve and this was rationalized by the authors by invoking the exciplex mechanism for the fluorescence quenching process, which apparently made the forward ET process more proficient than the BET process in their studied systems. In our present study, the $k_{q(TR)}$ vs ΔG^0 plot for the coumarin-Yb(III) pairs are seen to appear almost in the similar region as that of the theoretical Rehm-Weller curve constructed by Inada et al. based on their BET results. Since the fluorescence quenching studies in our cases are carried out in aqueous solution, we feel that in these cases the observed fluorescence quenching for all the coumarin-Ln(III) pairs occur simply through the PET mechanism, without involving the exciplex mechanism, which was suggested by Inada et al. for their fluorescence quenching results carried out in acetonitrile solution. In our present study, however, the $k_{q(TR)}$ vs ΔG^0 plot for the coumarin-Sm(III) systems is found to be shifted quite largely towards the lower exergonicity region, quite similar to the $k_{q(TR)}$ vs ΔG^0 plot obtained by Inada et al. involving the aromatic hydrocarbon-Ln(III) systems in acetonitrile solvent. We feel that, even though the $k_{q(TR)}$ vs ΔG^0 plot for the coumarin-Sm(III) systems appears in the similar exergonicity region as that of the aromatic hydrocarbon-Ln(III) systems studied by Inada et al., in our study there could be hardly any exciplex formation because the present study is carried out in highly polar aqueous solution, where exciplex formation is suggested to be extremely unfavorable.⁴⁴³ To be mentioned in the present context that even though there are few cases of covalently coupled donor-acceptor systems where weak exciplex formations in aqueous

solution have been reported and analyzed based on the pre-existing favorable orientations of the donor and acceptor units before photoexcitation that support intramolecular exciplex formation,⁴⁴⁴ there are hardly any report on intermolecular exciplex formation in aqueous solution, at least to the best of our knowledge. Further, in the present study, even if we consider the involvement of the exciplex formation process for the coumarin-Sm(III) systems in aqueous solution for which the $k_{q(TR)}$ vs ΔG^0 plot appeared to be in the similar exergonicity region as that of the aromatic hydrocarbon-Ln(III) systems studied by Inada et al. in acetonitrile solvent, then it becomes difficult to justify why the same would not be happening for the coumarin-Yb(III) systems as well. Hence, in the present study, we propose that the largely differ propensity for the fluorescence quenching processes in the coumarin-Yb(III) and coumarin-Sm(III) systems is mainly due to the differential extent of participation of the multichannel PET involving Yb(III) and Sm(III) ions as the electron acceptors. It is also interesting in the present content to recall some other literature reports that distinctly show unusually lower $k_{q(TR)}$ values involving Yb(III) ion as the quencher as compared to those with Sm(III) ion,^{226,227} very similar to the results obtained in our present study.

Considering the correlations shown in Figure 6.11, it is found that for the coumarin-Yb(III) systems the estimated λ value is much larger (~ 2.3 eV) as compared to that (~ 1.3 eV) obtained for the coumarin-Sm(III) systems. We feel that such a large difference in the λ values observed for the the coumarin-Yb(III) and the coumarin-Sm(III) systems are due to the differential involvements of the multichannel PET in the two respective cases. It is expected that the involvement of the multichannel PET would cause a large modulation in the associated intramolecular reorganization energy (λ_i), though the solvent reorganization energy (λ_s) would essentially remain similar for all the cases, as only one electron is transferred in all the coumarin-Ln(III) systems studied and the donor and acceptor radii involved in these cases are all in the very similar range. Since the total reorganization energy λ is the sum of λ_i and λ_s ,¹⁰⁻¹² and because λ_s effectively remains unchanged in all the systems studied, it evidently suggests that there is a large increase in the λ_i value for the coumarin-Yb(III) systems as compared to the coumarin-Sm(III) systems. Since the charge distribution in the different electronic states of the Ln(III) ions would necessarily be largely different, we can anticipate that λ_i values involving different electronic states of the hydrated Ln(III) ions would also differ quite largely from one state to other. Considering the observed results in the coumarin-Yb(III) and coumarin-Sm(III) systems, we can infer that the λ_i values are in general higher for the lower electronic states of the Ln(III) ions than the higher electronic states. Consequently, for the coumarin-Yb(III) systems, since only the lowest electronic state of the Yb(III) ion participates in the PET reactions, the concerned λ_i value for these systems becomes large enough to cause the total λ to be as high as ~ 2.3 eV, as estimated from the $k_{q(TR)}$ vs ΔG^0 correlation for these systems as shown in Figure 6.11. For the coumarin-Sm(III) systems, since the second higher electronic state of the Sm(III) ion also participates in the PET reactions, it causes the associated λ_i value to be much lower than that of the coumarin-Yb(III) systems, resulting the total λ for these systems to be quite low,

only ~ 1.3 eV. Along with the λ_i value, the electronic coupling (V_{el}) parameter for the coumarin-Ln(III) systems may also be modulated quite differently for different electronic states of the Ln(III) quenchers, and this might also become partly responsible for the observed differential behavior for the the $k_{q(TR)}$ vs ΔG^0 plots as revealed for the coumarin-Yb(III) and coumarin-Sm(III) systems, especially (cf. Figure 6.11). Since we do not have any priory information on the possible λ_i and V_{el} values for different electronic states of Ln(III) ions, we are not in a position to quantify the exact roles of these ET parameters in modulating the PET rates during the involvement of the multichannel PET process in the concerned coumarin-Ln(III) systems.

6.4. Conclusion

In the present study, PET reactions between a series of coumarin donors and selected Ln(III) acceptors have been investigated in aqueous solution following both SS and TR fluorescence quenching measurements. Among different coumarin-Ln(III) pairs, only the coumarin-Eu(III), coumarin-Yb(III) and coumarin-Sm(III) systems provide favorable free energy changes (negative ΔG^0 values) for the PET reactions, and accordingly in the present study the elaborate investigations could be carried out with the above three systems only, involving Eu(III), Yb(III) and Sm(III) ions as the quenchers. In the present study, it is interestingly seen that the correlation of the estimated $k_{q(TR)}$ values with the exergonicity ($-\Delta G^0$) of the PET reactions do not display a generalized single correlation incorporating all the three coumarin-Ln(III) systems together, as otherwise reported for most other chemically related donor-acceptor systems reported in the literature,^{130,260,264,375,416,442} but exhibit distinctly different trends for different Ln(III) ions, not showing a direct correspondence with their redox characteristics. Thus, it is interestingly observed in the present study that even though the exergonicity values for different donor-acceptor systems follow the order, coumarin-Eu(III) > coumarin-Yb(III) > coumarin-Sm(III), the corresponding $k_{q(TR)}$ values surprisingly follow the unusual trend as, coumarin-Eu(III) > coumarin-Sm(III) > coumarin-Yb(III). Based on the diffusion mediated bimolecular reaction scheme, we tried to correlate the $k_{q(TR)}$ values with the ΔG^0 values of the PET reactions in different coumarin-Ln(III) systems and thereby it is found that the total reorganization energy (λ) associated for the coumarin-Yb(III) systems is unusually large (~ 2.3 eV) as compared to the coumarin-Sm(III) and coumarin-Eu(III) systems ($\lambda \sim 1.3$ eV). Observed inconsistency in the trends for the $k_{q(TR)}$ and ΔG^0 values for different coumarin-Ln(III) systems and the unseemly high λ value estimated for the coumarin-Yb(III) systems are rationalized considering the participation of multichannel PET reactions in different extents involving different Ln(III) ions. This proposition is based on the consideration that different Ln(III) ions have different sequences of low lying electronic energy states associated with them and some of these states be accessed suitably by the available exergonicity ($-\Delta G^0$) for the concerned PET reactions. It is realized that for Eu(III) and Sm(III) quenchers, more than one electronic states of these ions can be involved to

support PET reactions in the coumarin-Eu(III) and coumarin-Sm(III) systems, causing these systems to involve significantly lower λ value and thus to display substantially higher $k_{q(TR)}$ values on correlating them with the exergonicity of the reactions. With Yb(III) ion, however, only its lowest electronic state can be accessed by the available exergonicity of the PET reactions of the used coumarin-Yb(III) systems. Accordingly, the $k_{q(TR)}$ values in these cases are significantly lower in comparison to those of the coumarin-Eu(III) and coumarin-Sm(III) systems. With the same reason, the λ value is also much larger for the coumarin-Yb(III) systems ($\lambda \sim 2.3$ eV) as compared to the coumarin-Sm(III) systems ($\lambda \sim 1.3$ eV), especially, in spite of the fact that the ΔG^0 values for the former systems are more favorable (more negative) than the latter systems. It is felt from the observed results that the λ_i values associated with the lower electronic states of the hydrated Ln(III) ions are much larger than those associated with higher electronic states of these ions. The intriguing involvements of the multichannel PET reactions in different coumarin-Ln(III) systems and their effects on the observed PET kinetics and in the associated λ values are very noteworthy results from the present study. The modulations in the PET kinetics as observed in the studied coumarin-Ln(III) systems can also be expected with the other suitably chosen electron donor-Ln(III) pairs and such systems are expected to find applications in the controlled utilization of the PET reactions in different applied areas.

References

- (1) G. R. Fleming, J. L. Martin and J. Breton, *Nature*, **1988**, 333, 190.
- (2) M. R. Wasielewski, *Chem. Rev.*, **1992**, 92, 435.
- (3) J. Barber, *Chem. Soc. Rev.*, **2009**, 38, 185.
- (4) M. Gratzel, *J. Photochem. Photobiol. C*, **2003**, 4, 145.
- (5) D. Gust, T. A. Moore and A. L. Moore, *Acc. Chem. Res.*, **2009**, 42, 1890.
- (6) S. S. Isied, M. Y. Ogawa and J. F. Wisharts, *Chem. Rev.*, **1992**, 92, 381.
- (7) L. Stryer, *Biochemistry* 3 ed.; San Francisco, 1995.
- (8) J. Jortner and M. Bixon, Electron Transfer from Isolated Molecules to Biomolecules. In *Advances in Chem. Phys., Part 1 & 2*, Wiley: New York, 1999; Vol. 106, 107,
- (9) J. R. Bolton, N. Mataga and G. L. McLendon, *Electron Transfer in Inorganic, Organic and Biological Systems* American Chemical Society: Washington DC, 1991.
- (10) R. A. Marcus, *J. Chem. Phys.*, **1956**, 24, 966–978.
- (11) R. A. Marcus, *J. Chem. Phys.*, **1956**, 24, 979.
- (12) R. A. Marcus, *J. Electroanal. Chem.*, **2000**, 483, 2.
- (13) W. F. Libby, *J. Phys. Chem.*, **1952**, 56.
- (14) R. A. Marcus and N. Sutin, *Biochim. Biophys. Acta*, **1985**, 811, 265.
- (15) R. A. Marcus, *Angew. Chem. Int. Ed. Engl.*, **1993**, 32, 1111–1121.
- (16) R. A. Marcus, *Annu. Rev. Phys. Chem.*, **1964**, 15, 155–196.
- (17) R. A. Marcus, *Faraday Disc.*, **1982**, 74, 7.
- (18) H. Sumi and R. A. Marcus, *J. Chem. Phys.*, **1986**, 84, 4894.
- (19) R. A. Marcus, *J. Chem. Phys.*, **1965**, 43, 679.
- (20) P. F. Barbara, T. J. Meyer and M. A. Ratner, *J. Phys. Chem.*, **1996**, 100, 13148.
- (21) G. J. Kavarnos, Fundamental concepts of photoinduced electron transfer. In *Topics in Current Chemistry*, J. Mattay, Ed. Springer-Verlag: Berlin, 1990; Vol. 156, pp 21
- (22) K. Yoshihara, K. Tominaga and Y. Nagasawa, *Bull. Chem. Soc. Jpn.*, **1995**, 68, 696.
- (23) N. Sutin, *Acc. Chem. Res.*, **1982**, 9, 275.
- (24) P. F. Barbara, G. C. Walker and T. P. Smith, *Science*, **1992**, 256, 975.
- (25) G. R. Fleming and P. G. Wolynes, *Physics Today*, **1990**, 43, 36.
- (26) H. Heitele, *Angew. Chem. Int. Ed. Engl.*, **1993**, 32, 359.
- (27) P. F. Barbara and W. Jarzeba, *Adv. Photochem.*, **1990**, 15, 1.
- (28) M. D. Newton and N. Sutin, *Annu. Rev. Phys. Chem.*, **1984**, 35, 437.
- (29) G. J. Kavarnos, *Fundamentals of Photoinduced Electron Transfer* VCH Publishers: New York, 1993.
- (30) M. A. Fox and M. Chanon (Eds.), *Photoinduced Electron Transfer* Elsevier: Amsterdam, 1988.
- (31) H. Eyring, S. H. Lin and S. M. Lin, *Basic Chemical Kinetics* Wiley: New York, 1980.
- (32) D. G. Truhlar, W. L. Hase and J. T. Hynes, *J. Phys. Chem.*, **1983**, 87, 2664.

- (33) P. Hänggi, P. Talkner and M. Borkovec, *Rev. Mod. Phys.*, **1990**, 62, 251.
- (34) R. A. Rossi, A. B. Pierini and A. B. Peñeñory, *Chem. Rev.*, **2003**, 103, 71.
- (35) A. I. Ivanov and V. A. Mikhailova, *Russ. Chem. Rev.*, **2011**, 79, 1047.
- (36) T. Kumpulainen, B. Lang, A. Rosspeintner and E. Vauthey, *Chem. Rev.*, **2017**, 117, 10826.
- (37) H. B. Gray and J. R. Winkler, *PNAS*, **2005**, 102, 3534.
- (38) M. Kumbhakar and H. Pal, *Sci. Lett. J.*, **2015**, 4:139, 1.
- (39) D. R. Weinberg, C. J. Gagliardi, J. F. Hull, C. F. Murphy, C. A. Kent, B. C. Westlake, A. Paul, D. H. Ess, D. G. McCafferty and T. J. Meyer, *Chem. Rev.*, **2012**, 112, 4016.
- (40) K. Wynne and R. M. Hochstrasser, *Advances in chemical physics : Electron transfer – from isolated molecules to biomolecules* John Wiley & Sons: NJ, USA, 2007; Vol. 107.
- (41) L. D. Zusman, *Chem. Phys.*, **1983**, 80, 29.
- (42) A. M. Fox, *Special Issue on Electron Transfer*. Chem. Washington, DC, 1992; Vol. 92, p365.
- (43) V. Balzani, *Electron Transfer in Chemistry* Wiley-VCH Publishers Inc.: New York, 2001; Vol. I-V.
- (44) S. J. Formosinho, L. G. Arnaut and R. Fausto, *Prog. Reac. Kin.*, **1998**, 23, 1.
- (45) D. F. Calef and P. G. Wolynes, *J. Phys. Chem.*, **1983**, 87, 3387.
- (46) L. D. Zusman, *Chem. Phys.*, **1980**, 49, 295.
- (47) I. Rips and J. Jortner, *J. Chem. Phys.*, **1987**, 87, 2090.
- (48) J. Jortner and M. Bixon, *J. Chem. Phys.*, **1988**, 88, 167.
- (49) M. Bixon and J. Jortner, *Chem. Phys.*, **1993**, 176, 467.
- (50) M. D. Newton, *Chem. Rev.*, **1991**, 91, 767.
- (51) I. Rips and J. Jortner, *J. Chem. Phys.*, **1987**, 87, 6513.
- (52) L. D. Zusman, *Chem. Phys.*, **1988**, 119, 51.
- (53) M. D. Newton, *Adv. Chem. Phys.*, **1999**, 107, 303.
- (54) C. Costentin, *Chem. Rev.*, **2008**, 108, 2145.
- (55) P. Chen and T. J. Meyer, *Chem. Rev.*, **1998**, 98, 1439–1477.
- (56) R. A. Marcus, *J. Chem. Phys.*, **1957**, 26, (872–877).
- (57) J. R. Miller, J. V. Beitz and R. K. Huddleston, *J. Am. Chem. Soc.*, **1984**, 106, 5057–5068.
- (58) G. L. Closs and J. R. Miller, *Science*, **1988**, 240, 440.
- (59) J. R. Miller, L. T. Calcaterra and G. L. Closs, *J. Am. Chem. Soc.*, **1984**, 106, 3047.
- (60) W. J. Royea, A. M. Fajardo and N. S. Lewis, *J. Phys. Chem. B*, **1997**, 101, 11152.
- (61) J. Ulstrup and J. Jortner, *J. Chem. Phys.*, **1975**, 63, 4358.
- (62) F. Sanchez, M. L. Moya and M. Galan, *Prog. Reac. Kin.*, **1994**, 19, 1.
- (63) N. Mataga and H. Miyasaka, *Prog. Reac. Kin.*, **1994**, 19, 317.
- (64) J. Burgess and E. Pelizzetti, *Prog. Reac. Kin.*, **1992**, 17, 1.
- (65) R. D. J. Miller, G. L. McLendon, A. J. Nozik, W. Schmickler and F. Willig, *Surface Electron Transfer Processes*, VCH Publishers, Inc.: New York, 1995.
- (66) A. Heller, *Acc. Chem. Res.*, **1981**, 14, 154.
- (67) M. Gratzel, *Coord. Chem. Rev.*, **1991**, 111, 167.
- (68) N. Serpone and E. Pelizzetti, *Photocatalysis: Fundamentals and Applications* Wiley: New York, 1989.

- (69) P. V. Kamat and D. Meisel, *Semiconductor Nanoclusters: Physical, Chemical and Catalytic Aspects* Elsevier: Amsterdam, 1997.
- (70) H. Weller, A. Eychmuller and P. V. Kamat, *Semiconductor Nanoclusters-Studies in Surface Science and Catalysis* Elsevier Science: 1996; Vol. 103, p 5.
- (71) D. F. Ollis, E. Pelizzetti and N. Serpone, *Environ. Sci. Technol.*, **1991**, 25, 1523.
- (72) G. J. Kavarnos and N. J. Turro, *Chem. Rev.*, **1986**, 86, 401.
- (73) J. N. Onuchic, *J. Chem. Phys.*, **1987**, 86, 3925.
- (74) I. Rips and J. Jortner, *J. Chem. Phys.*, **1988**, 88, 818.
- (75) M. Bixon, J. Jortner, J. Cortes, H. Heitele and M. E. Michel-Beyerle, *J. Phys. Chem.*, **1994**, 98, 7289.
- (76) D. DeVault, *Quantum Mechanical Tunneling in Biological Systems* Cambridge University Press: 1984.
- (77) J. T. Hynes, *J. Phys. Chem.*, **1986**, 90, 3701.
- (78) K. F. Freed, *Acc. Chem. Res.*, **1975**, 11, 74.
- (79) K. F. Freed and J. Jortner, *J. Chem. Phys.*, **1970**, 52, 6272.
- (80) K. V. Mikkelsen and M. A. Ratner, *Chem. Rev.*, **1987**, 87, 113.
- (81) R. R. Dogonadze, A. M. Kuznetsov, M. A. Vorotyntsev and M. G. Zakaraya, *J. Electroanal. Chem.*, **1977**, 75, 315.
- (82) N. Liang, G. L. Closs and J. R. Miller, *J. Am. Chem. Soc.*, **1990**, 212, 5353.
- (83) N. Sutin, *Prog. Inorg. Chem.*, **1983**, 30, 441.
- (84) J. Ulstrup, *Charge Transfer Processes in Condensed Media* Springer-Verlag: Berlin, 1979.
- (85) M. Bixon and J. Jortner, *Adv Chem. Phys.*, **1999**, 106, 35.
- (86) M. Bixon and J. Jortner, *J. Phys. Chem.*, **1988**, 92, 7148.
- (87) L. D. Landau and E. M. Lifshitz, *Quantum Mechanics* Pergamon: London, 1958.
- (88) H. Kandori, K. Kemnitz and K. Yoshihara, *J. Phys. Chem.*, **1992**, 96, 8042.
- (89) Y. Nagasawa, A. P. Yartsev, K. Tominaga, A. E. Johnson and K. Yoshihara, *J. Am. Chem. Soc.*, **1993**, 115, 7922.
- (90) Y. Nagasawa, A. P. Yartsev, K. Tominaga, A. E. Johnson and K. Yoshihara, *J. Chem. Phys.*, **1994**, 101, 5717.
- (91) Y. Nagasawa, A. P. Yartsev, K. Tominaga, P. B. Bisht, A. E. Johnson and K. Yoshihara, *J. Phys. Chem.*, **1995**, 99, 653.
- (92) H. Pal, H. Shirota, K. Tominaga and K. Yoshihara, *J. Chem. Phys.*, **1999**, 110, 11454.
- (93) H. Shirota, H. Pal, K. Tominaga and K. Yoshihara, *Chem. Phys.*, **1998**, 236, 355.
- (94) H. Shirota, H. Pal, K. Tominaga and K. Yoshihara, *J. Phys. Chem. A*, **1998**, 102, 3089.
- (95) H. Pal, Y. Nagasawa, K. Tominaga and K. Yoshihara, *J. Phys. Chem.*, **1996**, 100, 11964.
- (96) P. K. Singh, S. Nath, A. C. Bhasikuttan, M. Kumbhakar, J. Mohanty, S. K. Sarkar, T. Mukherjee and H. Pal, *J. Chem. Phys.*, **2008**, 129, 114504.
- (97) C. Wang, B. Akhremitchev and G. C. Walker, *J. Phys. Chem. A* **1997**, 101, 2735.
- (98) M. Kumbhakar and H. Pal, *J. Phys. Chem. B*, **2016**, 120, 9804–9809.
- (99) W. Nadler and R. A. Marcus, *J. Chem. Phys.*, **1987**, 86, 3906.
- (100) A. M. Kuznetsov and J. Ulstrup, *Electron Transfer in Chemistry and Biology: An Introduction to the Theory* Wiley: New York, 1998.

- (101) S. Dadashi-Silab, S. Doran and Y. Yagci, *Chem. Rev.*, **2016**, *116*, 10212.
- (102) B. M. Rosen and V. Percec, *Chem. Rev.*, **2009**, *109*, 5069.
- (103) A. Ito and T. J. Meyer, *Phys. Chem. Chem. Phys.*, **2012**, *14*, 13731.
- (104) C. J. Gagliardi, B. C. Westlake, C. A. Kent, J. J. Paul, J. M. Papanikolas and T. J. Meyer, *Coord. Chem. Rev.*, **2010**, *254*, 2459.
- (105) S. Doose, H. Neuweiler and M. Sauer, *Chem. Phys. Chem.*, **2009**, *10*, 1389.
- (106) R. A. Marcus, *Rev. Mod. Phys.*, **1993**, *65*, 599.
- (107) J. Zhu and J. C. Rasaiah, *J. Chem. Phys.*, **1991**, *95*, 3325.
- (108) J. Zhu and J. C. Rasaiah, *J. Chem. Phys.*, **1992**, *96*, 1435.
- (109) J. Zhu and J. C. Rasaiah, *J. Chem. Phys.*, **1993**, *98*, 1213.
- (110) J. Zhu and J. C. Rasaiah, *J. Chem. Phys.*, **1994**, *101*, 9966.
- (111) S. Lee and J. T. Hynes, *J. Chem. Phys.*, **1988**, *88*, 6853.
- (112) S. D. Choudhury, M. Kumbhakar, S. Nath and H. Pal, *J. Chem. Phys.*, **2007**, *127*, 194901.
- (113) M. Tachiya, Y. Tabata and K. Ohshima, *J. Phys. Chem.*, **1973**, *77*, 263.
- (114) M. Tachiya, *J. Phys. Chem.*, **1993**, *97*, 5911.
- (115) M. Tachiya, *J. Chem. Phys.*, **2008**, *129*, 066102.
- (116) M. Kumbhakar, A. Manna, M. Sayed, A. Kumar and H. Pal, *J. Phys. Chem. B*, **2014**, *118*, 10704–10715.
- (117) M. Kumbhakar, S. Nath, T. Mukherjee and H. Pal, *J. Indian Chem. Soc.*, **2010**, *87*, 173.
- (118) M. Kumbhakar, S. Dey, P. K. Singh, S. Nath, A. K. Satpati, R. Gangully, V. K. Aswal and H. Pal, *J. Phys. Chem. B*, **2011**, *115*, 1638.
- (119) A. K. Satpati, M. Kumbhakar, S. Nath and H. Pal, *J. Phys. Chem. B*, **2007**, *111*, 7550.
- (120) M. Kumbhakar, S. Nath, T. Mukherjee and H. Pal, *J. Chem. Phys.*, **2005**, *122*, 084512.
- (121) M. Kumbhakar, P. K. Singh, S. Nath, A. C. Bhasikuttan and H. Pal, *J. Phys. Chem. B*, **2008**, *112*, 6646.
- (122) M. Kumbhakar, P. K. Singh, A. K. Satpati, S. Nath and H. Pal, *J. Phys. Chem. B*, **2010**, *114*, 10057.
- (123) S. D. Choudhury, M. Kumbhakar, S. Nath, S. K. Sarkar, T. Mukherjee and H. Pal, *J. Phys. Chem. B*, **2007**, *111*, 8842.
- (124) M. Kumbhakar, S. Nath, H. Pal, A. V. Sapre and T. Mukherjee, *J. Chem. Phys.*, **2003**, *119*, 388.
- (125) M. Kumbhakar, S. Nath, T. Mukherjee and H. Pal, *J. Chem. Phys.*, **2004**, *120*, 2824.
- (126) M. Kumbhakar, T. Mukherjee and H. Pal, *Chem. Phys. Lett.*, **2005**, *410*, 94.
- (127) M. Kumbhakar, S. Nath, T. Mukherjee and H. Pal, *J. Chem. Phys.*, **2005**, *123*, 034705(1).
- (128) M. Kumbhakar, S. Nath, T. Mukherjee and H. Pal, *J. Photochem. Photobiol. A*, **2006**, *182*, 7.
- (129) P. Verma, S. Nath, P. K. Singh, M. Kumbhakar and H. Pal, *J. Phys. Chem. B*, **2008**, *112*, 6363.
- (130) D. Rehm and A. Weller, *Israel J. Chem.*, **1970**, *8*, 259.
- (131) M. Maroncelli, *J. Mol. Liq.*, **1993**, *57*, 1.
- (132) M. Maroncelli, J. MacInnis and G. R. Fleming, *Science*, **1989**, *243*, 1674.
- (133) M. Maroncelli and G. R. Fleming, *J. Chem. Phys.*, **1987**, *86*, 6221.
- (134) R. S. Fee and M. Maroncelli, *Chem. Phys.*, **1994**, *183*, 235.
- (135) R. S. Fee, J. A. Milsom and M. Maroncelli, *J. Phys. Chem.*, **1991**, *95*, 5170.

- (136) J. E. W. Castner, G. R. Fleming, B. Bagchi and M. Maroncelli, *J. Chem. Phys.*, **1988**, 89, 3519.
- (137) K. Bhattacharyya and B. Bagchi, *J. Phys. Chem. A*, **2000**, 104, 10603.
- (138) N. Sarkar, A. Datta, S. Das and K. Bhattacharyya, *J. Phys. Chem.*, **1996**, 100, 15483.
- (139) N. Nandi, K. Bhattacharyya and B. Bagchi, *Chem. Rev.*, **2000**, 100, 2013.
- (140) K. Hara, H. Kuwabara and O. Kajimoto, *J. Phys. Chem. A*, **2001**, 105, 7174.
- (141) P. Sen, S. Mukherjee, A. Halder and K. Bhattacharyya, *Chem. Phys. Lett.*, **2004**, 385, 357.
- (142) A. Datta, D. Mandal, S. K. Pal and K. Bhattacharyya, *J. Mol. Liq.*, **1998**, 77, 121.
- (143) A. Datta, S. K. Pal, D. Mandal and K. Bhattacharyya, *J. Phys. Chem. B*, **1998**, 102, 6114.
- (144) S. Vajda, R. Jimenez, S. J. Rosenthal, V. Fidler, G. R. Fleming and J. E. W. Castner, *J. Chem. Soc. Faraday Trans.*, **1995**, 91, 867.
- (145) D. M. Willard, R. E. Riter and N. E. Levinger, *J. Am. Chem. Soc.*, **1998**, 120, 4151.
- (146) R. E. Riter, E. P. Undiks and N. E. Levinger, *J. Am. Chem. Soc.*, **1998**, 120, 2705.
- (147) H. Shirota and K. Horie, *J. Phys. Chem. B*, **1999**, 103, 1437.
- (148) J. R. Lakowicz, *Principle of Fluorescence Spectroscopy* 3rd ed.; Springer: New York, 2006.
- (149) B. Verity and S. W. Bigger, *Int. J. Chem. Kinet.*, **1996**, 28(12), 919.
- (150) I. R. Schmolka, *J. Am. Oil Chem. Soc.*, **1977**, 54, 110.
- (151) J. Gonzalez-Lopez, C. Alvarez-Lorenzo, P. Taboada, A. Sosnik, I. Sandez-Macho and A. Concheiro, *Langmuir*, **2008**, 24, 10688.
- (152) T. Liu, G. Xu, H. Gong, J. Pang and F. He, *Langmuir*, **2011**, 27, 9253.
- (153) K. Mortensen and M. Annaka, *ACS MacroLett.*, **2016**, 5, 224.
- (154) J. Aguiar, P. C. J. Molina-Bolivar and C. C. Ruiz, *J. Colloid Interface Sci.*, **2003**, 258, 116.
- (155) D. Schmaljohann, *Adv. Drug Deliv. Rev.*, **2006**, 58, 1655.
- (156) C. Alvarez-Lorenzo, J. Gonzalez-Lopez, M. Fernandez-Tarrio, I. Sandez-Macho and A. Concheiro, *Eur. J. Pharm. Biopharm.*, **2007**, 66, 244.
- (157) J. K. Armstrong, B. Z. Chowdhry, M. J. Snowden, J. Dong and S. A. Leharne, *Int. J. Pharm.*, **2001**, 229, 57.
- (158) Y. Kadam, K. Singh, D. G. Marangoni, J. H. Mac, V. K. Aswal and P. Bahadur, *J. Colloid Interface Sci.*, **2010**, 351, 449.
- (159) A. V. Parmar, A. Bahadur, K. Kuperkar and P. Bahadur, *Eur. Polym. J.*, **2013**, 49, 12.
- (160) V. Singh, P. Khullar, P. N. Dave, A. Kaura, M. S. Bakshi and G. Kaur, *Phys. Chem. Chem. Phys.*, **2014**, 16, 4728.
- (161) P. Samanta, P. Halder, P. Bahadur, S. D. Choudhury and H. Pal, *J. Phys. Chem. B*, **2018**, 122, 10190–10201.
- (162) S. A. Pillai, B. Bharatiya, M. Casas, E. V. Lage, I. Sandez-Macho, H. Pal and P. Bahadur, *Colloid. Surf. B*, **2016**, 148, 411.
- (163) C. L. Zhao, M. A. Winnik, G. Riess and M. D. Croucher, *Langmuir*, **1990**, 6, 514.
- (164) E. Goddard, N. Turro, P. Kuo and K. Ananthapadmanabhan, *Langmuir*, **1985**, 1, 352.
- (165) M. Wilhelm, C. L. Zhao, Y. Wang, R. Xu, M. A. Winnik, J. L. Mura, G. Riess and M. D. Croucher, *Macromolecules*, **1991**, 24, 1033.
- (166) S. A. Pillai, C.-F. Lee, D. Ray, V. K. Aswal, H. Pal, L.-J. Chen and P. Bahadur, *RSC Adv.*, **2016**, 6, 87299.

- (167) S. A. Pillai, *Colloids Surf. A* **2016**, 506, 234.
- (168) M. Kumbhakar, T. Goel, T. Mukherjee and H. Pal, *J. Phys. Chem. B.*, **2005**, 109, 14168.
- (169) G. B. Dutt, *J. Phys. Chem. B*, **2002**, 106, 7398.
- (170) K. Streletsky and G. D. J. Phillies, *Langmuir*, **1995**, 11, 42.
- (171) J. H. Fendler, *Membrane Mimetic Chemistry* Wiley: New York, 1982.
- (172) R. Nagarajan, *Langmuir*, **2002**, 18, 31.
- (173) P. Atkins and J. D. Paula, *Atkins' Physical Chemistry* 8 ed.; Oxford University Press: Oxford, 2006.
- (174) S. A. Pillai, C.-F. Lee, D. Ray, V. K. Aswal, M.-R. Wang, L.-J. Chen and P. Bahadur, *J. Mol. Liq.*, **2018**, 252.
- (175) K. Mortensen, W. Brown and B. Norden, *Phys. Rev. Letts.*, **1992**, 68, 2340.
- (176) R. A. Ganguly, V. K.; Hassan, P. A.; Gopalakrishnan, I. K.; Kulshreshtha, S. K. , *J. Phys. Chem. B*, **2006**, 110, 9843–9849.
- (177) R. Ganguly, V. K. Aswal, P. A. Hassan, I. K. Gopalakrishnan and J. V. Yakhmi, *J. Phys. Chem. B*, **2005**, 109, 5653.
- (178) K. Mortensen and W. Brown, *Macromolecules*, **1993**, 26, 4128.
- (179) J. Jansson, K. Schillen, M. Nilsson, O. Soderman, G. Fritz, A. Bergmann and O. Glatter, *J. Phys. Chem. B*, **2005**, 109, 7073–7083.
- (180) Z. Zhou and B. J. Chu, *Colloid Interface Sci.*, **1988**, 126, 171.
- (181) G. Wanka, H. Hoffmann and W. Ulbricht, *Macromolecules*, **1994**, 27, 4145.
- (182) J. R. Lopes and W. Loh, *Langmuir*, **1998**, 14, 750.
- (183) P. Alexandridis, J. F. Holzwarth and T. A. Hatton, *Macromolecules*, **1994**, 27, 2414.
- (184) P. Alexandridis, T. Nivaggioli and T. A. Hatton, *Langmuir*, **1995**, 11, 1468.
- (185) K. Nakashima, T. Anzai and Y. Fujimoto, *Langmuir*, **1994**, 10, 658.
- (186) G. S. Hartley, *Q. Rev. Chem. Soc.*, **1948**, 2, 152.
- (187) K. Kalyansundaram, *Photochemistry in Microheterogeneous Systems* Academic Press: Orlando, 1987.
- (188) S. A. Pillai, *Colloids Surf. A*, **2016**, 506, 576.
- (189) J. Bhattacharjee, G. Verma, V. K. Aswal, V. Patravalec and P. A. Hassan, *RSC Adv.*, **2013**, 3, 23080.
- (190) A. Parmar, S. Chavda and P. Bahadur, *Colloids Surf. A*, **2014**, 441, 389.
- (191) N. V. Sastry and H. Hoffmann, *Colloid Surf. A*, **2004**, 250, 247.
- (192) K. C. Tama and E. Wyn-Jonesb, *Chem. Soc. Rev.* , **2006**, 35, 693.
- (193) N. Kaltsoyannis and P. Scott, *The elements* Oxford Chemistry Primers, Oxford Science Publications: Oxford, 1999.
- (194) S. Cotton, *Lanthanides and actinides* McMillan Physical Science Series, McMillan Education: London, 1991.
- (195) P. Atkins, T. Overton, J. Rourke, M. weller and F. Armstrong, *Shriver & Atkins' Inorganic Chemistry* 5 ed.; Oxford University Press: Oxford, 2010.
- (196) J.-C. G. Bünzli and C. Piguet, *Chem. Soc. Rev.*, **2005**, 34, 1048.
- (197) P. Verma and H. Pal, *Phys. Chem. Chem. Phys.*, **2015**, 17, 23214.
- (198) S. Faulkner, S. J. A. Pope and B. P. Burton-Pye, *Appl. Spectrosc. Rev.*, **2005**, 40, 1.

- (199) T. Terai, K. Kikuchi, S.-Y. Iwasawa, T. Kawabe, Y. Hirata, Y. Urano and T. Nagano, *J. Am. Chem. Soc.*, **2006**, *128*, 6938.
- (200) V. W. W. Yam and K. K. W. Lo, *Coord. Chem. Rev.*, **1999**, *184*, 157.
- (201) W. D. Horrocks Jr, *Coord. Chem. Rev.*, **1999**, *185–186*, 307.
- (202) N. Hildebrandt, K. D. Wegner and W. R. Algar, *Coord. Chem. Rev.*, **2014**, *273–274*, 125.
- (203) W. R. Kirk, W. S. Wessels and F. G. Prendergast, *J. Phys. Chem.*, **1993**, *97*, 10326.
- (204) T. Lazarides, M. A. H. Alamiry, H. Adams, S. J. A. Pope, S. Faulkner, J. A. Weinstein and M. D. Ward, *Dalton Trans*, **2007**, 1484–1491.
- (205) M. R. Kesama, S. R. Dugasani, S. Yoo, P. Chopade, B. Gnapareddy and S. H. Park, *ACS Appl. Mater. Interfaces*, **2016**, *8*, 22, 14109–14117.
- (206) Z. Ahmed and K. Iftikhar, *RSC Adv.*, **2014**, *4*, 63696.
- (207) X. Chen, T. Sun and F. Wang, *Chem. Asian J.*, **2019**, *15*, 21.
- (208) M. Roger, M. Regueiro-Figueroa, C. B. Azzeddine, V. Patinec, C. S. Bonnet, C. Platas-Iglesias and R. Tripier, *Eur. J. Inorg. Chem.*, **2014**, *2014*, 1072.
- (209) T. Gunnlaugsson, M. Glynn, G. M. Tocci, P. E. Kruger and F. M. Pfeffer, *Coord. Chem. Rev.*, **2006**, *250*, 3094.
- (210) H. Tan, B. Liu and Y. Chen, *ACS Nano*, **2012**, *6*, 10505.
- (211) P. Samanta, S. D. Choudhury and H. Pal, *J. Photochem. Photobiol. A*, **2020**, *401*, 112774.
- (212) M. C. Chuan, G. Y. Shu and J. C. Liu, *Water, Air, Soil Pollut.*, **1996**, *91*, 543.
- (213) J. F. McCarthy, W. E. Sanford and P. L. Stafford, *Environ. Sci. Technol.*, **1998**, *32*, 3901.
- (214) C. N. Mulligan, R. N. Yong and B. F. Gibbs, *Eng. Geol.*, **2001**, *60*, 193.
- (215) D. A. e. Atwood, *Radionuclides in the Environment* John Wiley & Sons: 2010.
- (216) C. Poinssot and H. Geckeis, *Radionuclide Behaviour in the Natural Environment: Science, Implications and Lessons for the Nuclear Industry* Woodhead Publishing: Cambridge, 2012.
- (217) J.-C. G. Bünzli, Rare Earth Luminescent Centers in Organic and Biochemical Compounds. In *Spectroscopic Properties of Rare Earths in Optical Materials*, G. K. Liu and B. Jacquier, Eds. Springer Verlag: Berlin, 2005; Vol. 83, p 462–499
- (218) S. Faulkner and J. L. Matthews, Fluorescent Complexes for Biomedical Applications. In *Comprehensive Coordination Chemistry II*, M. D. Ward, Ed. Elsevier: Amsterdam, 2004; Vol. 9, pp 913
- (219) K. Matsumoto and J. G. Yuan, Lanthanide Chelates as Fluorescent Labels for Diagnostics and Biotechnology. In *Metal Ions in Biological Systems*, A. Sigel and H. Sigel, Eds. CRC Press, Marcel Dekker Inc.: New York, 2003; Vol. 40, pp 191
- (220) A. J. Amoroso and S. J. A. Pope, *Chem. Soc. Rev.*, **2015**, *44*, 4723.
- (221) M. V. DaCosta, S. Doughan, Y. Han and U. J. Krull, *Anal. Chim. Acta*, **2014**, *832*, 1.
- (222) T. Inada, Y. Funasaka, K. Kikuchi, Y. Takahashi and H. Ikeda, *J. Phys. Chem. A*, **2006**, *110*, 2595.
- (223) F. Kielar, C. P. Montgomery, E. J. New, D. Parker, R. A. Poole, S. L. Richardson and P. A. Stenson, *Org. Biomol. Chem.*, **2007**, *5*, 2975.
- (224) D. Sykes, A. J. Cankut, N. M. Ali, A. Stephenson, S. J. P. Spall, S. C. Parker, J. A. Weinstein and M. D. Ward, *Dalton Trans.*, **2014**, *43*, 6414.
- (225) N. Sabbatini, S. Perathoner, G. Lattanzi, S. Dellonte and V. Balzani, *Inorg. Chem.*, **1988**, *27*, 1628.

- (226) Y. Tendler and M. Faraggi, *J. Chem. Phys.*, **1972**, 57, 1358.
- (227) Y. Nosaka, A. Kira and M. Imamura, *J. Phys. Chem.*, **1981**, 85, 1353.
- (228) G. E. Buono-Core, H. Li and B. Marciniak, *Coord. Chem. Rev.*, **1990**, 99, 55–87.
- (229) F. Martelli, S. Abadie, J.-P. Simonin, R. Vuilleumier and R. Spezia, *Pure Appl. Chem.*, **2013**, 85, 237.
- (230) L. R. Morss, *Chem. Rev.*, **1976**, 76, 827.
- (231) L. J. Nugent, R. D. Baybarz, J. L. Burnett and J. L. Ryan, *J. Phys. Chem.*, **1973**, 77, 1528.
- (232) W. J. Evans, *Coord. Chem. Rev.*, **2000**, 206–207, 263.
- (233) S. Maity and E. Prasad, *J. Photochem. Photobiol. A*, **2014**, 274, 64.
- (234) N. Sabbatini, M. T. Endelli, M. T. Gandolfi and V. Balzani, *J. Phys. Chem.*, **1982**, 86, 3585–3591.
- (235) M. Kumbhakar, T. Goel, S. Nath, T. Mukherjee and H. Pal, *J. Phys. Chem. B*, **2006**, 110, 25646.
- (236) H. Pal, *J. Indian Chem. Soc.*, **2017**, 97, 1311.
- (237) C. D. Clark and M. Z. Hoffmann, *Coord. Chem. Rev.*, **1997**, 159, 359.
- (238) A. A. Alkaitis, G. Beck and M. Gratzel, *J. Am. Chem. Soc.*, **1975**, 97, 5723.
- (239) M. A. J. Rodgers and J. C. Becker, *J. Phys. Chem.*, **1980**, 73, 5493.
- (240) A. V. Berzykin and M. Tachiya, *Heterogeneous Chem. Rev.*, **1996**, 3, 105.
- (241) M. Almgren, *Adv. Colloid Interface Sci.*, **1992**, 41, 9.
- (242) C. A. Bunton and G. Cerichelli, *Int. J. Chem. Kinet.*, **1980**, 12, 519.
- (243) S. K. Pal, D. Mandal, D. Sukul and K. Bhattacharyya, *Chem. Phys.*, **1999**, 249, 63.
- (244) E. J. C. Olson, D. Hu, A. Hormann, A. M. Jonkman, M. R. Arkin, E. D. A. Stemp, J. K. Barton and P. F. Barbara, *J. Am. Chem. Soc.*, **1997**, 119, 11458.
- (245) A. Bernas, D. Grand, S. Hauteclouque and C. Gianotti, *J. Phys. Chem.*, **1986**, 90, 6189.
- (246) D. Grand and S. Hauteclouque, *J. Phys. Chem.*, **1990**, 94, 837.
- (247) A. J. Frank, M. Gratzel and J. J. Kozak, *J. Am. Chem. Soc.*, **1976**, 98, 3317.
- (248) M. Gratzel, J. J. Kozak and J. K. Thomas, *J. Chem. Phys.*, **1975**, 62, 1632.
- (249) D. J. W. Barber, D. A. N. Morris and J. K. Thomas, *Chem. Phys. Lett.*, **1976**, 37, 481.
- (250) L. K. Patterson and M. Gratzel, *J. Am. Chem. Soc.*, **1975**, 79, 956.
- (251) P. Chen, R. Duesing, G. Tapolsky and T. J. Mayer, *J. Am. Chem. Soc.*, **1989**, 111, 8305.
- (252) P. Chen, R. Duesing, D. K. Graff and T. J. Mayer, *J. Phys. Chem.*, **1991**, 95, 5850.
- (253) N. E. Katz, S. L. Mecklenburg, D. K. Graff, P. Chen and T. J. Mayer, *J. Phys. Chem.*, **1994**, 98, 8959.
- (254) N. E. Katz, S. L. Mecklenburg and T. J. Mayer, *Inorg. Chem.*, **1995**, 34, 1282.
- (255) E. H. Yonemoto, R. L. Reley, Y. I. Kim, J. R. Atherton, S. H. Schmehl and T. E. Mallouk, *J. Am. Chem. Soc.*, **1992**, 114, 8081.
- (256) E. H. Yonemoto, G. B. Saupe, R. H. Schmehl, S. M. Hubig, R. L. Reley, B. L. Iverson and T. E. Mallouk, *J. Am. Chem. Soc.*, **1994**, 116, 4786.
- (257) M. R. Wasielewski, N. P. Niemczyk, W. A. Svec and E. B. Pewitt, *J. Am. Chem. Soc.*, **1985**, 107, 1080–1082.
- (258) S. L. Larson, L. F. Cooley, C. M. Elliott and D. F. Kelley, *J. Am. Chem. Soc.*, **1992**, 114, 9504.
- (259) L. S. Fox, M. Kozik, J. R. Winkler and H. B. Gray, *Science*, **1990**, 47, 1069.
- (260) I. R. Gould and S. Farid, *Acc. Chem. Res.*, **1996**, 29, 522–528.

- (261) H. Segawa, C. Takehara, K. Honda, T. Shimidzu, T. Asahi and N. Mataga, *J. Phys. Chem.*, **1992**, 96, 503.
- (262) J. S. Zhou and M. A. J. Rodgers, *J. Am. Chem. Soc.*, **1991**, 113, 7728.
- (263) C. Zou, J. B. Miers, R. M. Ballew, D. D. Dlott and G. B. Schuster, *J. Am. Chem. Soc.*, **1991**, 113, 7823.
- (264) C. Turró, J. M. Zaleski, Y. M. Karabatsos and D. G. Nocera, *J. Am. Chem. Soc.*, **1996**, 118, 6060.
- (265) K. Ishiguro, T. Nakano, H. Shibata and Y. Sawaki, *J. Am. Chem. Soc.*, **1996**, 118, 7225.
- (266) P. Thanasekaran, T. Rajendran, S. Rajagopal, C. Srinivasan, R. Ramaraj, P. Ramamurthy and B. Venkatachalapathy, *J. Phys. Chem. A*, **1997**, 101, 8195.
- (267) C. Li and M. Z. Hoffman, *J. Phys. Chem. A*, **1998**, 102, 6052.
- (268) S. Fukuzumi, Y. Yoshida, T. Umano, T. Suenobu and H. Imahori, *J. Am. Chem. Soc.*, **2001**, 123, 11331.
- (269) S. Fukuzumi, M. Nishimine, K. Ohkubo, N. V. Tkachenko and H. Lemmetyinen, *J. Phys. Chem. B*, **2003**, 107, 12511.
- (270) E. Prasad and K. R. Gopidas, *J. Am. Chem. Soc.*, **2000**, 122, 3191.
- (271) D. M. Guldi and K.-D. Asmus, *J. Am. Chem. Soc.*, **1997**, 119, 5744.
- (272) S. Fukuzumi, K. Ohkubo, H. Imahori and D. M. Guldi, *Chem. Eur. J.*, **2003**, 9, 1585.
- (273) M. Tachiya and S. Murata, *J. Phys. Chem.*, **1992**, 96, 8441.
- (274) E. L. Quitevis, A. H. Marcus and M. D. Fayer, *J. Phys. Chem.*, **1993**, 97, 5762.
- (275) N. C. Maiti, M. M. G. Krishna, P. J. Britto and N. Periasamy, *J. Phys. Chem. B*, **1997**, 101, 11051.
- (276) G. B. Dutt, *J. Phys. Chem. B*, **2003**, 107, 10546.
- (277) G. B. Dutt, *J. Phys. Chem. B*, **2003**, 107, 3131.
- (278) I. D. Charlton and A. P. Doherty, *J. Phys. Chem. B*, **2000**, 104, 8327.
- (279) J. A. Molina-Bolivar, J. Aguiar and C. C. Ruiz, *J. Phys. Chem. B*, **2002**, 106, 870.
- (280) J. E. Yambert and J. D. Philies, *Langmuir*, **1996**, 12, 3431.
- (281) J. D. Philies, R. H. Hunt, K. Strang and N. Sushkin, *Langmuir*, **1995**, 11, 3408.
- (282) K. Streletzky and J. D. Philies, *Langmuir*, **1995**, 11, 42.
- (283) N. Nandi, K. Bhattacharyya and B. Bagchi, *Chem. Rev.*, **2000**, 100, 2013.
- (284) J. B. Birks, *Photo Physics of Aromatic Molecules* Wiley-Interscience: New York, 1970.
- (285) A. Gilbert, J. Baggott and P. J. Wagner, *Essential of Molecular Photochemistry* Blackwell science Inc.: Cambridge, USA, 1991.
- (286) J. R. Lackowicz, *Principles of fluorescence spectroscopy* 3rd ed.; Springer: New York, 2006.
- (287) K. K. Rohatgi-Mukherjee, *Fundamentals of Photochemistry* Wiley Eastern Ltd: India, 1986.
- (288) R. A. Velapoldi and K. D. Mielenz, *Standard Reference Materials: A fluorescence standard reference material: Quinine sulfate dihydrate*, **1980**, Nat. Bur. Stand. (US) Spec. Publ. 260.
- (289) W. Becker, *Advanced time correlated single photon counting technique* Springer: New York, 2005.
- (290) J. N. Demas, *Excited state lifetime measurement* Academic press: New York, 1983.
- (291) D. V. O'Connor and D. Phillips, *Time Correlatated Single Photon Counting* Academic: New York, 1984.
- (292) W. R. Ware, *Creation and detection of the Excited State*. In A. A. Lamola, Ed. Marcel Dekker: New York, 1971; Vol. 1, Part A. ,

- (293) P. R. Bevington, *Data Reduction and Error Analysis for the Physical Sciences* McGraw-Hill: New York, 1969.
- (294) D. A. Gedcke and W. J. McDonald, *Nucl. Instrum. Meth.*, **1967**, 55, 377.
- (295) D. A. Gedcke and W. J. McDonald, *Nucl. Instrum. Meth.*, **1968**, 58, 253.
- (296) G. R. Haugen, B. W. Wallin and J. E. Lytle, *Rev. Sci. Instrum.*, **1972**, 50, 64.
- (297) J. Yguerabide, *Meth. Enzymol.*, **1972**, 26, 498.
- (298) A. E. McKinnon, A. G. Szabo and D. R. Miller, *J. Phys. Chem.*, **1977**, 81, 1564.
- (299) D. V. O'Connor, W. R. Ware and J. C. Andre, *J. Phys. Chem.*, **1979**, 83, 1333.
- (300) W. R. Ware, L. J. Doemeny and T. L. Nemzek, *J. Phys. Chem.*, **1973**, 77, 2083.
- (301) D. Bebelaar, *Rev. Sci. Instrum.*, **1986**, 57, 1116.
- (302) M. A. Duguay, *Progress in Optics* Amsterdam, Netherlands, 1976; Vol. XIV.
- (303) M. A. Duguay and J. M. Hansen, *Opt. Commun.*, **1969**, 1, 254.
- (304) M. A. Kahlow, W. Jarzeba, T. P. DuBruil and P. F. Barbara, *Rev. Sci. Instrum.*, **1988**, 59, 1098.
- (305) H. Mahr and M. D. Hirsch, *Opt. Commun.*, **1975**, 13, 96.
- (306) J. Shah, *IEEE J. Quant. Elect.*, **1988**, 24, 276.
- (307) P. K. Singh, M. Kumbhakar, H. Pal and S. Nath, *J. Phys. Chem. B*, **2009**, 113, 1353.
- (308) D. Bebelaar, *Rev. Sci. Instrum.*, **1986**, 57.
- (309) T. C. Kippeny, M. J. Bowers II, A. D. Dukes III, J. R. McBride, R. L. Orndorff, M. D. Garrett and S. J. Rosenthal, *J. Chem. Phys.*, **2008**, 128, 084713/1.
- (310) D. F. Underwood, T. Kippeny and S. J. Rosenthal, *J. Phys. Chem. B*, **2001**, 105, 436.
- (311) M. Ito, H. Kume and K. Oba, *IEEE Trans. Nucl. Sci.*, **1984**, NS-31, 408.
- (312) P. K. Singh, M. Kumbhakar, R. Ganguly, V. K. Aswal, H. Pal and S. Nath, *J. Phys. Chem. B*, **2010**, 114, 3818.
- (313) P. K. Singh, M. Kumbhakar, H. Pal and S. Nath, *J. Phys. Chem. B*, **2008**, 112, 7771.
- (314) P. K. Singh, M. Kumbhakar, H. Pal and S. Nath, *J. Phys. Chem. B*, **2009**, 113, 1353.
- (315) P. K. Singh, A. K. Satpati, M. Kumbhakar, H. Pal and S. Nath, *J. Phys. Chem. B*, **2008**, 112, 11447.
- (316) R. G. W. Norrish and G. Porter, *Nature*, **1949**, 164, 658.
- (317) G. Porter, *Proc. Roy. Soc.*, **1950**, A200, 284.
- (318) R. J. Hunter, *Zeta potential in colloid science: principles and applications* Academic Press: London, UK, 1988.
- (319) A. N. Singh, R. D. Thakre, J. C. More, P. K. Sharma and Y. K. Agrawal, *Polym. Plast. Technol. Eng.*, **2015**, 54, 1077.
- (320) H. Feng, X. Lu, W. Wang, N.-G. Kang and J. W. Mays, *Polymers*, **2017**, 9, 494(1).
- (321) Y. Mai and A. Eisenberg, *Chem. Soc. Rev.*, **2012**, 41, 5969.
- (322) P. P. Ghoroghchian, G. Li, D. H. Levine, K. P. Davis, F. S. Bates, D. A. Hammer and M. J. Therien, *Macromolecules*, **2006**, 39, 1673.
- (323) A. Rösler, G. W. Vandermeulen and H. A. Klok, *Adv. Drug Deliv. Rev.*, **2012**, 64, 270.
- (324) R. K. O'Reilly, C. J. Hawker and K. L. Wooley, *Chem. Soc. Rev.*, **2006**, 35, 1068.
- (325) P. Alexandridis, *Curr. Opin. Colloid Interface Sci.*, **1996**, 1, 490.
- (326) Z. L. Tyrrell, Y. Shen and M. Radosz, *Prog. Polym. Sci.*, **2010**, 35, 1128.

- (327) A. Rösler, G. W. Vandermeulen and H.-A. Klok, *Adv. Drug Deliv. Rev.*, **2012**, *64*, 270.
- (328) T. Smart, H. Lomas, M. Massignani, M. V. Flores-Merino, L. R. Perez and G. Battaglia, *Nano Today* **2008**, *3*, 38.
- (329) H.-C. Kim and S.-M. H. Park, W.D., *Chem. Rev.*, **2009**, *110*, 146.
- (330) B. Chu and Z. Zhou, Physical chemistry of polyoxyalkylene block copolymer surfactants. In *Nonionic surfactants*, V. M. Nace and M. Dekker, Eds. New York, 1996; Vol. 60, p 67
- (331) B. Chu, *Langmuir*, **1995**, *11*, 414.
- (332) K. Nakashima and P. Bahadur, *Adv. Colloid Interface Sci.*, **2006**, *123-126*, (75–96).
- (333) J. Li, X. Ni, X. Li, N. K. Tan, C. T. Lim, S. Ramakrishna and K. W. Leong, *Langmuir*, **2005**, *21*, 8681.
- (334) P. Alexandridis, D. Zhou and A. Khan, *Langmuir* **1996**, *12*, 2690.
- (335) P. Alexandridis and T. A. Hatton, *Colloids Surf. A*, **1995**, *96*, 1.
- (336) H. Suh and H. W. Jun, *Int. J. Pharm.*, **1996**, *129*, 13.
- (337) *Pluronic and Tetronic Surfactants Technical Brochure* BASF Corp.: Parsippany, NJ, 1989.
- (338) T. Nivaggioli, B. Tsao, P. Alexandridis and T. A. Hatton, *Langmuir*, **1995**, *11*, 119.
- (339) D. Attwood, J. H. Collett and C. A. O'Connor, *Int. J. Pharm.*, **1990**, *65*, 201.
- (340) Z. Sezgin, N. Yüksel and T. Baykara, *Eur. J. Pharm. Biopharm.*, **2006**, *64*, 261.
- (341) D. A. Chiappetta and A. Sosnika, *Eur. J. Pharm. Biopharm.*, **2007**, *66*, 303.
- (342) A. Bahadur, S. Cabana-Montenegro, A. V. K., E. V. Laged, I. Sandez-Machod, A. Concheiro, C. Alvarez-Lorenzo and P. Bahadur, *Int. J. Pharm.*, **2015**, *494*, 453.
- (343) K. S. Sonu and S. K. Saha, *J. Phys. Chem. B*, **2015**, *119*, 9751.
- (344) P. Mukherjee, M. Halder, M. S. Hargrove and J. W. Petrich, *Photochem. Photobiol.*, **2006**, *82*, 1586.
- (345) B. K. Paul, N. Ghosh and S. Mukherjee, *RSC Adv.*, **2015**, *5*, 9381.
- (346) B. D. Wagner, *Molecules*, **2009**, *14*, 210.
- (347) P. Samanta, S. Rane, P. Bahadur, S. Dutta Choudhury and H. Pal, *J. Phys. Chem. B*, **2018**, *122*, 6079–6093.
- (348) S. Dutta Choudhury, M. Kumbhakar, S. Nath, S. K. Sarkar, T. Mukherjee and H. Pal, *J. Phys. Chem. B*, **2007**, *111*, 8842.
- (349) A. Chakraborty, D. Seth, D. Chakrabarty, P. Hazra and N. Sarkar, *Chem. Phys. Lett.*, **2005**, *405*, 18.
- (350) M. Marchena and F. Sanchez, *Prog. React. Kinet. Mech.*, **2010**, *35*, 27.
- (351) F. Sanchez, A. Barrios, M. Lopez-Lopez, P. Lopez-Cornejo, E. Bernal, B. Sarrion, J. A. Lebron and M. Marchena, *Prog. React. Kinet. Mech.*, **2014**, *39*, 151.
- (352) M. Tachiya, *Kinetics of Non-homogeneous Processes*, Wiley: New York, 1987.
- (353) M. Tachiya, *Chem. Phys. Lett.*, **1975**, *33*, 29.
- (354) M. Tachiya, *Can. J. Phys.*, **1990**, *68*, 797.
- (355) M. Maroncelli and G. R. Fleming, *J. Chem. Phys.*, **1987**, *86*, 6221.
- (356) H. Pal, S. Nad and M. Kumbhakar, *J. Chem. Phys.*, **2003**, *119*, 443.
- (357) J. A. Dean, *Lange's Handbook of Chemistry* 13th ed.; McGraw-Hill: New York, 1987.
- (358) H. Masuhara, T. Hino and N. Mataga, *J. Phys. Chem.*, **1975**, *79*, 994.
- (359) H. Masuhara and N. Mataga, *Acc. Chem. Res.*, **1981**, *14*, 312.

- (360) A. Barik, S. Nath and H. Pal, *J. Chem. Phys.*, **2003**, *119*, 10202.
- (361) M. Kumbhakar, T. Goel, T. Mukherjee and H. Pal, *J. Phys. Chem. B*, **2004**, *108*, 19246.
- (362) M. Kumbhakar, S. Nath, T. Mukherjee and H. Pal, *J. Chem. Phys.*, **2004**, *121*, 6026.
- (363) M. C. Rath, H. Pal and T. Mukherjee, *J. Phys. Chem. A*, **1999**, *103*, 4993.
- (364) S. Nath, H. Pal and A. V. Sapre, *Chem. Phys. Lett.*, **2002**, *360*, 422.
- (365) G. B. Dutt, *J. Phys. Chem. B*, **2005**, *109*, 4923.
- (366) P. Debye, *Polar Molecules* Dover: New York, 1929.
- (367) C. M. Hu and R. Zwanzig, *J. Chem. Phys.*, **1974**, *60*, 4354.
- (368) P. G. Sen, S., K. Sahu, S. K. Mondal, D. Roy and K. Bhattacharyya, *J. Chem. Phys.*, **2006**, *124*, 204905.
- (369) J. C.-M. Lee, R. J. Law and D. E. Discher, *Langmuir*, **2001**, *17*, 3592.
- (370) J. T. Edwards, *J. Chem. Educ.*, **1970**, *47*, 261.
- (371) H. Shirota and H. Segawa, *J. Phys. Chem. A*, **2003**, *107*, 3719.
- (372) H. Shirota and H. Segawa, *Chem. Phys.*, **2004**, *306*, 43.
- (373) S. Ghosh, A. Adhikari, U. Mandal, S. Dey and K. Bhattacharyya, *J. Phys. Chem. C*, **2007**, *111*, 8775.
- (374) J. B. Birks, *Photophysics of Aromatic Molecules* Wiley-Interscience: New York, 1970.
- (375) S. Nad and H. Pal, *J. Phys. Chem. A*, **2000**, *104*, 673.
- (376) J. Sangster, *J. Phys. Chem. Ref. Data*, **1989**, *18*, 1111.
- (377) P. R. Jones, M. J. Drews, J. K. Johnson and P. S. Wong, *J. Am. chem. Soc.*, **1972**, *94*, 4595.
- (378) W. R. Fawcett, *J. Phys. Chem.*, **1993**, *97*, 9540.
- (379) W. R. Fawcett, Solvent Acidity and Basicity in Polar Media and Their Role in Solvation. In *Quantitative Treatments of Solute/Solvent Interactions*, P. Politzer and J. S. Murray, Eds. Elsevier: Amsterdam, The Netherlands, 1994; Vol. 8, pp 183
- (380) C. Reichardt, *Chem. Rev.*, **1994**, *94*, 2319.
- (381) V. Gutmann, *Coord. Chem. Rev.*, **1976**, *18*, 225.
- (382) Y. Marcus, *J. Sol. Chem.*, **1984**, *13*, 599.
- (383) P. M. E. Mancini, T. A., G. M. G. and L. R. Vottero, *J. Phys. Org. Chem.*, **1995**, *8*, 617.
- (384) J. Kroon, H. Oevering, J. W. Verhoeven, J. M. Warman, A. M. Oliver and M. N. Paddon-Row, *J. Phys. Chem.*, **1993**, *97*, 5065.
- (385) S. Murata and M. Tachiya, *J. Phys. Chem.*, **1996**, *100*, 4046.
- (386) H. B. Gray, J. R. Winkler and D. Wiedenfeld, *Coord. Chem. Rev.*, **2000**, *200-202*, 875.
- (387) H. N. Ghosh, H. Pal, D. K. Palit, T. Mukherjee and J. P. Mittal, *J. Photochem. Photobiol. A*, **1993**, *73*, 17.
- (388) V. Castelletto, P. Parras, I. W. Hamley, P. Baverback, J. S. Pederson and P. Panine, *Langmuir*, **2007**, *23*, 6896.
- (389) R. Ganguly, Y. Kadam, N. Choudhury, V. K. Aswal and P. Bahadur, *J. Phys. Chem. B*, **2011**, *1115*, 3425.
- (390) R. Ganguly, V. K. Aswal and P. A. Hassan, *J. Colloid Interface Sci.*, **2007**, *315*, 693.
- (391) Y. U. Paulechka, D. H. Zaitsau, G. J. Kabo and A. A. Strechan, *Thermochim. Acta*, **2005**, *439*, 158.

- (392) L. P. N. Rebelo, J. N. C. Lopes, J. M. S. S. Esperanca and E. Filipe, *J. Phys. Chem. B*, **2005**, *109*, 6040.
- (393) L. Gaillon, J. Sirieix-Plenet and P. Letellier, *J. Sol. Chem.*, **2004**, *33*, 1333.
- (394) J. Sirieix-Plenet, L. Gaillon and P. Letellier, *Talanta*, **2004**, *63*, 979.
- (395) S. Thomaier and W. Kunz, *J. Mol. Liq.*, **2007**, *130*, 104.
- (396) M. Blesic, M. H. Marques, N. V. Plechkova, K. R. Seddon, L. s. P. N. Rebelo and A. n. Lopes, *Green Chem.*, **2007**, *9*, 481.
- (397) B. Dong, N. Li, L. Zheng, L. Yu and T. Inoue, *Langmuir*, **2007**, *23*, 4178.
- (398) R. L. Vekariya, V. K. A. P. A. Hassan and S. S. Soni, *Langmuir*, **2014**, *30*, 14406–14415.
- (399) K. Thakkar, V. Patel, D. Ray, H. Pal, V. K. Aswal and P. Bahadur, *RSC Adv.*, **2016**, *6*, 36314.
- (400) P. Samanta, S. D. Choudhury and H. Pal, *J. Phys. Chem. B*, **2019**, *123*, 5942–5953.
- (401) A. K. Satpati, M. Kumbhakar, S. Nath and H. Pal, *J. Photochem. Photobiol. A*, **2008**, *200*, 270.
- (402) Y. Marcus, *Chem. Soc. Rev.*, **1993**, *22*, 409.
- (403) G. C. Walker, E. Akesson, A. E. Johnson, N. E. Levinger and P. F. Barbara, *J. Phys. Chem.*, **1992**, *96*, 3728.
- (404) S. Nad and H. Pal, *J. Chem. Phys.*, **2002**, *116*, 1658.
- (405) H. L. Tavernier, F. Laine and M. D. Fayer, *J. Phys. Chem. A*, **2001**, *105*, 8944.
- (406) H. L. Tavernier, A. V. Barzykin, M. Tachiya and M. D. Fayer, *J. Phys. Chem. B*, **1998**, *102*, 6078.
- (407) S. S. Kulthe, N. N. Inamdar, Y. M. Choudhari, S. M. Shirolikar, L. C. Borde and V. K. Mourya, *Colloid. Surf. B*, **2011**, *88*, 691.
- (408) M. Cagel, E. Bernabeu, L. Gonzalez, E. Lagomarsino, M. Zubillaga, M. A. Moretton and D. A. Chiappetta, *Biomed. Pharmacother.*, **2017**, *95*, 894.
- (409) D. Gust, T. A. Moore and A. L. Moore, *Acc. Chem. Res.*, **2001**, *34*, 40.
- (410) H. Petek and J. Zhao, *Chem. Rev.*, **2010**, *110*, 7082.
- (411) M. Lopez-Lopez, S. F. and M. Marchena, *Prog. Reac. Kin. Mech.*, **2012**, *37*, 203.
- (412) M. Kumbhakar, *J. Phys. Chem. B*, **2007**, *111*, 12154.
- (413) M. Kumbhakar, *J. Phys. Chem. B*, **2007**, *111*, 14250.
- (414) J. Jansson, K. Schillen, G. Olofsson, R. C. D. Silva and W. J. Loh, *Phys. Chem. B*, **2004**, *108*, 82.
- (415) P. Verma and H. Pal, *Phys. Chem. Chem. Phys.*, **2015**, *17*, 15400–15411.
- (416) R. Ganguly, V. K. Aswal, P. A. Hassan, I. K. Gopalakrishnan and S. K. Kulshreshtha, *J. Phys. Chem. B*, **2006**, *110*, 9843.
- (417) K. S. Mali and G. B. Dutt, *J. Chem. Sci.*, **2007**, *119*, 147.
- (418) P. K. Singh, M. Kumbhakar, H. Pal and S. Nath, *J. Phys. Chem. B*, **2008**, *112*, 7771.
- (419) J. Jansson, K. Schillen, M. Nilsson, O. Soderman, G. Fritz, A. Bergmann and O. Glatter, *J. Phys. Chem. B*, **2005**, *109*, 7073.
- (420) T. Thurn, S. Couderc, J. Sidhu, D. M. Bloor, J. Penfold, H. J. F. and E. Wyn-Jones, *Langmuir*, **2002**, *18*, 9267.
- (421) D. Chen, Z. Li, C. Yu, Y. Shi, Z. Zhang, B. Tu and D. Zhao, *Chem. Mater.*, **2005**, *17*.
- (422) T. K. Bronich, M. Ouyang, V. A. Kabanov, A. Eisenberg, F. C. Szoka and A. V. Kabanov, *J. Am. Chem. Soc.*, **2002**, *124*, 11872.
- (423) Y. Tan, S. Srinivasan and K.-S. Choi, *J. Am. Chem. Soc.*, **2005**, *127*, 3596.

- (424) K. S. Mali, G. B. Dutt and T. Mukherjee, *J. Phys. Chem. B*, **2007**, *111*, 5878.
- (425) A. Chakraborty, D. Seth, S. P. and N. Sarkar, *J. Chem. Phys.*, **2008**, *128*, 204510 (1.
- (426) U. Mandal, S. Ghosh, S. Dey, A. A. and K. Bhattacharyya, *J. Chem. Phys.*, **2008**, *128*, 164505 (1.
- (427) S. Sarkar, S. Mandal, R. Pramanik, C. Ghatak, R. V. G. and N. Sarkar, *J. Phys. Chem. B*, **2011**, *115*, 6100.
- (428) C. Ghatak, V. G. Rao, S. Mandal and N. Sarkar, *Phys. Chem. Chem. Phys.*, **2012**, *14*, 8925.
- (429) C. Tablet, I. Matei and M. Hillebrand, *J. Mol. Liq.*, **2011**, *160*, 57.
- (430) M. Porel, A. Klimczak, M. Freitag, E. Galoppini and V. Ramamurthy, *Langmuir*, **2012**, *28*, 7, 3355.
- (431) C.-H. Chuang, M. Porel, R. Choudhury, C. Burda and V. Ramamurthy, *J. Phys. Chem. B*, **2018**, *122*, 1, 328.
- (432) P. D. Wood and L. J. Johnston, *J. Phys. Chem. A*, **1998**, *102*, 5585.
- (433) C. A. Mebi, J. J. Trujillo and A. A. Bhuiyan, *Cent. Euro. J. Chem.*, **2012**, *10*, 1218.
- (434) W. T. Carnall, P. R. Fields and K. Rajnak, *J. Chem. Phys.*, **1968**, *49*, 4424.
- (435) W. T. Carnall, P. R. Fields and K. Rajnak, *J. Chem. Phys.*, **1968**, *49*, 4443.
- (436) W. T. Carnall, P. R. Fields and K. Rajnak, *J. Chem. Phys.*, **1968**, *49*, 4447.
- (437) W. T. Carnall, P. R. Fields and K. Rajnak, *J. Chem. Phys.*, **1968**, *49*, 4450.
- (438) L. Chen, P. D. Wood, A. Mnyusiwalla, J. Marlinga and L. J. Johnston, *J. Phys. Chem. B.*, **2001**, *105*, 10927.
- (439) J. Wachtveitl, R. Huber, S. Spörlein, J. E. Moser and M. Grätzel, *Int. J. Photoenergy*, **1999**, *1*, 153.
- (440) T. S. Singh, B. S. M. Rao, H. Mohan and J. P. Mittal, *J. Photochem. Photobiol. A*, **2002**, *153*, 163.
- (441) S. Nad and H. Pal, *J. Phys. Chem. A*, **2001**, *105*, 1097.
- (442) A. K. Satpati, S. Nath, M. Kumbhakar, D. K. Maity, S. Senthilkumar and H. Pal, *J. Mol. Struct.*, **2008**, *878*, 84.
- (443) S. Murata and M. Tachiya, *J. Phys. Chem. A* **2007**, *111*, 9240.
- (444) J. P. Dinnocenzo, A. Mark and S. Farid, *J. Org. Chem.*, **2019**, *84*, 7840–7850.
- (445) P. Alexandridis and T. A. Hatton, *Colloids Surf. A*, **1995**, *96*, 1.
- (446) P. Alexandridis, J. F. Holzwarth and T. A. Hatton, *Macromolecules*, **1994**, *27*, 2414.
- (447) E. D. Goddard, *J. Colloid Interface Sci.*, **2002**, *256*, 228.
- (448) K. Mortensen and J. S. Pederson, *Macromolecules*, **1993**, *26*, 805.
- (449) Z. Zhou and B. Chu, *J. Colloid Interface Sci.*, **1988**, *126*, 171.
- (450) V. Y. Alakhov and A. V. Kabanov, *Expert Opin. Invest. Drugs*, **1998**, *7*, 1453.
- (451) P. Bahadur and G. Riess, *Tenside, Surfactants, Deterg.*, **1991**, *28*, 173.
- (452) E. V. Batrakova, H. Y. Han, D. W. Miller and A. V. Kabanov, *Pharm. Res.*, **1998**, *15*, 1525.
- (453) M. Guzman, F. F. Garcia, J. Molpeceres and M. R. Aberturas, *Int. J. Pharm.*, **1992**, *80*, 119.
- (454) A. Kabanov, J. Zhu and V. Alakhov, *Adv. Genet.*, **2005**, *53*, 231.
- (455) T. G. Park, S. Cohen and R. Langer, *Pharm. Res.*, **1992**, *9*, 37.
- (456) M. Yokoyama, *Crit. Rev. Therapeutic Drug Carrier Syst.*, **1992**, *9*, 213.

Thesis Highlight

Name of the Student: **Papu Samanta**

Name of the CI/OCC: **BARC**

Enrolment No.: **CHEM01201604001**

Thesis Title: ***Photoinduced electron transfer processes in homogeneous and microheterogeneous media involving organic & inorganic donor-acceptor systems***

Discipline: **Chemical Sciences**

Sub-Area of Discipline: **Photochemistry**

Date of viva voce: **10.07.2021**

Electron transfer (ET) processes being the fundamental redox reactions occurring ubiquitously both in chemistry and biology, studies on these processes has been the topic of intense research for long time to understand the intricate details of the ET reactions using model systems. A significant part in this endeavor has been the studies involving photoinduced electron transfer (PET) reactions, also termed as photoinduced charge separation processes having direct relevance to conversion of solar energy into chemical or electrical energy.

Present thesis demonstrates how the elusive Marcus Inversion (MI) behavior can be observed convincingly for photoinduced bimolecular ET processes, conducting the reactions in constrained microheterogeneous media. In this thesis, PET processes have been investigated involving coumarin dyes as the acceptors and aromatic amines as the donors, conducting the studies in Tetronic and Pluronic block copolymer micelles, either using them independently, or using along with the additives like a salt (NaCl) or a co-surfactant $[\text{C}_n\text{MIm}][\text{BF}_4]$ series of ionic liquids and sodium dodecyl sulphate (SDS) as conventional surfactant) to modulate micellar microenvironments. In all the cases, MI behavior is observed very convincingly, which is attributed to the non-diffusional nature of bimolecular reactions that follow the two-dimensional ET (2DET) mechanism, as the micelles provide quite constrained reaction media and solvent relaxation within micelle is exceedingly slow. Interestingly, both the PET kinetics and the onset of MI along the exergonicity scale ($-\Delta G^0$) for the studied PET systems are seen to be modulated very significantly on using either characteristically quite different copolymer systems or on using either a salt or a co-surfactant as the modulating agent for a particular copolymer micelle. Different observations made in the present study involving different microheterogeneous media are concisely shown using **Panels A-C** of the included figure.

In the present thesis, another interesting aspect investigated is the involvement of multichannel ET in the forward PET processes, studied in homogeneous aqueous medium using Ln(III) ions as the unique electron acceptors and suitable coumarin dyes as electron donors. Since most Ln(III) ions have number of low lying electronic energy states that can be accessed by the available exergonicity of the studied PET reactions, they can support multichannel PET with different propensity, depending on used Ln(III) ion. Accordingly, the k_q versus $-\Delta G^0$ plots for the studied coumarin-Ln(III) systems show largely different correlations for different Ln(III) ions, as are displayed convincingly in **Panel D** of the included figure.

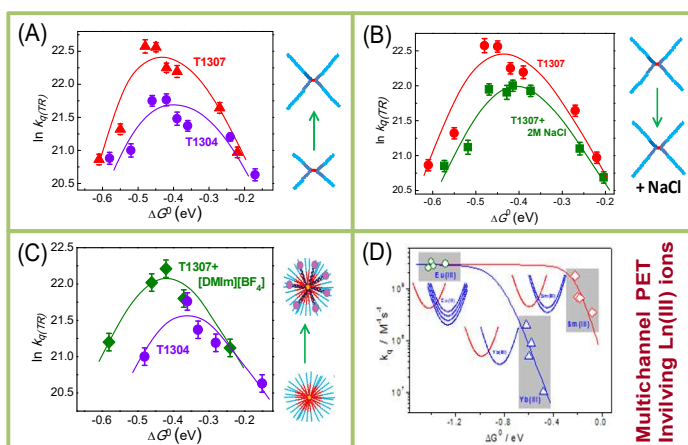


Figure: Modulation of the PET kinetics and energetics following different approaches. In micellar media: (A) Using different Tetronic systems, (B) With the addition of a salt, and (C) On using a co-surfactant. In homogeneous aqueous medium: (D) On using Ln(III) ions to support multichannel PET processes.